Progress in Polymer Science 42 (2015) 79–153

Contents lists available at ScienceDirect

Progress in Polymer Science

journal homepage: www.elsevier.com/locate/ppolysci

Editorial/Preface

Pressure sensitive adhesives based on interpolymer complexes

Mikhail M. Feldstein[a,b,c,*], Elena E. Dormidontova[d], Alexei R. Khokhlov[a,b]

[a] Faculty of Physics, M.V. Lomonosov Moscow State University, 119991, GSP-1, 1-2 Leninskiye Gory, Moscow, Russia
[b] A.N. Nesmeyanov Institute of Organoelement Compounds (INEOS), Russian Academy of Sciences, Moscow, Russia
[c] D.I. Mendeleyev University of Chemical Technology of Russia, Moscow, Russia
[d] Institute of Materials Science and Physics Department, University of Connecticut, Storrs, CT 06269, United States

ARTICLE INFO

Article history:
Received 9 January 2014
Received in revised form 15 October 2014
Accepted 22 October 2014
Available online 1 November 2014

Keywords:
Pressure-sensitive adhesives
Molecular design method
Free volume
Intermolecular cohesion
Interpolymer and polymer–oligomer complexes

ABSTRACT

Adhesion of noncovalent complexes formed between complementary polymers bearing functional groups capable of hydrogen bonding or ionic interactions is reviewed. The rational design of novel adhesive materials with tailored properties requires a molecular insight into the mechanism of their self-assembly. At the most fundamental molecular level, strong adhesion is the result of a delicate balance between two generally conflicting properties: high energy of intermolecular cohesion and large free volume. These conflicting properties can be achieved in self-assembling interpolymer complexes. The adhesive and mechanical properties of the polymer blends can easily be controlled by blend composition and the type of intermolecular bonding (hydrogen bonding or ionic interactions or combination of both), whereas their solubility and water absorbing capacity are dictated by the hydrophilicity of the parent components. Innovative self-adhering pressure sensitive adhesives are based either on nonstoichiometric interpolymer complexes or on stoichiometric complexes of long-chain polymers with telechelic oligomers. Once the molecular mechanism of self-assembly of adhesive materials has been established, the molecular design of new adhesives with tailored properties becomes feasible. The number of functional polymers suitable to serve as parent components for producing novel adhesives is very large, suggesting that the polymer blending approach, based on molecular design considerations, may revolutionize the adhesive industry in the coming decades.

Contents

1. What are pressure sensitive adhesives? 81
2. Molecular theory of pressure sensitive adhesion 82
3. Pressure sensitive adhesives based on stoichiometric complexes of high molecular weight polymers with telechelic oligomers 83
   3.1. Peel adhesion of PVP–PEG and PVCL–PEG blends 83
   3.2. Probe tack behaviors of PVP–PEG and PVCL–PEG PSAs 84
   3.3. Tensile properties of PVP–PEG blends 86

* Corresponding author at: A.N. Nesmeyanov Institute of Organoelement Compounds (INEOS), Russian Academy of Sciences, Moscow, Russia. Tel.: +7 499 135 0732.
E-mail address: mfeld@ineos.ac.ru (M.M. Feldstein).

http://dx.doi.org/10.1016/j.progpolymsci.2014.10.006
0079-6700/

3.4. Water absorbing properties of PVP–PEG blends 88
3.5. Phase state of PVP–PEG and PVCL–PEG blends 89
3.6. Nonequimolar stoichiometry and nanostructure of PNVAm–PEG network complex 91
3.7. Molecular mechanism of the PNVAm–PEG interaction and mixing throughout the entire composition range 92
3.8. Comparison of the T_g analysis data with the results of independent measurements 93
3.9. Energy of intermolecular H-bonding and free volume in PVP–PEG PSAs 95
3.10. "Smart" thermoswitchable PSA based on hydrophilic polymer possessing Lower Critical Solution Temperature in water 97
3.11. Pharmaceutical application of PVP–PEG adhesive 98
4. Fundamentals of interpolymer and polyelectrolyte complex formation 101
4.1. Cooperative mechanisms of self-assembling the interpolymer and polyelectrolyte complexes 101
4.2. Theoretical models of cooperative interpolymer and polyelectrolyte complex formation pertinent to their adhesive behaviors 103
4.3. Effects of topological chain entanglements between complementary polymer components on the structure of interpolymer complexes 104
4.4. Impact of polymer chain stiffness upon supramolecular structure of polyelectrolyte complexes 105
4.5. Effects of cohesive interaction strength, chain length, charge distribution, solvent quality, salt concentration, polybase–polyacid ratio, pH and temperature 106
5. Cohesive interaction forces between reactive functional groups in electrostatic and hydrogen-bonded interpolymer complexes governing molecular mechanisms of complexation, elasticity and adhesion 112
5.1. Probing the strengths of intermolecular bonds 112
5.2. Self-assembly of interpolymer and polyelectrolyte complexes examined with single-molecule force spectroscopy 117
5.3. Inherent stretching elasticity of single polymer chain 119
5.4. Understanding adhesion and interfacial phenomena on the level of single macromolecules 123
6. Pressure sensitive adhesives based on nonstoichiometric polyelectrolyte complexes 127
6.1. Mechanisms of intermolecular interactions and the strength of noncovalent bonds in a model polyelectrolyte complex 128
6.2. Phase behavior of the polyelectrolyte complexes in a solid state 130
6.3. Mechanical properties of polyelectrolyte blends 132
6.4. Adhesion of the PSAs based on nonstoichiometric polyelectrolyte complexes 132
6.5. Impact of the type of intermolecular bonding on adhesion of polyelectrolyte complexes 133
6.6. Electrorheology of solid polyelectrolyte complexes 135
6.7. Water-absorbing capacity of polyelectrolyte PSAs 136
7. Pressure-sensitive adhesive hydrogels based on ternary interpolymer complexes with telechelic oligomer 137
7.1. Mechanisms of competitive hydrogen bonding underlying phase behavior of ternary PVP–PEG–Polyacid blends 137
7.2. Tensile properties of PSAs based on ternary PVP–PEG–Polyacid complexes 139
7.3. Effects of the ladder-like and telechelic oligomer crosslinkers on adhesion of ternary PVP–PEG–Polyacid complexes 140
7.4. Mechanisms of swelling and dissolution of ternary PVP–PEG–Polyacid complex in water 142
7.5. Effect of absorbed water on adhesion of PVP–PEG–Polyacid hydrogels 143
8. Hydrophilic adhesives based on interpolymer and polymer–oligomer complexes compared with conventional PSAs and bioadhesives 144
9. Conclusions 145
Acknowledgements 146
References 146

List of abbreviations

AFM atomic force microscopy (microscope)
CFM chemical force microscopy
DMA dynamic mechanical analysis
DMAEMA N,N-dimethylaminoethyl methacrylate
DSC differential scanning calorimetry
F–D, f–d force–distance
FFP film forming polymer
FJC freely jointed chain model
FRC freely rotating chain model
FTIR spectroscopy Fourier transform infrared spectroscopy
Ig immunoglobulin
IPC, IPCs interpolymer complex(es)
ISDN isosorbide dinitrate
JKR Johnson–Kendall–Roberts theory of adhesion
L traveled distance (in SMFS experiments)
L_c contour length of polymer chain
LCST Lower Critical Solution Temperature
LLC ladder-like crosslinker
MW molecular weight
NCC noncovalent crosslinker
NMR nuclear magnetic resonance
OSF Odijk–Skolnick–Fixman theory
PAA polyacrylic acid
PAAm poly(acryl amide)
PAANa sodium salt of polyacrylic acid
PAH poly(allylamine hydrochloride)
PAAm poly(acryl amide)
PALS positron annihilation life-time spectroscopy
PDADMAC poly(diallyldimethylammonium chloride)
PDEAm poly(N,N-diethylacrylamide)
PDMAEMA-co-MMA/BMA copolymer of N,N-dimethylaminoethyl methacrylate with methyl methacrylate and butyl methacrylate
PDMAm poly(N,N-dimethylacrylamide)

PEC, PECs polyelectrolyte complex(es)
PEG poly(ethylene glycol)
PEM polyelectrolyte multilayer
PEO poly(ethylene oxide)
PFG NMR pulsed field gradient nuclear magnetic resonance
PIB polyisobutylene
PMA-co-MVE copolymer of maleic acid with methylvinyl ether
PMAA-co-EA copolymer of methacrylic acid and ethyl acrylate
PMMA poly(methyl methacrylate)
$PM2VP_{249}$-b-PEO_{134} poly(N-methyl-2-vinylpyridynium iodide)-block-poly(ethylene oxide)
PNVAm poly(N-vinyl amide)
PNIPAM poly(N-isopropyl acrylamide)
p/p_s relative water vapor pressure (Relative Humidity)
PS polystyrene
PSA, PSAs pressure-sensitive adhesive(s)
PSPMA poly(3-sulfopropyl methacrylate) brush
PTMAEMA poly(trimethylaminoethyl methacrylate)
PVA poly(vinyl alcohol)
PVAc poly(vinyl acetate)
PVAm poly(vinyl amine)
PVCL poly(N-vinyl caprolactam)
PVP poly(N-vinyl pyrrolidone)
QM-FRC quantum mechanical freely rotating chain model
QSPR quantitative structure–property relationship
RH relative humidity
R_g radius of gyration
S sol fraction
SA self-assembly
SAM self-assembling monolayer
SFM scanning force microscopy (microscope)
SIS styrene–isoprene–styrene triblock copolymer
SMFS single molecule force spectroscopy
TEC triethyl citrate
TDS transdermal delivery system
T_g glass transition temperature
TM-DSC Temperature Modulated Differential Scanning Calorimetry
UCST Upper Critical Solution Temperature
WAXS wide-angle X-ray scattering
WLC wormlike chain model
WMI wedge microinterferometry
W_a the practical work of adhesion (debonding energy)
W_b the work of viscoelastic deformation up to the break of polymer film under uniaxial extention
WMI wedge micro-interferometry
w_{*PEG} adjustable parameter in Eq. (2), defining the weight fraction of PEG chains that crosslink repeat units in the PVP chains by means of two H-bonds through both terminal OH-groups in the PEG chains.
α swell ratio

1. What are pressure sensitive adhesives?

Hydrogen or ionically bonded polymeric network structures, readily produced in a melt or in solution by mixing complementary polymers bearing functional groups, possess unusual physical and chemical properties not found in parent and conventional polymers. These new materials are finding innovative practical applications and have generated much interest in widely diverse scientific and engineering fields [1–5]. This review summarizes the formation, adhesive and viscoelastic behaviors of such self-assembling noncovalently crosslinked supramolecular structures and briefly outlines their applications.

Our everyday life is inconceivable without pressure-sensitive adhesives (PSAs). Applications of PSAs expand day by day in various areas of industry and medicine. They are widely used as surface protection films, as a component of pressure-sensitive tapes, labels, note pads or automobile trim. Also they serve as skin-contact adhesive platforms in medical plasters, wound dressings, transdermal patches, and a variety of other products. PSAs are designed for either permanent or removable applications. Removable PSAs serve to form a temporary bond and ideally can be removed after months or years without leaving residue on the surface of an adherend. Innovative PSAs with tailored properties can be produced by physical mixing of nonadhesive parent polymers bearing complementary reactive functional groups in their recurring units and (or) at the opposite ends of their short chains.

PSAs are a special class of viscoelastic polymers that form strong adhesive joints with substrates of varying chemical nature under application of light external bonding pressures (1–10 Pa) over short periods of time (1–5 s). To be a PSA, a polymer should possess high molecular mobility and fluidity under applied bonding pressure in order to form good adhesive contact, coupled with high intermolecular cohesive strength and elasticity. The latter requirement is necessary for resistance to debonding stress and for dissipation of the mechanical energy of adhesive bond failure under a detaching force.

According to definition of the Pressure Sensitive Tape Council [6], PSAs are aggressive and permanently tacky, adhere to different adherends (substrates) without the need of more than finger or hand pressure during very short time (a few seconds), require no activation by heat, solvent or water, and exert a strong holding force. PSAs have sufficient cohesive strength and elasticity so that they can be removed from smooth surfaces without leaving a residue.

PSAs are designed with a balance between flow and resistance to flow. The bond forms because the adhesive is soft enough to flow, wetting the adherend. The adhesive bond has strength because the adhesive is hard enough to resist flow when detaching stress is applied to the bond [7].

After some early uncertainty in the literature about the nature of the pressure sensitive adhesive bond [8], Dahlquist related the elasticity modulus data to the time-temperature tack dependence and established that the compression (shear) modulus of the adhesive had to be less than about 0.1 MPa before any adhesive tack was observed [9–11]. This was explained as the highest modulus that still allowed the adhesive to be sufficiently compliant to come into molecular contact with a substrate and form dispersive interfacial bonds. Investigators who followed Dahlquist have accepted this requirement [12–17], termed

Table 1
Common PSA polymer classes.

Inherently tacky	Need tackification
Polyalkylacrylate copolymers	Natural rubber
Poly(vinyl ethers)	Polyisobutylene (PIB)
Polyalphaolefins	Styrene–isoprene block copolymers
	Styrene–butadiene block copolymers
	Styrene–butadiene random copolymers
	Polysiloxanes

the "Dahlquist Criterion of Tack", even though the true criterion is defined as a dimensionless quantity.

Another general criterion for pressure sensitivity is that the glass transition temperature of the adhesive should be below ambient temperature, most frequently room temperature. Broadly speaking, the T_g of a PSA should be about 30–70 °C below the room temperature, depending on the base polymer and the added modifiers [7,14,15]. This observation implies that all PSAs are viscoelastic rubber-like polymers [17,18]. Based on this criterium, Chu [19] and Chang [20] have suggested that the first step in designing a PSA is to tailor an adhesive to a predetermined T_g and modulus window.

The first PSA was natural rubber. The era of modern PSA technology was ushered in during the 1930s with the appearance of synthetic rubbers. The list of currently commercially available elastomers that can be formulated into PSAs is presented in Table 1. Two subsets are differentiated in Table 1: those polymers that are inherently tacky, and those that require modification with tackifiers to meet the T_g and modulus criteria to become a PSA.

As is evident from Table 1, commercially available PSAs are mainly hydrophobic polymers. A common drawback of the hydrophobic adhesives is a lack of adhesion toward wet substrates [21,22]. Indeed, if an adhesive material is incapable of absorbing water, any accumulation of moisture at the adhesive–substrate interface will render the adhesive untacky [23]. In recent years PSAs have found ever-widening application in transdermal [24,25] and transmucosal [26,27] therapeutic systems for controlled drug delivery, wound dressings [28–30], topical drug plasters [24], tooth whitening strips [30], and as skin-contact adhesives for attachment of medical catheters and diagnostic electrodes [24]. Regrettably, hydrophobic PSAs have not yet been applied as broadly as the biomedical community initially hoped it would. The major limiting factor is the lack of adherence toward wet biological tissues that secrete moisture during the lifetime of adhesive joint, a factor that limits long-term wear of adhesive patches on skin. Thus, development of hydrophilic water-absorbing PSAs is vitally important.

The history of hydrophilic PSA technology abounds in numerous examples of mixing hydrophobic adhesives with hydrophilic absorbents of moisture [31–37]. The hydrophobic PSA therewith forms a continuous phase, whereas a disperse phase is formulated from the moisture-absorbent material. Upon contact with relatively large amounts of moisture, the hydrophilic polymer particles swell and cause the adhesive platform to phase separate. As a consequence, adhesion vanishes [31]. A radical resolution of this challenge could be achieved by developing water-absorbing PSAs based on hydrophilic polymers. Rational design of novel PSAs with tailored performance properties requires gaining an insight into the molecular structures responsible for pressure-sensitive adhesion of viscoelastic polymers. Thus the present review is focused on recent progress achieved in elaboration of the PSAs of controlled hydrophilicity and water absorption capacity and describes the molecular structures of the hydrophilic PSAs and states the principles for controlling their major performance properties. To avoid republication of earlier presented data, the present discussion considers the data of general significance, while for details a reader is referred to original publications.

2. Molecular theory of pressure sensitive adhesion

Pressure sensitive adhesion is very complex phenomenon including a variety of contributions. Because our final goal is rational development of innovative PSAs, in this review we mainly consider the bulk properties and supramolecular structures of adhesives, leaving aside the interfacial contributions which relate mainly to the properties of substrates (e.g., surface energy and roughness).

What are the molecular structures that control pressure-sensitive adhesion of polymers and polymer composites? By default, until recently this reasonable question was considered to be irrelevant and unanswerable because, as is seen from Table 1, existing PSAs exhibit markedly dissimilar chemical compositions and structures. As has been quite recently shown [38], the 180° peel force, P (N), to debond a PSA film from a rigid substrate is related to the factors defining pressure-sensitive adhesion of a PSA at the molecular level by Eq. (1) [38]:

$$P = kbl\frac{\pi NaD\tau}{k_BT}\sigma_b^2 \quad (1)$$

where b and l are the width and thickness of the adhesive film, k is a dimensionless constant that takes into account the contributions of a backing film deformation and the interaction between the adhesive and the substrate, N is the number of segments of size a in a polymer chain, D is the self-diffusion coefficient of a polymer segment, τ is apparent relaxation time of the adhesive polymer, σ_b is the ultimate tensile stress of the PSA film under uniaxial extension, k_B is Boltzmann's constant, and T is temperature (°K). The dependence of peel force on the adhesive layer thickness and the material properties of the backing film in hydrophilic PSAs were considered by Chalykh et al. in Ref. [39].

Eq. (1) is not useful for quantitative calculations of peel force due to a range of crude assumptions made in its derivation [38]. Nevertheless, Eq. (1) predicts qualitatively the significance of diffusion and relaxation processes (both of which require molecular mobility) for the adhesive properties of polymers. According to Eq. (1), pressure sensitive adhesion requires coupling of high molecular mobility (D) with long term relaxation processes (τ) and high cohesive strength of an adhesive polymer (σ_b). At the most fundamental, molecular level, cohesive strength is governed by intermolecular cohesion energy. The energy of

intermolecular cohesion and the molecular mobility are mutually conflicting properties, as most commonly a stronger intermolecular cohesion lowers the molecular mobility. This explains why pressure sensitive adhesion is a comparatively rare phenomenon.

High molecular mobility is a manifestation of a large free volume defined as the vacant space between neighboring macromolecules [40]. The self-diffusion coefficient of a polymer segment increases with the free volume fraction f_v. Hence, Eq. (1) shows that at the molecular level pressure sensitive adhesive capability of polymer materials requires both a high cohesive energy, as reflected by σ_b, and a large free volume.

As the molecular theory of pressure sensitive adhesion predicts [17,38,41], strong adhesion requires a high value of cohesive strength (σ_b), a large diffusion coefficient (D), and a long relaxation time (τ). Both the diffusion coefficient and the relaxation time are measures of molecular mobility, although they do vary in opposite directions as molecular mobility increases in the course of transition from a glassy polymer to viscous liquid, e.g., with the increase of temperature or the content of a plasticizer. Indeed, the longest relaxation times are featured for glasses (years, decades or centuries), whereas low molecular weight liquids relax almost instantaneously. In contrast, the lowest diffusion coefficients are observed for glasses, while the highest diffusion coefficients are demonstrated in liquids and gases.

According to Eq. (1), maximum peel strength, P, is related to the maximum magnitude of the product $D{\cdot}\tau{\cdot}{\sigma_b}^2$. Evidently, this product achieves its maximum magnitude over a limited range of values of relaxation times and diffusion coefficients, which are intermediate between those inherent for liquids and glasses. Materials exhibiting properties of both liquids and solids are viscoelastic [18] and that is why all PSAs are viscoelastic materials. Hence, the molecular theory of pressure sensitive adhesion predicts that adhesion strength goes through a maximum with the change of PSA molecular mobility as an adhesive material composition or temperature is varied [17,38,41].

As with any useful theory, the molecular theory of pressure sensitive adhesion not only explains the mechanisms underlying adhesion phenomenon but also has predictive power. High strength of PSA joints requires a compromise between two mutually conflicting factors, namely a high energy of intermolecular cohesion and a large free volume. To test the predictive capacity of this theory, we consider molecular structures of polymers that can fulfill this compromise. Successful combination of polymers chosen on this basis would provide strong evidence in favor of the theory, with accompanying insights toward molecular design of new PSAs with optimized performance properties.

3. Pressure sensitive adhesives based on stoichiometric complexes of high molecular weight polymers with telechelic oligomers

The derivation of Eq. (1) [38] and its forerunners [17,41] was based on consideration of a model PSA behavior, i.e., the blends of high MW poly(N-vinyl pyrrolidone), PVP, with oligomers of poly(ethylene glycol), PEG, ranging in molecular weight from 200 to 600 g/mol. In this connection it is quite logical to begin a discussion of polymer structures combining high molecular mobility and intermolecular cohesion strength with these model systems.

3.1. Peel adhesion of PVP–PEG and PVCL–PEG blends

Our earlier research established that blends of high molecular weight, glassy poly(*N*-vinyl amides) (PNVAm), such as poly(N-vinyl pyrrolidone) (PVP, M_w = 1,000,000 g/mol; M_n = 360,000 g/mol) [39,42] or poly(*N*-vinyl caprolactam) (PVCL) [43], with liquid poly(ethylene glycol) (PEG, M_w = 400 g/mol) demonstrate excellent pressure sensitive adhesion [38,39,42,43]. PVP has been shown to be easily soluble in low molecular weight PEG, yielding single phase homogeneous blends [44–46]. The miscibility of blended polymers is known to result most frequently from a specific favorable interaction between the macromolecules [47]. Since, as illustrated in Fig. 1, both PNVAm's and PEG contain only electron donating groups in the recurring units of their backbones, they would normally be expected to be immiscible.

At ambient temperature, PVP is immiscible with high molecular weight fractions of PEG (M_w > 600 g/mol) [45]. Miscibility of 400 MW PEG with PVP is therefore attributed to hydrogen bonding between the proton donor OH end groups on PEG with the PVP electron donating carbonyl groups. Such interactions are confirmed by Fourier transform infrared (FTIR) spectroscopy [44,48,49]. A schematic

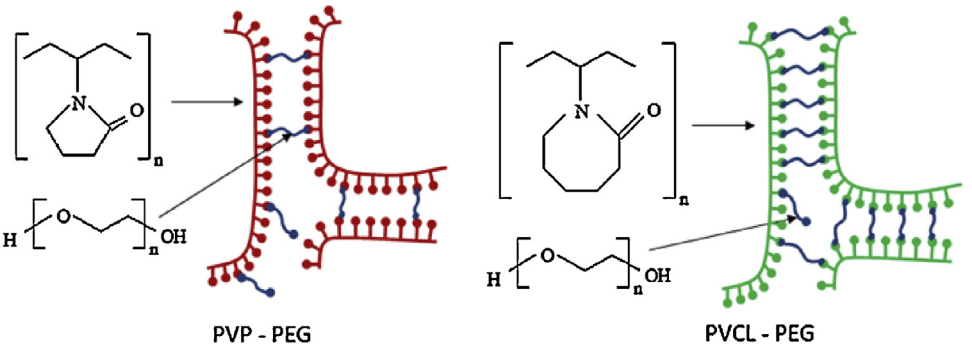

Fig. 1. Chemical structures of poly(N-vinyl pyrrolidone), poly(N-vinyl caprolactam) and schematic presentation of the corresponding network H-bonded complexes formed with poly(ethylene glycol) oligomer, PEG-400.

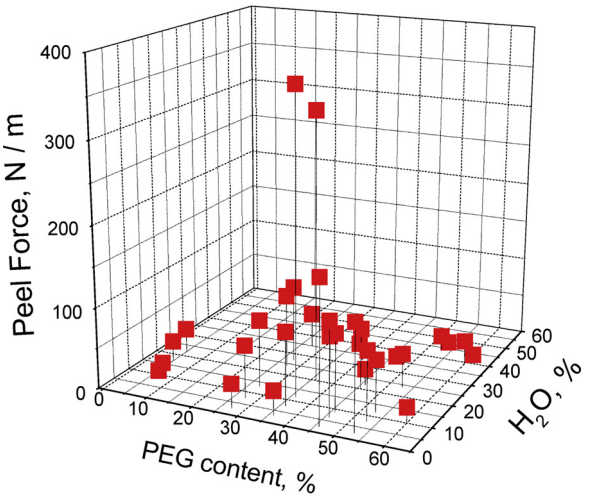

Fig. 2. 180° Peel adhesion of PVP–PEG blends as a function of PEG concentration and the content of absorbed water (percent water absorbed per 100% PVP + PEG). Peeling rate is 10 mm/min. A low-density polyethylene (PE) film of 100 μm in thickness, crystallinity ~45%, surface energy 28.5 mJ/m^2 is employed as a standard substrate.
[39], Copyright 2002. Reproduced with permission from Taylor & Francis.

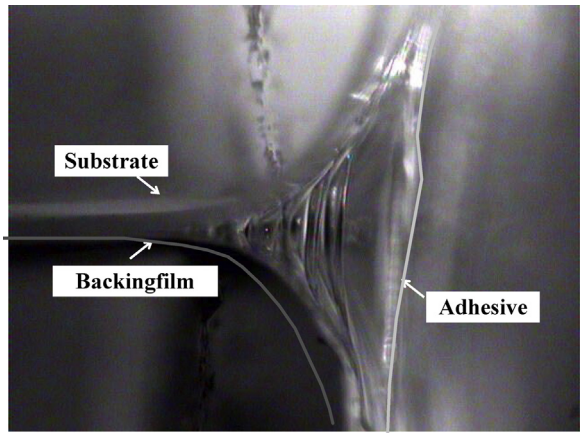

Fig. 3. A photomicrograph of PVP–PEG (36 wt. %) hydrogel adhesive joint failure with PE substrate viewed from the side. Initial thickness of adhesive layer is 250 μm. Prior to bonding the PVP–PEG adhesive was exposed to RH = 50% and absorbed 13% water.
[39], Copyright 2002. Reproduced with permission from Taylor & Francis.

view of the proposed structure of the PNVAm–PEG complexes is illustrated in Fig. 1.

Because every PEG chain bears two reactive terminal OH-groups, PEG acts as an H-bonding reversible crosslinker of longer PNVAm macromolecules and as a spacer between the PVP or PVCL chains.

In Fig. 2, the 180° peel adhesion, *P*, is plotted against PVP–PEG blend composition and content of water absorbed as vapor from the surrounding atmosphere [39]. Although neither parent component, PVP or PEG, demonstrates inherent pressure sensitive adhesion on its own, high adhesion appears in PVP blends with the PEG content in a narrow range around 36 wt.%. This finding is of critical industrial importance. Commonly, novel PSAs are produced by chemical synthesis or modification of initially tacky polymers. From Fig. 2 it is now evident that innovative PSAs can be also produced by physical mixing of nonadhesive polymers.

Properties of polymer blends are usually intermediate between those of the constituent polymers [47]. New properties, atypical of the pure components, arise most frequently from specific interactions or chemical reactions [50]. In polymer blends such interaction products are frequently interpolymer complexes which demonstrate properties alien to the parent components [1–5]. For blended PVP/PVCL–PEG PSAs mixing PVP or PVCL with PEG leads to formation of an H-bonded network complex shown schematically in Fig. 1. The cohesive strength of this complex is provided by hydrogen bonding between carbonyls in PNVAm recurring units and both terminal hydroxyl groups at opposite ends of PEG short chains. The large free volume is due to the length and flexibility of PEG crosslinks. In this way, self-assembled PVP–PEG and PVCL–PEG network complexes behave as new individual supramolecular structures and exhibit a tack that is not found in either parent component.

Debonding of pressure-sensitive adhesives in peel or probe tack tests has been found to occur not through the initiation and propagation of cracks in the plane of the adhesive layer along a PSA–substrate interface but rather through the formation of progressively extended fine fibrils in the tensile direction which span a joint prior to its complete separation. The fibrils may consume a reasonable portion of the force required to remove adhesive tape from the substrate. This general mechanism is typical of the PVP–PEG PSA joint fracture as well [39,42], exhibiting several important peculiarities, as is readily visible under the microscope when one observes the debonding process in the course of peel testing (Fig. 3) [39].

Similar to other PSAs, the PVP–PEG adhesive joints fail by elastic stretching of the adhesive bulk up to a critical value of tensile strain of ε = 1000–1500%, where a fracture occurs. The entire layer of the adhesive is thus subjected to elongational flow as fibrils which provides resistance to detachment and energy dissipation. Thus viscoelastic deformation of an adhesive in extension is a major energy dissipating mechanism in the course of adhesive bond failure.

3.2. Probe tack behaviors of PVP–PEG and PVCL–PEG PSAs

When developing novel PSAs, the probe tack test is a most informative and highly illustrative tool that enables not only characterization of an adhesive joint's strength, but also development of qualitative insight into the relative contributions of the intermolecular cohesion energy (E_c) and the free volume fraction (f_v) to adhesion. When the contribution of E_c dominates that of f_v, the probe tack stress–strain curve has a shape illustrated in Fig. 4 by curve 1, which is typical for debonding of solid-like PSAs [51]. This curve is characterized by a sharp maximum at rather low strains and a small area under the stress–strain curve. Adhesive joint failure in this case proceeds through interfacial crack propagation between the probe and the

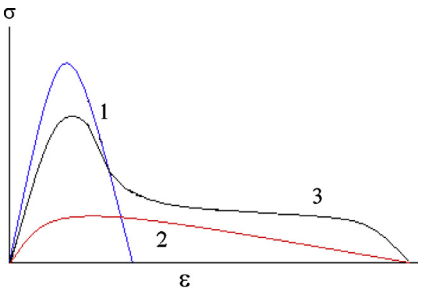

Fig. 4. Typical probe tack curves for solid-like PSA (high E_c:f_v ratio, curve 1), liquid-like adhesive (low E_c:f_v ratio, curve 2), and the PSA with optimized adhesion (intermediate value of E_c:f_v ratio, curve 3).

adhesive film surface and is called "adhesive debonding." At the other extreme, when f_v prevails, the probe tack curve is as that shown by curve 2 in Fig. 4 [51]. This type of adhesive joint failure is characteristic of fluid PSAs [52,53], which demonstrate comparatively low cohesion strength, indicated by a lower peak of debonding stress, σ, coupled with a relatively high value of elongation, ε. In this case, the adhesive joint breaks by cohesive fracture in the bulk of the adhesive layer and the debonding process are governed by viscous flow. This type of debonding is called "cohesive debonding," where some residue of adhesive are left on the probe at the end of the test.

In between these two cases, when a high E_c is accompanied by a large f_v, the area under the probe tack curve achieves its maximum value. Debonding proceeds via cavitation and fibrillation of the adhesive layer, which is typical for PSAs with optimized adhesion (Fig. 4, curve 3) [51]. The curve shows a peak of debonding stress followed by a more or less pronounced plateau, and then either gradual or sharp decrease of the detaching force to zero. Detachment in that case occurs at the interface between the probe and the adhesive layer [52,53], with no macroscopic residue left on the probe. When strain hardening in fibrils is present just before the final detachment, the probe tack stress–strain curve may demonstrate a slight increase in the stress or a second peak.

Fig. 4 provides a key for molecular insights into the probe tack behavior. In Probe Tack curves, the stress peak relates to the cavitation of adhesive material under the detaching tensile force [54–56]. The major factor providing dissipation of a large amount of mechanical energy in the course of debonding of PSAs is the fibrillation of the adhesive layer that is observed by the appearance of a plateau on the stress–strain curves (Fig. 4, curve 3). Adhesive joints of solid adhesives fail predominantly via the mechanism of cavitation that is not followed by fibrillation. The typical shape of their probe tack stress–strain curves is a symmetric peak (Fig. 4, curve 1). In a probe tack experiment, the maximum stress is generally considered as a measure of tack, the value of plateau stress characterizes the cohesive strength of fibrils, and the area under the stress–strain curve corresponding to the practical work of adhesion (W_a) is related to the total amount of mechanical energy needed for adhesive bond failure, and hence is a measure of adhesive strength.

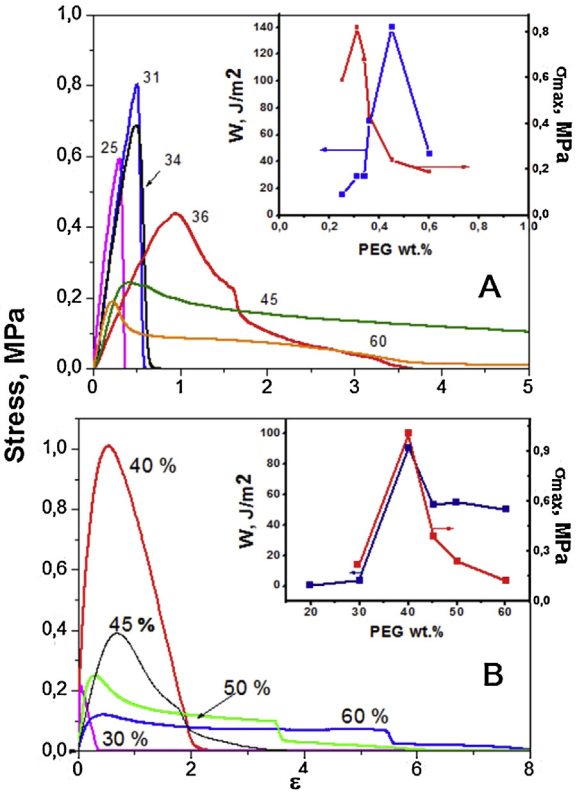

Fig. 5. Effect of PEG content on probe tack adhesion of PNVAm blends with PEG-400. The amount of absorbed water is 7 wt. %. The PEG concentrations are indicated in the Figure. Inset: Effect of blend composition on the values of the practical work of adhesion, W_a (J/m^2), and maximum stress, MPa. A: PVP–PEG blends; B: PVCL–PEG blends.

PSAs are known to possess the properties of both liquid-like and solid materials and the shape of stress–strain curves reflects this dualism [38]. In probe-tack curves, the liquid-like behavior relates to the material capability to develop very high values of maximum elongation ($\varepsilon \approx 10$–40) under a comparatively very low level of applied detaching stress (much lower than 0.1 MPa). In contrast, the solid-like behavior is evident when the debonding occurs at relatively small values of maximum elongation ($\varepsilon < 1$) provided by high values of tensile stress.

Taking into account that poly(N-vinyl caprolactam), PVCL, is a close homologue of PVP (containing respectively seven- and five-membered lactam rings in side-chains of their backbones, Fig. 1), it is logical to expect that blends of PVCL with PEG will also exhibit adhesive properties.

As follows from the data in Fig. 5, the curves for 25, 31, and 34 wt.% of PEG-400 in blends with PVP and 30% and 40% PEG in blends with PVCL are typical of solid-like PSAs, wherein the contribution of cohesive interaction energy dominates that of free volume. The debonding mechanism is adhesive when no macroscopic residue of an adhesive layer remains on the surface of a steel substrate. The transition to a more ductile type of deformation is observed for 34 wt.% of PEG in the blend with PVP and 45% in the PVCL–PEG blend. The curves for the higher PEG content in PSAs correspond to liquid adhesives and the cohesive

mechanism of debonding. The PVP–PEG blend containing 36 wt.% of PEG-400 and PVCL blend with 50% PEG demonstrate the debonding behaviors typical of PSAs when the contributions of cohesive interaction energy and free volume are properly counterbalanced. As the molecular theory of pressure-sensitive adhesion predicts [38], adhesive strength, evaluated in the terms of practical work of adhesion (area under the probe tack stress–strain curve, W_a), goes through a maxima at 45 and 40 wt.% of PEG-400 in the PVP–PEG and PVCL–PEG blends, respectively. As follows from Fig. 5, probe tack adhesion and mechanism of PVP–PEG and PVCL–PEG model PSA debonding can be easily tuned by varying the PSA composition. Note that the results of peel and probe tack tests need not be identical as in the course of an 180° peel test the major mechanism of PSA deformation is extension [54] while the probe tack testing also involves an appreciable contribution of shear [7,14,55,57–60].

Pressure sensitive adhesion is an interfacial property. When the fibrils detach from the probe (or substrate) interface rather than failing cohesively, it is described as a "clean detachment". An adhesive (clean) detachment is often preferable over having high tack energy.

3.3. Tensile properties of PVP–PEG blends

The E_c:f_v ratio also reflects such fundamental quantities of polymers as solubility parameter, glass transition temperature, or elastic modulus, G' [38]. In this connection it is of no surprise that adhesive properties of PSAs relate closely to their linear viscoelastic behaviors. This relationship is thoroughly examined and described in [51]. Here we consider the role of large tensile strain in the peel test behavior.

Because the major mode of deformation of an adhesive under high angle peeling is extension (Fig. 3), while the contribution of shear is negligible [57], it is logical to examine stress–strain curves of the model PVP–PEG adhesive blends under uniaxial extension up to fracture, and to compare the behaviors of peel force and work of deformation [38].

Fig. 6(A–C) illustrates the effect of PEG content on the stress–strain behavior to break for films formed from various of PVP–PEG blends [38,61]. In general, the stress–strain curves (Fig. 6A) resemble those of lightly crosslinked high molecular weight polymers [62]. PEG is a good plasticizer for PVP and addition of PEG results in increased elongation at break (ε_b). With increasing PEG concentration, the value of ε_b increases linearly, as shown in Fig. 6B [38,61]. For PVP blends containing <36% PEG, the ultimate tensile strength, σ_b, is comparatively high and practically unaffected by PEG content. For PEG concentrations >36%, σ_b declines rapidly with PEG content. The transition from ductile to tight deformation occurs over a fairly narrow range, between 36% and 34% PEG (Fig. 6A). This range corresponds to the transition from the fibrillar type of adhesive joint failure (36% PEG and higher) to brittle-like fracture without fibrillation [38,42].

The area under the stress–strain curve, W_b, which is the total work of viscoelastic deformation required to break the PVP–PEG adhesive blends, correlates well with both peel [39] and probe tack [42] behaviors and reveals a maximum at 36% PEG concentration for the blend demonstrating best

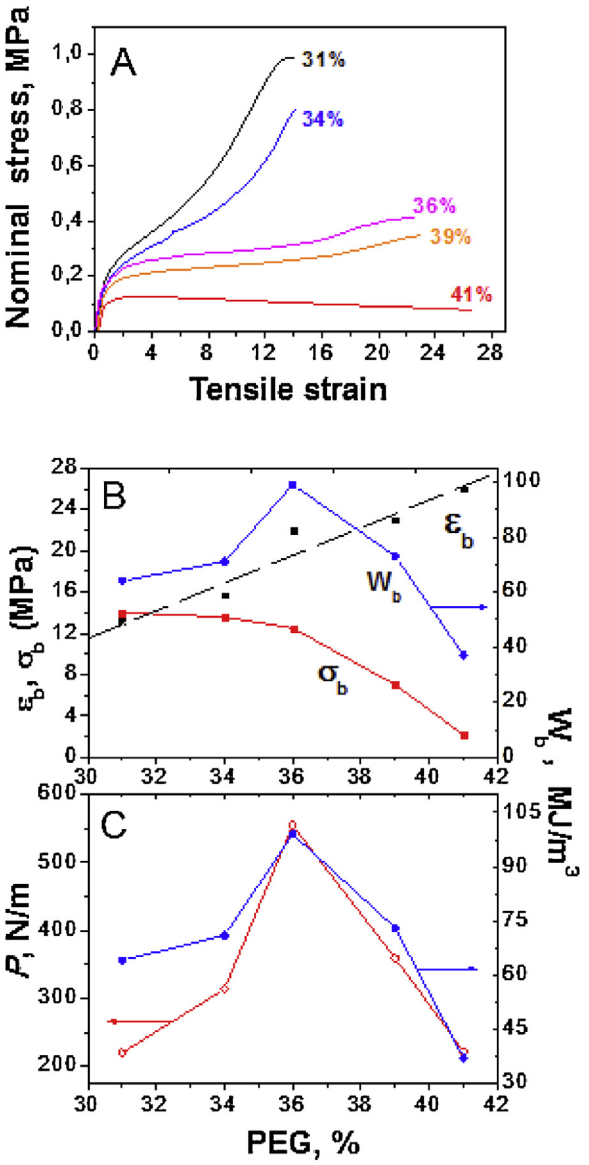

Fig. 6. Tensile properties of PVP–PEG blends as a function of PEG content. A: Tensile stress–strain curves to break the PVP–PEG blends, containing 31, 34, 36, 39, and 41 wt% PEG-400 at 8–9% degree of hydration. The drawing rate is 20 mm/min. B: Total work of viscoelastic deformation to break the PVP–PEG film, W_b, the ultimate tensile strength, σ_b and the break elongation, ε_b as a function of PEG concentration in blends. C: Effects of PVP–PEG composition on 180° peel force, P, and the work of viscoelastic deformation of the adhesive film up to break, W_b, under uniaxial extension. The peel and drawing rates are 20 mm/min.
[61], Copyright 2003. Reproduced with permission from Elsevier Ltd.

adhesion (Fig. 6C). An evident correlation between peel adhesion and work of viscoelastic deformation, illustrated in Fig. 6C, signifies the controlling contribution of viscoelastic deformation to adhesive performance [38]. In a similar manner with probe tack adhesion (Fig. 5), the tensile behavior of PVP–PEG PSA is easily controlled by the change of blend composition.

Fig. 7 illustrates the effect of PEG content on the stress–strain behavior of PVP–PEG blends under drawing

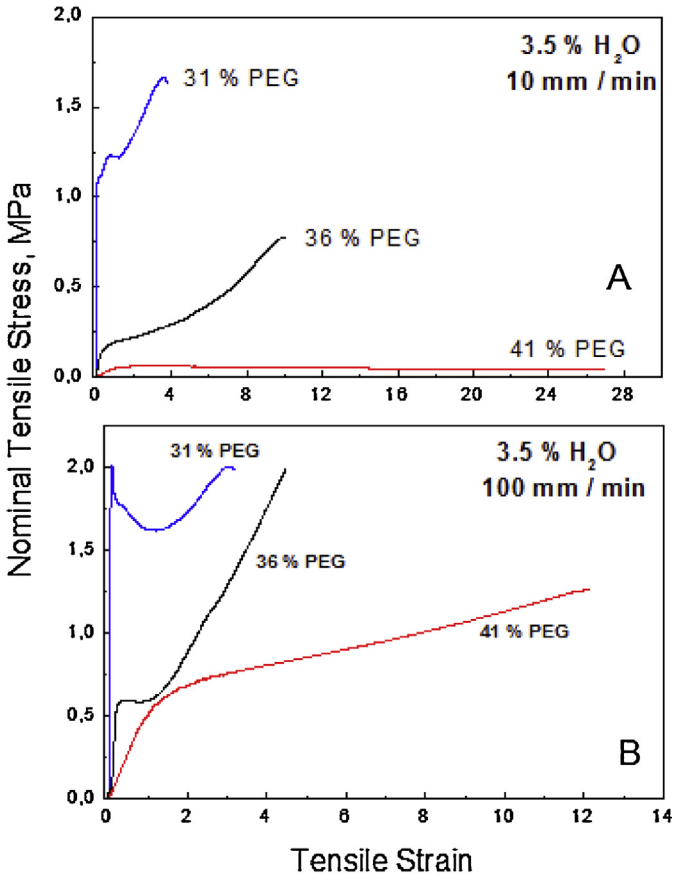

Fig. 7. Tensile stress–strain curves under uniaxial drawing to break with the rates of 10 (A) [39] and 100 (B) mm/min for PVP blends of 3.5% hydration with 31, 36 and 41 wt. % of PEG-40 [unpublished data by Novikov and Feldstein].

with extension rates of 10 and 100 mm/min [61]. With a lower drawing rate the PSA has enough time to relax in the course of uniaxial extension and the shape of the stress–strain curves is typical of rubbery polymers. Transition from elastic to brittle-like deformations occurs within a very narrow range of PVP–PEG composition. The ductile strain involving the fibrillation is typical of cohesive failure and high tack, exemplified by the blend containing 41% PEG, while the PVP blend with 36 wt.% PEG has been found to manifest the transitional type of adhesive bond fracture. In the transition point the intermolecular interaction forces within the adhesive polymer are properly counterbalanced by the force of adhesive–substrate interaction.

At higher tensile rate (Fig. 7B) the PSA no longer has time to relax in the course of stretching and behaves as a cohesively stronger adhesive. Likewise, the increase in tensile rate is equivalent to the decrease in PEG plasticizer concentration and the decrease of temperature. In this case the PVP blend with 36 wt.% PEG exhibits brittle-like fracture, whereas the blend containing 41 wt.% PEG-400 demonstrates strain-hardening and behaves as a slightly crosslinked elastomer. A tenfold increase in drawing rate affects the ductile-tight behavior of a hydrogen bonded PVP–PEG adhesive to a much greater extent than that of conventional hydrophobic adhesives (see Fig. 41 in [38]). In other words, the ductile-tight transition in the styrene–isoprene–styrene (SIS) and polyisobutylene-based adhesives is much wider than that in the PVP–PEG blends [61].

Thus, the behavior of hydrogen bonding is very dependent on the speed at which the materials are tested. H-bonds do not play the role of crosslinks if they have time to relax (slow debonding speed or slow speed of stretching) while they play the role of chemical crosslinks at high extension rates. Under slow extension the intermolecular H-bonds in PVP–PEG blends have time to rupture and reform anew at another place during deformation and do not contribute appreciably to the resistance to strain until the onset of a critical, strain hardening region, where the final rupture of H-bonded crosslinks between the PVP chains occurs. In contrast, at higher extension rates the H-bonds have insufficient time for rearrangement at new locations and behave like pseudo cross-links, which have to be ruptured in order to deform the polymer. The sharp transition from ductile to tight stretching with increased drawing rate corresponds to a well-defined rate of the rearrangement of the H-bonded network under drawing the PVP–PEG adhesive. The sharp transition between the

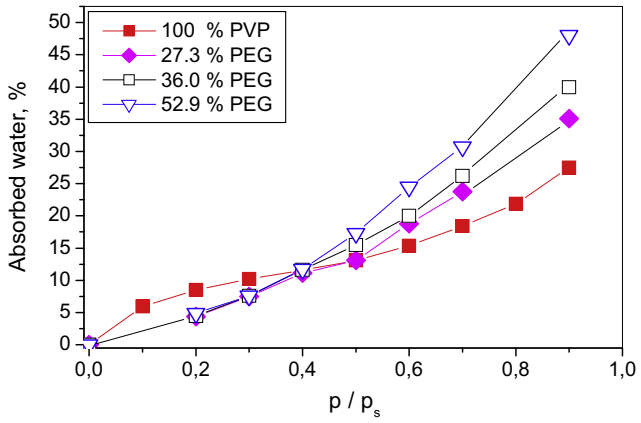

Fig. 8. Water vapor absorption isotherms for PVP and its blends with PEG-400 at ambient temperature as a function of relative humidity, p/p_s. [39], Copyright 2002. Reproduced with permission from Taylor & Francis.

ductile and tight deformation modes with the change of extension rate is observed only for H-bonded PVP–PEG system and is not typical of SIS and PIB based adhesives [38,61].

It is worth emphasizing the distinction between the PVP–PEG adhesive and a classical rubber/tackifier PSA system. Rubbers have low T_g values, that are increased by addition of tackifier while the plateau modulus is decreased. For the PVP–PEG hydrogels, the base polymer (PVP) has a high T_g. The PEG or water decrease T_g and plateau modulus simultaneously [60,62]. Although these additives produce tack, they are not acting as "tackifiers" in the classical sense because they do not increase T_g. Instead they are acting strictly as plasticizers. It is useful to make the point that PEG produces a higher deformation work (at a given T_g) than a lower molecular weight water plasticizer so that the peel force is higher [41].

Insights gained into the molecular structures responsible for pressure sensitive adhesion enable molecular design of new PSAs with optimized performance properties. The fundamental basis for molecular design has been established using PVP–PEG binary blends as a model PSA. Commonly, novel PSAs are produced by chemical synthesis or modification of initially tacky polymers. However, the data presented here show that innovative PSAs can be obtained by physical mixing of nonadhesive polymers bearing complementary functional groups that form noncovalent bonds. Adhesive and mechanical properties of PSA composites can be tuned by changing blend composition, once the function of each polymer blend component is understood. Thus, in the PVP–PEG model PSA, high MW PVP is the most important component that serves as a film forming polymer (FFP). Short chain PEG is a minor complementary component, which acts as a noncovalent crosslinker, NCC, i.e., as a curing agent. The NCC function is instrumental in forming the 3-dimensional supramolecular network structure and in enhancing the cohesive strength of the PSA. Owing to the low glass transition temperature and a telechelic structure, i.e., due to location of complementary hydroxyl groups at opposite ends of short chains (Fig. 1), PEG also acts as a plasticizer, increasing free volume and reducing T_g. Together, the PVP and PEG build up a PSA with ideally tailored performance properties.

3.4. Water absorbing properties of PVP–PEG blends

PVP is a highly hygroscopic polymer [41,63–66] and macroscopic physical properties of its blends with PEG depend on how much water vapor was absorbed. For this reason we consider first the water absorbing capacity of the PVP blends with PEG-400.

Being composed of typical hydrophilic polymers, PVP–PEG compatible blends absorb a large amount of water when exposed to water vapor at various relative humidities (RH) (Fig. 8) [39]. As a rule, the higher the PEG content, the higher the hydration, a trend that is especially prominent at higher RH. Unblended PVP is evidently an exception to this rule and a characteristic shoulder on the PVP isotherm within the lower RH region is traditionally attributed to the polymer degree of hydration, where the PVP undergoes a transition from a glassy to rubbery state [67–71]. Annealing PVP at 200 °C, followed by slow cooling with a rate lower than 1 °C min^{-1}, has been shown to cause the shoulder at the low relative water vapor pressure p/p_s to vanish but does not affect appreciably the rapid growth in water uptake in the upper RH region. This observation is attributed to the presence of the thermal history that relates to unrelaxed hole-free volume in glassy PVP. An absorbed water may accumulate within the holes [68].

The amount of absorbed water vapor, expressed as the number of water molecules absorbed in blends per one PVP unit, is plotted in Fig. 9 against the blend composition. The latter is expressed in terms of the number of PEG-400 macromolecules available in the blends per one PVP recurring unit [63]. All the plots in Fig. 9 are unequivocally linear with the intercepts relating to the number of water molecules associated with the PVP recurring unit at zero PEG concentration and with the slopes determining the average number of water molecules per PEG-400 macromolecule, [H_2O]/[PEG-400]. The degree of water binding with the PVP units, [H_2O]/[PVP], is found by subtraction of the quantity of water associated with PEG (the slope) from the total amount of absorbed water and shown to coincide exactly with the relevant intercepts. Only at RH = 20% is all the absorbed water solely associated with PVP units because the slope of this plot (Fig. 9) is zero. At higher RH

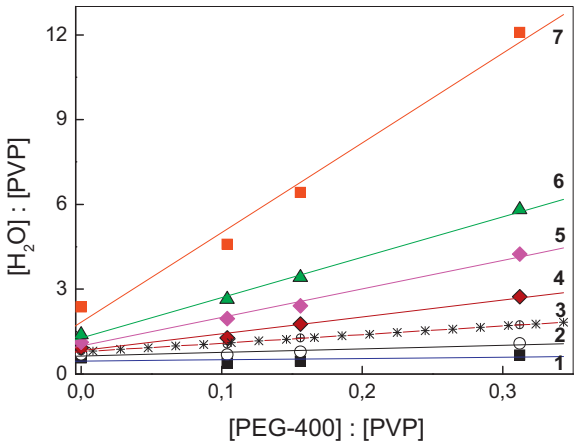

Fig. 9. The number of water molecules, absorbed in PVP–PEG blends per PVP unit, as a function of the blend composition for different values of the relative humidity (RH) at 20 °C. p/p_s = 0.2 (1), 0.3 (2), 0.4 (3), 0.5 (4), 0.6 (5), 0.7 (6) and 0.9 (7).
[63], Copyright 2000. Reproduced with permission from Elsevier Ltd.

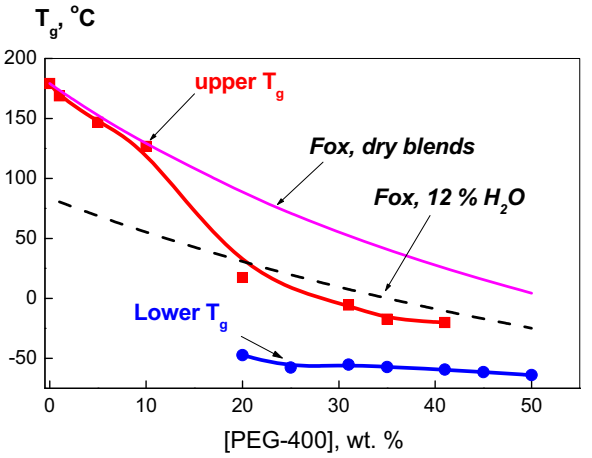

Fig. 10. Relation of T_g on composition of PVP blends containing 0–50 wt. % PEG-400.
[80], Copyright 2000. Reproduced with permission from Elsevier Ltd.

more water molecules are associated with PEG. The plot linearity provides evidence that hydrogen bonding of PEG hydroxyls to the carbonyls in PVP units proceeds directly via the water molecules located near PVP units and hence does not cause appreciable desorption of water. This conclusion also is confirmed by independent data obtained by FTIR spectroscopy in addition to quantum chemical modeling of the PVP hydrogen bonding with PEG-400 and water molecules (see Section 3.10 and Table 3 below [38,49,72]). As has been shown in this research, the most stable complexes in the PVP–PEG–H_2O system are those formed by the water molecules associated with the PVP monomer units in the first hydration shell [67,72]. Absorbed water is not a competitor but rather an assistant in the process of PVP–PEG H-bonded complex formation. In this respect the mechanism of PVP–PEG interaction in hydrogels may be treated as the binding of PEG terminal groups to hydrated PVP units. In other words, the ternary blend PVP–PEG–water may be regarded as a binary blend formed by PEG and equilibrium hydrated PVP [63].

3.5. Phase state of PVP–PEG and PVCL–PEG blends

We consider now the molecular mechanism, thermodynamics and stoichiometry of PNVAm complex formation with short chain telechelic PEG. Insight into these issues was obtained from the analysis of PNVAm–PEG phase behavior.

In many polymer systems, a homogeneous phase is obtained because of the existence of specific favorable interactions between different polymer components as the interactions allow mixing on a molecular scale. One such favorable interaction is hydrogen bonding as has been reported for many polymer blends [47,50]. Polymers containing ternary amide groups such as PVP are potentially good proton acceptors due to the basic nature of the functional groups [64,65]. At the same time, short-chain PEG carries two proton-donating hydroxyl groups at the chain ends [73] (see Fig. 1). Unlimited PVP solubility in liquid PEG is well established [45,66], and the PVP-PEG blends may be therefore treated as the solutions of high molecular weight PVP in liquid oligo(ethylene glycols).

The most unambiguous experimental evidence of polymer miscibility is the occurrence of a single glass transition temperature that is intermediate between the two T_g's corresponding to the blend components [74]. In miscible blends, the glass transition temperature generally depends on blend composition through a simple rule of mixing outlined by the Fox equation [75]. On the other hand, blends of immiscible polymers that segregate into distinct phases exhibit glass transitions identical to that of the unblended components. In the intermediate cases of partial polymer miscibility or if the size of the dispersed phase is very small, the T_g's of individual components may be shifted. The temperature shifts obscure the distinction between miscible blends and systems of partial miscibility. An elevation of the low-T_g transition temperature and a depression of the high-T_g transition in a two-phase polymer blend may indicate that the system is very close to being miscible.

Miscibility of high-MW PVP with PEG oligomers has been thoroughly studied with DSC [63,76–81] and optical microinterference [45,46] techniques. Despite the unlimited solubility of PVP in oligomers of ethylene glycol, unequivocally established with wedge optical microinterferometry, the PVP–PEG system demonstrates two distinct and mutually consistent temperatures of relaxation transitions within a certain concentration region. In DSC thermograms these relaxation transitions resemble heat capacity jumps at the glass transition temperature and in this case we use the same symbol T_g for designation of their temperatures. As is evident from the data in Fig. 10 [80], the composition dependence of the upper T_g satisfies a simple weight-average rule of mixing such as the Fox equation [75], indicating that the upper T_g-phase can be unambiguously attributed to a homogeneous PVP–PEG blend. As has been shown in the final research paper [80] of the series [63,76–81], the lower T_g unambiguously relates to some amorphous PVP–PEG interaction product

(polymer–oligomer complex) which nucleates and grows within the homogeneous upper T_g-phase.

The glass transition temperature, T_g, is one of the most fundamental parameters of polymers. The T_g directly relates to the cohesive energy and packing density [38,82,83]. The simple rule of mixing, stated by the Fox equation [75], neglects specific interactions between a polymer and a plasticizer and infers a complete uniformity of intermolecular forces. In practice, the plasticization effect often involves specific interactions or excess volume formation upon mixing a polymer and a plasticizer (solvent) so that the effect leads to negative T_g deviations. Large negative T_g deviations from the Fox equation have been observed for PVP blends with the plasticizers bearing two or more hydroxyl groups per molecule (PEG and glycerol) [78,79]. It has been found that the plasticization effect relates more to the fraction of hydroxyl groups in a blend than to the plasticizer weight fraction. Negative deviations of the blend T_g from the relationship predicted with the original form of the Fox equation were shown to be in direct proportion to the number of hydroxyl groups in plasticizer molecule [78].

Qualitatively the phase behavior of PVCL blends with PEG-400 is similar to the PVP–PEG phase behavior. However, negative deviations from the Fox equation in the PVCL blends with PEG-400 are appreciably larger, than those for the PVP–PEG system [43].

To fit the composition curve for T_g of PNVAm–PEG hydrated blends an adjustable parameter w_{*PEG} was introduced into the original form of the Fox equation [78–80]:

$$\frac{1}{T_g} = \frac{w_{PNVAm}}{T_{g_{PNVAm}}} + \frac{w_{H_2O}}{T_{g_{H_2O}}} + \frac{w_{PEG} + w_{*PEG}}{T_{g_{PEG}}} \quad (2)$$

where T_g refers to the glass transition temperatures and w to the weight fractions of PNVAm, water, and PEG, respectively.

Within the context of Eq. (2) the parameter w_{*PEG} has a clear physical meaning. It is established that the negative deviations come out only from the formation of more than one hydrogen bond (e.g., through both terminal OH groups in PEG molecule) [80]. Hence the w_{*PEG} defines the weight fraction of PEG chains that crosslink repeat units in the PNVAm chains by means of two H-bonds through both terminal OH-groups in the PEG chains.

Thus the w_{*PEG}/w_{PEG} ratio yields the average mole fraction of PEG chains crosslinking the PNVAm units by H-bonding through both terminal hydroxyls. This quantity is plotted in Fig. 11 against PVP–PEG blend composition expressed as the total number of PEG OH-groups per one PVP repeat unit.

Although the DSC data in Fig. 11A refer to the PVP–PEG blends of lower hydration (6–8%), they are in excellent agreement with the Temperature Modulated DSC (TM-DSC) results obtained for the blends of 12% hydration. This implies that the difference in blend hydration is properly accounted for by the modified Fox equation (Eq. (2)) and that the effect of water on the lower T_g behavior obeys the classical weight-average rule of mixing.

As is evident from the data in Fig. 11B, at low PEG content (20% and 25%) the w_{*PEG} fraction exceeds w_{PEG} (the total PEG content) (i.e., the w_{*PEG}/w_{PEG} ratio exceeds

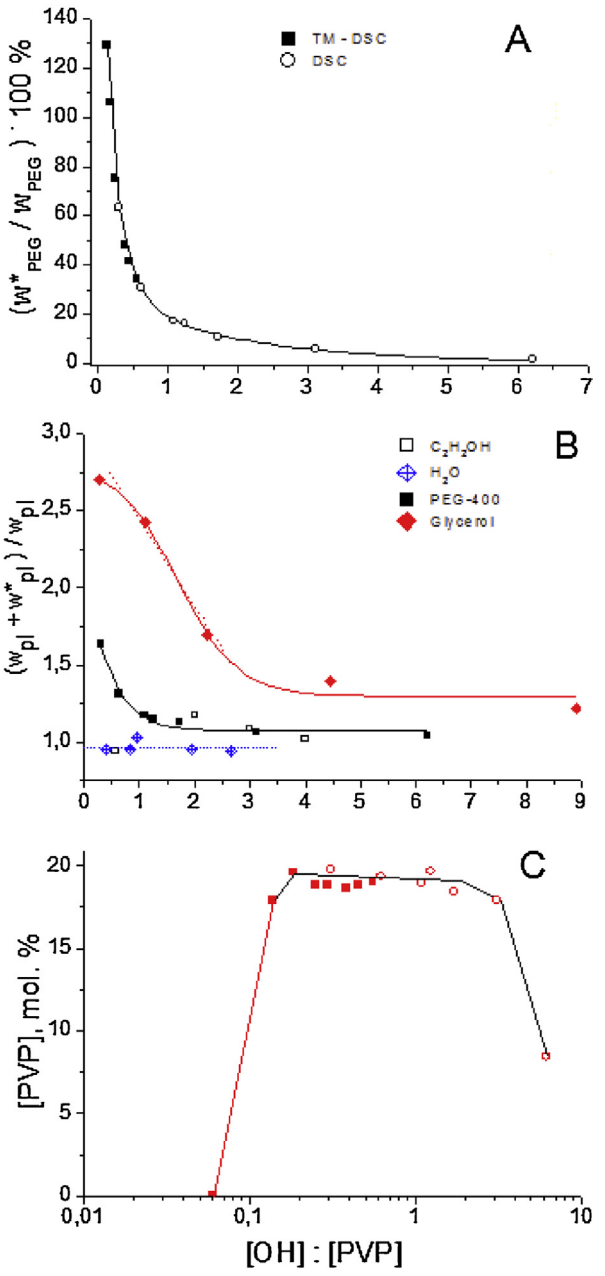

Fig. 11. Involvement of terminal hydroxyl groups in stoichiometric PVP complex formation with telechelic oligomers as a function of composition expressed in the terms of OH groups available in the blends per PVP carbonyl. A: The percentage of PEG-400 macromolecules crosslinking PVP units. Open symbols denote DSC data from reference [79], whereas solid symbols correspond to the values obtained using Temperature Modulated Differential Scanning Calorimetry (TM-DSC) technique [80]. B: The number of hydroxyl groups in a plasticizer molecule participating in hydrogen bonding with PVP units over the composition range for various noncovalent crosslinkers: ethanol, water, PEG-400 and glycerol [80]. C: The compositional behavior of the percentage of PVP repeat units crosslinked through PEG-400 chains into a hydrogen-bonded network complex. [80], Copyright 2003. Reproduced with permission from Elsevier Ltd.

100%). This seemingly unrealistic conclusion results from the fact that the T_g value indicates the presence of a certain phase formation within the polymer blend. The value, however, does not define directly the amount of formed phase. At low PEG content, the PEG chains will crosslink only some fraction of PVP macromolecules, leaving other PVP chains unoccupied. In other words, discrete nuclei of a noncovalently crosslinked PVP–PEG complex (lower T_g-phase) are formed within the continuous upper T_g-phase.

According to Eq. (2), the $(w_{PEG} + w*_{PEG})/w_{PEG}$ quantity is the number of hydroxyl groups per plasticizer (e.g., PEG) molecule involved into H-bonding with PVP. Indeed, as is obviously demonstrated in Fig. 11B [80], as the plasticizer concentration decreases in the blends, this quantity tends to unity for water and ethanol, two for PEG, and three for glycerol that contains three reactive OH groups per molecule.

3.6. Nonequimolar stoichiometry and nanostructure of PNVAm–PEG network complex

Taking the product of the total number of PEG OH-groups per PVP repeat unit ([OH]/[PVP]) and the molar fraction of PEG chains crosslinking the PNVAm units ($w*_{PEG}/w_{PEG}$), we obtain the mole percent of OH groups involved in the H-bonded cross-links. Assuming that every OH group forms an H-bond only with a single PNVAm carbonyl, this product yields the mole percent of PNVAm units noncovalently crosslinked through PEG chains, M_H^+ [80]:

$$M_H^+ = \frac{w*_{PEG}}{w_{PEG}} \cdot \frac{[OH]}{[PNVAm]} \times 100\% \quad (3)$$

M_H^+ shown in Fig. 11C is remarkably independent of PEG content within a wide composition range. This provides unambiguous evidence of the PVP–PEG network complex stoichiometry. The stoichiometric composition of the PVP–PEG network complex, derived from the concentration dependence of the lower T_g, has been found to correlate fairly reasonably with the direct results of FTIR measurements [44,48,49] as well as with the data obtained from the depression of heat of PEG melting in blends with amorphous PVP [79].

The crosslinking capability of PEG chains increases with the decrease of their length as well as with the reduction in the number of PEG hydroxyls available per one PVP repeat unit. Using this ratio, the dynamics of hydrogen bonding and crosslinking of the PVP units has been assessed in terms of the quantities outlined by Eq. (3). As one compares the variations in the state of PVP repeat units over the composition of the PVP blends with PEG-200, 300, 400, and 600, the impact of PEG chain length upon the state of PVP carbonyls becomes clear. To make the comparison more apparent, the concentration profiles of the mol% of PVP units crosslinked through PEG chains with molecular weight from 200 to 600 are presented in Fig. 12.

The content of crosslinked PVP units is nearly invariant with PEG concentration over a wide composition range for PEGs with various molecular weights, indicating the stoichiometry of hydrogen bonded network PVP–PEG complexes. Although all the PEG chains bear two reactive

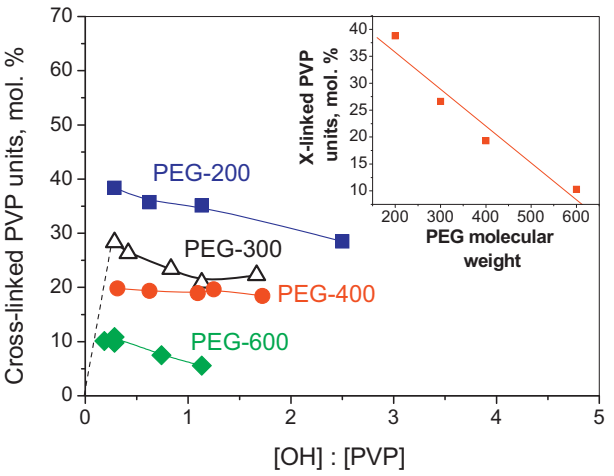

Fig. 12. Impact of PEG molecular weight on the percentage of PVP repeat units noncovalently crosslinked through PEG chains as function of PVP – PEG blend composition. Inset: The content of PVP units (in mole percent) crosslinked by PEG chains in the blend [OH]: [PVP] = 1.132, plotted against the PEG molecular weight.
[79], Copyright 2001. Reproduced with permission from Elsevier Ltd.

hydroxyl groups, their hydrogen bonding activity, assessed in terms of the $(w_{PEG} + w*_{PEG})/w_{PEG}$ ratio, is inversely related to the chain length at fixed concentration of OH groups in a blend (see the insert in Fig. 12). As the PEG molecular weight increases and approaches 1000 g/mol, the PEG ceases crosslinking the PVP units. This conclusion has been confirmed experimentally [48].

Recall that the $w*_{PEG}$ quantity is defined as the weight fraction of PEG chains that crosslink the PVP repeat units by H-bonding through both terminal hydroxyls. Then, taking into account that every PEG cross-link forms two H-bonds, the mole fraction of H-bonded network junctions is:

$$\frac{2w*_{PEG}}{MW_{PEG}} \quad (4)$$

where MW_{PEG} is the PEG molecular weight (400 g/mol). Dividing the total number of PNVAm repeat units in 1 g of PNVAm–PEG blend (w_{PNVAm}/MW_{PNVAm}) (where MW_{PNVAm} is the molecular weight of either the PVP or PVCL monomeric unit) by the mole fraction of H-bond junctions, Eq. (4) yields the average number of recurring PNVAm units between neighboring junctions:

$$\frac{w_{PNVAm} \cdot MW_{PEG}}{MW_{PNVAm} \cdot 2w*_{PEG}} \quad (5)$$

As is seen from Fig. 12, the shorter the chains of the PEG crosslinker the greater the density of the H-bonded network. In PVP blends with PEG-400 and PEG-600, respectively, approximately every 5th and 10th PVP unit is involved in crosslinking through an H-bonded PEG chain. The network supramolecular structure of the PVP complex with PEG-400 is illustrated schematically in Fig. 1.

In a recent publication, the contour lengths of PEG chains and PVP segments between neighbor crosslinks were predicted, taking into account the valence angles

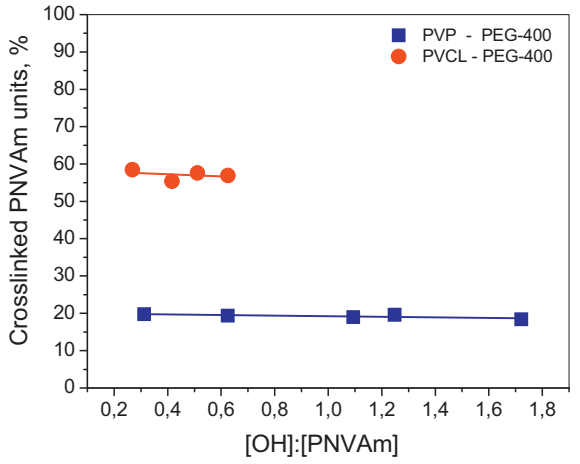

Fig. 13. The percentage of poly(N-vinyl amide) (PNVAm, i.e. PVP or PVCL) repeat units noncovalently crosslinked through PEG chains in hydrogen-bonded network complex.
[43], Copyright 2014. Reproduced with permission from the American Chemical Society.

between covalent bonds linking the atoms of the polymer backbones [84]. As has been established, the average length of PVP chain segments between neighbor crosslinks is approximately half the length of crosslinking PEG chain. For PEG-400, the contour length PEG chain is 2.5 nm, whereas the length of PVP segment in the mesh of stoichiometric network complex is 1.23 nm. The most plausible explanation to this fact is that the PVP chain is much stiffer than the PEG chain, which is appreciably bent due to its flexibility. In this connection, one can expect that the lengths of PVP chain segment and PEG crosslink in the mesh of H-bonded network are commensurable [84].

The negative T_g deviations for the PVCL–PEG blends were found to be about 25–30 °C greater than those for the PVP–PEG system at comparative contents of PEG-400 [43]. It is therefore no wonder that the content of noncovalently crosslinked PNVAm units through PEG-400 chains, shown in Fig. 13 for PVCL-PEG and PVP-PEG blends, is remarkably independent of PEG content within a wide composition range, which is direct evidence of the nonequimolar stoichiometry of the PVP and PVCL complexes with PEG-400. At the same time, approximately 60% of the PVCL monomer units form a H-bonded network junctions with PEG-400, while in PVP–PEG blends the amount of noncovalently crosslinked polymer repeat units is only about 20% (Figs. 11C and 12), i.e., three times lower than in PVCL–PEG blends (see Fig. 13, [43]).

It follows that the PEG chain length is one of the factors that controls the nonequimolar stoichiometry of PNVAm–PEG network complexes. Hydrogen bonding of PEG terminal hydroxyls to the PNVAm carbonyls leads to a gain in enthalpy as a result of complex formation and loss in entropy due to reduced conformational and translational freedom of the PEG chains. Unblended PVP or PVCL are in a glassy state and their segmental mobility is essentially frozen. As illustrated in Fig. 1, telechelic PEG chains act as spacers between longer PNVAm chains that increase the free volume and molecular mobility of PNVAm segments between neighboring H-bonded network junctions. The longer the crosslinking PEG chains, the greater is the loss in entropy due to fixation of conformation and limitation of PEG chain translational mobility. To enable PNVAm–PEG network complex formation a compensating mechanism is needed, counterbalancing the loss in entropy of PEG cross-links. This mechanism can be provided by the increase in molecular mobility of PVPNVAm chain segments between two neighboring H-bonded network junctions. The longer the crosslinking PEG chains, the longer the mobile PNVAm chain segments and the sparser the H-bonded network. When the entire PNVAm chain has already achieved sufficient mobility in the meshes of the flexible H-bonded PNVAm–PEG network (Fig. 1), the compensating mechanism does not exist any longer and the network PNVAm–PEG complex has reached its nonequimolar stoichiometry. In this way, the entropy loss compensating mechanism governs the noncooperative polymer–oligomer network complex formation [84]. While the stoichiometry of low molecular weight compounds is determined by their valency, the stoichiometry of interpolymer complexes is defined by entropic contributions to the free energy of the complex formation.

3.7. Molecular mechanism of the PNVAm–PEG interaction and mixing throughout the entire composition range

Knowledge of the $w*_{PEG}$ quantity makes it feasible to estimate many useful characteristics of the PNVAm–PEG complex network structures and the PNVAm–PEG mixing process. The critical molecular weight of a PVP chain segment (M_c; g/mol) in the mesh size of H-bonded network can be estimated as:

$$M_c = \frac{w_{PVP} \cdot MW_{PEG}}{2w*_{PEG}} \tag{6}$$

Here M_c is connected to the H-bond network density via the following equation:

$$\frac{\nu_H}{V_o} = \frac{\rho}{M_c} = \frac{2w*_{PEG} \cdot \rho}{w_{PVP} \cdot MW_{PEG}} \quad (mol/cm^3) \tag{7}$$

where ρ is the polymer blend density (g/cm^3), ν_H is the number of H-bonded junctions per molar volume of PVP–PEG complex, V_o. The blend density ρ can be evaluated as:

$$\frac{1}{\rho} = \frac{w_{PVP}}{\rho_{PVP}} + \frac{w_{PEG}}{\rho_{PEG}} + \frac{w_{H_2O}}{\rho_{H_2O}} \tag{8}$$

where $\rho_{PVP} = 1.25$, $\rho_{PEG} = 1.125$, and $\rho_{water} = 1.0$ g/cm^3, respectively.

The equilibrium constant of PNVAm–PEG stoichiometric complex formation, K_H^+ (mol/g), can be calculated following Eq. (9):

$$K_H^+ = \frac{2w*_{PEG}}{(2w_{PEG} - w*_{PEG}) \cdot ((w_{PVP}/MW_{PVP}) - (2w*_{PEG}/MW_{PEG}))} \tag{9}$$

Since both PVP and PVCL are soluble in PEG, their blends can be treated as solutions in PEG. The equilibrium between

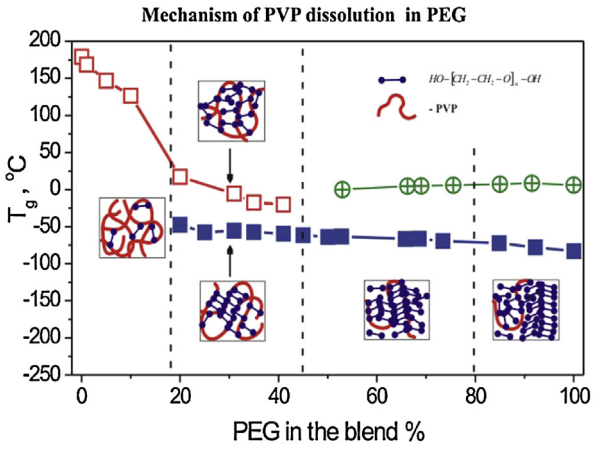

Fig. 14. Schematic representation of the scenario of PVP dissolution in liquid PEG along with the upper and lower T_g data (open and solid squares) and melting transition temperature for PEG (circles with cross). [80], Copyright 2003. Reproduced with permission from Elsevier Ltd.

crosslinked PNVAm units and those free of crosslinking may be evaluated in terms of the dissociation degree (α):

$$\frac{\alpha^2}{1-\alpha} = \frac{MW_{PEG}}{K_H^+ \cdot 2w_{*PEG}} \quad (10)$$

The term ($2w_{*PEG}/MW_{PEG}$) is the mole fraction of PEG OH-groups involved into H-bonding and crosslinking the PNVAm units per 1 g of the blend; the ratio is equal to the mole fraction of crosslinked PVP units.

Knowing the equilibrium constant of the complex formation, the free energy change corresponding to this process can be calculated through the van't Hoff equation:

$$\Delta G_H^+ = -RT \ln K_H^+ \quad (11)$$

The network density (Eq. (7)) and the critical molecular weight of PVP segment between neighboring junctions of H-bonded network (Eq. (6)) remain independent of the PEG concentration within a wide composition range (20–80% of PEG-400), just as the degree of crosslinking remains independent of the same factor (Figs. 11C and 12). The average length of the PVP chain segments between neighboring H-junctions is about 5–6 PVP units, whereas the corresponding length of the PEG chain between cross-links is up to 9–10 oxyethylene units (400 g/mol). The network is fully formed at 25% of PEG content in the blend and reveals no signs of swelling or breakdown up to 80% of PEG concentration. The network formation and failure occurs in narrow ranges of composition. It follows that the nature of the crosslinked complex is cooperative.

Large K_H^+ values correspond to the large negative ΔG_H^+ magnitudes. The PVP–PEG complex formation is an exothermic process. The gain in energy is greater at the first stage of PVP plasticization due to hydrogen bonding with PEG (w_{PEG} = 0.2–0.45) than at the subsequent stages of the PVP–PEG complex mixing with PEG, followed by the swelling of the H-bonded network and dissolution of disengaged PVP macromolecules in excess PEG (Figs. 11C and 14) [80]. In turn, the gain in energy is greater for the PVCL–PEG stoichiometric complex formation than in the course of PVP bonding with PEG. Taking into consideration that the contributions of hydrogen bonding between PNVAm and PEG molecules are approximately the same for PVP and PVCL polymers [43], it is logical to suppose that the PVCL–PEG complex is more energetically favorable on account of hydrophobic interactions. Due to greater density of the noncovalent network (Fig. 13), the mechanical properties and adhesion of the PVCL–PEG hydrogel are much less sensitive to the polymer molecular weight than for the PVP–PEG system.

Fig. 14 and Table 2 summarize the understanding of the mechanism of glassy PVP dissolution in liquid PEG outlined by the data presented in Figs. 11–13 [80]. At low PEG concentrations (0–20%), PVP plasticization occurs. However, as the PEG content reaches 20%, the PVP gel crosslinked by H-bonding with PEG chains begins to form, a process which is manifested by the occurrence of the second relaxation transition. The stoichiometric complex involves 18–19% of PVP units crosslinked by PEG terminal hydroxyls (via H-bonding) and requires about 14 OH-groups of PEG per 100 PVP units (26 wt.% of PEG-400 in blends) (Table 2).

It is well known from the literature that polymer crosslinking usually causes T_g to increase [85,86]. Nevertheless, in PNVAm–PEG systems, as PVP or PVCL chains become crosslinked by means of PEG, T_g gets appreciably reduced compared to uncrosslinked PNVAm (Figs. 10 and 13). This apparently anomalous behavior of the PNVAm–PEG blends has also been shown to be due to the appreciable length and flexibility of PEG chains that couple the properties of the H-bonding crosslinker and spacer [44,63,76,77,80,87]. By creating space between longer PNVAm macromolecules the PEG chains increase the free volume and, eventually, the molecular mobility of the PNVAm chain segments between neighboring H-bonded network junctions [84,88–90]. In addition to crosslinking of PNVAm units, PEG chains behave also as a cohesive strength enhancer [61]. It is the combination of the features of both cohesive strength and free volume enhancers that make the short chain PEG responsible for pressure-sensitive adhesion.

As follows from the data in Fig. 11A, if the PEG concentration increases the involvement of its chains in crosslinking the PNVAm units is reduced. As the amount of crosslinked monomer units in the PVP chains achieves its stoichiometric value (19% for PVP), the upper T_g vanishes. This occurs within the range of PEG concentrations between 41% and 50% (Figs. 10 and 14). As PEG is mixed with the complex in excessive amounts, a crystalline PEG phase appears below its melting temperature T_m (Fig. 11A and Table 2). If PVP solutions are relatively dilute, containing 80–90% of solvent (PEG-400), the PVP–PEG H-bonded network is thought to swell (Figs. 11C and 14). The concentration region where the PEG content is more than 90% corresponds to PVP dissolved in PEG-400 [80].

3.8. Comparison of the T_g analysis data with the results of independent measurements

DSC scans characterize heat capacity as a function of temperature. In turn, the heat capacity is a measure of molecular mobility that relates to the energy of

Table 2
Phase state of the PVP – PEG system and underlying molecular mechanisms corresponding to different stages of the dissolution of glassy PVP in liquid PEG [80].

% PEG	$\frac{[OH]_{PEG}}{[PVP]}$	Stage of Spontaneous PVP–PEG Mixing	Composition	Phase state
0–10	0–0.06	1. Homogeneous PVP–PEG mixing	Homogeneous PVP–PEG mixture	Single amorphous phase with T_g obeying the Fox rule of mixing for dry blends + water in vapour state.
10–20	0.06–0.14		Homogeneous PVP–PEG–water mixture	Single amorphous phase with T_g obeying the Fox rule of mixing for hydrated blends
20–35	0.14–0.3	2. Stoichiometric PVP–PEG H-bond complex formation within homogeneous PVP–PEG mixture	Homogeneous PVP–PEG mixture + Stoichiometric complex	Two amorphous phases with different composition–dependent T_g's
35–41	0.3–0.39		Stoichiometric PVP–PEG complex + homogeneous PVP–PEG mixture	Two amorphous phases with different composition-dependent T_g's; Presumably phase inversion
45–80	0.46–2.22	3. Dissolution of PVP–PEG stoichiometric complex in excess PEG	Mixing the stoichiometric PVP–PEG complex with excess PEG: PVP–PEG complex + PEG	Single amorphous phase (above PEG T_m); Amorphous–crystalline phase separation (below PEG T_m)
80–90	2.22–5.0		H-bonded network failure and gradual disengagement of PVP chains from the *stoichiometric complex*: PVP–PEG complex + PVP–PEG mixture	
>90	>5.0		PVP solution in PEG	

Reproduced with permission from Feldstein M.M., Roos A., Chevallier C., Creton C., Dormidontova E.E., Polymer, 44(6) (2003) 1819–1834 [80]. Copyright 2000, Elsevier Ltd.

cohesive interaction and free volume. Traditionally, molecular mobility of macromolecules is evaluated in terms of self-diffusion coefficients. These quantities have been measured for the PVP–PEG systems by a Pulsed Field Gradient NMR (PFG NMR) technique as a function of the composition, hydration, molecular weights of the components involved, and temperature [88,89]. The composition profiles of the activation energy for PEG-400 self-diffusion in the blends with high molecular weight PVP (E_A) and the energy of crosslinking PVP units (ΔG_H^+) were compared. At the stage of crosslinked complex formation ($w_{PEG} < 0.4$), the PVP–PEG interaction is especially strong, and the E_A curve reveals an abrupt increase (with a decrease in PEG content). It follows that the PEG loses its diffusivity due to its involvement with the crosslinked PVP–PEG complex (see Fig. 1). When the complex is mixed with unbound PEG that is capable of crystallizing below T_m ($w_{PEG} = 0.4–0.8$, Fig. 14 and Table 2), the equilibrium constant of PVP crosslinking is reduced and the strength of PVP–PEG interaction becomes weaker. Correspondingly, E_A decreases at this stage. When the PEG concentration achieves 70–80%, the failure of the PVP–PEG network complex occurs (Figs. 11C and 14) due to the corresponding decrease of crosslinking energy. Within this concentration range, the complex dissociates, and the activation energy for PEG self-diffusion matches closely the value found for bulk PEG-400 ($E_A = 38$ kJ/mol). This indicates that PEG interaction with PVP provides no obstacles for PEG diffusion in the diluted polymer solutions containing more than 70% of the solvent (PEG-400). Thus, the composition profile of short-chain PEG diffusivity in blends with PVP (evaluated with the PFG NMR method) follows the pattern of free energy of PVP H-bond crosslinking; the pattern was obtained from the analysis of deviations of the lower T_g from weight-average values using the modified Fox Eq. (2) [80].

It has also been shown by wedge interferometry that diffusion of short chain PEG in the blends overloaded with low molecular weight PVP is restricted by a kind of entanglement process which resembles chain reptation [47]. Since the chain reptation is thought to be a rather atypical mode of diffusion for such a highly flexible and short macromolecules as oligomeric PEG-400, the observed effect has been explained by the process of PEG chain engagement into H-bonded network formed in the PVP–PEG blends.

Both heat capacity and diffusivity are microscopic properties of PVP–PEG blends. The macroscopic properties, such as rubber-like viscoelasticity [90] and pressure sensitive character of adhesion [38], involve numerous processes acting on the molecular level. It comes therefore as no surprise that evident correlations have been established between the mechanism of PVP–PEG interaction discussed above and the composition dependence of viscoelastic and adhesive properties of the PVP–PEG blends.

The PVP–PEG system is plausibly among the first and most illustrative examples of miscible single-phase polymer blends, which reveal two distinct glass transition temperatures with a consistent compositional behavior. As is shown in Fig. 11C and 14, the behavior of the upper T_g

in the PVP–PEG blends obeys the well-known Fox equation, indicating homogeneous PVP–PEG mixing or glassy PVP dissolution in liquid PEG. At the same time, the lower T_g is due to the formation of a hydrogen bonded PVP–PEG network complex (gel), which behaves like a new chemical entity.

Nevertheless, the PVP–PEG blend is not a unique single-phase polymer system displaying two heat capacity jumps, resembling glass transitions, in DSC thermograms. A similar behavior has also been observed for such single-phase systems as partially denaturated proteins and polypeptides. In this case a low-temperature relaxation transition is generally treated as a glass transition, whereas the high-temperature heat capacity jump refers to the processes of thermal denaturation and α-helix-coil transition [91–97]. In both cases, the existence of two relaxation transitions may be attributed to the occurrence of highly ordered supramolecular structures, exhibiting disparate relaxation properties which result from hydrogen bonding. Relaxation properties of PVP–PEG PSAs and their relation to adhesion are described in a series of recent publications [98–102] and briefly discussed in the review [38].

3.9. Energy of intermolecular H-bonding and free volume in PVP–PEG PSAs

As Eq. (1) has shown, the factor responsible for pressure sensitive adhesion at a molecular level is specific balance between sufficiently strong intermolecular cohesion energy (ΔE_c) and large free volume (unoccupated space between neighboring macromolecules). With the ΔE_c and free volume behaviors in model PVP–PEG PSA's properly characterized, we can answer key questions: What values of free volume are responsible for high adhesion in the PVP–PEG blends? The answer to this question is of fundamental significance since it establishes direct correlations between nanoscopic and macroscopic properties of PSA material.

Mechanisms of intermolecular interactions in the system PVP–PEG–water have been studied by FTIR spectroscopy [38,44,48,49,87], which provides unambiguous identification of interacting functional groups in complementary macromolecules. Formation of hydrogen bonds between functional groups is manifested in IR spectra by a shift of their characteristic frequencies toward lower wavenumbers. IR absorption bands of the carbonyl bond in the amide group of PVP are observed in the region 1720–1650 cm^{-1}, and the bands of hydroxyl groups at the ends of PEG short chains fall within the range 3600–3200 cm^{-1}.

Mixing dehydrated PVP with PEG-400 results in a shift of the band related to PVP carbonyl group stretching vibrations from 1679 to 1655 cm^{-1}, and a corresponding shift of PEG terminal hydroxyl vibrations from 3455 to 3332 cm^{-1} [38,44,48,49,87]. These results are indicative of strong H-bond formation between these groups. For PVP containing 6–7 wt.% absorbed water, the carbonyl group vibration band lies at 1661 cm^{-1}, indicating association of PVP carbonyl groups with water [49]. Under these conditions mixing PVP with PEG-400 shifts the band related to PVP carbonyl group stretching vibrations from 1679 to 1655 cm^{-1}, and that of PEG terminal hydroxyls vibrations from 3455 to 3332 cm^{-1}.

WAXS studies have shown that the binary PVP–PEG400 system reveals reorientation of PEG chains, with terminal PEG hydroxyl groups becoming no longer self associated or bound with the oxyethylene units of neighboring chains [48,79]. The differential FTIR spectrum of the PVP–PEG blend in the region of PVP carbonyl group stretching vibration demonstrates bands at 1716, 1680, and 1650 cm^{-1}, which can be assigned to PVP carbonyls that are free, loosely bound, and strongly bound with PEG OH groups, respectively [47,86]. The loosely bound mode at 1680 cm^{-1} most likely relates to PEG chains forming single H-bonds with PVP carbonyl groups through one terminal hydroxyl group. The strongly bound mode at 1650 cm^{-1} corresponds to H-bonds formed by PEG chains through both terminal OH groups.

To evaluate the competition in hydrogen bonding between reactive functional groups of PVP and PEG in blends containing absorbed water, based on data from FTIR spectroscopy, the energies of formation of different types of hydrogen bonded structures that exist in the blends should be taken into account. For this purpose, quantum chemical calculations of energy of formation for more than 110 complexes of various types have been performed. Relevant results of the calculations are presented in Table 3 and are arranged in order of diminishing magnitudes of the complex formation energy [49]. According to the calculations, the strength of hydrogen bonded complexes in PVP–PEG–H_2O system diminishes in the order: PVP–H_2O–PEG–H_2O–PVP ($-\Delta E_c$ = 79.4 kJ/mol) > PVP–H_2O–PEG–PVP (78.9 kJ/mol) ≫ PVP–H_2O–PEG (50.1 kJ/mol) ≫ PVP–PEG–PVP (33.7 kJ/mol) > PVP–H_2O (26.4 kJ/mol) > PEG self-association through terminal OH-groups (24.6 kJ/mol) > PEG–H_2O (20.4 kJ/mol) > PVP–PEG (20.3 kJ/mol). As is obvious from these data, the most stable complexes in the PVP–PEG–H_2O system are formed owing to the participation of water molecules associated with the PVP monomer units in the first hydration shell [49]. Absorbed water is not a competitor, but rather assists in the process of PVP–PEG H-bonded complex formation. The formation energies of PVP–PEG–H_2O complexes underlie the cohesive strength of PVP–PEG model PSA at the molecular level.

Positron annihilation lifetime spectroscopy (PALS) has been employed to characterize the size and content of subnanoscopic free volume in a model PSA based on a stoichiometric hydrogen-bonded network complex of PVP and oligomeric PEG [84]. The size and number density of free volume domains in the PVP–PEG blends were determined as functions of blend composition and relative humidity of the surrounding atmosphere, which controls the amount of absorbed water.

Both PEG-400 and absorbed water are good PVP plasticizers. Interestingly, while an increase in PEG concentration increases the free volume radius and fraction, absorbed water leads to the increase in number density of free volume holes, having no effect on the size of free volume cavities. The depth profile of free volume radius in the

Table 3
Schematic structures and the energies of formation of hydrogen-bonded complexes in the system PVP–PEG–H_2O [38].

Complex	Schematic structure	$-\Delta E$ (kJ/mol)
PVP-H_2O–PEG-H_2O–PVP	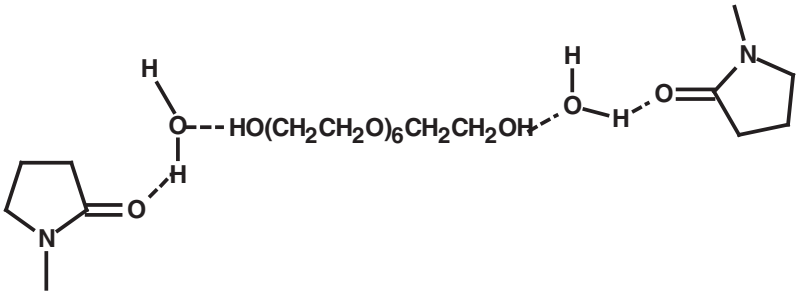	79.4
PVP–PEG-H_2O–PVP	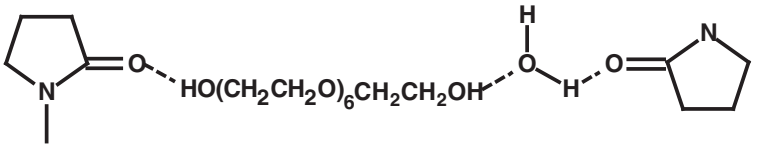	78.9
PVP-H_2O–PEG	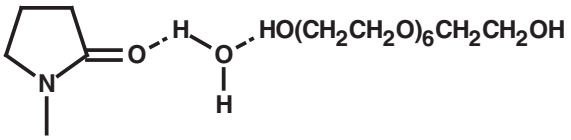	50.1
PVP–PEG–PVP	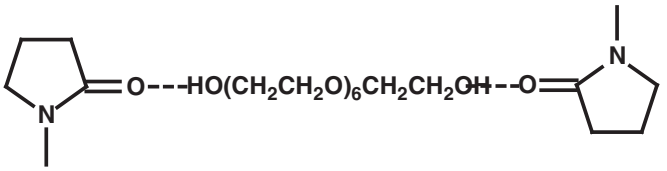	33.7
PVP-H_2O	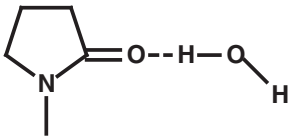	26.4
PEG–PEG	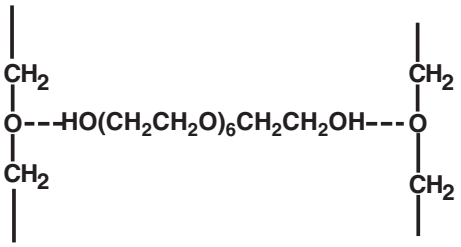	24.6
PEG-H_2O	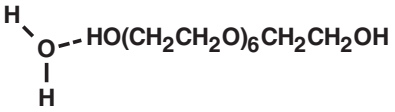	20.4
PVP–PEG	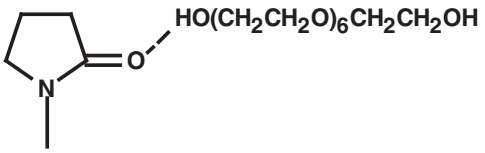	20.3

Reproduced with permission from Feldstein M.M., Siegel R.A., Journal of Polymer Science, Part B: Polymer Physics 50 (2012) 739–772. Copyright 2012, Wiley Periodicals, Inc.

PVP–PEG-400 PSA demonstrates excess free volume near the surface of the adhesive film (~3.25 Å at ~20 nm into the film) compared with the bulk (3.08 Å at 1.4 μm and beyond). Excess free volume at the surface facilitates substrate wetting by the PSA polymer under slight bonding pressure, as shear deformation dominates. On the other hand residual free volume in the bulk facilitates dissipation of mechanical energy under a detaching force, during which the PSA polymer exhibits large tensile strain and fibrillation. Thus, the depth profile of free volume radius in the PVP–PEG model PSA promotes its pressure sensitive adhesion.

The strongest adhesion is observed at 6.3–7.0% free volume content and free volume radius varying between 2.95 and 3.08 Å [84]. In probe tack curves, if the contribution of interfacial adhesive–substrate interaction dominates that of cohesive strength of PSA material, then the radius and the relative fraction of free volume govern the value of maximum elongation. Finally, in tensile stress-strain curves the size and relative fraction of free volume relate linearly to the maximum elongation to break in the PSA's, whereas both the ultimate tensile strength and elasticity modulus vary inversely with free volume, as these quantities are determined by cohesive strength [38,84]. Free volume fraction is more important than free volume hole size in controlling the tensile and adhesive properties of PVP–PEG PSA's. Thus, the presented research bridges the gap between molecular structure at the nanoscopic level and macroscopic physical properties of PVP–PEG model PSA's.

3.10. "Smart" thermoswitchable PSA based on hydrophilic polymer possessing Lower Critical Solution Temperature in water

Despite evident progress in adhesion technology over the last few decades, it remains challenging to produce materials that are sticky on demand. Recent efforts in developing reversibly switchable adhesives that exhibit the ability to trigger adhesion in response to environmental stimuli – pH, solvent, temperature, mechanics and electromagnetic field – are reviewed in a feature article by Kamperman and Synytska [105]. Polymers which demonstrate low critical solution temperature (LCST) behavior in an aqueous environment, including polyacrylamides, polyvinylcaprolactone, polyethyleneglycols, and polypeptides [106], have been employed to design reversibly switchable adhesives. In this case, the reversible formation of hydrogen bonds is responsible for switching. At room temperature, for example, polyacrylamide chains form hydrogen bonds with surrounding water molecules and adhesion is poor. As the hydrogen bonding becomes weaker with increased temperature while hydrophobic interactions persist through 37–50 °C temperature range, such polymers lose their solubility in water at the LCST. Thus, increasing the temperature induces a phase transition (LCST) and leads to a change in adhesion [107].

Since the PVP is a much more hydrophilic polymer than PVCL, the former exhibits a LCST around 170 °C that was evaluated theoretically from the temperature

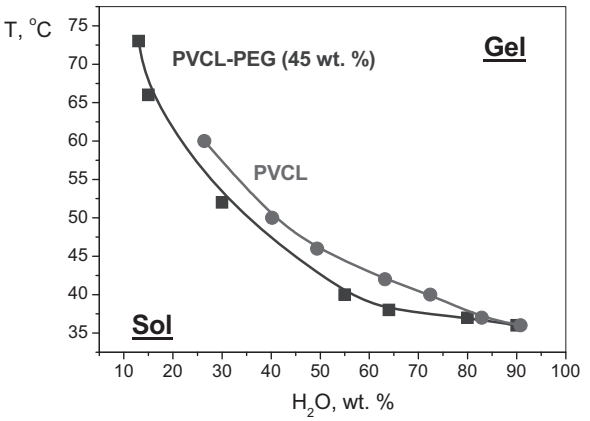

Fig. 15. The effects of temperature and the content of absorbed water on the cloud point behavior of PVCL and its blend with 45 wt. % PEG-400. [43], Copyright 2014. Reproduced with permission from the American Chemical Society.

relationship of PVP swelling degree in water [108,109] and confirmed experimentally. The PVCL demonstrates a LCST and becomes insoluble in water in the vicinity of 37–40 °C [110–116]. In our recent research [43] we analyzed the influence of the LCST on the adhesive properties of the PVCL–PEG composites.

As follows from the comparison of the equilibrium constants and dissociation degree behaviors of the PVP–PEG and PVCL–PEG complexes, calculated using Eqs. (9) and (10), the PVCL–PEG H-bonded complexes are characterized by much greater stability, a higher density noncovalent network and a higher complexation constant. These data are in good agreement with the results by Kirsh et al. on hydrogen bonding of phenols to PVP and PVCL [117].

The effects of temperature and solution composition on the cloud point behavior in PVCL–water and PVCL–PEG–water system are demonstrated in Fig. 15. The shape of the curve for the binary PVCL–water system is in good agreement with the literature data of Meeussen et al. [110]. The LCST is observed at 36 °C and its position is shifted toward dilute solutions (10 wt.% of polymer). The LCST is slightly higher than the value reported by Meeussen et al. (~30 °C) for a somewhat similar molecular weight polymer, but agrees perfectly with the data by Kirsh, measured for the same HMW PVCL sample [108]. With an increase of PVCL concentration the cloud point temperature climbs smoothly, achieving 60 °C at 26 wt.% of water in polymer.

In general, the behavior of ternary PVCL–PEG (45 wt.%)–water system follows the pattern shown by the PVCL solution in water. At high water content (80–90%) the curves are practically superimposed. This behavior is expected, because at such high concentrations of water it forms H-bonds with both polymer (PVCL) and oligomeric crosslinker (PEG), so the formation of a stoichiometric PVCL–PEG complex can hardly be possible. At higher PVCL concentrations the curves become parallel to each other, with the polymer–oligomer complex curve running 3–5 °C below that of pure PVCL (Fig. 15).

In the connection with reported phase behavior the question arises: how does the LCST affect the adhesion

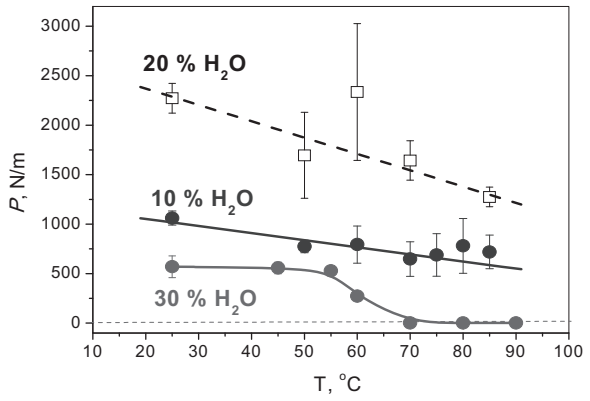

Fig. 16. Temperature dependence of the 180° peel adhesion force for PVCL–PEG (45 wt. %) hydrogels containing 10, 20 and 30 wt. % of absorbed water. Peel rate is 10 cm/min.
[43], Copyright 2014. Reproduced with permission from the American Chemical Society.

behavior of PVCL–PEG hydrogels in the course of their swelling (upon water addition) and temperature elevation? To answer this question we performed 180° Peel Tests, which enabled the control of water content captured by the hydrogel in the course of heating if a water impermeable film is employed as a substrate.

The effects of temperature and the amount of absorbed water on the 180° Peel Adhesion of the HMW PVCL with 45 wt.% PEG-400 are illustrated in Fig. 16. As follows from these data, in the temperature range from 20 to 90 °C the PVCL–PEG hydrogels containing 10 and 20 wt.% of water exhibit gradual reduction of adhesion with an increase in temperature. In contrast to this behavior, the hydrogels containing 30 wt.% of water and more demonstrate the loss of adhesion in rather narrow temperature ranges. Thus, the PVCL blend with 45 wt.% of PEG-400, containing 30 wt.% of absorbed water, loses its adhesion sharply between 55 and 70 °C. The higher the content of absorbed water, the lower the temperature of spontaneous detachment of the adhesive film. Thus the temperature behavior of adhesion in the PVCL–PEG hydrogels correlates fairly reasonably with the temperature dependence of the cloud point, as shown in Fig. 15 [43].

The temperature transitions of the mixing–demixing behavior and the change of adhesion, presented in Figs. 15 and 16, respectively, are fully reversible. As an opaque detached adhesive film is removed from warm aqueous solution, it becomes transparent and tacky within 1–1.5 min as the result of both cooling and partial evaporation of absorbed water. The fact that the PVCL–PEG-400 blends containing 10 and 20 wt.% of water demonstrate only a smooth decrease of adhesion with increasing temperature implies that the amount of absorbed water in these hydrogels is too low to inhibit adhesion [43]. The absolute values of peel force in Fig. 16 are extremely high, ranging from 2280 to 570 N/m at 20 °C. The PVCL–PEG network is much denser than the PVP–PEG one, resulting in stronger adhesion.

The comparison of PVP–PEG and PVCL–PEG stoichiometric complexes shows that their remarkable adhesive properties is a common feature of the whole class of polyvinyl lactam or even polyvinylamide polymers. One of the arguments against their application is the difficulty to control the material humidity, which would affect the adhesive and mechanical properties of these materials. Still, there are numerous scientific reports on consistent and reproducible PVP behavior obtained in different laboratories around the world with various natural humidity levels. The fact is that the normal range of weight percent of water tightly bonded (via hydrogen bonding) with PVP is rather wide: 4–12%. Thus this water can be considered as a natural intrinsic component of any PVP-containing system which mediates interactions of PVP with other substances. This is the reason for the consistent behavior and solid performance of PVP- and PVCL-containing systems obtained under different natural humidity conditions. Thus, we believe that adhesives based on PVP–PEG and PVCL–PEG complexes have a great potential to become an important part of hydrophilic water-absorbing adhesive materials worldwide.

3.11. Pharmaceutical application of PVP–PEG adhesive

Eq. (1) establishes the direct relationship between adhesion and diffusion transport properties of PSAs. High diffusivity of PSAs favors their strong adhesion and makes them useful as diffusion matrices in transdermal drug delivery systems (TDS). TDS have found increasing applications in pharmacy for controlled delivery of drugs into systemic blood circulation across intact skin with predetermined release rate. In addition, both components of the PVP–PEG PSA have been approved for medical applications and are generally regarded as safe. For these reasons, the PVP–PEG PSA was originally designed as adhesive platform for transdermal drug delivery. Currently five transdermal patches based on the PVP–PEG PSA with nitroglycerin, isosorbide dinitrate (ISDN), clonidine, cytisine and phenazepam, known as Nitropercuten, Nisopercuten, Clopercuten, Cypercuten and Phenapercuten, respectively, have been approved for medical applications in Russia following their successful large scale clinical trials. The PVP–PEG PSA has been also employed as adhesive platform in a topical antimycotic drug plaster with chinosol. The latter is approved for treatment of onychomycosis in Russia as Chinasive.

Concerns have been usually voiced of whether the high hydrophilicity and sensitivity of adhesion and mechanical properties of the PVP–PEG blends to absorbed water makes this PSA a sufficiently stable product. In this connection it should be noted that the state of absorbed water in PVP–PEG blends was studied extensively with DSC [62], FTIR [47,48,66,71,86], NMR [87,88,103], PALS [83], DMA [60,89], and other techniques [41–44,46,67]. As is obvious from these data, the absorbed water is tightly bound to PVP recurring units until the total amount of water in blends reaches 20 wt.% [66,103]. As has been clearly demonstrated by the experimental data presented above, the tightly bound water affects the adhesive and mechanical properties of the blends in a quite favorable manner.

Free water appears in the PVP–PEG blends above the 20% threshold [89,103,117]. The kinetics of PVP–PEG PSA

film hydration have been studied both in vitro, under experimental conditions typical of drug delivery rate measurement in aqueous solution, and in vivo, using placebo PVP–PEG patch application to forearm and chest skin of 3 male volunteers [118–121]. The patch consists of a PVP–PEG adhesive layer laminated to a water impermeable metalized PET backing film that possesses an occlusive effect and assists skin hydration which in turn enhances percutaneous drug penetration. To decrease the matrix sensitivity to hydration over the 20% limit and increase creep resistance, a thin cotton woven fabric with a water absorption capacity of 7 times its weight was incorporated into the adhesive layer. Inclusion of the woven absorbent into the adhesive layer increases the 20% threshold to 35%. The equilibrium water content in the PVP–PEG films ranges from 8 to 12 wt.%. In vivo absorption of moisture by PVP–PEG PSA has been found to be less than 30%.

For 14 examined drugs with various chemical structures, delivery rates from the hydrophilic PVP–PEG based PSA matrices is higher than hydrophobic PSA matrices and depend on drug solubility in the PSA [122–124]. Delivery of propranolol, glyceryl trinitrate (nitroglycerin) and isosorbide dinitate (ISDN) from the hydrophilic TDS matrix across human cadaver skin epidermis or skin-imitating polydimethylsiloxane-polycarbonate block copolymer Carbosil membrane in vitro is characterized by high rate values and zero-order drug delivery kinetics up to the point of 75–85% drug release from their initial matrix contents [123,124].

As follows from Fig. 17A, the steady-state propranolol concentration in rabbit and human plasma is achieved not later than 24 h after TDS application [122]. The drug plasma level is held constant during the whole period of TDS application (up to 6 days), suggesting that in vivo transdermal drug delivery kinetics are zero-order.

PVP–PEG PSA based TDS with propranolol exhibits effective hypotensive and antianginal action beginning 20–24 h after the first TDS application with an area of 30–48 cm^2, which was maintained over the course of a 2-week alternative application with patch replacement in every 5 days. A negative chronotropic effect was noted in 74% patients and was evident in a 12–15% systolic blood pressure decrease, an 11–15% diastolic blood pressure decrease and a 20–28% heartbeat frequency decrease (Fig. 17A–C). After 24–48 h of TDS application, antianginal action was recorded in 67% of patients and was expressed in a 37–39% increase in the mean time to development of moderate anginal attacks on a treadmill exercise test. The decrease in the daily requirement for nitroglycerin tablets was more than 50%.

Antianginal action of nitroglycerin hydrophilic TDS in 53% of patients was expressed 2 h after the patch application to skin area of 35 cm^2 (Fig. 18) [125,126]. This effect was permanent over the course of >24 h of every TDS application. The daily requirement for nitroglycerin tablets was reduced to 45% on the first and second days after the first Nitropercuten TDS application. For the other 27.5% of patients, the decrease in the above-mentioned indexes was 25–50%. In patients with acute myocardial infarction, the antianginal effect was more evident [122].

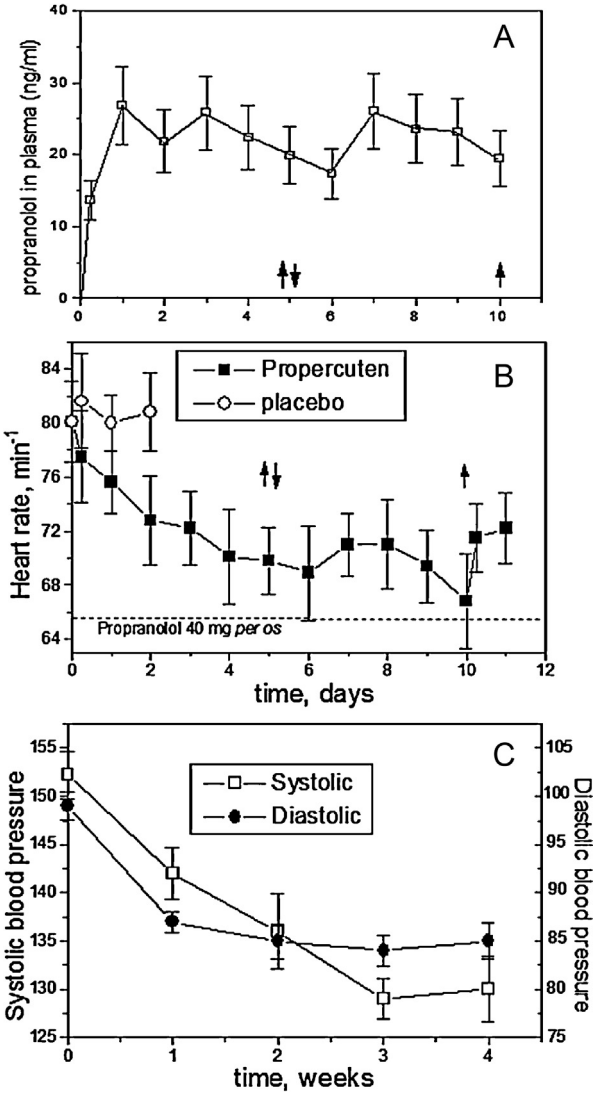

Fig. 17. A: Propranolol concentration in human plasma (ng/ml) for twelve patients following the Propercuten-forte TDS skin application with patch area $S = 48\ cm^2$. Replacements of patch applications are marked by the arrows. [122], Copyright 1996. Reprinted with permission from Elsevier Ltd. B: Pharmacodynamics of heart rate (min^{-1}) in 12 hypertensive patients (sitting) following placebo-controlled Propercuten-forte patch application, replacement () and removal (). $S = 48\ cm^2$ (L.I. Pavlova, A.S. Rumyantsev, A.K. Starodubtsev and V.G. Kukes, unpublished report). Dashed line denotes the mean effect of propranolol 2 h after peroral tablet administration dose of 40 mg. C: Decrease of blood pressure in 40 patients with mild to moderate hypertension within repeated Propercuten-forte TDS application for 4 weeks. $S = 48\ cm^2$ (L.I. Zavolovskaya, V.A. Orlov, unpublished report).

The antianginal effect of ISDN hydrophilic TDS was determined from the tolerance to physical exercises. For 57% of patients, a stable effect has been attained 6 h after the PVP–PEG TDS skin application and was permanent even after 48 h. In 92% of patients, the ISDN therapeutic dose was 1–2 patches (30–60 cm^2). This dose is significantly below the Frandol tape application area (100–300 cm^2) [127] and indicates that the ISDN transdermal delivery rate is enhanced from the hydrophilic PVP–PEG matrix. The

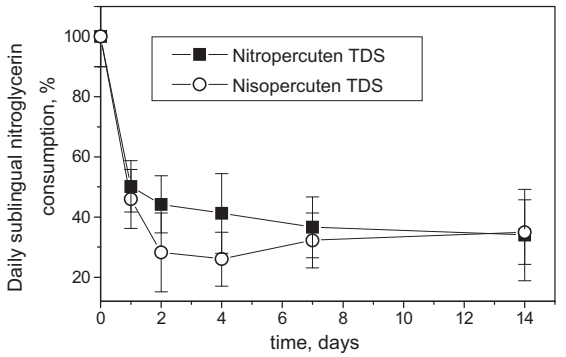

Fig. 18. Reduction in daily consumption of sublingual nitroglycerin (%) to stop anginal attacks in 25 and 14 patients with angina pectoris treated by the Nitropercuten and Nisopercuten TDS respectively.
[122], Copyright 1996. Reprinted with permission from Elsevier Ltd.

daily requirement for nitroglycerin tablets to prevent anginal attacks was reduced to 50% and 64% on the first and second day, respectively, after Nisopercuten application [122].

The Cypercuten TDS has offered a nonnicotine transdermal medication in smoking cessation. A total of 222 heavy smokers aged were involved in placebo-controlled clinical trials of the Cypercuten TDS, performed in 4 specialized clinics. Persons who smoked 20–30 cigarettes daily were treated initially with one 30 cm^2 patch, and the others, smoked 30–50 cigarettes, with the double dose. All the patches were repeatedly applied to forearm skin for 2–3 days. The treatment duration varied from 6 days to 2 weeks and averaged 12.4 days. 37.8% of participants were treated in hospitals and 62.2% on out-patient basis.

The vast majority of the smokers (79–92%) were affected by the Cypercuten TDS 1.5–2 h after the first patch application. They declared the disturbance of their craving for cigarettes as a consequence either of evoking a bitterness or disgusting sweetness in mouth (58.7%) or a sickness (53.0%) during smoking. These unpleasant feelings were most often spontaneously transient after smoking. As a result of the first day of trials 79% of the smokers not only reduced their daily cigarette consumption by over 50%, but they also left 2/3 of every cigarette unsmoked. The control group did not respond to the placebo patch application by the attenuation of craving for cigarettes. In the end of a short term study of the Cypercuten TDS as a monotherapy drug in smoking cessation, 25.7% of the patients were abstinent and did not resume smoking one month after treatment. The abstinence onset was documented 4 days following initial patch application and the abstinence rate achieved its steady state level 6 days after beginning of treatment. 15.4% of the abstainers ceased smoking after one 30 cm^2 Cypercuten TDS application, whereas the other 84.6% of the abstainers were treated by 2 patches. The attenuation in the craving for cigarettes in 79–90% of the heavy smokers was evident 1.5–2 h after the first patch application and lasted as long as 3 days in 81% of the patients. In average 63.2% of the smokers declined their cigarette consumption by over 50% from the first day. No systemic effects were observed that could definitely have been ascribed to the administration of cytisine. Symptoms inherent in nicotine abstinence syndrome (headache, dizziness, dry mouth) were only documented in 1 smoker (0.5%) and tachycardia in 2 patients (0.9%). Cytisine patches had been readily accepted by 89–95% of the smokers.

PVP–PEG and PVCL–PEG blends are not unique examples of high molecular weight hydrophilic polymers and short-chain telechelics that form adhesive interpolymer complexes. As has been shown earlier, PVP and PVCL may be replaced by other polymers, bearing H-bonding recurring units. As has been recently demonstrated by Takemoto et al., poly(N-vinyl acetamide) forms H-bonded complexes with PEGs varied in molecular weight from 200 to 600 g/mol and with glycerol [128]. These complexes have excellent compressive strength and have great potential in biomaterials industry such as alternative tissues. As the noncovalent crosslinkers of N-vinyl amide polymers, other hydroxyl-, carboxyl-, phenol- or aminoterminated telechelics can be employed, e.g., succinic acid, hydroquinone, etc. The examples are described in patent [129].

Silva et al. recently reported on the preparation of films based on chitosan polyelectrolyte complexes for transdermal drug delivery [130]. Their PEC was based on the blends of polybase (chitosan) and crosslinked poly(acrylic acid) (PAA). Hydrogels prepared with a wide range of ratios between chitosan and crosslinked PAA were earlier successfully applied for the amoxicillin site-specific delivery in stomach, for buccal delivery of acyclovir, and provided a suitable controlled drug release profile. The aim of their study was the development and characterization of PEC films based on chitosan and PAA with good functional properties and cosmetic attractiveness for a potential application as a universal skin drug delivery system.

Due to the very low bioadhesive properties of their formulations, an additional layer of the hydrophilic PSA composed of long chain PVP and PEG-400 was applied to the film to provide best functional performance and the properties of the resulting formulation. This PVP–PEG-400 PSA was reported to demonstrate enhanced transdermal delivery of various drugs, is compatible with drugs of different physicochemical properties, does not act as a penetration barrier to drug diffusion and is nontoxic. The authors have decided to apply the hydrophilic PVP–PEG PSA in order to keep the hydrophilic nature of the skin delivery system and because this type of adhesive offers several advantages over hydrophobic ones: improved skin adhesion, compatibility with a higher variety of drugs and excipients, and expanded capability to control/manipulate adhesion–cohesive properties. As has been noted in reference [130], the PVP–PEG PSA exhibits all ideal properties for the development of a universal matrix for enhanced transdermal delivery of drugs.

Summing up, the data presented in this section represent the structure–property relationship and quantitative approach to the molecular design of hydrophilic PSAs with tailored performance properties and universal transdermal systems for enhanced and controlled delivery of numerous drugs [131].

4. Fundamentals of interpolymer and polyelectrolyte complex formation

As Eq. (1) and the molecular theory of pressure sensitive adhesion have demonstrated, PSAs should combine two mutually opposing properties: a large unoccupied space between neighboring macromolecules (free volume) and a high energy of intermolecular cohesion (cohesive strength) [38]. Another example of supramolecular network structures that couple high molecular mobility with intermolecular cohesion strength, are interpolymer complexes (IPCs), in particular polyelectrolyte complexes (PECs).

In polymer blends, where formation of an interpolymer complex between macromolecules of a polybase and a polyacid takes place, high cohesion strength is provided by hydrogen, electrostatic, or ionic bonding between macromolecules that carry complementary reactive groups in recurring units of their main chains, whereas a large free volume can result from the occurrence of loops and other defects in the supramolecular network structure.

4.1. Cooperative mechanisms of self-assembling the interpolymer and polyelectrolyte complexes

In this brief sketch we consider several theoretical studies analyzing molecular mechanisms of the IPC and PEC formation. Basing on their interaction forces, IPC can be divided into four classes i.e., hydrogen-bonded complexes, polyelectrolyte complexes (PECs), stereocomplexes and charge–transfer complexes [132]. PECs are formed mainly due to long-range Coulomb forces by mixing oppositely charged polyelectrolytes, i.e., by polyanions and polypolycations. Hydrogen-bonded complexes are formed by a combination of complementary polymers bearing proton-accepting functional groups in their recurring units (polybase) and proton-donating groups (polyacid). The family of such proton-accepting and proton-donating complementary polymers also includes polymers forming either polycations or polyanions upon ionization of their reactive functional groups. Thus in this connection the term polyelectrolyte complex (PEC) is somewhat ambiguous: it relates also to hydrogen-bonded complexes of uncharged polybases and polyacids. In following analysis of published data we discuss the molecular mechanisms formation of IPC and PEC with a specific balance between the energy of polybase–polyacid interaction and the free volume (i.e., unoccupied space) between complementary macromolecules as the factors governing pressure sensitive adhesion [38]. The majority of published papers describe mechanisms of IPC and PEC formation in dilute solution. In the present review we are mainly focusing on interpolymer complexes in the solid state, and consider complexation in solution in so far as they illustrate fundamental principles.

Theoretical studies on cooperative mechanisms of H-bonded IPC formation date back to the end of 1960 and beginning of 1970 when Kargin, Kabanov, Papisov and Zezin took into consideration the unfavorable contributions of conformational, translational and combinatorial entropy to the thermodynamics of the IPC and PEC formation in solution [133–145]. In particular, the review [134] considered theoretical aspects and experimental results on the cooperative intermolecular bonding and selectivity of both IPC and PEC formation. The paper [133] was the first research work where IPC formation was treated as a cooperative selective chemical reaction when a stronger proton-accepting polymer displaces a weaker one from an IPC formed with a proton-donating polymer. The selectivity of competitive chemical reactions occurring in IPC formation was later reviewed in [135].

Earlier reports of the Moscow University team, originally published in Russian, became internationally known owing to cooperation with Osada [146,147], who worked with the Russian team during that time [148]. As a result, cooperativity of the IPC and PEC formation is now generally recognized due to the fundamental review by Tsuchida and Abe [132].

Due to the long-chain structure of the complementary macromolecules and more or less regular sequence of monomer units in polymer backbones, in the formation of intermacromolecular assemblies between a polybase and a polyacid the energy for breaking one bond of the inner repeat unit is not compensated by an increase in entropy. Actually, such IPC formation is not accompanied by addition of conformational and translational degrees of freedom, as occurs when the bond between two corresponding separate monomer units is broken. In other words, the cooperative mechanism of IPC formation is governed by the entropy factor [132].

As one of the functional groups reacts with a complementary one, the neighboring functional groups in the recurring units have more favorable entropy to form new interchain bindings. Thus, the activation energy is highest for the first intermacromolecular bond formation and becomes substantially lower with an increase of the number of interchain bonds. For this reason, the cooperative reaction between two complementary macromolecular chains advances very rapidly according to the "all-or-none" type principle, like a zipping mechanism as the segments of interacting complementary macromolecules also interlock. The zipper effect is the neighboring group effect in the course of cooperative IPC formation. As a result of the cooperative zipper mechanism between complementary macromolecules, e.g., oppositely charged polyelectrolytes, a 1:1 complex stoichiometry can be achieved. The term of "all-or-none" was originally borrowed from protein physics. The cooperativity of the α-helix-coil conformational transitions in proteins and synthetic polypeptides led Ptitsyn and Uversky to conclude that the transition in question is of the "all-or-none" type [149].

The thermodynamics of IPC formation controls the IPC stability. The enthalpy gain is not very large and only slightly depends on the number of reactive functional groups in polymer chains, because the IPC formation may be regarded as a kind of substitution reaction between counterions. In aqueous solution the hydrophobic interactions also act in concert [132]. On the other hand, the entropy change (ΔS_i) is the sum of the entropy changes caused by fixing the polymer chain positions and their conformations (the loss of translational and conformational freedom, ΔS_p), the entropy gain caused by the

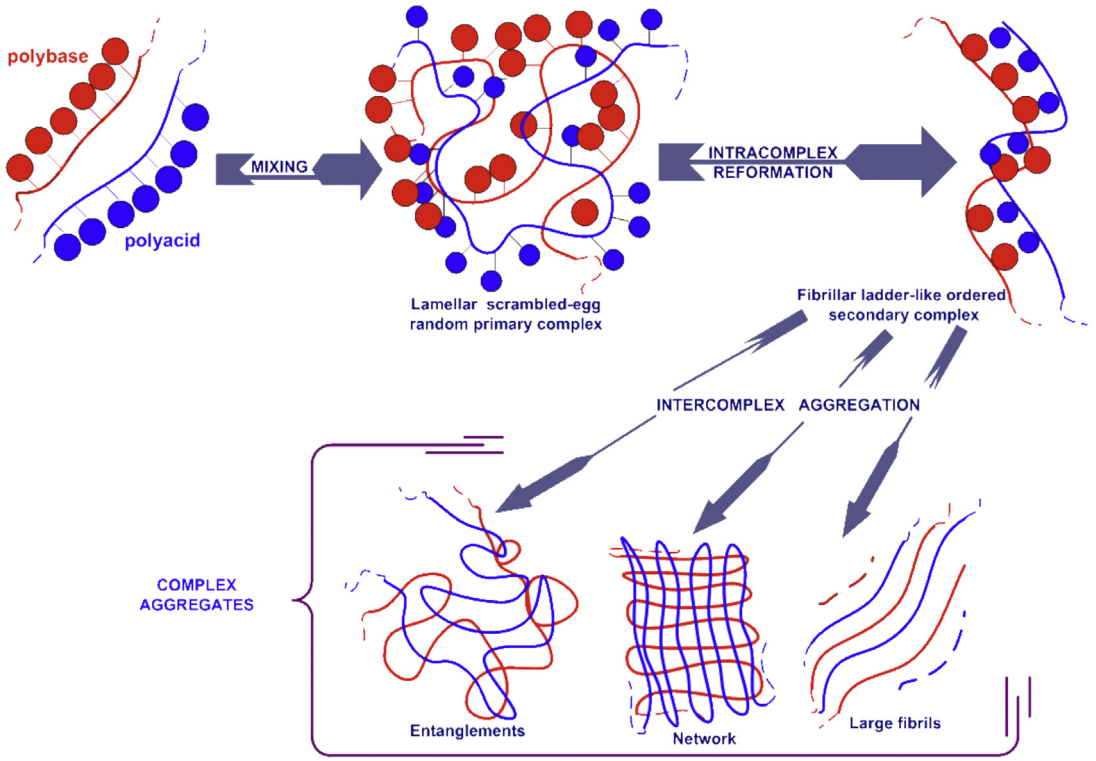

Fig. 19. Schematic representation of the association and aggregation of interpolymer and polyelecrolyte complexes.

released low molecular weight counterions (ΔS_m) and the entropy change resulting from hydrophobic interactions (ΔS_h). Note that release of counterions occurs only for self-assembly of complementary polyelectrolytes and does not take place in the case of H-bonded IPC formation. When the increase in ΔS_h and ΔS_m exceeds the decrease in ΔS_p, the reaction between macromolecular chains is entropically favorable. ΔS_m is not appreciably affected by the number of reactive sites in the polymer chain whereas ΔS_h increases and ΔS_p decreases with the chain length of the complementary polymers. Therefore, the total entropy change under the IPC formation gradually increases with increased chain length of the polymer components. The free energy change ($\Delta F_i = \Delta H_i - T\Delta S_i$) first decreases with the increase in polymerization degree and then increases to about zero because the loss in entropy becomes compensated by the enthalpy gain [150]. Thus, the total free energy change (ΔF) associated with the complex formation may gradually become more negative with increasing chain length of the polymer components [132]. PEC formation is significantly affected by the nature of the individual complementary polymer components and the complexation conditions. Depending on the polybase–polyacid ratio, PECs either may separate from the solution as solids or liquids, remain soluble in solution or may settle as gels. In hydrogen-bonded IPCs, polybases and polyacids typically interact with each other almost stoichiometrically. In dilute solutions the complex stoichiometry approaches almost unity and 2/3 in concentrated solutions [132].

Investigations of the complexation mechanisms provide important information about both supramolecular structures and functional properties of the intermacromolecular complexes. The primary complexes formed by mixing complementary macromolecules frequently demonstrate further rearrangements of their supramolecular structure and aggregations under particular conditions. It is expected that the complex has a random conformation in dilute solution because the complexation reactions proceed very rapidly such that the IPCs formed at the contact of complementary polymer macromolecules exist in a metastable state and then gradually transform into more stable structures. Thus, a characteristic feature of such IPC formation is their self-assembly into the most energetically stable supramolecular structures.

PEC (IPC) formation process follows through three main steps or stages (Fig. 19):

(1) primary complex formation,
(2) rearrangement of the primary complex structure into most energetically stable state,
(3) intercomplex aggregation process, i.e., supramolecular structure formation.

The first step occurs through hydrogen bonding in IPCs or Coulomb forces in PECs. It should be particularly emphasized that Coulomb forces are long-range attractions between cations and anions that can be fairly far apart, whereas H-bond formation requires direct contact between proton-donating and proton-accepting functional groups. Both reactions are very fast. The second step takes the time of the order of an hour if the complex is formed in dilute solutions and involves spontaneous breakage of

the bonds and their subsequent reformation at another site, resulting in a relaxation of the polymer chain conformation. If the complex formation occurs in concentrated solution or in the melt the duration of the second stage accordingly increases and takes few weeks depending on chain length and mixing temperature. The third step represents aggregation of secondary complexes into supramolecular structure mainly through hydrophobic interactions.

The final PEC and IPC aggregates are often insoluble, and their stoichiometry tends to unity. Moreover, in contrast to the primary complex precipitates, the final product is believed to be packed comparatively densely [132]. Notwithstanding the hydrophilicity and water solubility of both polybase and polyacid macromolecules, in their secondary 1:1 stoichiometric fibrillar complexes all the complementary hydrophilic groups are strongly associated through hydrogen or electrostatic bonding as the scheme in Fig. 19 illustrates, resulting in hydrophobization and aggregation of fibrillar ladder-like complex structures.

As Fig. 19 illustrates, the random primary complex is less densely packed and exhibits a much larger free volume than the ordered secondary complex, formed in the course of complementary chain association leading to energetically more favorable and stable state. As we shall see subsequently from our own experimental data presented in Section 6.2 of this review, the random primary complexes of hydrogen and ionically bonded complementary macromolecules display lamellar structures in solution, while for ordered secondary complexes fibrillar structures are usually typical. This observation is in good agreement with the results of other authors [5,132,151–153].

4.2. Theoretical models of cooperative interpolymer and polyelectrolyte complex formation pertinent to their adhesive behaviors

As both polybase and polyacid are random copolymers, wherein reactive functional groups in monomeric units are diluted with inert recurring units, a steric inconsistency occurs between the location of complementary groups along a polybase and a polyacid chains. As will be shown below, this mismatch is another powerful factor that contributes to the loop and free volume formation.

Although a considerable research efforts have been devoted to investigation of the formation mechanisms and the properties of interpolymer and polyelectrolyte complexes in solutions [1,4,5,132,154–158], there is a lack of experimental data on the phase behavior of oppositely charged polyelectrolyte blends in a solid state [2,3,159,160].

We now turn our attention to the discussion of theoretical models describing cooperative processes of IPC and PEC self-assembly from the point of view of coupling a high molecular mobility (large unoccupied space between complementary macromolecules) with intermolecular cohesion energy as a design principle for pressure sensitive adhesives (PSAs). Taking into account that intermolecular cohesion energy is very high in the course of cooperative IPC formation, our major concern is to reveal the factors making free volume in the IPCs and PECs as large as possible.

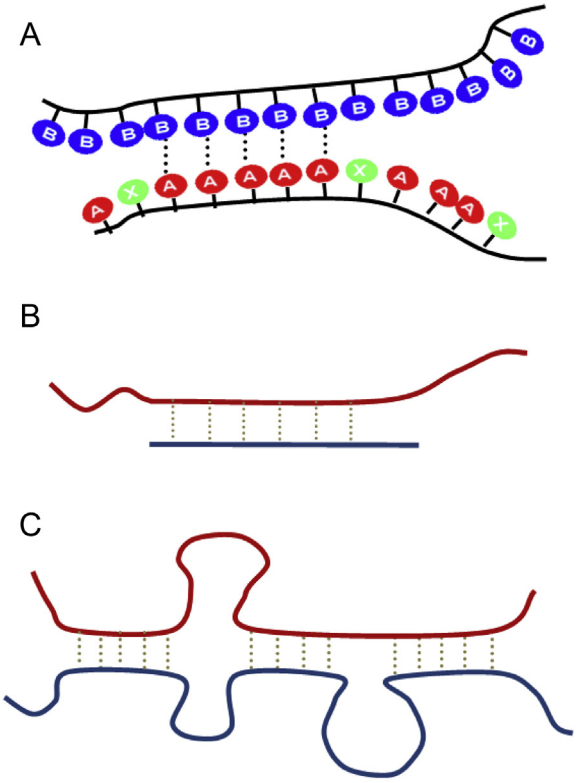

Fig. 20. Schematic illustration of the effect of macromolecular steric mismatches on the structure of interpolymer complexes. A: The IPC cooperative formation process between complementary polymer and copolymer. A is repeat unit containing acidic functional group, B is a basic unit, X is a monomeric unit that cannot interact with A and B units. B: The structure of a "zipper" 1:1 stoichiometric ladder-like interpolymer or polyelectrolyte complex. C: Ladder-like interpolymer or polyelectrolyte complex with disordered positions of intermolecular bonds, consisting of the sequences of regularly bonded ("ladder") and unbound recurring units (loops).

Despite a large number of studies devoted to IPC formation and properties, comparatively few of them included a theoretical approach [134,141–153]. Iliopoulos and Audebert offered a semiquantitative theoretical model especially adapted for the study of reversible IPCs stabilized through weak interaction such as H-bonding [160,161]. In such a situation the cooperative effect plays a great role. This means that oligomers of a given A-type polymer (polyA) cannot be complexed with a long B-type macromolecule (polyB) if the length of polyA chain is not large enough (i.e., if their polymerization degree is smaller than a critical chain length, l_c,). More generally they discussed the situation of a mixture of proton-accepting homopolymer (polybase, polyB) with a random polyacid copolymer (copolyA*X*) where *X* is a unit which cannot interact with B units (Fig. 20A).

In this way, steric mismatches between the positions of reactive recurring units in complementary polymers were taken into account [161].

Only polymers or oligomers with a degree of polymerization equal to or higher than the critical chain length can be complexed with long chains of the complementary

polymer. From a thermodynamic point of view, the formation of one noncovalent bond (H-bonding, electrostatic attraction) between two macromolecular species in solution is quite improbable, while the formation of a large number of such bonds leads to a thermodynamically stable complex [132]. For this reason, many authors have proposed a zipping mechanism for the complexation between complementary macromolecules and a ladder structure for the resulting complex. This structure can be represented by the scheme shown in Fig. 20B [162].

Obviously, if the two complementary chains are very long, such an uninterrupted ladder structure is rather improbable. Moreover, experimental results showed that even in the case of homopolymer couples, the complexation is not perfect: a fraction of the interactive monomers is not involved in the complex. The structure proposed for such complexes is illustrated by the scheme shown in Fig. 20C [162].

There is a dramatic influence of the inactive group content, ***K***, on the complexation reaction between a homopolymer (polybase) and a copolymer (polyacid). In dilute solution and for low values of ***K***, the complex exhibits a compact structure, leading to a sharp decrease in the viscosity. On the other hand, in concentrated solutions of high molecular weight polymers and for sufficiently high values of ***K*** (about 4–5% for PEO and 10–15% for PVP), mixtures of very high viscosity are obtained. This implies that a network supramolecular structure is formed.

In this way, as the theory of Iliopoulos and Audebert predicts, the structures and properties of IPS depend appreciably on the chain flexibility of the parent complementary polymers. The PEO is much more flexible polymer than the PVP as the Kuhn chain segment for PEO consists of 4–5 recurring units, whereas that for PVP includes 11 units [85].

The effects of polymer chain lengths and positional mismatches on the viscosity of IPC solution, measured in [162], can be easily explained on the basis of the statistical theory of globular polyelectrolyte complexes proposed later by Borue and Erukhimovich [163]. One of major features of their approach to the structure of PEC formed between weakly charged polyelectrolytes is the interpretation of a transition between a random primary complex to ordered secondary complex, shown in Fig. 19 [132] as a phase coil–globule transition. The main difference between the polymer coil and globule appears most clearly when the degree of polymerization of the chain, ***N***, is sufficiently large [164]. The equilibrium globule density, ρ, characterizing its spatial structure, fills space an approximately constant density, which is determined by the balance between forces of electrostatic attraction and excluded-volume repulsion, and is independent of ***N***. Therefore, PEC can be considered as a polymer globule. From this point of view, approach [163] differs from other models, which considered PEC as a more or less contracted coil.

Treating a PEC as a polymer globule not only enables application of statistical theory of polymer globules [164,165] and thus calculation of the equilibrium PEC properties (monomer density, surface tension of coacervate particles, etc.), but also provides a natural framework to account for the various experimental observations (e.g., salt effects) [166–169].

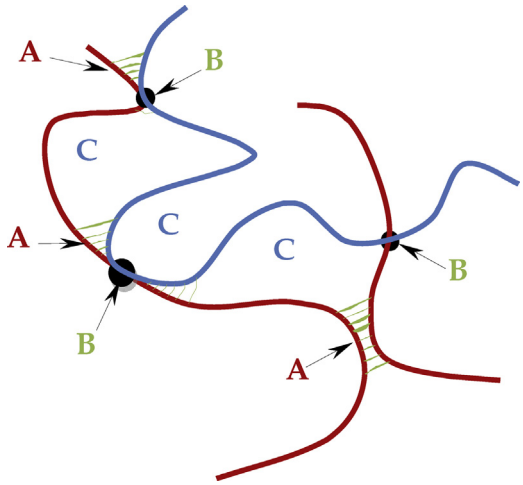

Fig. 21. Schematic representation of a non-covalently crosslinked network structure of interpolymer complexes. A: Noncovalent crosslinks consisting of sequences of hydrogen, electrostatic, or ionic bonds formed between functional groups in monomer units of complementary macromolecules. B: The entanglement junctions of long polymer chains. C: Loops consisting of the segments of macromolecules free of interpolymer bonding.

4.3. Effects of topological chain entanglements between complementary polymer components on the structure of interpolymer complexes

As has been noted above, strong intermolecular cohesion and the cooperative mechanism of interpolymer polyelectrolyte complex formation lead to a drastic decrease in the distance between neighboring complementary macromolecules and therefore to reduction of the free volume. Hence, in order to reconcile the strong intermolecular bonding with large free volume, that is a prerequisite of pressure sensitive adhesion [38], special technological practices should be applied. Fig. 21 presents a schematic illustration of such methods.

The scheme shown in Fig. 21 [160] covers the blends of complementary polymers including the interpolymer complexes. High cohesion energy can be provided by the formation of intermolecular hydrogen, electrostatic, or ionic bonds. The bonds crosslink the chains of complementary polymers into three-dimensional network structures [38]. The cohesive strength of the network is controlled by the number and strength of interchain junctions. Two kinds of junctions may be distinguished. Junctions A represent the ladder-like sequences of interchain bonds. Their strength depends on the energy and the amount of these bonds, i.e., on the length of the ladder-like bond sequences. Junctions B emerge due to physical entanglements of macromolecules in the blend. Their number and strength are affected by the polymer concentration in the blend and the chain length (molecular weight). The free volume of interpolymer complexes, along with other defects of the supramolecular network structure, can be produced by loops (C) of unbonded macromolecular chains (Fig. 21 [160]). The size and the number of the loops, or their degree of conversion in the cooperative chemical reaction of solid state interpolymer complex formation, are

governed by the content and the strength of topological polymer chain entanglements B. These entanglements constrain the mobility of complementary polymer chains and hamper the formation of the ladder-like network junctions A. In other words, the topological entanglements of complementary polymer chains B assist in stopping the cooperative process of interpolymer complex formation at an intermediate nonequilibrium stage. Thus, the free volume in the polyelectrolyte blends depends on the specific features of the polyelectrolyte PSA preparation method, rather than the contribution of interpolymer cohesion energy.

The mechanisms of IPC and PEC formation under the conditions of restricted molecular mobility of complementary macromolecules (i.e., in concentrated solutions or in the melt) have not yet been theoretically described. The "zipper effect" is based on the assumption that both polybase and polyacid remain as individual disentangled chains before complexation. However, it has been well-established in the literature that polyelectrolytes form "multimacroion domains" [170–174] in salt-free or low-salt solution. When polyelectrolytes or ionomers are studied by dynamic light scattering in dilute solution two diffusive relaxation modes are observed, with neither mode representing the diffusion of a single polymer chain. The fast mode is attributed to the coupled diffusion of polyion/counterions [175–181], while the interpretation of the slow mode has not reached full agreement yet [172,173,176]. Since the slow mode disappears at elevated salt concentration, the major driving force is attributed to electrostatic interactions. Herein, the term of "multimacroion domains (or clusters)" has been used to denote such associations.

The first and as a whole insufficiently successful attempt to describe theoretically the effect of topological obstacles on the structure of self-assembled IPC was made by Son and Pak [182]. Employing their earlier topological network theory based both on a tetrahedral lattice model and on the earlier theory of Iwata et al. [183,184], they extended the theory of Iliopoulos and Audebert [161,162] for aqueous polymer solutions. Despite the improved characterization of the complexation degree and viscosity of IPC in solutions, their conclusions suffered from a lack of insight into the structure and self-assembly mechanism of these complexes. More recently Deng et al. re-examined of the "zipper effects" in hydrogen-bonding IPC [185]. The mechanism of hydrogen-bonding complexation turned out to be more complicated than expected. The complication has originated from the association of component polymers before mixing. As was demonstrated in [185], polybase and polyacids form "multimacroion domains" (giving rise to a slow mode in dynamic light scattering) at the conditions suitable for complexation. After mixing, the hydrogen-bonded complex evolved from "multimacroion domains" rather than single polymer chains. Therefore, the slow mode process played a key role in determining the structure and physical properties of the formed complexes.

These results should also apply to polyelectrolyte complexation at low salt concentrations. The first observation of the slow mode of polyelectrolytes was in 1978 [175], decades later than the study of interpolyelectrolyte complexation [147], and the interpretation of the slow mode was still controversial. It was probably the reason why the effect of slow mode on complexation was ignored. Moreover, the interpolymer complexes generally involved multiple interactions and were controlled by both thermodynamics and kinetics [172]. A proper control on the association of the component polymers before mixing is crucial for development of interpolymer complexes with novel properties and desirable behavior.

It is widely believed that the structure and the physical properties of solid materials based on polyelectrolyte complexes are poorly reproducible due to the cooperativity of the complex formation mechanism, the difficulty to achieve complex dissociation at high temperatures, and a large number of variables that determine complex formation. All of these properties are known to be influenced not only by the relative molecular weights and stereochemical matching of complementary polyelectrolyte chains, charge densities and so on, but also by the secondary experimental conditions such as the concentrations, the order of polyelectrolyte mixing, mixing ratio, ionic strength, pH, temperature of the solution, and the stirring rate. In this connection, it is pertinent to note that the experimental conditions of complex preparation, as practiced in our research, make the T_g's of the complexes of different compositions [160] quite reproducible (with accuracy of 2–5 °C). This was indirect evidence in favor of uniformity of the polyelectrolyte blends. The major principle underlying the uniformity of such blends is simple: avoiding local supersaturations in the course of complementary polyelectrolyte mixing.

4.4. Impact of polymer chain stiffness upon supramolecular structure of polyelectrolyte complexes

In addition to steric mismatch effects on free volume in cooperatively formed IPS, the data by Idiopoulos and Audebert [162] suggest that polymer chain stiffness affects greatly the supramolecular structure and density of IPC. Recently Lazutin et al. [186] have employed Monte Carlo simulations to analyze the structure of polyelectrolyte complexes consisting of two identical but oppositely charged macroions of different chain stiffness. Computer simulation is one of the most illustrative methods of PEC structure investigation [187–195]. The formation of a complex consisting of two oppositely charged macroions of equal length and charge density was studied in ref. [187–190]. The complex formation was shown to occur in two stages: at first macroions come close and entangle with each other, then the complex size decreases sharply and dense particles appear.

PECs are normally formed by many reversible salt bonds between oppositely charged groups, stabilizing their supramolecular structure. The "ladder" model [5,196,197] (Fig. 20) assumes that PEC is organized in such a manner that all oppositely charged groups of two complementary macromolecules are facing each other and form ion pairs. By this mechanism the resulting supramolecular structure is characterized by 1:1 stoichiometry and resembles a ladder. In the "scrambled-egg" complex the monomer units of oppositely charged macromolecules are randomly

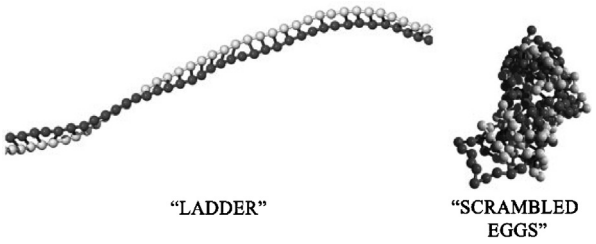

Fig. 22. Snapshots of PEC in the "ladder" and "scrambled eggs" states. [186], Copyright 2012. Reprinted with permission from Wiley-VCH.

mixed just as yolk and white in scrambled eggs, forming the loops of unbound macromolecular segments as Fig. 22 illustrates [5,132,158,161,162,198]. In this way, the stoichiometry of the "scrambled-egg" complex deviates from equimolar composition. In real systems the intermediate case is often encountered: oppositely charged units form ion pairs but the chains are randomly mixed (entangled) to some extent [186].

An ideal "ladder" structure of interpolymer complex could be realized only for macroions with equal lengths and charges, i.e., with matching distances between charged groups on associating polycation and polyanion chains. Another important factor stabilizing such a structure is the stiffness of polymer chains.

Visual analysis of the Monte Carlo simulations (Fig. 23 [186]) allows us to conclude that PECs have "ladder" structure of 1:1 stoichiometry at high values of stiffness parameter ε_{st}. In this case almost all oppositely charged groups of macroions form ion pairs ($n_{bond} = N$) and the complex looks like a tape bending in the space (Fig. 23a). Stiff chains are predominantly organized into complexes having an ideal "ladder" structure. In such complexes all monomer units form ionic pairs. As the stiffness parameter ε_{st} decreases, defects appear in the "ladder" structure, the polyion chains bend, the complex size decreases, and the total number n_{bond} of ion pairs somewhat decreases as well. In such complexes some parts of macroions are involved in the ladder structures whereas other parts form small droplets with disordered arrangement of monomer units (Fig. 23b). With a further decrease of ε_{st} the fraction of ladder conformation decreases while the fraction of unconnected monomer units increases. Polyelectrolyte complex of flexible chains appears like a "scrambled egg," i.e., as a set of randomly located monomeric units of oppositely charged ions with rather short "ladder" blocks (Fig. 23c–d).

PECs of semiflexible chains ($\varepsilon_{st} = 4$) contain several "ladder" fragments separated by one or two free monomer units. In a PEC consisting of flexible chains ($\varepsilon_{st} = 0$) the fraction of free monomer units increases while monomer units forming an ionic pair typically have rather different positions along their respective chains although, short "ladder" fragments emerge as well. The majority of ion pairs between complementary monomer units are not ordered for low ε_{st} (scrambled egg).

The dependence of the mean order parameter η on the stiffness parameter ε_{st} for macromolecules of different lengths N is shown in Fig. 24 [186]. One can see that the order parameter increases with the growth of macromolecule stiffness ε_{st} and that for different macromolecule length N a sharp growth of the order parameter is observed at $\varepsilon_{st} \approx 4$. The parameter η is close to zero at $\varepsilon_{st} = 0$. This implies that ladder-type ordering is practically not observed in a complex of flexible chains. At high values of stiffness parameter ε_{st}, the ladder-ordering parameter is rather high, but still it is lower than unity. Thus, even very stiff and short macromolecules do not always exhibit an ideal "ladder" conformation (as is evident from Fig. 23). In the course of complex formation some ionic pairs can be destroyed and then reformed again. The longer is the macromolecule the higher is the disorder leading to smaller values of the ladder order parameter at both high and low macromolecule stiffness ε_{st} [186].

The two limiting structures – "ladder" and "scrambled egg" – differ in macromolecular organization, structure compactness, and, consequently, free volume. Within a complex of flexible macromolecules ($\varepsilon_{st} = 0$) the total number of long-range electrostatic bonds is rather high, while at high backbone stiffness ($\varepsilon_{st} > 8$) such bonds are totally absent [186]. In full agreement with the prediction of the statistical theory of globular polyelectrolyte complexes [163], the structural transformation of PECs from the "ladder" to "scrambled egg" structure may be treated as a phase transition [186].

4.5. Effects of cohesive interaction strength, chain length, charge distribution, solvent quality, salt concentration, polybase–polyacid ratio, pH and temperature

Polymer networks crosslinked in the presence of a large amount of diluent are very labile systems and one needs only small changes of external parameters (e.g., temperature, pressure, solvent quality, salt concentration) to induce a drastic jump-like conformational transition accompanied by a significant shrinking of the network. The phenomenon of a collapse of a polymer network was first explicitly described by Tanaka in 1978 [199]. Since then much theoretical and experimental research has been devoted to this problem [188,189,191,200–212].

Fig. 25 illustrates the density of the PEC clusters for different interaction strengths ($\lambda = 0.4$, 4, 40) [188,189]. For the chain length $N = 40$ no compact structure is formed at $\lambda = 0.4$, although the radius of gyration of a chain is already smaller than in a good solvent. At $\lambda = 4.0$ the formation of a denser structure occurs. A further increase of λ leads to an even more compact cluster. A local crystalline-like structure is obtained for even larger interaction strengths ($\lambda > 50$).

The size of the PEC particles is determined by the strength of electrostatic interactions between oppositely charged macroions. The stronger are these interactions the denser is the PEC structure and the smaller the free volume. The snapshots presented in Fig. 25 illustrate the coil-globule transition predicted by the theory of Borue and Erukhimovich [163]. Under comparatively weak intermolecular cohesion the polyelectrolyte chains in the coil form loops, which are distinctive feature of scrambled egg supramolecular structure (Fig. 25, left). The coil collapse is accompanied by the reduction of free volume and enhancement of intermolecular cohesion energy. Complexes with

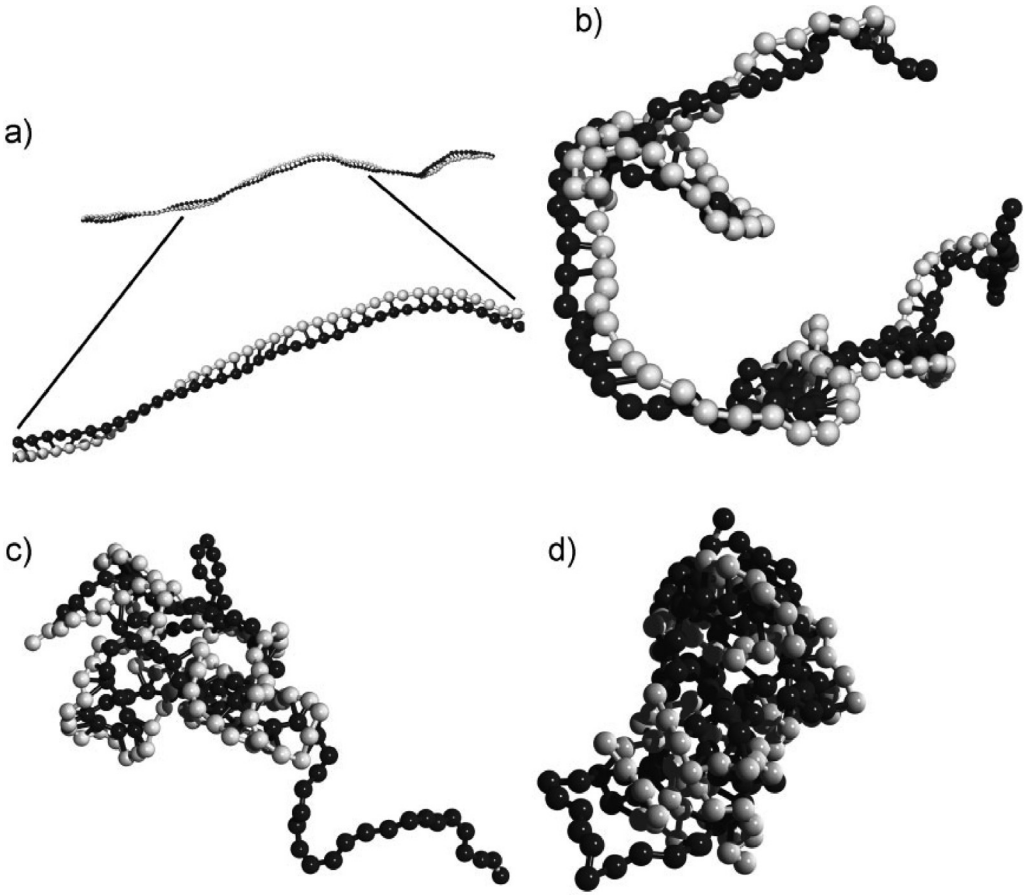

Fig. 23. Snapshots of PECs at different values of the stiffness parameter ε_{st}:ε_{st} = 50 (a), 4 (b), 3 (c), 0 (d). Number of repeat units N = 100. [186], Copyright 2012. Reprinted with permission from Wiley-VCH.

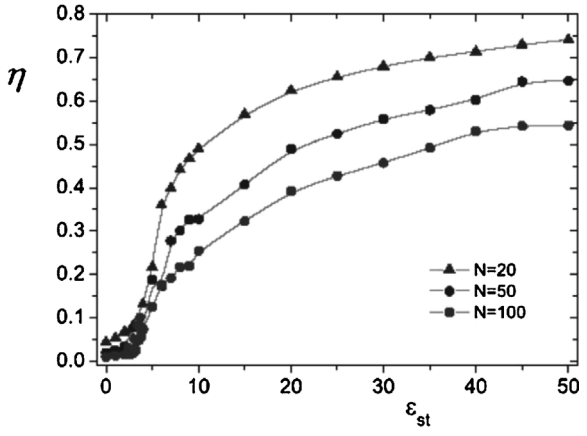

Fig. 24. Dependence of the "ladderness" order parameter η (normalized number of "matching" pairs of A–B bonds) on the stiffness parameter ε_{st}. [186], Copyright 2012. Reprinted with permission from Wiley-VCH.

globular structure can emerge when electrostatic attraction forces are strong enough. In a collapsed globule (Fig. 25, right) the polyelectrolyte chains are aligned in ladder-like structure. For very strong electrostatic bonding the PEC globules often show dense glass-like structures with a distinct round surface and pronounced local order [189].

In [188] the kinetics of PEC cluster formation was also investigated. The simulations were started with well separated chains. Turning on the Coulomb interaction, the chains start to attract each other. In a first step of the aggregation process (at sufficiently large interaction strengths) the chains start to wind around each other and form helical-like supramolecular structures as is seen from the snapshots presented in Fig. 26. However, the chains do not form perfect helices. In a second step the chains fold into a compact structure because of the attractive interaction between dipoles formed by oppositely charged monomers (Fig. 26). The imperfect helix supports the formation of the compact aggregate. Due to the lack of the perfect twist, monomers and groups of monomers are rather mobile and can therefore easily rearrange to form the cluster. Untwisting a perfect helix before the collapse requires more time than for a disordered helix. Indeed, the folding process of the system was observed to be very fast.

The effects of charge distributions along the chains of interactive polyelectrolytes are described in [191] and [212]. Macro-ions in aqueous solution are surrounded by an electrical double layer: a zone with an increased concentration of counterions and a reduced concentration of

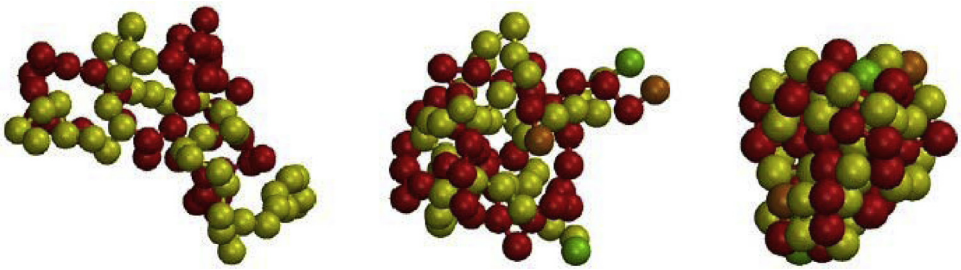

Fig. 25. Snapshots of PEC aggregates with chain length N = 40 and the interaction strengths λ = 0.4, 4 and 40 (from left to right).
[189], Copyright 2004. Reproduced with permission from IOP Publishing & Deutsche Physikalische Gesellschaft. CC BY-NC-SA.

co-ions. When two oppositely charged macro-ions form a complex, the double layers are destroyed to a certain extent and the counterions are released in the form of an ordinary salt solution. This implies changes in both the energy (enthalpy) and the entropy of the system. Both contributions vary with the concentration of salt (ionic strength) [213].

The PEC self-assembling process can be treated as a chemical reaction leading to the formation of a stoichiometric complex and the release of free low molecular weight counterions. The number of released counterions matches the number of formed intermacromolecular ionic pairs. The polyelectrolyte complexation is an equilibrium reversible process and is characterized by an equilibrium constant. In accordance with Le Châtelier's principle, if the concentration of free ions is increased by adding a salt, the position of equilibrium moves in such a way as to counteract the concentration change, i.e., to increase the concentration of free polyelectrolytes. As a result, salts suppress PEC formation. Moreover, when increasing the salt concentration (ionic strength) in polyelectrolyte solution, the following phenomena are also observed:

(1) reduction of electrostatic interactions between polycations and polyanions due to the screening effect of ions,
(2) acceleration of weak polyelectrolyte dissociation owing to the decrease of intramolecular electrostatic repulsion,
(3) increase of PEC hydrophobicity caused by the charge neutralization and the contraction of polyelectrolyte chains [132].

A large number of comprehensive experimental studies of PECs, including preparation and structure characterization, have been reported in recent decades

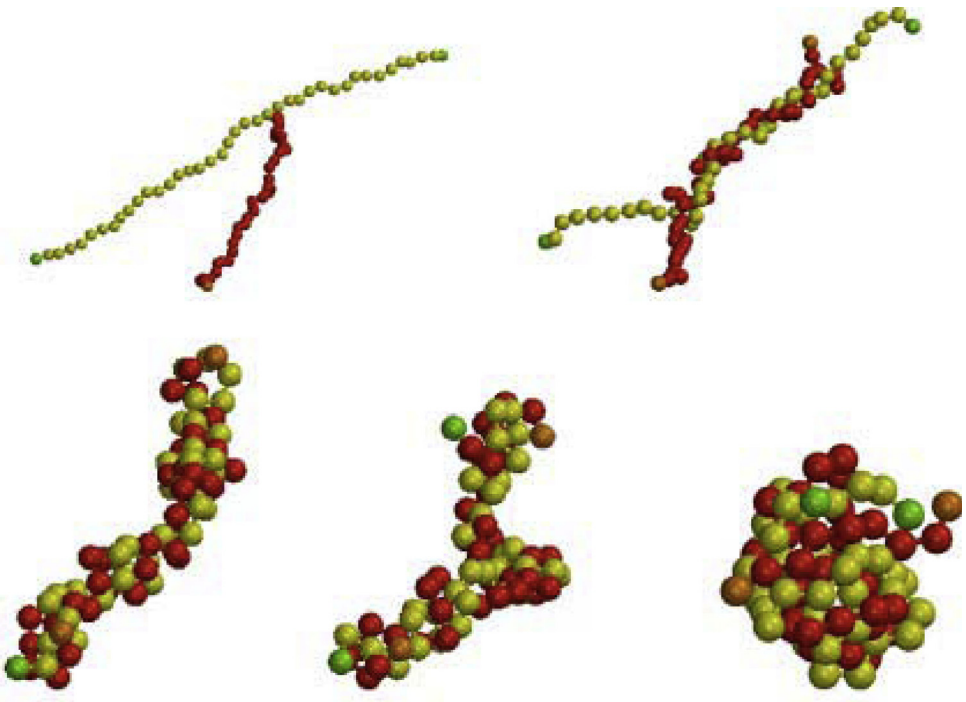

Fig. 26. Successive conformations of chains of length $N = 40$ at the interaction strength $\lambda = 8$ during the formation of a globule; t/τ=0, 6×10^4, 1.2×10^5, 4.75×10^5, and the equilibrium state (from top left to bottom right).
[188], Copyright 2002. Reproduced with permission from the American Physical Society.

[132,151,153,213,214]. It has been shown that PEC properties depend strongly on the ratio of positive to negative charges within mixtures. Nonstoichiometric complexes appear if there is an excess of charges of one sign in the solution. They take the form of hydrodispersed tiny particles or micellar aggregates stabilized by the presence of a surface net charge. In contrast with nonstoichiometric ones, stoichiometric PECs contain equal numbers of opposite charges with a zero net charge, resulting in the PECs aggregation and precipitation [215].

Recently, it was shown that the phase separation in stoichiometric mixtures could be prevented if at least one of the polyelectrolytes is a diblock amphiphilic copolymer that includes a hydrophilic nonionic block [216–218]. The interactions between monomer units of this block and the solvent stabilize the formation of finite-size particles in the solution. These particles have a well-defined core–shell structure where the core is surrounded by a corona formed by the hydrophilic block. Theories have been proposed for such complexes that are referred to as block–ionomer complexes [219–222].

It is well known that salt ions screen electrostatic interactions and can destabilize PECs when their concentration is high enough. In the case of the core–shell complexes, the introduction of salt ions can play a double role. On one hand, screening of electrostatic interaction does weaken the electrostatic attraction between oppositely charged ions and destabilizes PECs. On the other hand, the decrease in electrostatic interaction between oppositely charged core and shell of the complex can lead to the increase in the thickness of the protective shell and thus stabilizes of complexes with respect to aggregation within a certain range of salt concentration [222].

The thermodynamic stability of nanodispersed, stoichiometric polyelectrolyte complexes (PECs) consisting of oppositely charged macromolecules having different affinity to water was considered in the presence of increasing salt concentration [215]. It was shown that such complexes have a core–shell structure, the shell accommodating the polyion with the higher affinity to water preferentially. According to the theory [215], at low salt concentrations the fraction of hydrophilic units forming the complex shell is rather small and grows smoothly with the salt concentration up to a critical salt concentration, where the complex size increases sharply. This change is associated with a "decollapse transition" undergone by the complexed macromolecules by analogy to corresponding transitions in polyelectrolyte gels [215]. After the "decollapse" transition, macroions still form complexes. At this point, the separation is unfavorable from the entropic viewpoint. Indeed, separating both macroions requires a much higher concentrations of oppositely charged counterions to compensate the total charge. Separation occurs at salt concentration when the polyions separate totally; that is, each becomes freely moving in the aqueous medium. At higher concentrations, polyions undergo normal charge screening that can lead to precipitation.

The volume fraction of the polymers in the interior and external parts of the PEC clusters composed of polyions with sufficiently long chains is almost independent of the chain length, and primarily depends on the salt concentration. The critical salt concentration increases with the degree of ionization of the macromolecules and hydrophobicity of the polycation, whereas it decreases when the degree of polymerization increases or when the affinity of the anionic hydrophilic sites with water increases. The higher the degree of ionization of the macroions, the higher the concentration at which total separation occurs; this concentration does not depend on interaction parameters or on the degree of polymerization of macroions. It was shown that in both the collapsed and swollen states the interpolymer complexes are stable with respect to their aggregation. The sharp increase in PEC particle size with an increase in salt concentration was not due to aggregation, that is, to an increase in the number of macromolecules forming the complexes, but rather to the "decollapse" of complex particles themselves.

The formation of complexes in solutions containing positively charged polyions (polycations) and a variable amount of negatively charged polyions (polyanions) has been investigated by Monte Carlo simulations in [168]. It was found that the propensity for cluster formation can be rationalized by four simple rules. For electrostatic reasons, (I) coexistence of oppositely charged clusters is unlikely and (II) charged clusters prefer to be large with (III) a low absolute net charge, whereas from an entropic point of view (IV) many and consequently smaller clusters are preferred.

In the absence of added salt, when the screening of the charges comes only from the counterions of the polyions, the electrostatic energy dominates over entropy. In a system which contains 10 polycations and 5 polyanions with the same absolute charge, the scene is dominated by 2:1 clusters, kept apart by a net repulsion. Close to an equivalent amount of polyions, there is an increasing propensity to form large clusters. This may be seen as the excess polycations collecting the available neutral pairs of positive and negative polyions to share the excess charge, although small neutral clusters still appear for entropic reasons. The largest complex is, thus, observed when there is only one excess polycation. When equal amounts of polyions are present, neutral clusters of small to intermediate size dominate the system, since, the attractive electrostatic correlation interactions between neutral clusters do not yet dominate over the entropy.

The addition of salt was investigated by varying the screening length. When the screening length is short, the electrostatic interactions are reduced and rules I–III become less significant in relation to rule IV. This is manifested by a larger fraction of smaller clusters. Also, clusters of opposite charge may be present. Moreover, the attractive interactions, which lead to associations into complexes, and the repulsion between charged complexes are characterized by different length scales and are, thus, affected differently by the variation of the screening length. In system containing 10 polycations and 5 polyanions with the same absolute charge, an intermediate regime is found where 2:1 clusters dominate but repel each other only weakly or even show some net attraction, due to the short-range nature of the interactions [168]. Solvent quality for the polymer backbone plays an important role in determining the structure of a polyelectrolyte chain in

Table 4
Typical conformations of polyelectrolyte chains[a] [223].

Salt concentration	$l_B = 1\sigma$	$l_B = 2\sigma$	$l_B = 3\sigma$
0	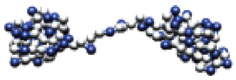	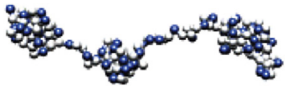	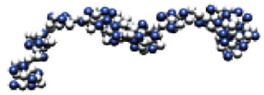
5×10^{-5}	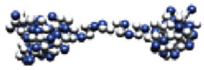	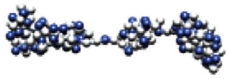	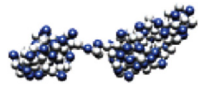
2.5×10^{-4}	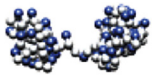	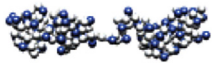	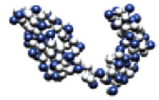
5×10^{-4}	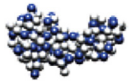	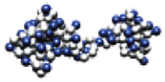	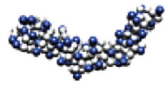
1.25×10^{-3}	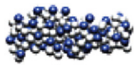	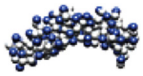	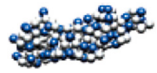

Reproduced with permission from Jeon J., Dobrynin A.V., Journal of Physical Chemistry B 110 (2006) 24652–24665 [223]. Copyright 2006, American Chemical Society.

[a] The negatively charged monomer units of a polyelectrolyte chain are blue and neutral monomers are gray.

solution. Polyelectrolytes in a poor solvent form a necklace like structure of beads connected by strings of monomers [223–236].

Table 4 demonstrates how the salt concentration and strength of the electrostatic interactions influence polyelectrolyte chain conformations [223]. In a poor solvent condition for the polymer backbone, a polyelectrolyte chain adopts a necklace-like conformation of beads connected by strings of monomers. The necklace parameters such as the number of beads, n_b, number of monomers in a bead, bead size, number of monomers in a string, and string length depend on the strength of the electrostatic interactions and salt concentration. The three-bead necklace is the most probable chain conformation for the system with the value of the Bjerrum length $l_B = 3\sigma$ at zero salt concentration. As salt concentration increases the probability of the necklaces with $n_b > 2$ decreases while necklaces with two beads become more favorable. A sausage-like aggregate appears in the systems at $c_s \approx (5 \times 10^{-4})\sigma^{-3}$ (see Table 4) and continues to dominate the chain conformations as salt concentration increases further.

Similar effects of salts have been reported not only for PEC solutions, but also for IPCs stabilized by hydrogen bonds. Association of macromolecules in aqueous media through hydrogen bonding results in the formation of discrete interpolymer complexes (IPCs). In [237], the effect of added salt on the stability of IPCs consisting of polyacrylic acid and either a flexible polymer (polyethylene oxide or polyvinylpyrrolidone) or a semirigid polymer (hydroxypropyl cellulose) is examined by a combination of spectrophotometry, viscometry and potentiometry. Addition of a neutral salt (e.g., NaCl) typically results in IPC aggregation.

The foregoing studies deal with PECs and IPCs in solutions. However, in the last few years the rheological behavior and physical properties of PECs in a solid state has been also examined [3,153,238–248]. As has been demonstrated in [238], the rheological response of polyelectrolyte complexes to an oscillatory strain depends strongly on salt concentration. At low salt concentration the response is similar to that of soft solids [249], whereas the response is liquid like at high salt concentration. These observations are in line with results on biological electrostatic complexes [250]. Thus, in the rheology of electrostatically assembled soft materials, the salt concentration plays a similar role as temperature for polymer melts, and as the strain rate for soft solids [251].

Coacervation is a phenomenon in which a macromolecular aqueous solution separates into two immiscible liquid phases. The denser phase, which is relatively concentrated in macromolecules, is called the coacervate and is in equilibrium with the relatively dilute macromolecular liquid phase [252]. The phenomenon can be divided into "simple" and "complex" coacervation. The former involves only one macromolecule and may result from the addition of a dehydrating agent that promotes polymer–polymer interactions over polymer–solvent interactions. In the latter, two or more oppositely charged macromolecules or colloidal species are present. For this case, Piculell and Lindman [253] have recommended the term "associative phase separation" to replace "complex coacervation".

The mechanism of complex formation depends on many factors, i.e., molecular weight, polymer concentration,

ratio between concentrations of the two interacting polyelectrolytes, ionic strength, pH, and temperature of the solution. This has been recognized from the beginning of PEC formation studies [1–5,132,151,153–156,158]. Recently new insights into associative phase separation were reported [254–261].

In the recent paper [255] Chollakup et al. presented intriguing data on combined effects of the polyacid/polybase mixing ratio, total polymer concentration, salt concentration, pH, and the temperature on the phase behavior in solutions of the PAA–PAH systems. However, the interpretation of their results suffers from a serious drawback. Sample turbidity in their research was utilized as a direct indicator of PEC formation. Such an approach disregards the formation of water soluble polyelectrolyte complexes that are well described by Kabanov et al. [3,125,158,198,214,218]. Thus, the lack of turbidity at mixing the complementary polyelectrolytes in solution cannot be taken as unequivocal evidence that no complexation occurs and implies merely the absence of phase separation. The oppositely charged polyelectrolytes can be simply considered as multivalent counterions and charge screening of the collapsed PEC is achieved by the polyelectrolyte in excess. The redissolution transition in initially multivalent ion-induced precipitated polyelectrolytes takes place with further addition of multivalent particles (polyions), as predicted for flexible linear polyelectrolyte chains in multivalent salt solutions [248,260].

A new type of temperature-sensitive polymer systems based on mixtures of poly(acrylic acid) (PAA) and poly(diallyldimethylammonium chloride) (PDADMAC) in strongly acidic aqueous medium is described in [261]. The mixtures exhibit reversible separation into two liquid phases upon a decrease in temperature. The phase separation is induced by the intermolecular bonding between PAA and PDADMAC due to ion–dipole interactions between the protonated carboxylic groups of PAA and the quaternary nitrogen atoms of PDADMAC. The PEC is formed between a weak polyacid and a strong polybase under conditions when carboxylic groups are fully protonated and ionic pairing between the polyacid and the polycation does not occur. Lowering the solution temperature enhances both ion-dipole and hydrogen bonding interactions within the PEC, eventually resulting in phase separation of complexes within a concentrated phase. It is particularly remarkable that the acidic PDADMAC/PAA mixture shows a completely reversible Upper Critical Solution Temperature (UCST)-type transition, which is rarely found in other polymer systems. Therefore, the mixtures of PAA and polycations in acidic media can be referred to as a new type of equilibrium temperature-responsive polymer systems [261].

The recent paper by Spruijt et al. [256] is aimed at bridging the gap between experimental reports on polyelectrolyte complexation and theoretical models. The authors have measured the binodal compositions of polyelectrolyte complexes of strongly charged poly(acrylic acid) (PAA) and poly(N,N-dimethylaminoethyl methacrylate) (PDMAEMA) directly using fluorescently labeled polymers. They focused on the effect of chain length and salt concentration on phase behavior, but their approach can easily be extended to measure phase behavior as a function of composition, pH, and temperature as well. The experimental data is described using a theoretical model for polyelectrolyte complexation with only a single adjustable parameter. The insights of this quantitative description enabled them to better understand polyelectrolyte complexation in general and the effect of chain length and salt concentration on complexation between other strongly charged flexible polyelectrolytes in particular. The mean field lattice model of Voorn and Overbeek [262] was used to describe the experimental binodal compositions of PAA–PDMAEMA polyelectrolyte complexes [256].

The critical salt concentration is the salt concentration beyond which phase separation into a dilute phase and a complex coacervate phase is suppressed. It can be seen that the critical salt concentration strongly depends on charge density. A similar dependence of critical salt concentration on polymer chain length was found by Chodanowski and Stoll in Monte Carlo simulations [263].

Thus, despite decades of extensive research, control of PEC structure and properties is still a challenge, in contrast to the above described IPCs between complementary polymers and telechelic oligomers, which act as noncovalent crosslinkers and plasticizers.

As stated above, for proper pressure sensitive adhesion the cooperative process of both IPC and PEC formation should be interrupted at an intermediate stage, so that cohesive interaction energy due to hydrogen or electrostatic bonding could be counterbalanced with large free volume within self-assembled supramolecular network PSA structures. In this respect, using a sufficiently high salt content in PEC-based PSA can be regarded as a useful tool to control the free volume. However, improving viscoelastic properties of the PSAs by incorporation of low molecular weight inorganic electrolytes has been shown to inhibit the tack (adhesive bond-forming property). Nevertheless as the data on polybase–polyacid blend stoichiometry demonstrate, the complex becomes enriched with free volume as the PEC components are taken in the ratio far apart from the 1:1 composition.

Summing up above presented fundamental mechanisms of IPC and PEC formation, we have drawn following general principles of PSA production:

1. Selection of polymers bearing in their recurring units comparatively weak proton-donating and proton-accepting groups;
2. Employment of random copolymers wherein reactive monomer units are diluted with inert units;
3. Mixing the polymers in amounts that strongly deviate from a 1:1 stoichiometric ratio;
4. Using the polymers of disparate chain lengths;
5. Blending the polymers in viscous media: either in concentrated solutions or in melts;
6. Avoiding local supersaturations in the course of polymer mixing;
7. Utilizing the copolymers preferentially forming relatively weaker hydrogen bonds as the materials of choice.

5. Cohesive interaction forces between reactive functional groups in electrostatic and hydrogen-bonded interpolymer complexes governing molecular mechanisms of complexation, elasticity and adhesion

Many macroscopic processes and phenomena in condensed phases, such as mechanisms of IPC formation, polymer adhesion and elasticity, are driven by intermolecular interactions that extend beyond the basic pair-wise adhesive interactions of functional groups. The spectrum of these interactions ranges from the long-range forces that by necessity involve large ensembles of functional groups, to polymer deformation processes that involve constant breaking and reforming of noncovalent bonds at different length and time scales. Often these interactions are accompanied by substantial energy dissipation, and thus rigorous quantitative treatment of these events becomes a considerable challenge.

In this section, we will focus on three basic problems:

1. Molecular mechanisms of IPC self-assembly expressed in the terms of bonding forces;
2. Elastic behavior of single polymer chain studied by single-molecule force spectroscopy (SMFS).
3. Understanding the origin of adhesion at the level of single macromolecules.

Chemical Force Microscopy (CFM), also known as single-molecule force spectroscopy (SMFS), provides an excellent opportunity to probe these events with an unprecedented degree of chemical specificity. SMFS has been widely used in exploring the intra- and intermolecular interactions at the level of single molecules, therefore providing a lot of information about the nanomechanics of single polymer chain which is not available by conventional methods [264–270].

This section describes the progress in applying SMFS techniques for measuring equilibrium and time-dependent force profiles of molecular interactions, which has led to a greater understanding of the origin of interfacial forces in adhesion. Measurements of force profiles with chemically modified probes are more appropriately termed 'chemical force spectroscopy' (CFS) (with the whole spectrum of 'force vs probe-surface distance' dependences), while the term 'chemical force microscopy' (CFM) implies chemically sensitive imaging with such probes. While the names of Single Molecule Force Spectroscopy (SMFS), Chemical Force Spectroscopy (CFS), Chemical Force Microscopy (CFM), Dynamic Force Spectroscopy (DFS), Atom Force Microscopy (AFM), Scanning Force Microscopy (SFM) have been used interchangeably in the literature to describe the force–distance experiments in testing the strength of weak chemical bonds, we will use the above CFS nomenclature to make the distinction [271,272].

5.1. Probing the strengths of intermolecular bonds

For testing the strengths of noncovalent chemical bonds, SMFS techniques utilize scanning force microscope (SFM). A chemically modified SFM tip interacts with a functionalized polymer surface (Fig. 27, [273]). The tip is coated with a thin layer of gold, which has been modified with a self-assembled monolayer of ω-functionalized alkanethiols. The wide range of functional groups that can be incorporated in these monolayers allows one to tune the chemical character of the tip; thus, by tuning the tip's surface free energy, the type and strength of the interactions with functional groups at the polymer surface can be controlled over a broad range.

Aside from synthetic polymers, the SMFS method has been also successfully used to explore weak interactions in cell biology, such as ligand–receptor bonds, lipid anchoring in membranes, unfolding of immunoglobulin (Ig) domains in the muscle protein titin and in recombinant proteins, cooperative unbinding of short DNA duplexes, etc. [274].

At the outset, it is important to define the relevant length, force, and energy scales. The length scale for molecular dimensions and interactions is obviously the nanometer (nm = 10 Å). One nanometer is comparable to

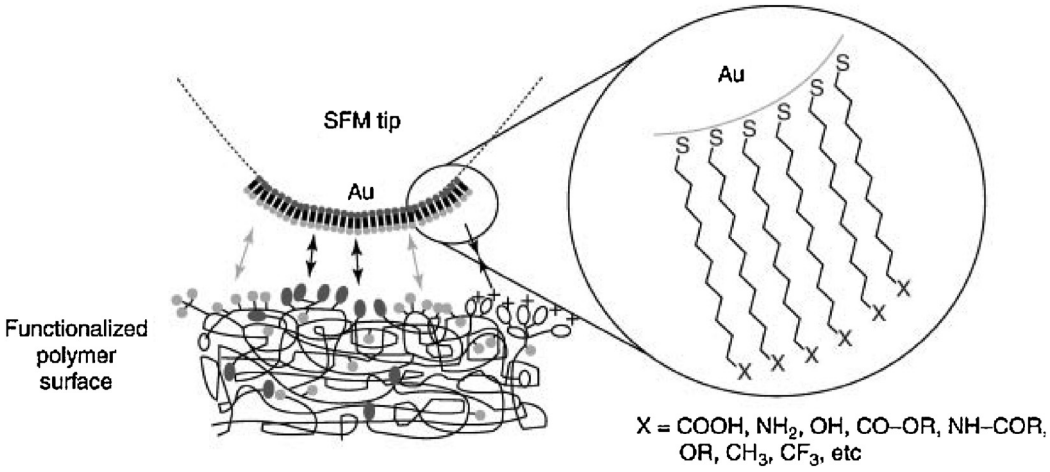

Fig. 27. Schematic illustration of probing the strength of chemical bonds with the SMFS technique. [273], Copyright 2004. Reproduced with permission from John Wiley & Sons Inc.

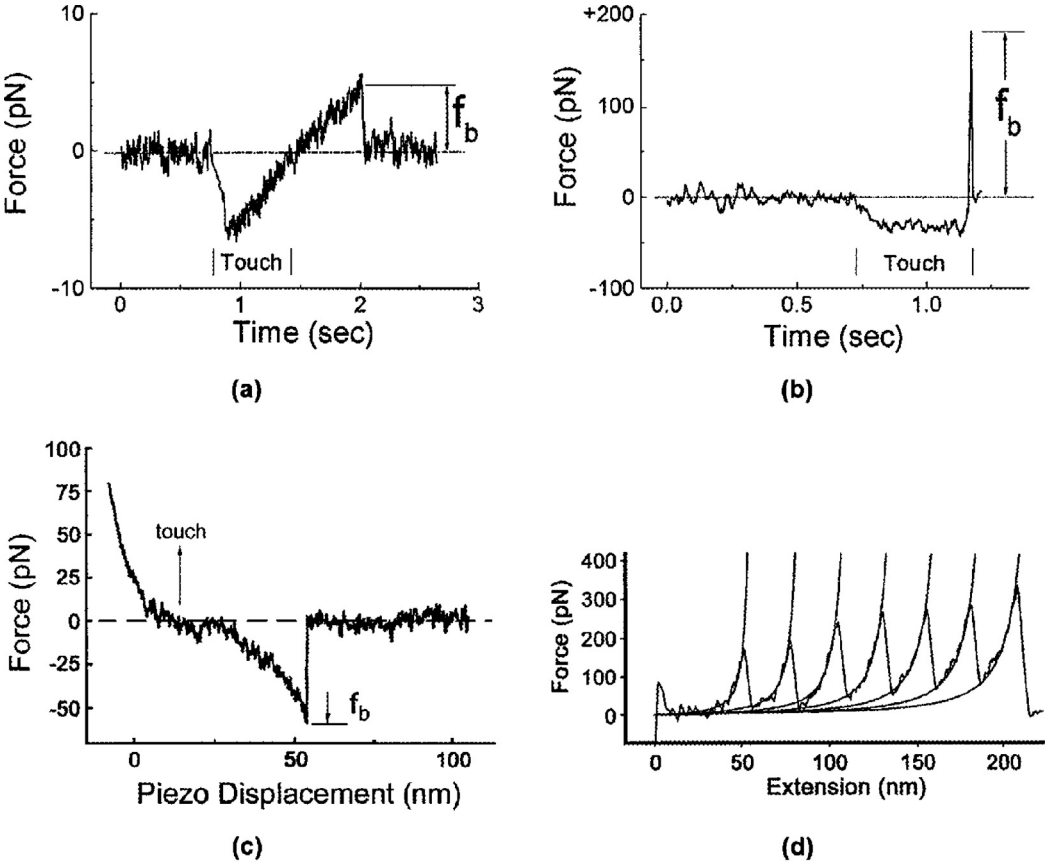

Fig. 28. Rupture of single bonds with ultrasensitive force probes. (a, b) Steady loading of bonds with a micron-size glass tip decorated with a specific carbohydrate ligand in contact with a second glass microsphere decorated with a receptor. (a) Moved toward the tip, contact (touch) by the test particle was sensed at a force of ~5 pN and fed back to signal retraction of the test particle. Slow retraction exposed a bond that held the tip to the test particle for ~0.5 sec and broke at $f_b \sim 5$ pN under a loading rate of ~10 pN/s. (b) Similarly moved to contact the tip, a test particle was stopped, paused for ~0.5 s after sensing a force of ~30 pN, then retracted at high speed. Here, a bond held the tip to the surface for ~0.003 s and broke at higher force $f_b \sim 180$ pN under the extremely fast loading rate of ~60,000 pN/s. (c, d) Nonsteady loading of bonds through soft polymer linkages to stiff atomic force cantilevers AFM. (c) A substrate decorated with PEG-linked strands of short DNA was retracted after contact with an AFM tip decorated with complementary PEG-linked strands of DNA (taken from Strunz et al, [275]). The formation of a duplex resulted in tensile forces (negative in the convention of AFM) that increased steeply as the linkage was stretched beyond 50 nm at a speed of 100 nm/s. The asymptotic stiffening is consistent with the 30 nm lengths of the PEG chains. (d) The famous saw-tooth pattern of force versus extension obtained from unfolding Ig domains in a recombinant construct of 8-Ig domains under constant pulling speed with an AFM (taken from Rief et al. [276]). Each unfolding event produced a precipitous drop in force and added ~30 nm to the contour length. The curves superposed on each event are correlations with the worm-like chain model for polymer elasticity.
[274], Copyright 2001. Reprinted with permission from Annual Reviews Inc.

spacing of molecules at a concentration of ~1 mole/liter. In the case of force, weak noncovalent bonds break in the piconewton (pN) range. One piconewton is the gravitational force generated by about one ten-billionth of a gram (10^{-10} g) which is ten thousand-fold smaller than what can be measured with an analytical microbalance. Together, the product of length and force scales provides the appropriate scale for energy-thermal energy k_BT – which is ~4 pN·nm at temperatures ~300 °K or ~0.6 kCal/mol (~2.5 kJ/mol) for Avogadro's number (~6×10^{23}) of molecules [274].

With few exceptions, tests of bond strength with force probes follow a common approach. The tips and substrates are first decorated with reactive molecules using methods that vary from serendipitous physisorbtion to specific covalent attachment through heterobifunctional polymer spacers and attachment mediated by high-affinity noncovalent complexes. Once prepared, the probe and substrate are repeatedly brought to/from contact by steady, precision movements. If decorated with a very low density of reactive sites, contact between the probe tip and the test surface will only produce an occasional bond. When a rare bond has formed, the tip is held to the substrate during separation of the surfaces and the transducer is stretched. Bond rupture is signaled by rapid recoil of the transducer to its rest position with no intervening arrests. Rupture force is quantified by the maximum transducer extension. Histories of force over the course of approach–touch–separation with formation and rupture of a bond are demonstrated in Fig. 28a and b. After hundreds of touches, the few detachment forces are cumulated into a histogram and the peak (most likely force for rupture) establishes the statistical measure of bond strength. Bond forces are always spread in value, and the most frequent force depends on how fast the bonds are loaded. The subtle feature of the generic

method is that the force experienced by an attachment is not constant but increases in time. As shown by comparison of Fig. 28a and b, bonds under slow loading have long lifetimes but only withstand small forces, whereas bonds under fast loading have shorter lifetimes and withstand larger forces. Molecular structures associated with a bond play an important role in the rate of force application to the bond. Bonds held by polymer-like connections experience highly nonlinear loading dynamics (Fig. 28c and d). Rupture occurs most often in the asymptotic regime as the separation distance approaches the stretched polymer chain length where the force diverges [274].

An extensive and systematic SMFS study of hydrogen bonding, van der Waals, and Coulombic interactions between tip and substrate, both of which have been modified with a variety of functional groups (CH_3, OH, NH_2, COOH, $CONH_2$), has been presented in the classical research by van der Vegte and Hadziioannou [277]. The interactions are quantified in terms of their adhesion forces. The Johnson–Kendall–Roberts theory of adhesion mechanics [278] has been applied to deduce single-bond forces, the number of interacting molecules, and the surface and interfacial free energies.

The force interaction between a functionalized tip and a chemical functionality on the surface was probed via force–distance curves. The attractive force in the unloading part of the force–distance curve reflects the intermolecular adhesion between tip and sample. Well-defined and highly reproducible model substrates and probes were prepared, using COOH, OH, NH_2, $CONH_2$, and CH_3 functional groups. The force–distance dependences were measured for the various tip-sample combinations, reflecting for the *uncharged* functional groups, the hydrogen bonding (e.g., COOH—$CONH_2$, OH—NH_2, etc.) and the purely van der Waals interactions (e.g., CH_3—OH, CH_3—CH_3, etc.).

As a result, distributions of adhesion forces were obtained, which are depicted in the histograms of Fig. 29 for the $CONH_2$-modified tip. From this distribution, the numerical average and standard deviation were calculated. All possible tip-sample interactions were characterized by measuring their adhesive force distributions. The mean adhesive force values in nN for the various tip-sample combinations are summarized in Table 5.

For a CH_3-modified tip, for which only van der Waals interactions play a role, small adhesive forces are found, compared to the hydrogen-bonding capable tips (e.g., OH, NH_2, COOH, and $CONH_2$ tip). As expected [278], the cohesive CH_3—CH_3 van der Waals interaction is found to be larger than the van der Waals forces for dissimilar pairs, e.g., CH_3—COOH. In the case of an introduced hydrogen bond, e.g., for a COOH or NH_2 tip, again the pure van der Waals interaction with a CH_3-model surface is found to give the lowest adhesive force, whereas the observed trend in hydrogen bond formation for OH-, NH_2-, COOH-, and $CONH_2$-model surfaces is found to coincide with the trend in hydrogen bond energies.

The Johnson–Kendall–Roberts (JKR) theory of adhesion mechanics [279] can be applied to these systems and adequately describes the measured data. The use of a variety of functionalized tips should give a better insight into the applicability of the JKR theory.

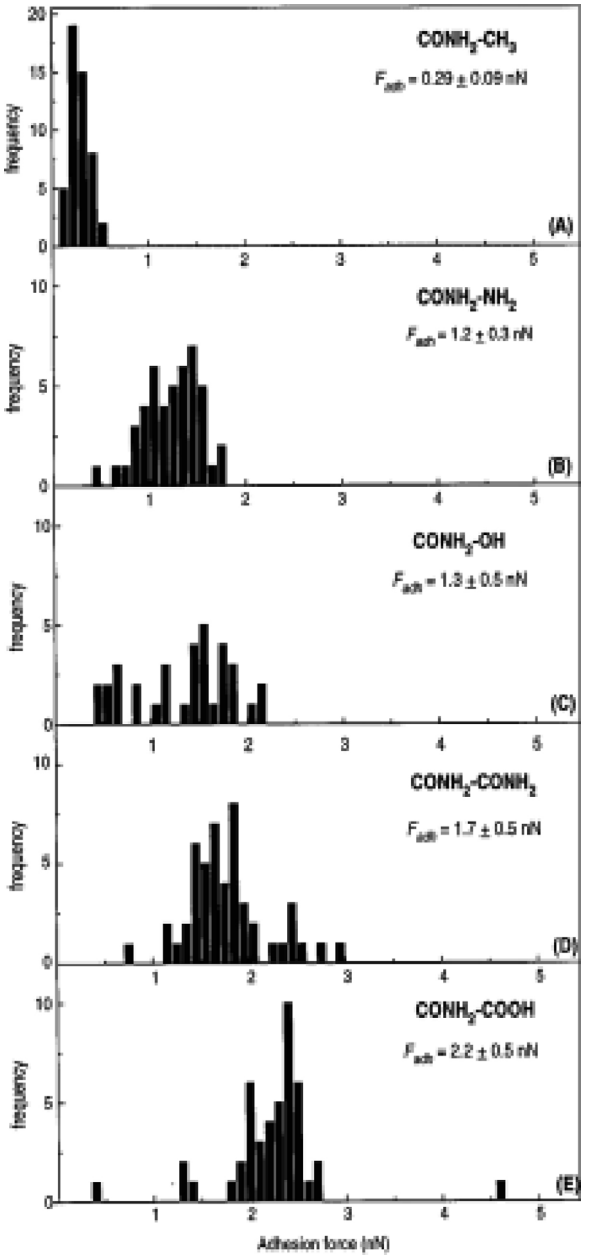

Fig. 29. Histograms of the adhesion force distribution for a $CONH_2$-functionalized tip on the various model substrates: (A) CH_3-functional SAM, (B) NH_2-functional SAM, (C) OH-functional SAM, (D) $CONH_2$-functional SAM, (E) COOH-functional SAM. Each histogram was constructed from at least 50 force-distance measurements in ethanol. [277], Copyright 1997. Reproduced with permission from the American Chemical Society.

The JKR theory describes the adhesion between a spherical tip 1 and a flat surface 2 in a medium 3. The adhesion force F_{adh} is given by the following equation:

$$F_{adh} = -\left(\frac{3}{2}\right)\pi R W_{12} \quad (12)$$

where W_{12} is the work of adhesion to pull the tip off the sample and R is the radius of curvature of the tip. W_{12} can

Table 5
Mean intermolecular adhesion forces (in nN) for each functionalized tip-substrate combination[a] used in [277].

Tip	Substrate				
	CH_3	OH	NH_2	COOH	$CONH_2$
CH_3	0.9	0.3	0.3	0.3	0.3
OH	0.1	0.9	1.2	1.2	1.4
NH_2	0.2	0.5	0.8	0.7	0.9
COOH	0.7	1.2	1.2	1.3	2.2
$CONH_2$	0.3	1.3	1.2	2.2	1.8

Data from [277].
[a] All measurements were performed in ethanol. The values represent the average adhesive forces out of 50 f/d curves. The experimental error in the measurements is approximately 20%.

be expressed in surface free energies: $W_{12} = \gamma_{13} + \gamma_{23} - \gamma_{12}$, where γ_{13} is the tip surface free energy in equilibrium with the medium (in cited measurements ethanol), γ_{23} the sample surface free energy in equilibrium with the medium (ethanol), and γ_{12} the interfacial free energy of the tip-sample contact interface. For identically functionalized tip-sample combinations, e.g., OH–OH or CH_3–CH_3, the work of cohesion is $W_{12} = 2\gamma$, where $\gamma = \gamma_{13} = \gamma_{23}$ is the surface free energy of the particular surface functionality against the medium (ethanol), the interfacial free energy γ_{12} being zero.

To check the validity of the JKR theory, an adhesion force of $F_{adh} = 0.82$ nN for a CH_3–CH_3 tip-sample pair was calculated on the basis of Eq. (12). This value is in good agreement with the measured value of $F_{adh} = 0.9 \pm 0.3$ nN.

The JKR theory has been applied to calculate the surface free energies and the interfacial free energies of all possible tip-sample combinations and the results are summarized in Table 6. From the values of γ in Table 6 it is clearly seen that hydrogen bond interactions (e.g., $CONH_2$—COOH) have small positive or even negative and thus favorable interfacial energies, which lead to high adhesive forces, whereas purely van der Waals interactions such as CH_3—$CONH_2$ exhibit high interfacial free energies (resulting from unfavorable contacts), which account for their small adhesive forces [264].

To calculate single-bond forces, the JKR theory was used to estimate the number of interacting molecules between the modified tip and sample. The number of interacting molecules can be calculated from the radius a of a spherical contact area at pull-off, for which JKR theory gives:

$$a_s = \left[\frac{3\pi W_{12} R^2}{2K}\right]^{1/3} \quad (13)$$

Table 6
Surface and Interfacial Free Energies (in mJ/m^2) (γ_{13} against ethanol) for all possible tip-substrate combinations, calculated from the measured adhesion forces using the JKR theory of adhesion mechanics.

Functional group/medium	Surface free energy, γ_{13}	Interfacial free energy, γ_{12}
CH_3	2.5	
OH	3.0	
NH_2	2.8	
COOH	4.5	
$CONH_2$	5.3	
CH_3-OH		4.4
CH_3-NH_2		3.8
CH_3-COOH		4.8
CH_3-$CONH_2$		6.1
HO-NH_2		−1.9
HO-COOH		−1.7
HO-$CONH_2$		−2.0
H_2N-COOH		−2.4
H_2N-$CONH_2$		0.6
HOOC-$CONH_2$		−6.0

Data from [277].

wherein K is the elasticity modulus of the tip and sample, R is the radius of curvature of the tip, and W_{12} is the work of adhesion to separate tip and sample.

Single chemical bond forces are calculated from the determined number of interacting molecules using the average adhesion forces for every tip-sample combination and are summarized in Table 7. The trend observed for the average adhesive forces, depending on the nature of the interaction between tip and sample, is exactly reflected in the single bond forces [277].

The use of ionizable functional groups like COOH, NH_2, OH, and $CONH_2$ in molecular adhesion force measurements has allowed the direct evaluation of charge–charge interactions and the determination of the acid–base

Table 7
Single chemical bond forces (in pN) for every tip-substrate combination, calculated on the basis of the JKR theory of adhesion mechanics.[a]

Tip	Substrate				
	CH_3	OH	NH_2	COOH	$CONH_2$
CH_3[b]	81	57	59	61	60
OH	50	101	113	112	117
NH_2	54	88	98	95	100
COOH	95	109	105	114	137
$CONH_2$	62	110	102	125	120

Data from [277].
[a] All bond strengths apply to measurements in ethanol.
[b] Although the van der Waals interaction is not a "two-center" bond interaction in this experimental setup, the calculated values for F_{single} presented in this table represent an effective binding force experienced by the molecular pairs and are listed for comparison reasons.

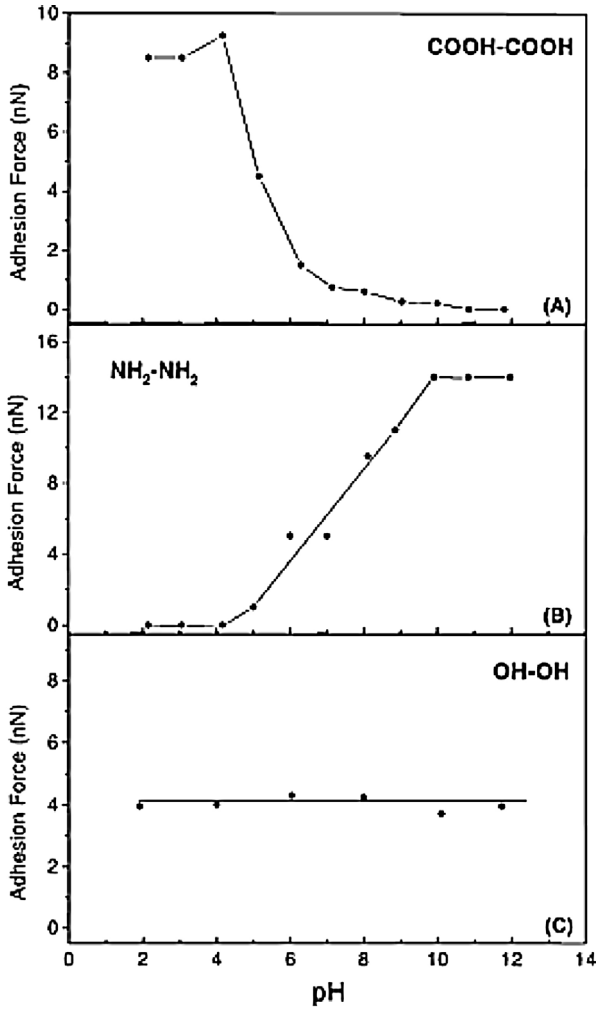

Fig. 30. Adhesion forces as a function of the pH at constant ionic strength: (A) COOH—COOH tip-substrate combination, (B) NH_2—NH_2 tip-substrate combination, (C) OH—OH tip-substrate combination.
[277], Copyright 1997. Reproduced with permission from the American Chemical Society.

behavior of surface acid and base groups [280]. The ionization behavior of surface-bound carboxylic acid (COOH) groups was directly measured by performing pH-dependent adhesion force measurements of the COOH—COOH tip-substrate combination, while maintaining a constant ionic strength. The measured adhesion force as a function of the pH of the medium is presented in Fig. 30A [277]. The plot shows a sharp decrease in adhesive force when the pH of the medium is increased and data points follow a curve that resembles a general titration curve for acids as was obtained from contact angle measurements. The pH-dependence can be understood considering the nature of the interaction between tip and substrate COOH groups. At low pH levels (pH = 1–4), the acids groups are protonated and hydrogen bonding is essentially responsible for the magnitude of the measured adhesion force. As the pH of the medium increases, the COOH groups gradually get deprotonated and become negatively charged. Because tip and sample bear the same functionality COOH, both tip and sample become negatively charged, which results in a repulsive Coulombic contribution to the total adhesive force acting between tip and sample. As more COOH groups become deprotonated with increasing pH, the larger is this repulsive contribution, resulting in a decreasing adhesive force. At pH = 10, the total adhesive force becomes zero and only Coulombic repulsion can be measured at still higher pH.

The same pH-dependent measurements were performed to determine the base behavior of surface-bound amine. The results are shown in Fig. 30B. For the NH_2 group, the expected pH-dependent behavior is found, opposite to the behavior of acidic COOH groups. An increase in adhesive force with increasing pH is found, i.e., at low pH levels, both tip and substrate are positively charged (NH_3^+ groups) resulting in electrostatic repulsion, whereas at higher pH levels, the NH_2 groups are recovered, changing the tip-substrate interaction into an attractive hydrogen-bonding interaction.

In order to assess the acid behavior of surface hydroxyl (OH) groups, an OH—OH tip-sample combination was employed in the pH-dependent adhesion force measurements. The results are given in Fig. 30C. A nearly pH-independent adhesion force was obtained, which indicates that there is no detectable acid behavior (ionization) of surface OH groups in the pH regime studied.

More recently Cranford et al. performed atomistic-level molecular dynamics (MD) studies to investigate the tunable adhesion properties of a polyelectrolyte complex in order to elucidate the complexation and electrostatic cross-linking behavior of the constituent polymers of polyelectrolyte multilayer (PEM) systems [281].

Later Gaub et al. reported on the applicability of the SMFS technique for measuring the strengths of covalent bonds [282]. The authors have found that the Si—C bond ruptured at 2.0 ± 0.3 nN, whereas the sulfur–gold anchor ruptured at 1.4 ± 0.3 nN. Thus, the SMFS technique enables direct and illustrative evaluation of the strength of chemical bonds. The forces required to rupture C—C and C—O covalent bonds were estimated theoretically as a function of bond lifetime and found to range from 6.1 to 2.5 and from 6.5 to 2.5 nN, respectively, as the lifetime varies from 1 ps to 10^{12} s [283–285]. It is of interest that the rupture strength of highly flexible C—O bonds is somewhat higher than C—C bonds.

The strength and length scale of hydrophobic interactions were also directly measured by SMFS in several experimental studies [286–288] and reviewed in [264,266]. Adhesion forces between tips and substrates modified with SAMs terminating in CF_3, CH_3, OCH_3, CH_2Br, OH, COOH, $COCH_3$, $CONH_2$, and NH_2 groups have been evaluated in organic and aqueous solvents and inert dry atmosphere. The results are reviewed in [266,271,289]. Even a quick glance through these data shows that the notion of determining a well-defined bond strength for a particular functional group pair interaction is too simplistic. Interaction forces measured between the same functionalities in different solvents and media can differ by almost an order of magnitude; and, even more troubling, measurements performed by different research groups using similar probe functionalization in the same solvent

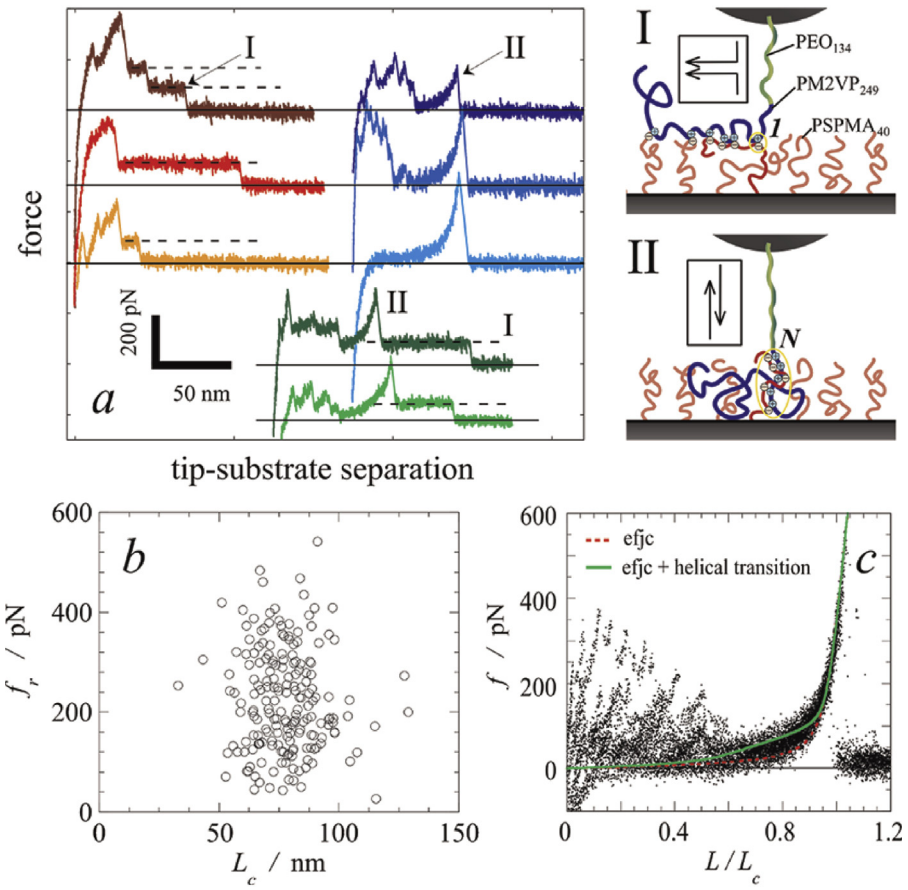

Fig. 31. Disruption of ionic bonds between a single polycation and a polyanionic brush measured by SMFS. (a) Tip retract curves show disruption of a zipper of ionic bonds, one at a time (I) and simultaneous disruption of cooperative complexes with multiple bonds (II). These curves are measured for the same tip-substrate combination at 1.0 M salt concentration. (b) Distribution of rupture forces and contour lengths of 200 type II events at 1.0 M salt concentration. (c) Rescaled overlay of 30 F-D curves with a type II event and fits to the extensible freely jointed chain (EFJC) model (dotted line) and the EFJC model with a helical to planar transition of the PEO block (solid line).
[291], Copyright 2012. Reproduced with permission from the American Chemical Society.

sometimes produce different results [271]. It is clear that the measured interaction force can be influenced by many different parameters: tip and substrate material, medium, temperature and testing regime. In this connection, the results of SMFS measurements cannot be regarded as absolute data. Nevertheless if the tests are performed by the same research team, using the same instrument and experimental conditions, as e.g., the measurements of van der Vegte and Hadziioannou [277], they are quite informative and indicative for comparative examination of various materials.

5.2. Self-assembly of interpolymer and polyelectrolyte complexes examined with single-molecule force spectroscopy

In this section we consider PECs on a single-molecule level. The ultimate self-assembling system forms designed structures rapidly, reversibly and controllably [290]. In aqueous systems, attractive electrostatic interactions have proven to be very promising as a driving force for self-assembly [213]. The strength of these interactions can be tuned continuously by screening the charge interactions and by changing the dielectric properties or the temperature of the medium. Disassembly can be induced easily by increasing the salt concentration [213,215,222,223,237,238,254–258,263].

Recently Spruijt et al. [291] performed direct SMFS measurements of the strength of single ionic bond between a cationic diblock copolymer and an anionic polymer brush. In this study (poly(N-methyl-2-vinylpyridynium iodide)-block-poly(ethylene oxide), $PM2VP_{249}$-b-PEO_{134}, was covalently attached to a silicon nitride AFM cantilever by its PEO-end, which acts as a neutral, flexible linker, while the PM2VP block is positively charged. The cantilever was then brought in contact with a substrate on which an anionic poly(3-sulfopropyl methacrylate) brush ($PSPMA_{40}$) was grown. Upon contact, the oppositely charged polyelectrolytes formed complexes consisting of one or multiple ionic bonds. The strength of these bonds was measured in aqueous solutions at various salt concentrations.

Fig. 31a shows some examples of force–distance curves for a salt concentration of 1.0 M [291]. Because of both the polydisperse nature of the polymer and the uncontrolled

stretching point of an AFM tip, the apparent contour lengths of polymer chains L_c may vary. The distance L values are therefore normalized so that different curves can be compared [270].

The measured interactions due to polyelectrolytes come in two characteristic types. In a part of the obtained F–D curves constant force plateaus were found (type I). These plateau regions were attributed to the continuous disruption of successive bonds, one by one, in a zipper-like fashion. In a reviewed particular case, such a zipper-like disruption of single bonds is expected when the polymer on the AFM tip binds to an oppositely charged polymer in the brush in a parallel fashion as depicted in Fig. 31a-I. Alternatively, the polymer attached to the tip may form single ionic bonds with several brush polymer chains, as if it was adsorbed on top of the brush. When the tip is retracted, the linker is stretched and a force is exerted on the first ionic bond. Upon failure, partial relaxation of the stretched polymer occurs and only part of the built-up load is transferred to the next ionic bond. This bond in turn breaks at a similar load, resulting in a plateau of constant force during separation [291].

Another part of F–D curves display a characteristic polymer stretching before a rupture event (type II). These rupture forces are typically much larger than the rupture forces of type I events at the same salt concentration. This must mean that rupture involves multiple ionic bonds between the same two polymers, in such a way that the applied force is shared between the bonds, i.e., a shear alignment of antiparallel polymer chains (Fig. 31a-II) [291]. Combinations of modes I and II are possible, since part of the long polymer on the AFM tip can bind antiparallel to a brush polymer chain (II), while another part can bind a second brush polymer in a parallel fashion (I). The authors attributed both rupture modes to interactions of single polymer chains with the brush on the substrate.

If the rupture events shown in Fig. 31a indeed correspond to the breaking of ionic bonds between the oppositely charged polyelectrolytes, then their magnitudes should be highly sensitive to the concentration of added salt. Indeed, the rupture forces of both type I and II events have been found to decrease with increasing salt concentration, as shown in Fig. 32 [291]. The critical point is reflected by a sudden jump to a lower mean rupture force between 1.2 and 1.5 M for both types of events, after which the mean rupture force remains approximately constant up to 3.0 M. The nonzero residual rupture force beyond 1.5 M salt was attributed to nonelectrostatic interactions between the two types of polymers that do not depend on salt concentration. Ionic bonds have strongly salt-dependent strength and collectively they can become as strong as covalent bonds.

Fig. 33 demonstrates the force histograms for type II rupture events for one, two, and three layers on the substrate. With two or more layers type I events were no longer found. Interestingly, the rupture force of the type II rupture events decreases significantly with the number of layers [291]. This experiment is of great importance to gain a molecular insight into the molecular mechanisms of adhesive debonding for the adhesive joints of PSAs based on

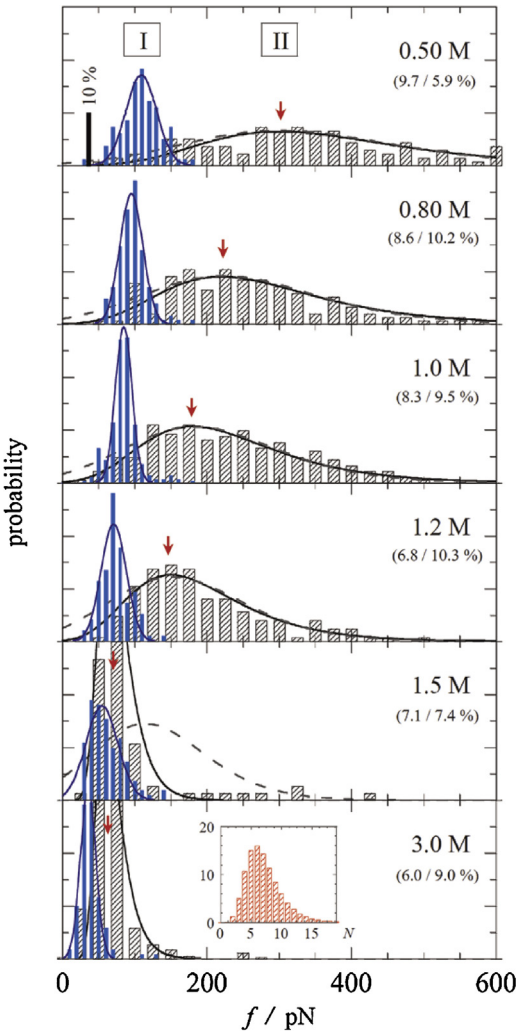

Fig. 32. Histograms of type I and II ionic bond rupture forces at various salt concentrations. For each histogram at least 1200 F-D curves were analyzed. The percentages indicate the fraction of rupture events (I/II). Solid lines are Gaussian (type I) and Gumbel (type II) fits of the data. Dashed lines are predictions of the distribution of type II rupture forces with molecular rupture mode for ionic bonds [278]. The arrows indicate the most probable rupture force of type II rupture events. The inset shows the Gumbel probability distribution of the number of ionic bonds in a type II complex used as a model for the force distribution data of type II rupture events. [291], Copyright 2012. Reproduced with permission from the American Chemical Society.

polyelectrolyte complexes, which are considered in Section 6 of the present review.

Ionic bonds are reversible and highly tunable connections. For the N-methyl-2-vinylpydidinium/3-sulfopropylmethacrylate bonds considered in [291], the strength ranges from roughly 1 k_BT close to the critical salt concentration to over 6 k_BT at low salt concentration. The cooperativity of the ionic bonds further amplifies this difference. As a result, the lifetime of ionic bonds in natural aqueous systems can range from milliseconds for a single ionic bond at high salt concentration to tens of years for small complexes of five ionic bonds at low salt concentration. This versatility offers many opportunities for use of

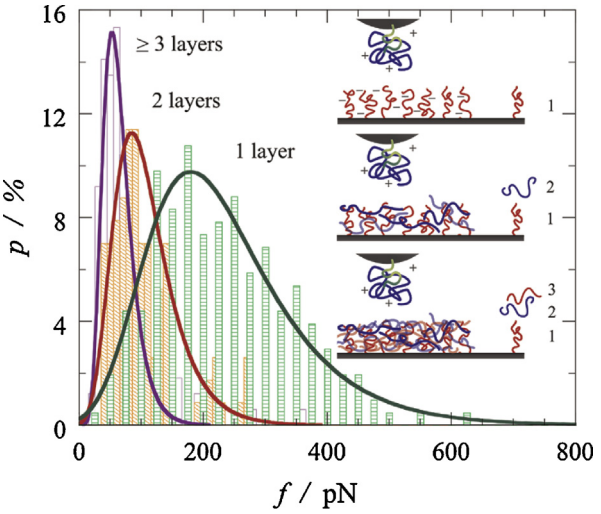

Fig. 33. Histograms of rupture forces of a PM2VP249 cationic block from a substrate with a varying number of polyelectrolyte "layers" at 1.0 M salt concentration. One layer corresponds to a PSPMA brush only, two layers indicate that free PM2VP is adsorbed on the PSPMA brush, and three layers indicate a second adsorption step with free PSPMA. Solid lines are Gumbel fits to the data.
[291], Copyright 2012. Reproduced with permission from the American Chemical Society.

ionic bonds in innovative materials. Under the right conditions a small complex of ionic bonds may be stronger than a covalent bond [282], yet remains completely reversible: it can be "unlocked" at any time by addition of salt [294]. When disassembly involves separation of the charges, much higher forces are required than for multilayer assemblies [291].

In another research article by Spruijt et al. [294] polyelectrolyte brushes of either positive or negative charge were grown on particles to prepare hairy colloids. For measurements of the interactions between oppositely charged particles, cationic particles were immobilized onto an anionic brush, grafted onto the substrate. Although all particles aggregate into large clusters at low salt concentrations, this aggregation is completely reversible. When the salt concentration is increased above the critical salt concentration all aggregates redisperse and a homogeneous suspension can be obtained [294]. PEC formation is a time-dependent process. When two oppositely charged polyelectrolyte brushes are brought into contact, they form a small volume of complex coacervate phase between them. Initially, the complex layer is thin, but the energy of ion pair formation and the entropy of counterion release drive growth of this complex phase. Growth involves further interpenetration of the chains, which is slowed down increasingly by friction. As a result, the growth of such complex phases between the two surfaces can easily take minutes [295]. This obviously leads to a transient force between two such surfaces. The salt concentration influences both the driving force for complexation and the friction that slows down the interpenetration, leading to a strongly salt-dependent transient force. In solution and in gels, interpenetration of the brushes between two unlike particles strengthens their connection and restricts their individual mobility. As a result, the aggregation mechanism may change from weak to strong, eventually leading to kinetically arrested gels [294,296].

In order to determine the strength of the cohesive ion–ion pair forces in a polyelectrolyte complex, van der Gucht et al. attached both positively and negatively charged polyelectrolytes as brushes to the solid surface of a colloidal probe (Fig. 34a) [213]. The surfaces were immersed in aqueous solutions with varying salt concentration. During a typical experimental approach-and-retract cycle (Fig. 34a), the brushes come into contact and form a thin complex layer. Initially, the brushes on both sides of the complex layer are compressed, but as the brushes are kept in contact, they start to interpenetrate. This interpenetration is driven by the growth of the complex phase on both sides of the initial layer. When the surfaces are separated again, the polyelectrolyte chains are stretched until enough energy is stored to disrupt the complex phase. In this case, disruption involves breaking all formed ion–ion pairs between the brushes.

The force–distance curves corresponding to this cycle show that the ion–ion pair forces depend strongly on salt concentration. Fig. 34b–d presents a few examples for PTMAEMA and PSPMA brushes. At salt concentrations above 1.5 M the interaction between the positive and the negative brushes is simply repulsive (Fig. 34d). At about 1.5 M, attraction sets in as can be seen in both the approach and retraction curves. This salt concentration is the equivalent of a critical salt concentration for complex coacervate phases. As long as the attraction remains weak, that is, in a narrow window close to the critical salt concentration (e.g., for 1.4 M), an almost reversible approach–retraction cycle is possible (Fig. 34c), when scanning slowly and avoiding extensive compression of the brushes. Reversibility is the result of formation and breaking of ion–ion pairs in the initial contact layer without subsequent growth of the complex phase. The forces exerted to separate positively and negatively charged chains are strong enough to break covalent bonds, showing that the cohesive interactions that hold the complex together are very strong, up to hundreds of k_BT per chain [213].

5.3. Inherent stretching elasticity of single polymer chain

The deformation of polymer chains is a classical problem in polymer science; however, it is very difficult to directly measure the elasticity of a single polymer chain. Recently, AFM has been successfully applied to study the deformation of individual polymer chains. The SMFS technique has been implemented in Gaub's group [276,282,292,293,297,298]. Some specific fingerprint information of nanomechanical properties of polymer chains has been obtained, which is not available by conventional methods [299–303].

The stretching elasticity of a single polymer chain is a classic problem which still arouses broad interest [265,270,304]. On the basis of the pioneering work of Flory and others [305], several models have been proposed to describe the single-chain behavior of polymers. Among others, the freely jointed chain (FJC) model [280,305], the wormlike chain (WLC) model [306,307], and the freely

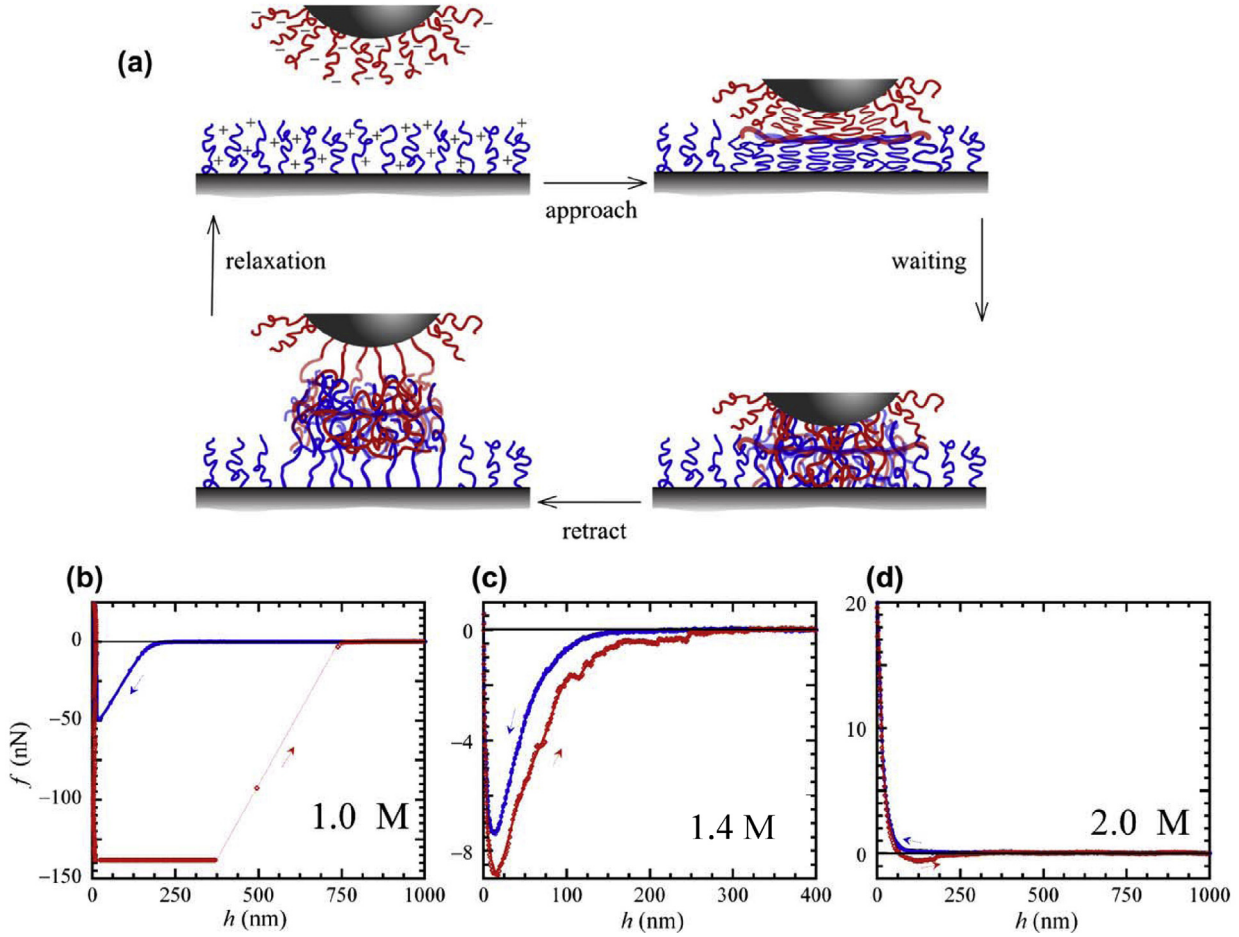

Fig. 34. (a) Schematic picture showing the SMFS measurement of the interactions between two oppositely charged polyelectrolyte brushes. (b–d) Measured force–distance curves between a surface covered with a PTMAEMA brush and a surface covered with a PSPMA brush for KCl concentrations of 1.0 M (b), 1.4 M (c), and 2.0 M (d) [198,282].
[295], Copyright 2010. Reproduced with permission from the American Chemical Society.

rotating chain (FRC) model and their modified forms [165,308,309] have often been used in the recent literature. In the past 20 years the many advances in single-molecule experimental methods have provided a good opportunity to test these models [270,281,309,310]. To date, the stretching behavior of many kinds of polymers, including neutral polymers and polyelectrolytes, has been investigated at the single-chain level [281,304].

According to the FJC elasticity model, the polymer is divided into N rigid elements (Kuhn's segments), each exhibiting a length of l_K connected through flexible joints without any long-range interactions. The pulling force (F)–extension (R_z) traces of single polymer chains can be fitted by Eq. (14) [270]:

$$R_z = N \cdot l_K \cdot \left[\coth\left(\frac{F \cdot l_K}{k_B T}\right) - \left(\frac{k_B T}{F \cdot l_K}\right) \right] = N \cdot l_K \cdot L \cdot \left(\frac{F \cdot l_K}{k_B T}\right) \quad (14)$$

where L is the Langevin function. The fit parameters in Eq. (14) are N and l_K.

Being expressed as the pulling force function of extension, Eq. (14) can be presented in the form:

$$F(R_z) = \frac{k_B T}{l_K} L^{-1}\left(\frac{R_z}{N \cdot l_K}\right) \quad (15)$$

Within the framework of the WLC model [311], the $F(R_z)$ function includes two fitting parameters: polymer chain contour length $L = N \cdot l_K$ and persistence length L_p:

$$F(R_z) = \frac{L_p}{k_B T}\left(\frac{R_z}{L} + \frac{1}{4(1-(R_z/L))^2} - \frac{1}{4}\right) \quad (16)$$

The persistence length, like the Kuhn length, is a measure of the flexibility of polymer chain [312,313]. In this way, the pulling force–extension traces by the SMFS provide a lot of valuable information about the elasticity of a single polymer macromolecule [270,309].

In the classical research article by Hugel et al. [314] the SMFS technique was used for the investigation of a single polyelectrolyte chain. Namely, the elasticity of poly(vinyl amine), PVAm, chains and their adhesive debonding (desorption) from solid surfaces was studied as a function

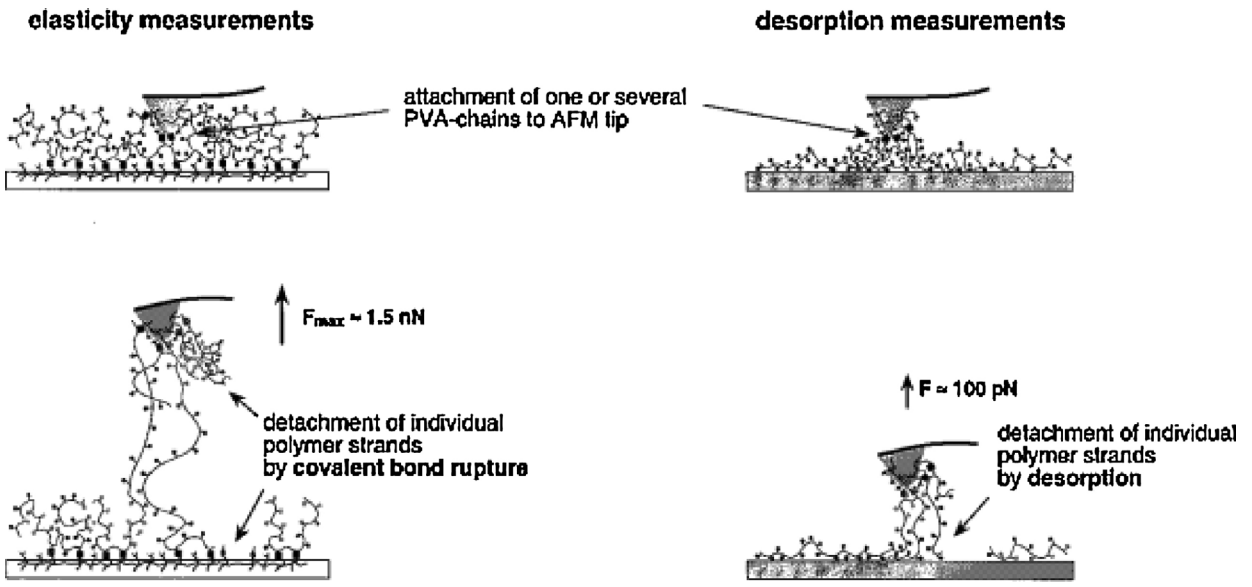

Fig. 35. Comparison of elasticity and desorption experiments.
[314], Copyright 2001. Reproduced with permission from the American Chemical Society.

of the polymer's charge density and electrolyte concentration. Experimental force–distance profiles were fitted by the wormlike chain model, including elastic contributions arising from the stretching of bond angles and covalent bonds. The force–distance curves according to the extended Hookean WLC model are described by Eq. (17) [314]:

$$F\frac{L_p}{k_BT} = \frac{R_z}{L} - \frac{F}{K_o} + \frac{1}{4(1-(R_z/L)+(F/K_o))^2} - \frac{1}{4} \qquad (17)$$

where L is the contour length of the stretched chain (polymer strand) under zero force. The polymer chain bending stiffness is expressed by the persistence length, L_p, and the polymer chain extensibility upon stretching is described by the normalized segment elasticity, K_o. Thus, Eq. (17) contains three fitting parameters: L, L_p and K_o.

Fig. 35 compares the experimental setups to measure single chain elasticity and adhesive debonding. In the elasticity experiment (Fig. 35a), the polymer is covalently fixed to both substrate and AFM tip. In the adhesive desorption experiment (Fig. 35b), single polymer chain is physisorbed to the substrate and only covalently attached to the AFM tip. Detachment in elasticity experiments occurs when a covalent bond ruptures along the stretched polymer strand (nanonewton forces). Upon single chain adhesive debonding the ionic bonds between substrate and polymer break under forces in the piconewton range [314].

For quantitative comparison of the experimental data with theoretical predictions for polyelectrolyte elasticity, the experimental F–D curves were fitted by an extended wormlike chain (WLC) model including linear elastic contributions arising from the stretching of bond angles and covalent bonds, see Eq. (17), [315]. The evaluated single chain elasticity data are presented in Table 8 as a function of polyelectrolyte ionization degree and salt concentration [314]. The increase in linear charge density

Table 8
Persistence length, L_p, and segment elasticity, K_o, of poly(vinyl amine) with different degrees of ionization (Line charge density), measured under conditions of varied salt concentration as obtained from WLC fits to the experimental force–distance SMFS curves.

Ionization degree	C_{salt} (mM)	Persistence length, L_p (nm)	K_o (pN)
10%	5	0.8	5100
	10	0.9	4100
	100	0.95	3600
30%	5	0.45	4800
	10	0.85	4500
	40	1.0	3000
	100	0.9	3700
50%	5	1.45	4000
	10	1.75	4500
	40	1.65	5000
	100	0.85	4000
70%	5	2.0	5200
	10	1.2	5700
	100	1.2	6500

Data from [314].

along the polyelectrolyte chains results in the unfolding of polymer chains and increase of persistence length. Increasing salt concentration has a comparatively weak effect on polymer chain stiffness. The single chain elasticity is reduced with increased salt concentration in partly ionized PVAm and is increased in strongly charged polyelectrolyte due to the screening of electrostatic interaction.

The results, obtained by Hugel et al. [314], illustrate the effect of intramolecular interactions on persistence length of polyelectrolytes. How intermolecular contributions may affect polymer elasticity can be illustrated by the effect of ionic charges on the measured persistence lengths of other polyelectrolytes (e.g., DNA) [270,316]. According to the Odijk–Skolnick–Fixman (OSF) theory [317,318], the

bending rigidity of a polyelectrolyte chain is increased as its like-charged segments electrostatically repel each other. The electrostatic persistence length L_{el} depends on the salt concentration and the polymer charge density [270,318].

It has been shown that the stretching elasticity of a single neutral polymer chain can be influenced by several factors, including the side chain structure, solvent, temperature, and cosolute [301,319–321]. However, it is expected that, in an unperturbed state, the polymer chain should present its inherent stretching elasticity (hereafter referred to as elasticity). Recently Wang et al. [304] utilized the SMFS technique to investigate the single-chain elasticity of neutral polymers with a carbon—carbon (C—C) backbone in a nonpolar solvent, aiming at measuring the inherent chain elasticity of this very important class of polymers. The nonpolar solvent was selected to minimize the effects of intermolecular interactions on chain elasticity. Three kinds of examined polymers were poly(N,N-diethylacrylamide), PDEAm, poly(acryl amide), PAAm, and polystyrene, PS.

Using the freely rotating chain model, FRC, the relationship between the extension (R_z) of a polymer chain and the stretching force (F) can be written in a good approximation as:

$$R_z = L[F] \cdot \left(1 - \frac{k_B T}{2bF}\right) \tag{18}$$

where $L[F]$ is the contour length of the chain at a given stretching force, b is the length of the rotating unit, k_B is the Boltzmann constant, and T is the temperature on the Kelvin scale [322,323].

Note that the chain contour length $L[F]$ is force dependent. Bond angles as well as bond lengths are altered upon stretching. These effects were recently investigated in great depth with an ab initio quantum mechanical (QM) calculation of the C—C backbone elasticity [323]. Upon normalization of the extension in Eq. (18) by the value of the chain contour length at zero force, L_o, one obtains:

$$\frac{R_z}{L_o} = \frac{L[F]}{L_o} \cdot \left(1 - \frac{k_B T}{2bF}\right) \tag{19}$$

where R_z/L_o is the normalized extension of a polymer chain.

The FRC model (Eq. (19)), which is integrated with the quantum mechanical results, is called the QM-FRC model [323].

The force curves of all three kinds of polymers can be superposed well with the QM FRC model. This result confirms that both the size and the polarity of the side chain have no detectable effect on the single-chain elasticity of neutral polymers with C—C backbones under conditions hindering interpolymer interactions between the side chains. This common single-chain elasticity is regarded as the inherent chain elasticity of neutral polymers with C—C backbones [304].

Side-group effects on single chain elasticity of two homologues, poly(acryl amide), PAAm, and its derivative poly(N-isopropyl acrylamide), PNIPAM, were studied with SMFS in aqueous solutions by Zhang et al. [265,324,325]. Based on this study, it is obvious that lager side groups make the polymer chain stiffer [324–326].

The SMFS technique allows probing conformational transitions in polymer chains [270]. In the present review we restrict the discussion to the case of synthetic polymers, omitting abundant theoretical and experimental data on the conformational transitions in proteins and DNA.

Single-chain mechanical properties of poly(N-vinyl pyrrolidone), PVP, were examined by Liu et al. [321]. The force–extension curves of PVP in water deviated appreciably from the behavior obtained in ethanol and tetrahydrofuran, suggesting that the elasticity of PEG individual chains is governed by hydrogen bonding with water. The fitting of the force–extension curves of the PVP chains in DI water with the modified FJC model yields the Kuhn length $l_K = 0.63$ nm, and $K_o = 41{,}580$ pN [321].

The macromolecular elasticity of poly(acrylic acid), PAA, was probed by Li et al. [300]. Good superposition of the normalized force–extension curves was taken as evidence that the elastic properties of the PAA chains scale linearly with their contour lengths. Thus it was deduced that interchain interaction does not contribute strongly to the PAA elasticity, because interchain interactions would scale nonlinearly with the chain length. By fitting the force–extension curves with the FJC model it was established that the PAA macromolecules possess almost identical Kuhn length of 0.64 ± 0.05 nm and a segment elasticity of $13{,}000 \pm 2000$ pN/nm, although the lengths of the PAA filaments varied from 60 nm to more than 1 μm [300].

Unexpected temperature-dependent single chain mechanics was observed for poly(N-isopropyl acrylamide), PNIPAM, in water [301]. The temperature behavior of the PNIPAM aqueous solutions is characterized with the LCST in the vicinity of 32–37 °C. Below the LCST the force curves obtained at different temperatures have no remarkable difference; while above LCST, an unexpected temperature dependent elasticity is observed, mainly in the middle force regime.

Amongst the synthetic polymers probed with SMFS technique, poly(ethylene glycol) [293,302,310] and poly(vinyl alcohol) [303] show transitions between two conformations, which are not observed in apolar media. For the case of poly(ethylene glycol), PEG, the force spectroscopy was carried out in either phosphate buffer saline (PBS), or in hexadecane. It was in the intermediate force regime that the behavior in the two solvents was different. Under 100 pN the PEG chain in water has shown only 80% of the elongation seen in hexadecane. This indicates the presence of a solvent-mediated polymer supra-structure. For PEG in aqueous solution fitting the superimposed force–extension traces demonstrated a Kuhn length l_K of 7 Å and a segment elasticity $K_{segment}$ of 150,000 pN/nm per monomer. The PEG conformational transition could be attributed to a breakdown of the hydrogen bonded solvation superstructure in water upon overstretching the helically folded equilibrium conformation of the polymer [293]. This illustrates how environmental changes may have a strong influence on the elastic response of a single polymer chain and how the manifestation of conformational transitions results from the coupling of intermolecular and intramolecular interactions.

The SMFS examination of poly(vinyl alcohol), PVA, has been described in [299,303]. As is shown in [299], the PVA in aqueous solution exhibits the Kuhn segment length l_K = 6.2 Å and segment elasticity $K_{segment}$ = 17,000 pN/nm. This shows that PVA is much stiffer than PEG.

The WLC model can only describe the elastic behaviors of PVA in water at either low-force regime or high-force regime. This indicates that PVA in water does not assume an ideal random coil conformation, but a suprastructure mediated by the interaction between polymer segments or the polymer–solvent interaction. Hydrogen-bonding interactions are so pronounced in PVA aqueous solution that the WLC model may no longer hold.

To prove the above assumption, the SMFS studies of poly(vinyl acetate), PVAc, were performed [303]. In PVAc, the hydroxyl groups are esterified, and thus the long-range interaction due to the hydroxyl groups is prevented. Interactions between acetate groups in nonaqueous solvents are very weak [327], and it is thus expected that PVAc behaves like an ideal random coil. It was found that the force–extension curves of PVAc were fitted with the WLC model very well, indicating that the PVAc behaves like an ideal random coil.

Earlier studies suggested that PVA exists as a helical structure in aqueous solution due to the hydrogen bonding of hydroxyl groups and that PVA undergoes a helix-coil transition upon increasing temperature [327]. As was shown in [303], a kink in the single-molecule force spectra always occurs at ~200 pN. The elasticity of PVA helix changes dramatically before and after the kink. This indicates that the suprastructure of the PVA undergoes a conformational change from a relaxed to a more stretched helical structure at ~200 pN. When a single PVA helix was repetitively stretched and relaxed, there was no hysteresis, indicating that the conformational change is fully reversible and takes place under equilibrium conditions. When stretching speeds were varied from 0.02 to 10 μm/s, no effect was observed on the force required for the conformational change (~200 pN) or its reversibility. This implies that this conformational change occurs much faster than the experimental time scale [303].

Hydrogen bonds can occur intermolecularly as well as intramolecularly. This is particularly important in macromolecular and biological assemblies, such as proteins and nucleic acids. In the native state of protein and DNA, hydrogen bonds are responsible for stabilizing ordered secondary structures, such as α helices and β sheets in proteins and double helices in DNA. Upon exposure to denaturants (such as urea), the hydrogen bonds (along with hydrophobic interactions) are broken, and thus the ordered secondary structure of proteins is destroyed.

The persistence length of PVAc in 3-heptanone (0.31 nm) is larger than that of "denatured" PVA in urea (0.16 nm). This may be due to the fact that the acetate side group in PVAc is much lager than the hydroxyl group in PVA, and the steric effect of acetate groups may become pronounced and make PVAc stiffer.

A comparison of the normalized force single molecule force spectra has shown that in the high-force regime the slope of the force curve (the stiffness of the molecule) of PVA in water (35,000 pN/nm) is much larger than that of denatured PVA in urea (13,000 pN/nm). This suggests that the suprastructure of PVA in water is a double- or multiple-stranded helix. If the helix of PVA in water were a single-stranded structure, the mechanical stretching of PVA would unravel the suprastructure and stretch the polymer chain to an almost fully stretched state where deformation of the polymer chain is dominated by the stiffness of bond angle potentials and independent of solvent [293]. Hence, the force curve of PVA at high-force regime would then superimpose that of denatured PVA, since denatured PVA is a random coil of a single polymer chain. This, however, was not observed, indicating that the PVA helix in water is a multiple-stranded structure [303]. In contrast to the multiple-stranded helix of PVA in water, PEG exists in water as a single-stranded helix [293].

Thus, for a detailed understanding of the macroscopic properties of polymer materials, in particular viscoelastic behavior and adhesion, it is desired to address the two issues separately: intramolecular forces governing the elastic response of a single polymer chain (including conformational transitions), and intermolecular forces responsible for the stability of supramolecular structures. The SMFS technique is a powerful and insightful tool for these purposes.

5.4. Understanding adhesion and interfacial phenomena on the level of single macromolecules

Pressure sensitive adhesion is very complex macroscopic phenomenon resulting from numerous molecular and nanoscale events. Understanding adhesion phenomena requires an intimate knowledge of the intermolecular forces from which they arise. Although indirect measurements on a macroscopic level have provided significant information on the molecular origin of adhesion, the true nanoscopic nature of the adhesive interaction is accessible only through a direct measurement. At present, our progress in understanding adhesion interactions at the interfaces is closely linked to the development of physical techniques for measuring such interactions. Typical interaction strength ranges from 10 pN for very weak van der Waals interactions to 2–10 nN for a strong covalent bond [278]. The interaction strength also varies significantly, depending on the properties of the surrounding medium. Therefore, an ideal technique for measuring interactions at the interfaces must be capable of measuring forces in the pN to nN range with a sub-nanometer distance resolution under a variety of environmental conditions and in different solvent media. The SMFS is an example of such a technique.

Interpretation of the SMFS experiments is based on a range of theoretical models, described and discussed in reviews by Noy et al. [271] and Vezenov et al. [272]. In addition to above-mentioned the Johnson, Kendall and Roberts theory of adhesion (JKR) [279], such models include Derjagin, Muller and Toporov theory (DMT) [328], Maugis–Dugdale (M–D) approximation [329], revised by Carpick et al. [330], Dzyaloshinskii, Lifshitz, Pitaevskii theory [331] and generally recognized acid–base interaction theory proposed by Fowkes, van Oss, Chaudhury and Good (FOCG) [332].

In order to demonstrate how the SMFS experiment allows one to gain insight into adhesive debonding mechanism at the level of single polymer chain, we turn now back to Fig. 31b and classical research paper of Hugel, Seizt et al. [314]. In their research, the poly(vinyl amine), PVAm, was adsorbed physically onto glass substrates from aqueous salt solutions and the desorption force was measured as a function of salt concentration and PVAm ionization degree. As indicated in Fig. 31b, the weakest links in this system are the ionic bonds between polymer and substrate. Therefore, the resulting force profiles are determined by the detachment of the polyelectrolyte chains from the substrate at forces of several hundred piconewtons while the covalent link to the AFM tip persists to forces up to the nanonewton range [282]. In this case, contact between tip and substrate was established for several seconds in each cycle followed by retraction of the tip until no more adhesive force was detected.

A force–distance trace recorded upon detachment of a single polyvinylamine chain from bare glass substrate is shown in Fig. 36a. In some cases, one loop of the polymer chain is picked up upon covalent attachment to the AFM tip at a random position, such that its two strands bridging between substrate and tip are of different length. While retracting the cantilever, the shorter strand is stretched which gives rise to the characteristic stretching trace at low forces until a plateau region of constant force ($F \approx 50$–100 pN) is observed.

Thus, each observed plateau region can be interpreted as the continuous desorption of one or several polyelectrolyte strands. In Fig. 36a, both ends of the loop are being stretched and desorbed simultaneously from the substrate as the length of the stretched (initially shorter) strand becomes comparable in size to the other strand of the loop. As a result, the required desorption force doubles, as indicated in the recorded trace by a stepwise increase followed by a second plateau region at twice the height of the first plateau. Finally, full desorption of both ends results in rupture of the system and the recorded (adhesive) force drops to zero.

However, the stretching and desorption of a single loop was only the simplest case observed. Fig. 36b shows a force curve which was found for the adhesive debonding of multiple molecules (loops). At short distances, a steep increase of the force resulting from the simultaneous stretching of several polymer strands is recorded. As the distance between tip and substrate is increased, their continuous desorption is again indicated by a plateau of constant force. As the shortest PVAm strand fully detaches from the substrate, a decreasing step in the force profile is measured, followed by the successive detachment of all polymer chains, each reflected by a stepwise decrease in the overall desorption force.

Although most of the recorded traces were more complex than the two most illustrative examples shown in Fig. 36, in all cases the typical plateaus of constant force were observed. In accordance with the discussion of the underlying molecular processes, the step heights were thus interpreted as the contribution of individual PVA strands to the overall recorded desorption forces. Although the simultaneous detachment of two or even three strands was occasionally observed, most of the steps indeed originated from single PVA strands. Thus we can refer to the plateau steps as desorption forces.

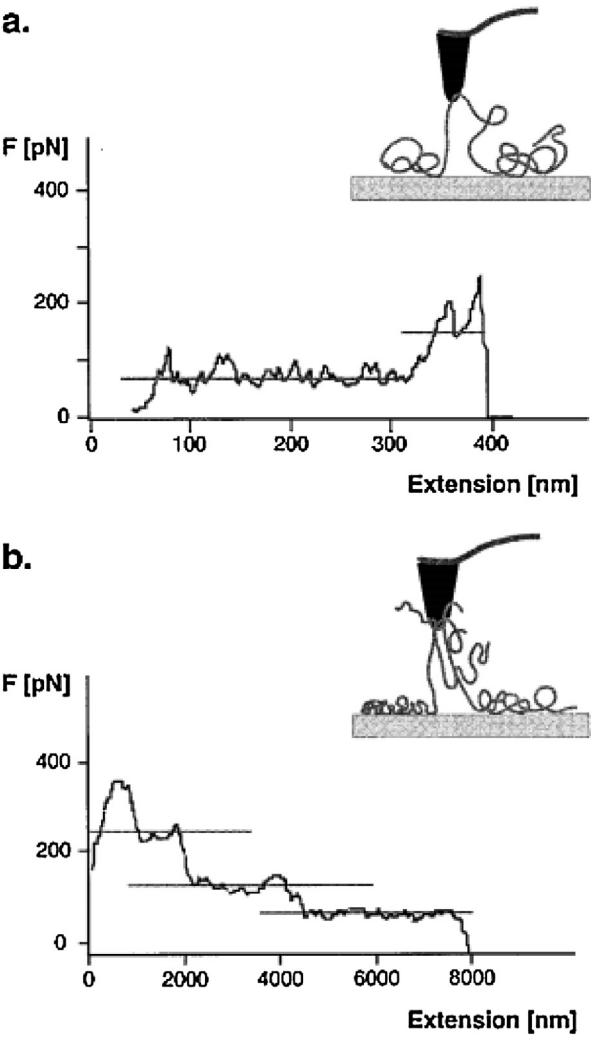

Fig. 36. Typical force-distance profiles measured upon detachment of physisorbed polyvinylamines (PVA) from a charged surface: (a) stretching and desorption of a single loop; (b) stretching and desorption of multiple strands.
[314], Copyright 2001. Reproduced with permission from the American Chemical Society.

The dissociation rate of ionic bonds between the positively charged amino groups of the polymer and the negatively charged surface sites is much faster than the pulling rate. Thus, on the time scale of the SMFS experiment, the polyelectrolyte chain can be considered as a string of constant charge continuously desorbing from the charged substrate against the attractive potential of the surface. The electrostatic contribution to the force that needs to be applied in order to induce this continuous desorption can be quantified as follows. The electrostatic potential, $V^{el}(z)$, of the substrate in electrolyte buffer is given in the Debye–Hückel approximation by

$$\frac{V^{el}(z)}{k_B T} = 4\pi \cdot l_B \sigma \cdot k^{-1} \exp(-kz) \tag{20}$$

in which σ is the surface charge density, k^{-1} the Debye length which describes the screening of the electrostatic potential in polyelectrolyte solution and l_B is the Bjerrum length [278]. Upon desorption of one polymer segment of length a, the entire polymer chain is moved against the electrostatic surface potential; i.e., the separation of each charged segment from the substrate is increased by the distance a. Therefore, the force that needs to be applied for this process can be determined simply from the transfer of one charged segment from $z = 0$ to $z = \infty$ while all other segments stay in place (Fig. 37a) leading to

$$F_{des}^{el} = (4\pi \cdot l_B \cdot k_B T) \cdot \sigma \cdot k^{-1}\tau \quad (21)$$

Thus, at constant surface charge density, a linear dependence of the desorption force on the Debye length, k^{-1} (for constant polymer charge), as well as on the line charge density, τ (for constant electrolyte concentration), is expected. The data obtained for the desorption of PVAm from silica substrates are plotted in Fig. 37b (F_{des} vs k^{-1}) and Fig. 37c (F_{des} vs τ), and their dependence on the given parameters is as predicted.

A decrease in polymer charge density in PVAm (50, 30, and 10% ionization degree) resulted in smaller average desorption forces. As in the elasticity measurements, no significant pH dependence in the range from pH 5–9 was observed [314].

As shown for PVAm (30% ionization) and PVAm (70% ionization), a linear increase in the adhesive desorption force is found with increasing Debye length resulting from the electrostatic interaction between polymer and substrate. By extrapolation to $k^{-1} = 0$, $F_0 \approx 33$ pN is obtained, which can be considered a "zero charge" contribution to the desorption force of PVAm chains from silica. It is independent of electrostatic charges and most likely is dominated by van der Waals interactions between polymer and substrate. In a first approximation, the electrostatic force, F_{el} (Eq. (21)), is therefore supposed to be the only additive term to the overall desorption force, F_{des}, such that

$$F_{des} = F_0 + (4\pi \cdot l_B \sigma \cdot k_B T) \cdot k^{-1}\tau \quad (22)$$

Thus, the surface charge density, σ_{SiOx}, of the silica substrates used in the experiments can be extracted from the slopes of the line fits for the two different polymers shown in Fig. 37b [314].

In Fig. 37c, the experimental data for different PVAm samples in 5 mM NaCl solution are plotted against the charge density of the polymers. Again, the expected increase in the average desorption force is observed, and zero charge contribution $F_0 \approx 38$ pN from this fit is in agreement with the constant term of the desorption force, which again indicates its nonelectrostatic origin. Finally, the surface potential, Ψ_0, of the substrate is obtained from Eqs. (20) and (22) as:

$$\psi_0 = \frac{F_{el}}{\tau} \quad (23)$$

According to the employed simple model, the surface potential of the silica substrate is thus given by the slope of the linear fit to the experimental data in Fig. 37c. Although its value is slightly higher than expected [278], it still indicates that the simple linear model used here is a good first

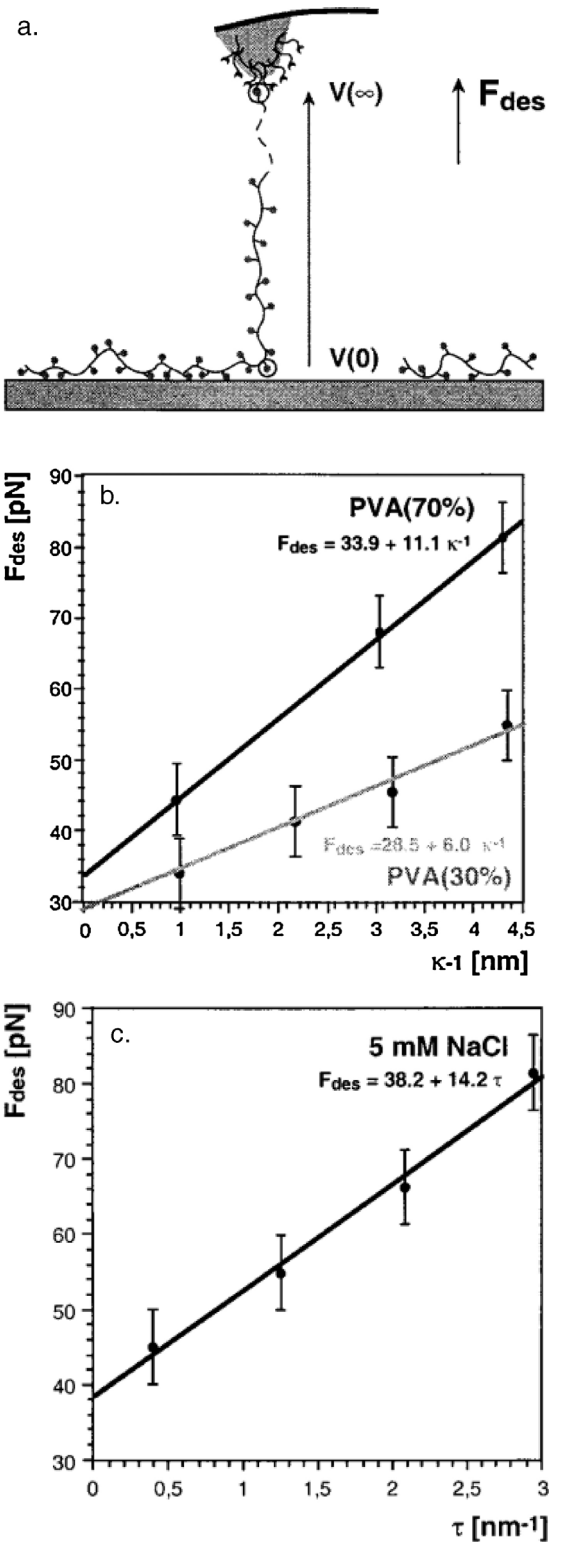

Fig. 37. (a) Continuous adhesive debonding of charged polymer chains from a charged substrate. (b) Dependence of desorption force on the Debye screening length plotted for PVA 30% and 70% ionization degrees. (c) Dependence of debonding force on polymer line charge density measured in 5 mM NaCl solution ($k^{-1} \approx 4.3$ nm).
[314], Copyright 2001. Reproduced with permission from the American Chemical Society.

approximation and well-suited to explain the observed desorption forces of polyelectrolytes from charged substrates [314].

Thus, the detachment force of single polyvinylamine chains from silicon oxide surfaces has been determined as a function of polymer line charge density as well as electrolyte concentration. Within the experimental errors, the results could be described by a simple model with a linear dependence of the detachment force on the polymer line charge density as well as the Debye screening length. On the basis of this model, the surface charge density as well as the surface potential of the silica substrate could be deduced from the experimental data. In addition to the electrostatic contribution, a constant detachment force presumably due to the nonelectrostatic interaction between polymer and substrate surface was found. Single molecule force spectroscopy by AFM thus allows the measurement of adhesive forces on the single molecule level and gaining detailed insight into fundamental adhesive interactions in polymer systems [314].

Chemical force titration is defined as SMFS probing the pH-dependence of adhesion forces between basic and acidic functional groups [272]. The effects of pH on force-extension SMFS curves are considered in a range of publications [272,281,333,334].

Considering the presence of multiple isoelectric points with different pK_a values on the interacting surfaces, the pH dependence of adhesion forces between amino-terminated probe spheres and silica can be qualitatively explained by the interplay of electrostatic and van der Waals (vdW) forces between the surfaces [333]. Within the contact area, van der Waals forces and other relevant adhesion interactions such as ionic bonding, hydrogen bonding, etc. make up the overall adhesion forces that can be calculated according to the JKR theory [279]. Outside the contact area, the van der Waals interactions and electrical double layer forces between a truncated sphere and a flat surface add an additional contribution to total adhesion forces. The balance of all these contributions can range from predominantly adhesive to nonadhesive contact, depending on the nature of interfacial bonding, charge on the surfaces and solution conditions [333].

At very low pH, the probe surface is strongly positively charged due to protonation of amino groups, while silica surface carries fewer positive charges due to protonation of silanol groups [335]. In addition to the noncompensated strong van der Waals forces within the contact area, ammonium groups of protonated amino-terminated polymer form strong hydrogen bonds with OH groups on the surface of silica substrate [336]. Such hydrogen bonds become especially strong in the presence of chloride counterions, as has been shown in [336]. As a result of such strong interfacial hydrogen bonding, a maximum adhesion force was measured. An increase in pH causes a steady decrease in adhesion forces due to a gradual decrease in protonation of surface amino groups at an intermediate solution pH. The reduced protonation translates into a reduced positive surface charge density on the probe particle, diminishing the attractive H-bond contribution which, in turn, leads to a decrease in adhesion forces. At higher pH, above 10, the amino-terminated probe contains no

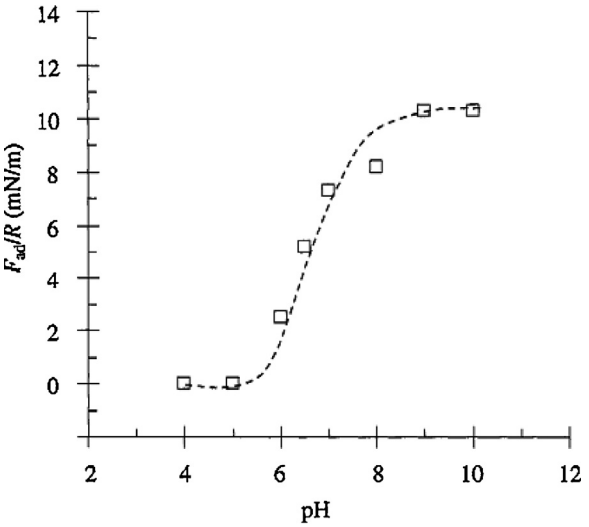

Fig. 38. Normalized adhesion force (F_{ad}/R) measured between an amine-functionalized polymer sphere and amine-functionalized silica wafer in 1 mM KC1 solution as a function of pH.
[333], Copyright 2005. Reprinted with permission from Taylor & Francis.

proton-donating ammonium groups, while silica surface is covered by hydroxyl groups, which capable of forming very weak hydrogen bonds with nonprotonated amino groups [336], resulting in a decrease of adhesion asymptotically approaching zero.

The adhesion forces were also measured using an amino-terminated polymer sphere and amino-terminated silica flat. The results in Fig. 38 show that at pH below 5, the surfaces are not in adhesive contact in 1 mM KC1 solution. At this pH the amino-terminated surfaces can be considered to be protonated and to carry strong positive surface charges. As pH increases above 5 the surfaces become less protonated, although remain positively charged overall. Under such conditions, a reduction in electrostatic repulsive interactions occurs with increasing solution pH. At pH above 10, the amino groups are anticipated to be fully deprotonated. Under such conditions, amino-groups on the contacting sphere and flat surfaces form hydrogen-bonded self-associates [336] and adhesion increases. A similar adhesion force profile between an amino-terminated AFM tip and an amino-terminated flat surface was reported by Vezenov et al. [337].

Noy and co-workers [271] studied the strength of the interactions between several different surfaces as a function of temperature. Intuitively, we expect the bonding force to decrease as the temperature increases and the thermal fluctuations gain more energy to break the bond. Surprisingly, the researchers observed that for interactions between COOH-terminated surfaces in a polar, hydrogen-bonding solvent the interaction strength increased with the temperature. This behavior was also present for interactions of other hydrophilic functionalities in polar solvents. Conversely, when the liquid medium was switched to a nonpolar solvent (hexane) the temperature trend reversed. These researchers attributed this behavior to the large negative entropy accompanying ordering of solvent molecules at the interface. This negative entropy destabilizes the

unbound state and leads to the observed counterintuitive temperature dependence. Nonpolar solvents do not tend to form ordered layers and, thus, do not contribute to these entropic solvation barriers.

Expressing the temperature dependence of the pull-off force, Eq. (24) presents a quantitative interpretation of this phenomenological picture [271,272].

$$f_{\text{pull-off}} = \frac{\Delta H}{x_\beta} - \frac{\Delta S}{x_\beta} T - \frac{k_B T}{x_\beta} \ln\left[\frac{k_B T}{r_f \tau_D x_\beta}\right] \quad (24)$$

where ΔH and ΔS are enthalpic and entropic contributions into free energy of transition, x_β is the distance to the energy potential barrier, r_f is the loading rate and τ_D represents the inverse of the diffusion-limited attempt frequency [272].

The first two terms in Eq. (24) describe the enthalpic and the entropic contributions to the adhesive bond strength and the third term describes the contribution of thermal motion to the bond strength. In other words, the first two components describe the true energy-barrier contribution and the (always negative) third component describes the 'thermal weakening' of a bond caused by the thermal fluctuations helping the system to get over the activation barrier.

Eq. (24) highlights another bit of nontrivial physics of chemical bond behavior under external load. The third term in Eq. (24) ('thermal weakening') always increases in magnitude as the temperature increases, leading to an overall decrease in the observed force, in full agreement with the intuitive picture of bond 'loosening'. Yet the entropic term can lead to either an increase or decrease in the overall interaction force, depending on the sign of the entropy change for the debonding process. Therefore, for the cases when the energy barrier has a large entropy component (i.e., in cases of entropic interactions) we expect the bond strength to increase with the temperature. The relative magnitudes of the entropic and the kinetic terms in Eq. (24) define two regimes of bond rupture:

(1) thermally dominated kinetics, where the kinetic weakening leads to a decrease in the observed bond strength with the increase in temperature, and
(2) barrier-dominated kinetics, where the entropic term overwhelms the kinetic term and leads to an increase in interaction strength with an increase in temperature. Furthermore, Eq. (24) also indicates that the entropic regime of debonding should exist only over a limited range of temperatures. As the temperature increases, the kinetic term which increases as $T\cdot \ln T$ will overwhelm the entropic term which increases only linearly. For the entropic forces caused by the ordering of the solvent molecules at the surface, this cross-over point simply corresponds to the situation when the thermal motion becomes too strong and overwhelms molecular ordering in the solvent layers [271,272].

A fruitful strategy to test the scaling relationship between the adhesion forces and the interfacial free energies predicted by the contact mechanics theories for quasi-equilibrium unbinding is to use the same tip and sample pair and vary either the solvent composition or the SAM composition on the probe. This arrangement preserves the geometrical parameters of the system while varying the interfacial free energies of the interacting system in a smooth and predictable manner. For example, Vezenov et al. used the same tip-sample pair terminating in CH_3 groups to determine adhesion forces in a series of methanol–water mixtures [338]. These measurements produced an unambiguous linear correlation between adhesion forces and corresponding surface free energy values determined from independent contact angle measurements, thus providing an additional corroboration of the scaling relationships predicted in such systems by the contact mechanics models (Fig. 39).

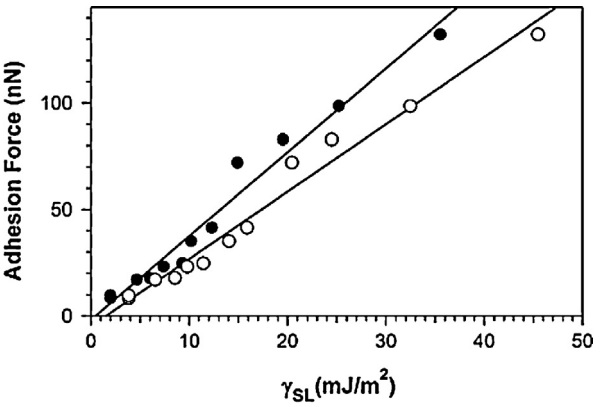

Fig. 39. Adhesion between CH_3-terminated tips and samples versus solid-liquid surface free energy determined from advancing (open symbols) and receding (closed symbols) contact angles for CH_3-terminated SAM (γ_{SV} = 19.3 mJ/m^2).
[338], Copyright 2002. Reproduced with permission from the American Chemical Society.

As was well recognized in classical adhesion science, there were no reliable tools to measure tack, i.e., adhesion bond-forming property, in terms of mechanical forces. In this connection the capability of well-known adsorption theory of adhesion and thermodynamic work of adhesion to predict the practical work of adhesive debonding was at the center of extensive debates [8,38]. The SMFS technique made it possible to probe bridging adhesion on the single macromolecule level. Nowadays, the results of SMFS measurements establish direct correlation between surface energies of an adhesive and a substrate on the one hand, and the strength of their adhesive joint at the level of single polymer chains on the other hand. We are just beginning to understand these complex processes, which involve stretching of polymer strands, their sliding on the surface, and their subsequent debonding [339–342].

6. Pressure sensitive adhesives based on nonstoichiometric polyelectrolyte complexes

Now, armed with molecular insights into the mechanisms of PEC self-assembly and their supramolecular structures, we consider structure–property relationship of composite adhesive materials based on self-associates of proton-donating and proton-accepting polymers, i.e.,

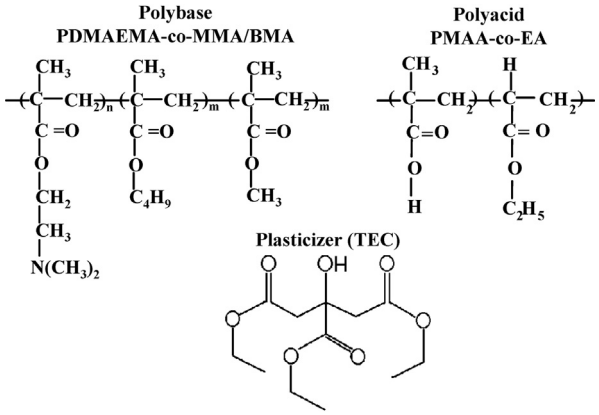

Fig. 40. Molecular structures of PDMAEMA-co-MMA/BMA polybase, PMAA-co-EA polyacid and TEC plasticizer.

polyacids and polybases. Because pressure sensitive adhesion requires coupling large free volume with strong intermolecular cohesion [38], and ionic interactions are much stronger than the hydrogen bonds [278], we will start our description with PECs formed by uncharged polyelectrolyte molecules, i.e., with H-bonded PECs.

6.1. Mechanisms of intermolecular interactions and the strength of noncovalent bonds in a model polyelectrolyte complex

In our study a model PEC PSA is formed by mixing various ratios of a polybase (e.g., copolymer of N,N-dimethylaminoethyl methacrylate with methyl methacrylate and butyl methacrylate PDMAEMA-co-MMA/BMA, 2:1:1), with a polyacid (e.g., copolymer of methacrylic acid and ethyl acrylate, PMAA-co-EA, 1:1) in the presence of triethyl citrate (TEC) as a plasticizer. The structures of PDMAEMA-co-MMA/BMA, PMAA-co-EA and TEC are illustrated in Fig. 40.

In our further discussion the following terminology will be used in accordance with the definitions set out below. The term complex or interpolymer complex refers to the association of macromolecules of two or more complementary polymers by means of favorable noncovalent interactions. The term ladder-like defines the complex or the mechanism of complexation leading to the association of the complementary macromolecules, wherein specific interactions occur between the functional groups in repeating units of polymeric backbones. Functional groups of complementary polymers are interacting in a cooperative manner (see Section 4.1 of this review). This means that due to entropic reasons, the complementary groups tend to form relatively long sequences of strong interchain bonds, rather than separate crosslinking bonds. As is seen from Figs. 20 and 22, the schematic structure of such a complex resembles a ladder.

In general, an interpolymer complex between a film forming polymer and a ladder-like crosslinker (LLC) is formed by hydrogen bonding, electrostatic bonding, ionic bonding, or their combination. The ladder-like complexes are reversibly crosslinked due to specific interactions between the functional groups in the complementary macromolecules and thus represent “networks”. In the present context the term “network” is used interchangeably with the term “complex”. However, the latter term refers more specifically to the supramolecular structure of the interpolymer complex.

In the PSAs based on polyelectrolyte complexes, the same polymer component may be used as either a film-forming polymer (FFP) or as a ladder-like noncovalent crosslinker (LLC) since both the FFP and LLC represent the same class of complementary functional polymers. The component presented in the greatest quantity serves as a film-forming polymer so that the difference between FFP and LLC is a function of their concentration. While the predominant component is typically referred to as a film-forming polymer, the minor component is referred to as a ladder-like noncovalent crosslinker. It must be noted that in further description the model FFP is always a polybase (PDMAEMA-co-MMA/BMA), whereas the model LLC is a polyacid (PMAA-co-EA).

FTIR-spectroscopy allows identification of interacting functional groups in polyelectrolyte PDMAEMA-co-MMA/BMA–PMAA-co-EA blends. To evaluate the structure and formation energies of the interpolymer complexes that involve both hydrogen and ionic bonding, quantum chemical calculations have been performed [336]. The results of quantum chemical calculations appreciably facilitate the interpretation of FTIR-spectra. Comparison of the molecular mechanisms of the polybase–polyacid interaction to the values of complexation energies gives an insight into the most energetically favorable interaction mechanisms between complementary functional groups of the polymers in the blends.

According to the quantum analysis of more than 300 polyelectrolyte complex structures examined in [336] (see Table 9), the ionic complexes formed with the participation of charged polyelectrolyte functional groups (ammonium cation and carboxylate anion) are from 4 to 16 times more energetically favorable than the strongest H-bonded complexes of uncharged complementary polybase and polyacid groups [336]. These energies control both the phase state and the cohesive strength of the PSAs based on the polyelectrolyte complexes.

The PSAs based on polyelectrolyte complex represent a new generation of water-absorbing adhesive materials. For this reason, the structures including water molecules associated with polymer functional groups were also taken into consideration in the course of the quantum chemical analysis. Molecules of absorbed water are not competitors but rather facilitators for the formation of stable energetically favorable polyelectrolyte complexes. The proton-donating capacity can be significantly improved in the presence of Cl^- ions. The Cl^- counterion effect may be appreciably inhibited if Na^+ cations are present in the solution. Proton-accepting capability weakens in the order: Uncharged aminogroup > Carboxylate anion > Uncharged carboxyl group > Hydroxyl group [336].

The carboxyl and aminogroups in the model PDMAEMA-co-MMA/BMA–PMAA-co-EA system are typical of a variety of polyelectrolytes. This enhances the fundamental

Table 9
Comparative strength of ionic and hydrogen bonding between amino groups of polybase, carboxyl group of polyacid and hydroxyl group of plasticizer [336].

Complex type	Complex structure	Formation energy (kJ/mol)
Complex of uncharged carboxyl group with two ammonium cations and chlorine counterion	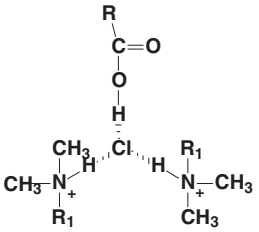	689.5
Ternary complex of uncharged carboxyl group, ammonium cation and water in the presence of chlorine counterion	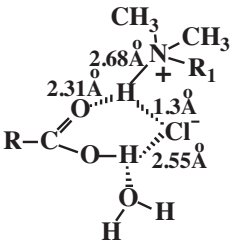	650.2
Hydrogen bonded complex of carboxylate anion and ammonium cation, stabilized with chlorine counterion	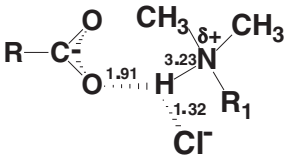	644.0
Ternary charge transfer complex of ionized carboxyl group, ammonium cation and water	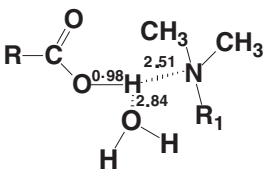	593.1
Ternary H-bonded complex of ammonium cation with carboxylate anion and water in the presence of chlorine counterion	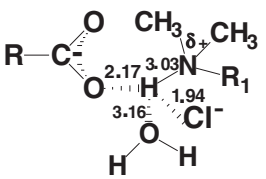	524.0
Ionic complex of carboxylate and ammonium counterions	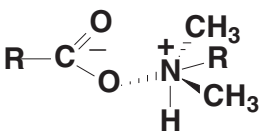	404.4
H-bonded complex of carboxylate and ammonium ions	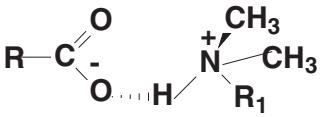	257.5
Ternary complex of uncharged carboxyl group, ammonium cation and water	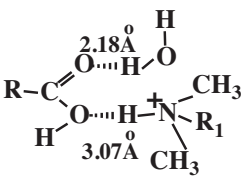	152.4

Table 9 (*Continued*)

Complex type	Complex structure	Formation energy (kJ/mol)
H-bonded complex of uncharged carboxyl group with ammonium cation	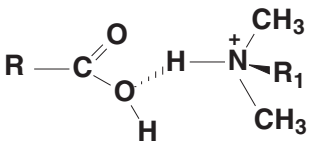	114.0
Complexes of carboxyl group and carboxylate anion	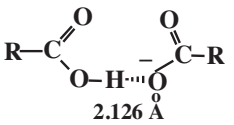	89.9
	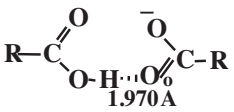	73.5
H-bonded TEC complex with carboxyl group	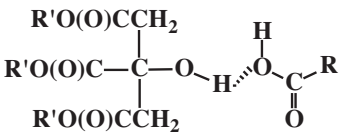	47.6
Ternary complex of uncharged carboxyl group, aminogroup and water	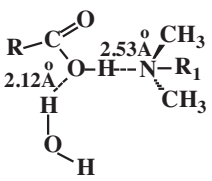	42.9
H-bonded complex between uncharged amino and carboxyl groups	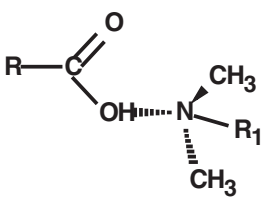	26.2
H-bonded complex of TEC with aminogroup	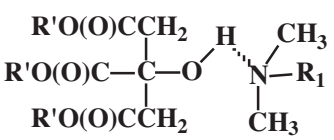	19.7

Reproduced with permission from Feldstein M.M., Kiseleva T.I., Bondarenko G.N., Kostina J.V., Singh P., Cleary G.W., Journal of Applied Polymer Science, 112(3) (2009) 1142–1165 [336]. Copyright 2009, Wiley Periodicals, Inc.

significance of the results obtained with this model system for the field of polyelectrolyte complexes.

6.2. Phase behavior of the polyelectrolyte complexes in a solid state

As has been shown in [38,81–83,160,343], the value of the glass transition temperature is an important indicator of the ratio between the energy of intermolecular cohesion and free volume in polyelectrolyte blends. The growth of cohesion results generally in the increase of the T_g value, while the rise of free volume leads to T_g reduction. The blends of PDMAEMA-co-MMA/BMA polybase with PMAA-co-EA polyacid and a TEC plasticizer exhibit a single glass transition temperature indicating that 20:1 and 10:1 plasticized polybase–polyacid blends are single-phase, whereas the blends of the polybase with larger amount of the polyacid LLC, closer to 1:1 stoichiometry, display signs of microphase separation. The composition behavior of T_g in the PDMAEMA-co-MMA/BMA blends with PMAA-co-EA and TEC demonstrates a predominant contribution of large free volume to the T_g. It is surmised that polyelectrolyte

mixing in a solid state or in concentrated solutions, which leads to polymer chain entanglements, favors the formation of loops of unbound polymer chains [160].

Ionization of polyelectrolyte functional groups significantly affects the phase behavior of unblended components but has only a minor impact on the T_g of the blends [160]. Measured T_g values correlate reasonably well with the earlier established mechanisms of molecular interaction in the PDMAEMA-co-MMA/BMA blends with PMAA-co-EA and TEC as a plasticizer.

Mixing a polybase with a polyacid in solution, in the vicinity of 1: 1 concentration ratio results in formation of a sol and gel fractions. The sol fraction consists predominantly of a nonstoichiometric complex of so-called "scrambled egg" structure. In contrast, the gel fraction represents a stoichiometric ladder-like network polyelectrolyte complex of a "zipper" structure [160]. The T_g values are always higher for the stoichiometric ladder-like complex than for the nonstoichiometric polyelectrolyte complexes of the "scrambled egg" structure (Figs. 19 and 22). This fact is a direct confirmation that intermolecular cohesion dominates free volume in a stoichiometric ladder-like polyelectrolyte complex, while in a slightly crosslinked nonstoichiometric complexes of "scrambled egg" structure the free volume dominates the energy of intermolecular cohesion due to loop formation.

When the stoichiometric and nonstoichiometric polyelectrolyte complexes are not separated by filtration of the casting solution prior to the dry blend preparation, the "scrambled egg" complex forms a continuous phase of lower T_g, while the finely divided particles of the ladder-like complex in the dispersed phase have microscopic sizes and do not show a separate T_g value. Supramolecular structures of nonstoichiometric and stoichiometric polyelectrolyte complexes have been studied with electron microscopy. The nonstoichiometric "scrambled egg" complex in the sol phase exhibits a lamellar structure or spherical-like domains (Fig. 41A), while a stoichiometric ladder-like complex in the gel phase forms a well developed fibrillar network structure that resembles a nanosized web (Fig. 41B) [160].

The state diagram of polybase–polyacid blends (Fig. 42, [160]) reveals areas of partial component miscibility and the formation of a nonstoichiometric complex of "scrambled egg" structure, which are separated by a field occupied by a ladder-like polyelectrolyte complex of stoichiometric composition. The ladder-like complex is immiscible with both parent polymers at temperatures below 172 °C. Melting of the ladder-like complex and polybase–polyacid miscibility above this critical temperature is thought to be a result of the complex dissociation at high temperatures, when intermolecular hydrogen bonds do not exist any longer. The plasticized polybase–polyacid blends of 20: 1 and 10: 1 concentration ratios, that demonstrate pressure sensitive adhesion, relate to the area of the phase diagram which corresponds to the nonstoichiometric polyelectrolyte complex of the "scrambled egg" structure. The stoichiometric ladder-like polyelectrolyte complex in the blends of 1: 1 polybase–polyacid composition ratio with plasticizer exhibits no adhesion.

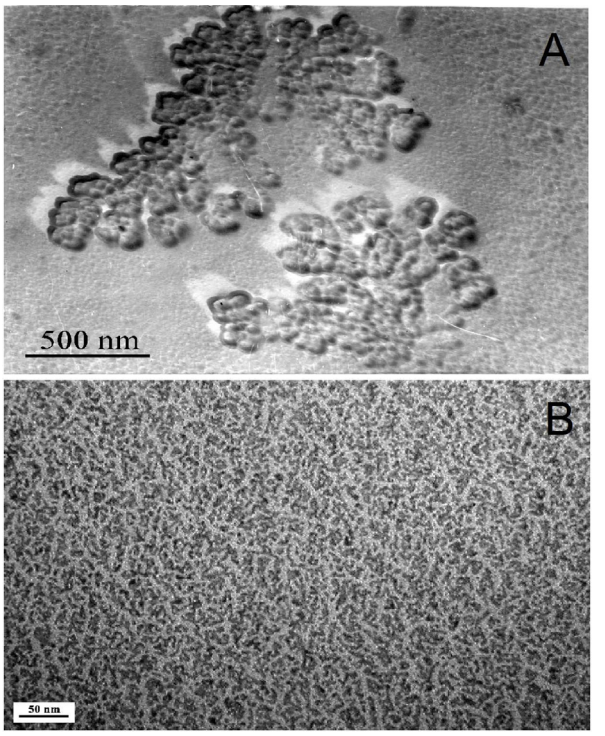

Fig. 41. TEM microphotographs of the PDMAEMA-co-MMA/BMA–PMAA-co-EA complex particles in a sol 70:30 (A, top) and gel 50:50 (B, bottom) phases.
[160], Copyright 2011. Reproduced with permission from Wiley Periodicals Inc.

As the most recent data of positron annihilation lifetime spectroscopy (PALS) measurements have shown [343], the value of hole free volume for the model polyelectrolyte complex PSA at 20 °C is 179 Å^3 (±2 Å^3), whereas for other typical PSAs it ranges from 145 to 183 Å^3 (±2 Å^3). Thus, in spite of the fact that the intermolecular cohesion

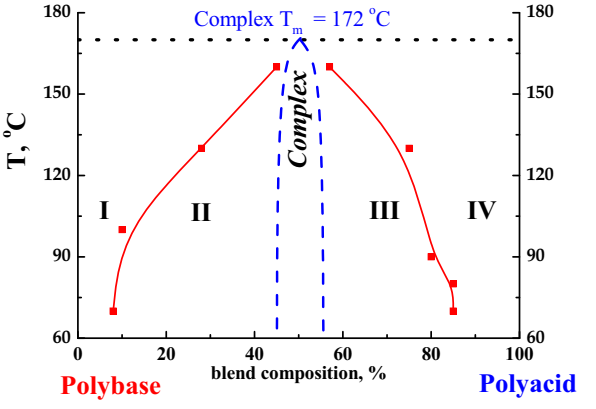

Fig. 42. State diagram of polybase PDMAEMA-co-MMA/BMA blends with PMAA-co-EA polyacid in the absence of TEC plasticizer. (I) Mixture of the polyelectrolyte complex with the PDMAEMA-co-MMA/BMA polybase. (II, III) Nonstoichiometric polybase–polyacid complex and (IV) mixture of the nonstoichiometric complex with PMAA-co-EA polyacid. The central zone is occupied by a stoichiometric polyelectrolyte complex of a ladder-like structure (T_m = melting temperature).
[160], Copyright 2011. Reproduced with permission from Wiley Periodicals Inc.

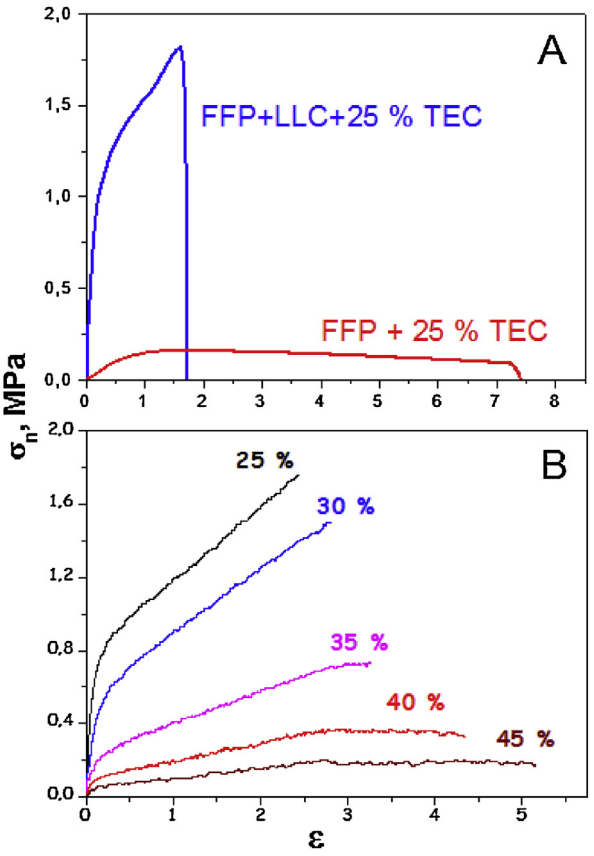

Fig. 43. Tensile properties of polyelectrolyte complexes. A: Nominal stress–strain curves for uniaxial drawing of the mixture of FFP with 25 wt % TEC plasticizer and the nonstoichiometric polyelectrolyte complex ([FFP]:[LLC] = 10:1) plasticized with the same amount of TEC. B: Effect of plasticizer concentration on tensile stress–strain curves of polyelectrolyte blends (FFP/LLC = 10/1). TEC content is indicated. Drawing rate is 20 mm/min.
[343], Copyright 2012. Reproduced with permission from Wiley Periodicals Inc.

energy of the polyelectrolyte complex PSA is essentially higher than for other typical representatives of the PSA family, the behavior of free volume conforms well to the values which are observed for typical PSAs of other chemical compositions.

6.3. Mechanical properties of polyelectrolyte blends

We come now to the macroscopic physical properties of polyelectrolyte PSAs. Direct correlation occurs between adhesion and large-strain tensile properties of the PSAs. Hence, consideration of the tensile behavior of the PSA allows us to establish and illustrate the role and function of each component in a polyelectrolyte blend. Since stretching is the main type of deformation of the PSAs during adhesive joint failure [14,41,53,54,58,344], the study of the mechanical characteristics of polymer materials during uniaxial drawing to break is of utmost importance.

As is seen from Fig. 43A [343], the stress–strain curve for the binary blend of the FFP (polybase) with 25 wt.% plasticizer is typical of the deformation of viscoelastic liquids, such as entangled linear macromolecules and non-crosslinked rubbers. Our experimental data shows that the polyacid in the blend with the polybase FFP plays the role of the noncovalent ladder-like polymer crosslinker (LLC), thereby increasing the cohesive strength of the material and decreasing its free volume. The incorporation of even small amounts of the polyacid (PMAA-co-EA; polybase:polyacid = 10:1) causes dramatic changes in the type of deformation and in the profile of the curve. This type of extension is typical for densely crosslinked rubbers. In this case, the breaking strength of the films increases by a factor of 6.6, while the maximum elongation decreases by a factor of 4.3. The ultimate fracture stress is a direct measure of the cohesive strength of deformed material, whereas the maximum elongation at break is proportional to the value of free volume fraction, as measured by positron annihilation spectroscopy [38,84].

Fig. 43B illustrates the effect of the plasticizer content on the tensile stress–strain curves of the polyelectrolyte blend [343]. The stress–strain curves for the blend under study are similar in shape to the corresponding curves for lightly crosslinked elastomers. All the PSAs belong to that class. This is manifested by the high ultimate strains (ε_b) typical for rubbers, as well as the occurrence of ductile or "plastic flow" regions characteristic of plastic deformation.

As has been shown earlier, while conducting a phase behavior study of the polyelectrolyte complexes [160], TEC is a good plasticizer of the PDMAEMA-co-MMA/BMA blends with PMAA-co-EA. This conclusion is now confirmed by the analysis of tensile stress–strain curves. As the concentration of plasticizer increases, the ultimate tensile strength and the work of viscoelastic deformation to break (the area under the stress–strain curve) decrease, whereas the maximum elongation increases. It is pertinent to recall once again that both former values are the indirect measures of cohesion strength, whereas the latter relates directly to the content of free volume [38,84].

Thus, varying the composition of the FFP–LLC blends with plasticizer provides easy tuning of the mechanical properties. The ultimate strength and ductility of the blends are such that they can be useful in many practical applications.

6.4. Adhesion of the PSAs based on nonstoichiometric polyelectrolyte complexes

The probe tack profiles (Fig. 44) provide valuable information about the mechanism of debonding [343]. The PSAs are known to couple the properties of liquid-like and solid-like materials. The shape of the stress–strain curves illustrates qualitatively this dualism (see Fig. 4 above).

Fig. 44 illustrates the effect of LLC on the probe tack curves of the polyelectrolyte complex at two concentrations of plasticizer (25 and 35 wt.% TEC). As follows from the curves, a ladder-like noncovalent cross-linking of FFP (PDMAEMA-co-MMA/BMA polybase) with LLC (PMAA-co-EA polyacid) results in a dramatic change in the debonding mechanism. The mechanism changes from the one typical of liquid PSAs (observed for plasticized FFP) to more elastic and solid-like, as found for the behavior of ternary PDMAEMA-co-MMA/BMA blends with PMAA-co-EA and

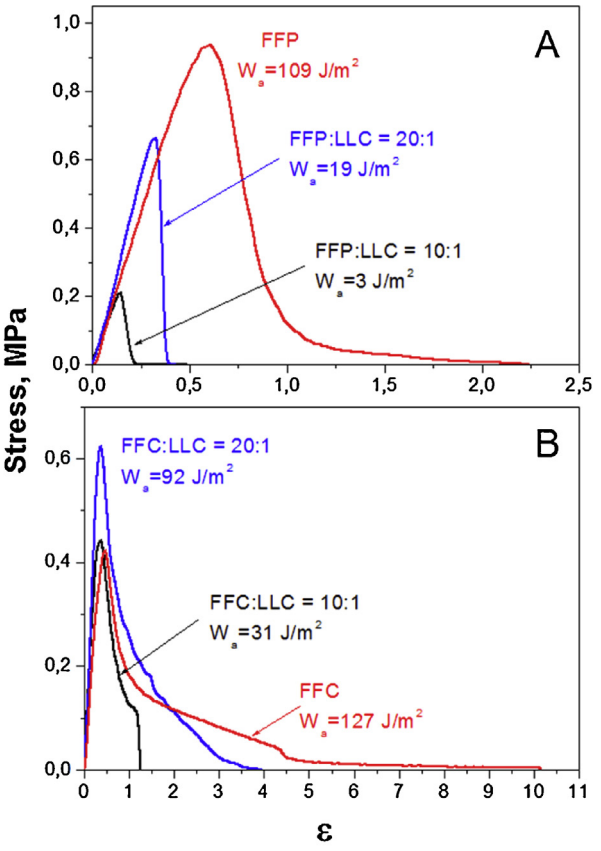

Fig. 44. Probe tack curves of the PDMAEMA-co-MMA/BMA polybase (FFP), and its polyelectrolyte complexes with LLC (polyacid, PMAA-co-EA). FFP:LLC = 20:1 and 10:1. The rate of probe detachment is 0.1 mm/s. Corresponding values of the practical work of adhesion (debonding energy) are indicated in the Figure. A: 25 wt % of TEC plasticizer. B: 35 wt % of TEC plasticizer.
[343], Copyright 2012. Reproduced with permission from Wiley Periodicals Inc.

TEC. The LLC behavior, observed also based on the data for tensile test (compare Figs. 44 and 43), implies the dominance of intermolecular cohesion over the free volume [38,51].

As illustrated in the Probe Tack curves, Fig. 44(A and B), a binary blend of PDMAEMA-co-MMA/BMA containing 25 and 35 w/w% of plasticizer TEC and no polyacid crosslinker is a tacky liquid that debonds cohesively at relatively high elongation. Upon cohesive joint failure a significant amount of adhesive is left on the surface of the probe. The higher the TEC concentration the more the PSA is liquid-like. This is obvious from the values of the maximum adhesive layer stretching at the point of debonding, ε_{max}. At 35 wt.% TEC in the blend, mixing the FFP with complementary LLC in the ratios of [FFP]:[LLC] = 20: 1 and 10: 1 leads to an immediate change in the debonding mechanism from cohesive to adhesive. Ladder-like crosslinking of FFP decreases the work of debonding from 126 to 92 and 31 J/m^2, respectively. The 20: 1 nonstoichiometric polyelectrolyte complex demonstrates a better balance between elastic and plastic behaviors, as theoretical models reviewed above in Section 4.5 predict. Although the debonding energy is somewhat decreased as compared to uncrosslinked FFP, this lightly crosslinked PSA exhibits an adhesive type of debonding. Further increase of LLC concentration lowers both the maximum debonding stress and the adhesive layer stretching. Thus, the dominance of the cohesive interactions over the free volume is produced by ladder-like cross-linking of FFP that affects the adhesive properties.

As is seen from Fig. 45A [343], in the course of mixing the PDMAEMA-co-MMA/BMA–PMAAco-EA polyelectrolyte complex with TEC plasticizer, the deformation mechanism typical of solid adhesives (25 wt.% TEC) changes to that inherent to viscoelastic adhesives. With an increase in the plasticizer concentration, the maximum stress of debonding increases, passes through a maximum at 35–45 wt.% TEC, and finally declines. The appearance of the plateau in the Probe Tack curves indicates the contribution of adhesive layer fibrillation. The maximum elongation of fibrils tends to increase as the amount of plasticizer increases. The work of adhesive joint failure passes through a maximum at 50–55 wt.% of the plasticizer [343].

At the same time, the Probe Tack curve obtained for the blend containing 50 wt.% of the plasticizer suggests the adhesive type of joint failure and indicates that, for the blend containing 60 wt.% TEC, detachment of the adhesive layer from the steel probe surface proceeds according to the cohesion mechanism. The adhesive bond failure in the Probe Tack curves is manifested as a sharp drop of debonding stress, whereas the cohesion mechanism is characterized by a gradual decrease of the debonding stress in the final section of the curve (Fig. 45A) [343].

As is obvious from Fig. 45B [343], the plasticizer hydrophilicity significantly affects the failure mechanism of adhesive joints of the FFP–LLC polyelectrolyte complex. The higher is the plasticizer hydrophilicity, the higher is the adhesion. The work of probe detachment from the adhesive film surface grows as the plasticizer hydrophilicity increases in the sequence: acetyltributyl citrate (ATBC) ≈ tributyl citrate (TBC) < acetyltriethyl citrate (ATEC) ≈ triethyl citrate (TEC). If the blends with hydrophobic plasticizers (ATBC and TBC) behave as solid adhesives and fail without essential fibrillation of the adhesive layer, the blends of the polyelectrolyte complex with the hydrophilic plasticizers (ATEC and TEC) demonstrate the existence of fibrillation, which is most pronounced in the case of the most hydrophilic plasticizer – TEC.

PDMAEMA-co-MMA/BMA polybase and PMAA-co-EA polyacid are not unique FFP and LLC suitable for the preparation of adhesives based on the mechanism of the ladder-like polyelectrolyte complex formation. As Fig. 45C illustrates, replacement of PMAA-co-EA polyacid by a copolymer of maleic acid with methylvinyl ether (PMA-co-MVE) increases adhesion appreciably, implying that the approach illustrated in this research has a general character [343].

6.5. Impact of the type of intermolecular bonding on adhesion of polyelectrolyte complexes

Partial ionization of polybase or polyacid in the blend, achieved with the addition of a strong inorganic acid (HCl)

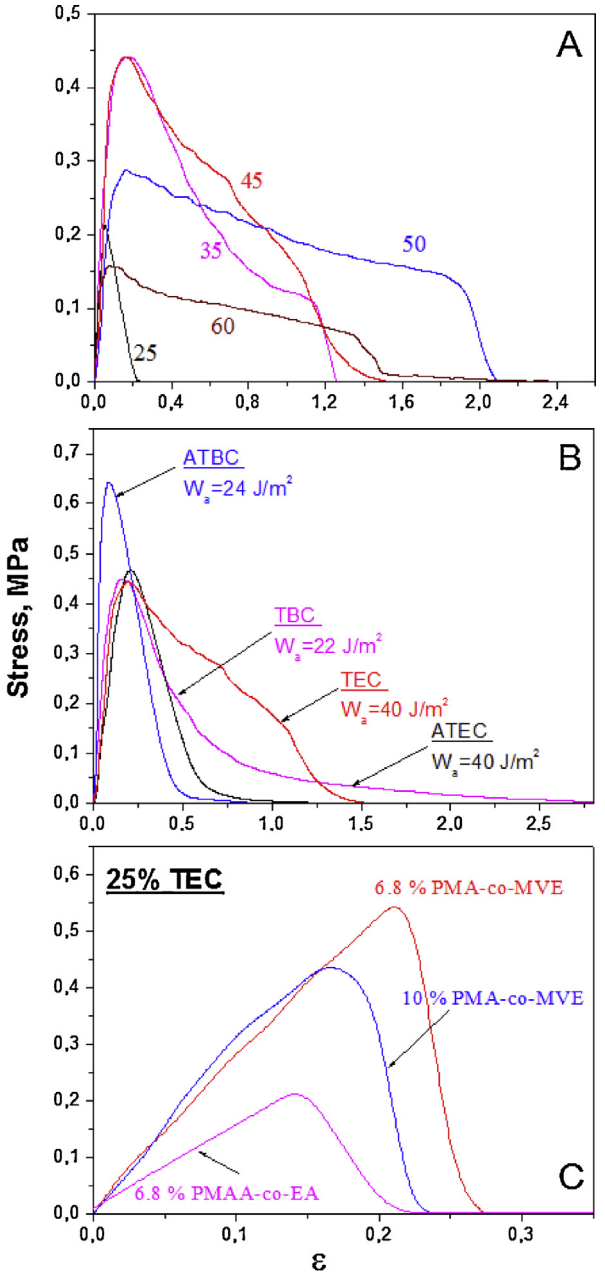

Fig. 45. Effects of composition on Probe Tack adhesion (stress-strain behavior) of polyelectrolyte complex PSAs. A: Effect of triethyl citrate concentration on the deformation mechanism of the adhesive layer in the 10: 1 polyelectrolyte complex of PDMAEMA-co-MMA/BMA with PMAA-co-EA. The rate of probe detachment is 0.1 mm/s. The TEC concentrations are indicated in the Figure. B: Impact of plasticizer hydrophilicity on Probe Tack curves of the blends composed of the 10: 1 polybase complex with polyacid. Plasticizer content is 45 wt %. ATBC is acetyl tributyl citrate, ATEC is acetyl triethyl citrate, TBC is tributyl citrate, and TEC triethyl citrate. C: Probe Tack behavior of interpolymer complexes containing ladder-like cross-linkers of different hydrophilicity and hydrogen-bonding capability: PMAA-co-EA and PMA-co-MVE. TEC content in blends is 25 wt %.
[343], Copyright 2012. Reproduced with permission from Wiley Periodicals Inc.

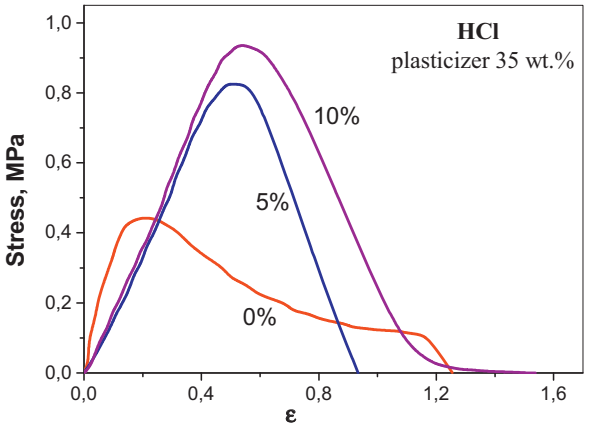

Fig. 46. The effect of partial ionization of the amino groups in PDMAEMA-co-MMA/BMA copolymer on Probe Tack curves of a ladder-like interpolymer complex plasticized with TEC. Ionization degrees are indicated in the Figure.
[343], Copyright 2012. Reproduced with permission from Wiley Periodicals Inc.

or base (NaOH), also improves the adhesive properties and changes the mechanism of debonding from fibrillar to solid-like (Fig. 46) [343]. The implication of this Probe Tack data is that the adhesive properties are affected by a mechanism of specific interaction between the components of the polyelectrolyte complex (hydrogen or ionic bonding). In turn, the molecular interaction governs the structure of the complex and determines the balance between cohesive energy and free volume.

The electron-donating amino groups of PDMAEMA-co-MMA/BMA polybase are capable of forming hydrogen bonds with the proton-donating carboxylic groups of PMAA-co-EA polyacid (Scheme 1).

According to the quantum chemical modeling data (see Table 9, [323]), such H-bonded complexes of uncharged complementary functional groups are characterized by the formation energy of ~26 kJ/mol. Inclusion of water molecule into the bonding makes the complex more stable (ΔE = 43 kJ/mol). Treatment of PDMAEMA-co-MMA/BMA by HCl in aqueous solutions causes partial ionization of the polybase and the formation of ammonium cations, which can interact with the carboxyl groups of PMAA-co-EA through the exchange reaction [31,336,343] (Scheme 2).

Ionic bonds are much stronger than hydrogen bonds [278,336] with an energy that ranges between 251 and 404 kJ/mol. Involving the associated water molecule into the ionic complexes enhances intermolecular bonding energy up to 524–650 kJ/mol [336]. As the data presented in Fig. 46 illustrate, the increase in the energy of interpolymer bonding increases both the energy of intermolecular cohesion and the practical work of adhesion (the area under probe tack curve). This allows us to assume that the

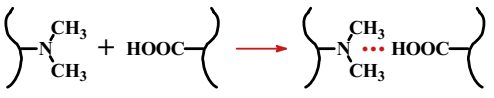

Scheme 1. Neutralization reaction of H-bonded interpolymer complex formation between uncharged polybase and polyacid macromolecules.

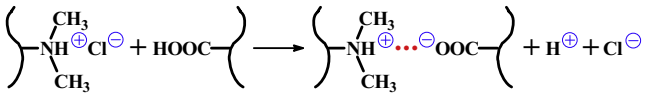

Scheme 2. Exchange reaction of ionic complex formation between ammonium salt of polybase and uncharged polyacid.

free volume in ionic ladder-like polyelectrolyte complex increases accordingly. Electrostatic repulsion of cationic ammonium groups in ionized PDMAEMA-co-MMA/BMA macromolecule leads to the increase in free volume.

Partial neutralization of the carboxylic groups of LLC (PMAA-co-EA–polyacid) by treatment with NaOH solution results in the formation of carboxylate anions that are unable to interact with the uncharged amino groups of FFP (PDMAEMA-co-MMA/BMA–polybase) and therefore do not contribute to the increase of cohesive energy. However, electrostatic repulsion between these anions increases the free volume. As a result, adhesion increases likewise [343]. Finally, the combined effect of ammonium cations in FFP and carboxylate anions in LLC enhances adhesion [343].

In this way, adhesion of PEC-based PSAs is controlled by the same fundamental factors (polybase–polyacid stoichiometry, charge density, etc.) which also govern supramolecular structure, single-chain elasticity and intermolecular interaction mechanisms. Analyzing the role of each component in blend (FFP, LLC, plasticizer) makes possible tuning the adhesion and development of novel PSAs with tailored mechanical and adhesion properties. The PSAs based on the ionic polyelectrolyte complexes, described in this section of the review, represent an example of "smart" pH-responsive PSAs. They can be employed in various areas of industry and medicine as electroconductive adhesives with ionic type of conductivity.

6.6. Electrorheology of solid polyelectrolyte complexes

Fig. 47 shows how the total voltage affects linear viscoelastic properties of PEC. Fig. 47A relates to a H-bonded

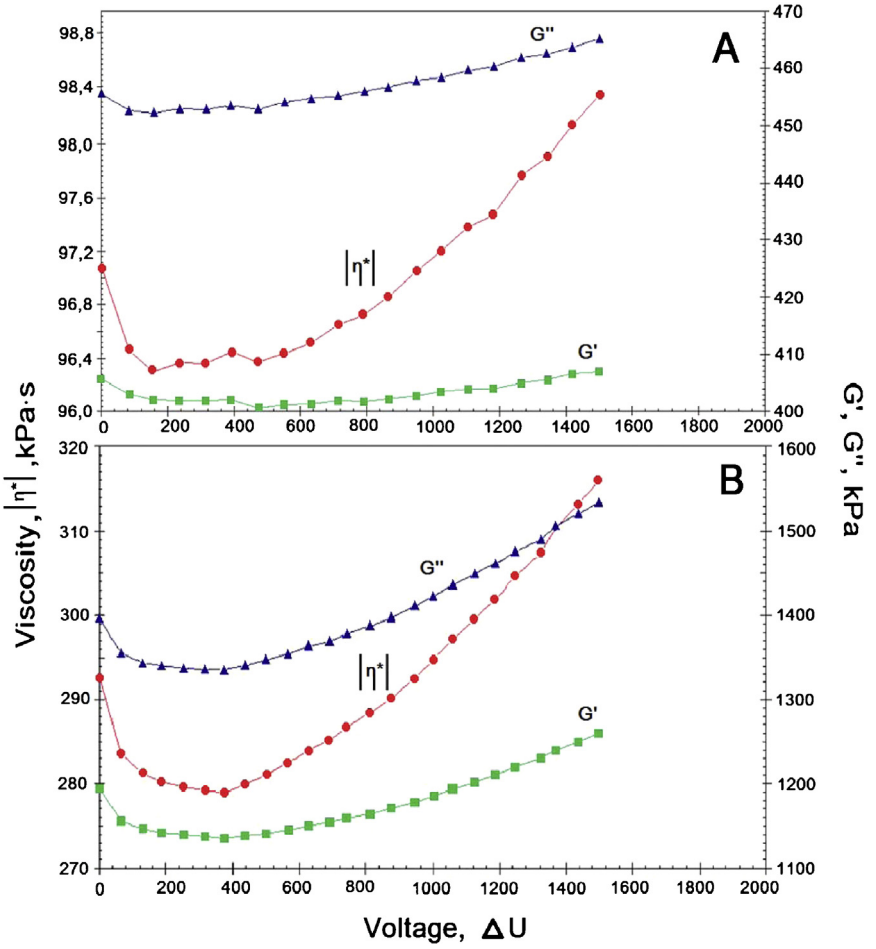

Fig. 47. Effects of total voltage on elastic modulus G′, loss modulus G″ and viscosity of 10:1 PDMAEMA-co-MMA/BMA – PMAA-co-EA polyelectrolyte complexes containing 25 wt. % of TEC plasticizer. A: uncharged complex formed by polybase–polyacid hydrogen bonding. B: polyelectrolyte complex of the same composition including 10 mol % of ionic bonds. Unpublished data by A.P. Moscalets, S.M. Khusyainov, K.A. Bovaldinova and M.M. Feldstein (2014).

10:1 complex of PDMAEMA-co-MMA/BMA polybase with PMAA-co-EA polyacid, containing 25 wt.% of plasticizer (TEC). Fig. 47B illustrates the changes of elasticity modulus G', loss modulus G'' and complex viscosity η of ionic PEG complex of the same composition based on HCl treated polybase (10% protonization degree of the aminogroups).

As follows from Fig. 47, for both uncharged and charged polyelectrolyte complexes the changes of moduli are relatively small as compared with the variation of viscosity. The viscosity relates to the elasticity modulus via the Maxwell equation $\eta = G' \cdot \tau$, where τ is the relaxation time, a measure of the polymer material molecular mobility. Longer relaxation times correspond to lower molecular mobility. As is seen from Fig. 47, all the curves go through a minimum. This means that under the influence of total voltage the changes of complex viscosity are governed by the variation of molecular mobility to much greater extent tnan the change of elasticity and, consequently, the supramolecular structure of the PEC. At small voltage the molecular mobility increases and the relaxation time is reduced, whereas at high voltage the mobility decreases, resulting in an increase of the relaxation time. As comparison of Fig. 47A and 4B demonstrates, the PECs formed by hydrogen and ionic bonds exhibit much greater viscosity, elastic and loss moduli than the complexes formed by solely hydrogen bonds.

6.7. Water-absorbing capacity of polyelectrolyte PSAs

Owing to the formation of three-dimensional network of noncovalent intermolecular bonds, the PSAs based on nonstoichiometric ladder-like polyelectrolyte complexes are partially water insoluble, rubber-like gels capable of absorbing a large amount of water. As illustrated by the data in Fig. 48A, polyelectrolyte complex formation leads to a loss of solubility of the polymer blend in water, expressed in terms of its sol fraction (S), and a reduction of swell ratio (α), defined as the weight of material in a swollen state divided by the dry weight of its gel fraction [343].

The swell ratio is a fundamental characteristic of cross-linked polymeric gels that relates to the density of network junctions. The higher the density of a ladder-like network, the lower the swell ratio [345]. As the LLC concentration increases i.e., the FFP: LLC ratio decreases, the ladder-like network gets denser. The reduction of both values is more pronounced at the comparatively small LLC concentrations (below 40 wt.%) (Fig. 48A). A further increase in LLC content has only a comparatively negligible effect on dissolution and swelling properties [343]. With an increase of the LLC content in blends, the solubility (Sol Fraction) and the swelling of the examined interpolymer complex significantly decreases. As Fig. 48B illustrates, the density of cross-links, which is expressed in terms of the swell ratio, controls the solubility of the ladder-like interpolymer complex. The swell ratio and the content of the soluble fraction in the ladder-like nonstoichiometric complex of PDMAEMA-co-MMA/BMA with PMAA-co-EA increase with pH and the concentration of plasticizer (Fig. 48C). The linear relationship that exists between the plasticizer concentration and the content of sol fraction attests that the soluble component of the hydrogel blend is mainly formed by the plasticizer.

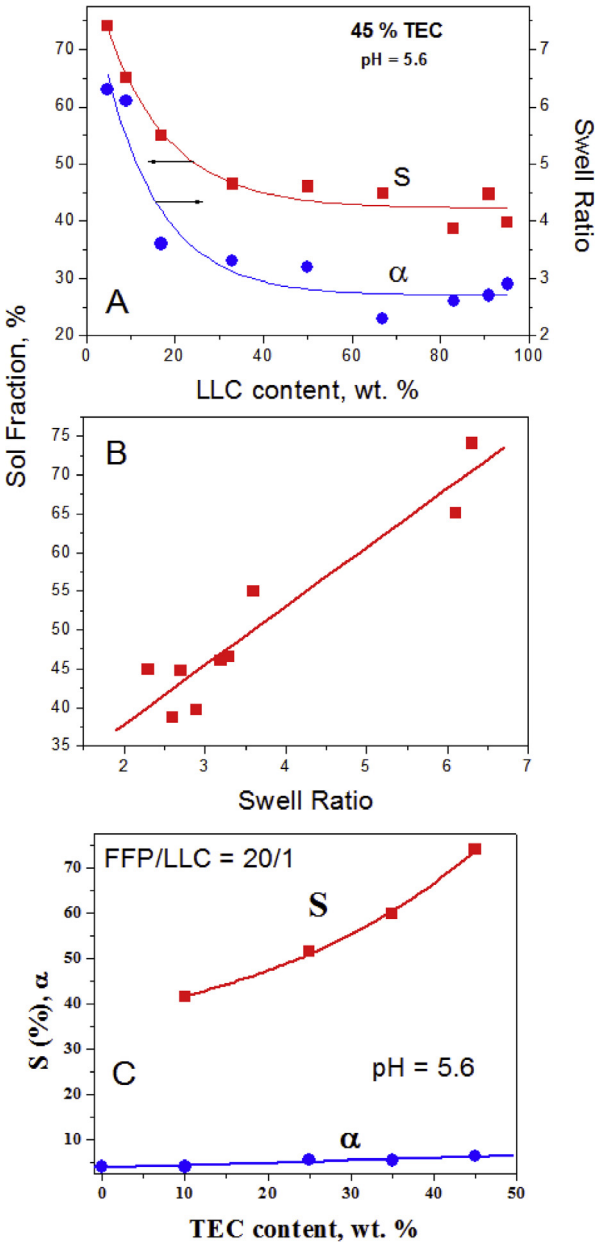

Fig. 48. Swelling and Sol–Gel behavior of PDMAEMA-co-MMA/BMA – PMAA-co-EA polyelectrolyte complexes. A: Effect of LLC concentration on sol fraction (S) and swelling ratio (α) of polyelectrolyte complex with 45 wt % TEC in water; pH 5.6. B: The soluble fraction content in the polyelectrolyte complex as a function of the swell ratio value; pH 5.6. The plasticizer concentration is 45 wt %. C: Effect of plasticizer concentration on solubility and water-absorbing capacity of the polyelectrolyte complex (FFP:LLC = 20:1).
[343], Copyright 2012. Reproduced with permission from Wiley Periodicals Inc.

The higher the hydrophilicity of the plasticizer, the greater the sol fraction and the swell ratio of the blends. The 10% ionization of PDMAEMA-co-MMA/BMA and PMAA-co-EA polymers increases their solubility in water [343].

Replacement of PMAA-co-EA by a more hydrophilic copolymer of maleic acid with methylvinyl ether (PMA-co-MVE) dramatically increases both the swell ratio and the sol fraction of their blends with PDMAEMA-co-MMA/BMA. The content of the soluble fraction in this case is 88% and 49% for the complexes with 6.8 and 10 wt.% PMA-co-MVE, respectively [343].

Thus, the adhesive, mechanical, and water-absorbing properties of polyelectrolyte blends can be easily manipulated by changing the relative concentrations of various copolymers in the blends and the ionization of their functional groups. Coupling adhesive properties with high water-absorbing capacity, typical for hydrogels, defines the polyelectrolyte PSAs as an innovative class of polymer composites with unique combination of performance properties. Owing to the presence of polar (ionic) and nonpolar groups in the copolymers, materials based on polyelectrolyte complexes may be classified as "amphiphilic" adhesives. Such adhesives are compatible with both hydrophilic and hydrophobic substances and can be developed for diverse applications in various fields of industry, particularly in pharmacy for controlled drug delivery. In addition, they can serve as electroconducting PSAs and respond to changes of voltage by varying their viscoelastic and adhesive properties.

7. Pressure-sensitive adhesive hydrogels based on ternary interpolymer complexes with telechelic oligomer

As has been shown in the Section 3 of this review, PVP blends with 30–40 wt.% PEG-400 demonstrate peel strength and probe tack adhesion typical of conventional (hydrophobic) PSAs. However, in contrast to the hydrophobic PSAs, the adhesion of PVP–PEG blends increases appreciably with the moistening of the surface of substrates or in the course of water absorption. Nevertheless, practical use of the PVP–PEG PSA in hydrated environments is essentially restricted by the limitless dissolution of the PVP–PEG complex in water. At the same time, it is well known that ladder-like interpolymer complexes of hydrophilic water-soluble polymers formed via hydrogen bonding or electrostatic interactions between complementary functional groups present in the repeat units of both polymer backbones behave as hydrogels that mainly swell but are insoluble in water (see Section 4 of this review). For this reason, we have used the ladder-like type of interpolymer complex formation to render the PVP–PEG hydrophilic PSA insoluble in water. With this purpose in mind, a third polymeric component is incorporated into the PVP–PEG blend, namely the polyacid, a copolymer of methacrylic acid (MAA) with ethyl acrylate (EA), PMAA-co-EA. The carboxyl groups of the polyacid are capable of forming a ladder-like complex with the carbonyls in the repeat units of long-chain PVP [31,48,72,103,104]. Fig. 49 illustrates schematic structure of the ternary interpolymer–oligomer complex formed by two complementaty high MW polymers and telechelic oligomer bearing hydrogen bonding groups at the ends of its short chains.

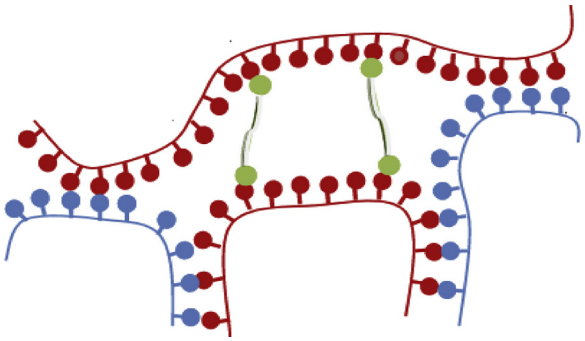

Fig. 49. Schematic illustration of the molecular structure of ternary complex formed by two long-chain polymers containing complementary functional groups in their repeat units and a telechelic oligomer.

7.1. Mechanisms of competitive hydrogen bonding underlying phase behavior of ternary PVP–PEG–Polyacid blends

Strong competition between PEG and PMAA-co-EA for interaction with PVP was a subject of a recent investigation [49]. The hydrogen bonding in partially miscible ternary PVP–PEG–PMAA-co-EA blends has been characterized with FTIR spectroscopy. In order to evaluate the relative strengths of hydrogen bonds in PVP–PEG–PMAA-co-EA blends, quantum-chemical calculations were performed. The results are presented in Tables 3 and 10 [49].

According to this analysis, the most stable complexes are the ternary PVP–PMAA-co-EA–PEG(OH) one and the complex wherein comparatively short PEG chains simultaneously form two hydrogen bonds with PVP carbonyl groups through both terminal OH-groups, acting as H-bonding crosslinks between longer PVP backbones. Incorporation of water molecules into hydrogen bonding of complementary functional groups of polymer components is capable of significantly increasing the strength of ternary interpolymer–oligomer complexes [49]. As a result, the most energetically favorable complex in the PVP–PEG–PMAA-co-EA–H_2O system is a network structure formed by hydrogen bonding of both PEG terminal hydroxyl groups to the carbonyl groups in PVP recurring units through the two water molecules located between the functional groups of the polymers (PVP–H_2O–PEG–H_2O–PVP). The mechanism of specific interaction in PVP–PEG–PMAA-co-EA blends affects the phase behavior of the polymer system. In turn, the interaction mechanism controls the physical properties of the composite material at a macroscopic scale, such as adhesion, viscoelasticity, and swelling [44].

Blends containing less than 30 wt.% of PMAA-co-EA have been shown to possess a single glass transition and are miscible. However, the PVP–PEG blend with 35.7% PMAA-co-EA demonstrates two T_g's of −38 and 55 °C [80]. Both T_g values are atypical of the parent components and are composition-dependent. It follows that the values relate to mixed phases and that the system is partially compatible. Based on the results of the phase behavior investigation of binary PVP–PEG blends [44,80], the lower-T_g phase can

Table 10
Schematic structures and the energies of hydrogen bonds formed between carboxyl groups of polyacid with proton-accepting groups in PVP and PEG in the presence of absorbed water [49].

Complex	Schematic structure	−ΔE (kJ/mol)
PVP-COOH–PEG-H_2O	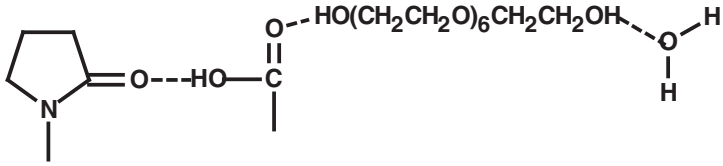	66.0
PVP-H_2O-COOH	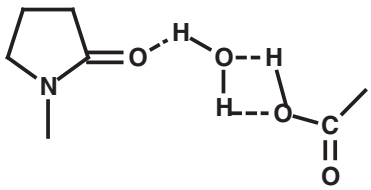	44.1
PVP-COOH–PEG	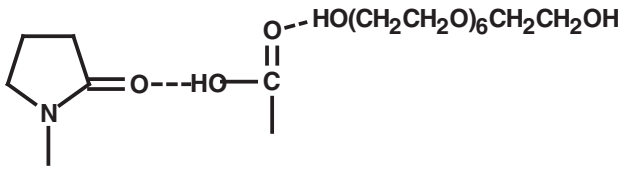	40.7
COOH–HOOC	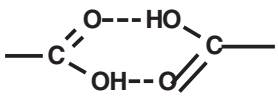	26.5
COOH-H_2O	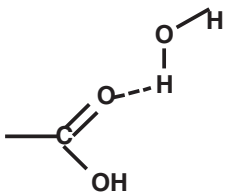	22.6
COOH-PEG (OH)	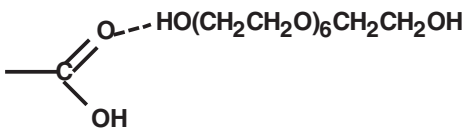	23.5
COOH-PEG (COC)	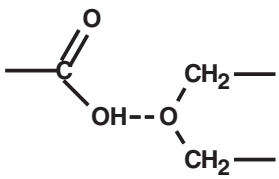	18.5
PVP-COOH	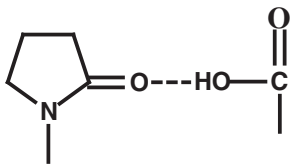	14.7

be logically related to PVP–PEG–PMAA-co-EA complex, whereas the upper-T_g phase corresponds most likely to the phase enriched with PMAA-co-EA. Further increase in the PMAA-co-EA concentration leads to rapid growth of the upper T_g value [49].

In the blends containing less than 9 wt.% of PMAA-co-EA all PEG is associated with PVP in the amorphous phase and is unavailable for crystallization. This fact is readily explained since in the binary PVP blends with PEG-400 the crystalline phase appears as the PEG content achieves 45–50 wt.% [44,76]. The most surprising feature of the DSC traces shown in an earlier paper of our research group (Fig. 4 in [49]) is that the endotherm of PEG melting appears in the range between 10 and 30 wt.% of PMAA-co-EA and vanishes as its amount becomes as high as 36%. Even very small amount of absorbed water (~ 2%) appreciably lowers the PEG binding degree.

The increase in the LLC content begets crystallizable (unbound) PEG due to partial replacement of the PEG in PVP–PEG complex by the LLC (PMAA-co-EA). On the basis of this observation we are able to propose that the carboxyl groups of PMAA-co-EA form stronger hydrogen bonds with the PVP carbonyls than with complementary hydroxyl groups in PEG-400 [49].

The ladder-like cross-linking in the blends of favorably interacting polymers leads to an appreciable increase in cohesion and a decrease in free volume. Thus, it is logical to expect that the PMAA-co-EA polyacid, having a pronounced effect on the balance between the cohesion and free volume in the blends with PVP polybase and PEG telechelic oligomer, will appreciably affect the adhesive performance.

7.2. Tensile properties of PSAs based on ternary PVP–PEG–Polyacid complexes

Tensile deformation accompanies the failure of adhesive joints under a detaching force. At the moment of debonding, the elongation of PSAs reaches many hundreds or thousands of percents and involves orientation of polymer chains in the direction of stretching. It is, therefore, no surprise that close correlation has been observed between the adhesion and the mechanical properties of soft viscoelastic adhesives under tension [346–350], including hydrophilic PVP–PEG adhesives [41,61].

The effect of LLC (PMAA-co-EA) concentration on the tensile properties of ternary PVP–PEG–PMAA-co-EA blends containing 50% PEG-400 is shown in Fig. 50A [72]. The shape of the stress–strain curve changes significantly with the increase in polyacid content. The increase in LLC concentration causes an appreciable gain in mechanical strength (ultimate tensile stress at break σ_b) and a loss of compliance, manifested by a decrease of the maximum elongation ε_b. The mechanical behavior of the binary PVP–PEG blend is similar to that of the ternary PVP–PEG–PMAA-co-EA system containing 4 wt.% LLC. While the blends containing 6% and 8% polyacid reveal the deformation mechanism typical of rubbers, the blend of 12% LLC shows the behavior typical of cured elastomers. The tensile modulus E can be determined as the slope of the initial linear region of a stress–strain curve, where Hooke's law is applicable, and is considered as a material constant

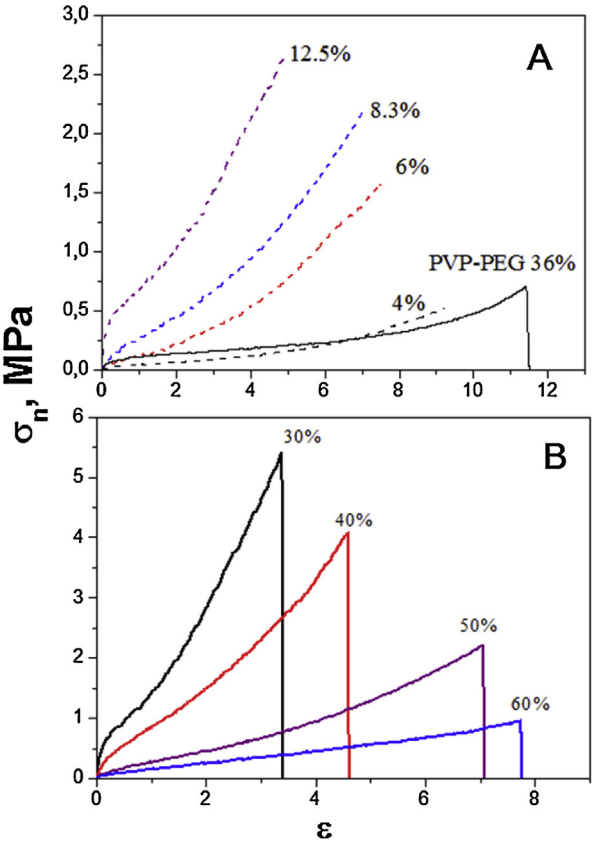

Fig. 50. Tensile properties of ternary PVP–PEG–Polyacid complexes. A: Stress–strain curves for ternary PVP–PEG–LLC blends containing 50% PEG and a constant content of absorbed water (7 wt%) obtained under uniaxial drawing at the rate of 1 mm/s. The solid curve corresponds to a PVP–PEG binary blend containing 36 wt% PEG-400. The dashed curves are for ternary blends with different fractions of the LLC indicated in the Figure. B: Impact of PEG weight % on tensile deformation of PVP–PEG–LLC blends. The PVP:LLC ratio is 5:1. The content of absorbed water is 7 wt%. Tensile rate is 1 mm/s. PEG wt.% are indicated in the Figure. σ_n, nominal stress (MPa), ε, relative elongation.
[72], Copyright 2007. Reproduced with permission from Taylor & Francis.

that characterizes polymer elasticity. With the increase of LLC concentration the modulus increases significantly, indicating a sharp increase in the ladder-like network density [72].

The value of ultimate tensile stress at break of a stretched film is a measure of cohesive strength of a strained material. As has been shown for binary PVP–PEG blends, the larger the free volume the higher the value of the maximum elongation-at-break [38,84]. The formation of polymer–oligomer cross-linked PVP–PEG complex has been shown earlier to lead to enhanced cohesive strength and large free volume. Their combination determines the adhesive properties of PVP–PEG blends. In contrast to this behavior, the formation of a ladder-like complex is accompanied by an increase of cohesive strength coupled with a decrease in free volume.

We consider now the effect of PEG concentration on tensile deformation of ternary PVP–PEG–PMAA-co-EA blends (Fig. 50B) [72]. The blend containing 30% PEG deforms as a tough-solid material exhibiting a pronounced effect of

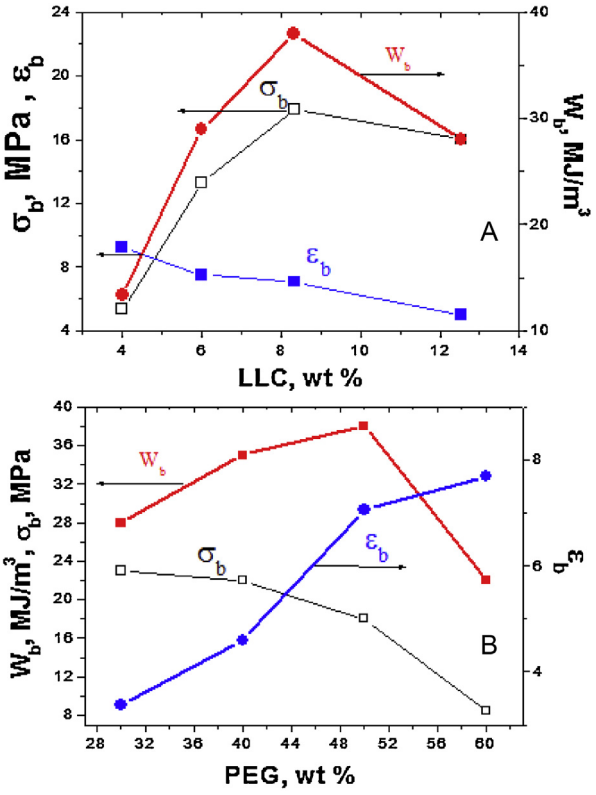

Fig. 51. Effects of LLC and PEG contents on the total work to deform and break the PVP–PEG–LLC adhesive film, W_b; ultimate tensile strength, σ_b; elongation-at-break, ε_b. Tensile rate is 1 mm/s. The content of absorbed water is 7 wt%.
[72], Copyright 2007. Reproduced with permission from Taylor & Francis.

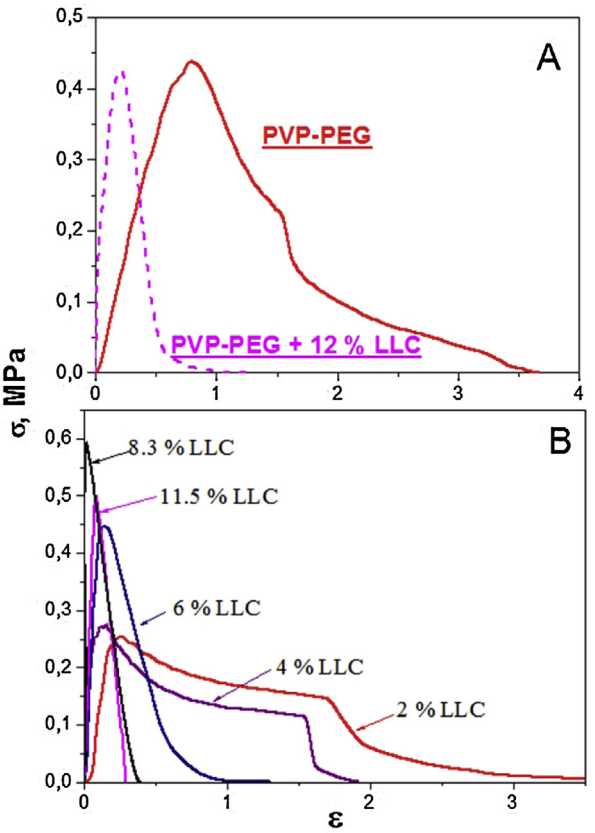

Fig. 52. Adhesion properties of ternary PVP–PEG–Polyacid complexes. A: Probe tack curves of binary PVP–PEG (36 wt%) and ternary PVP–PEG (29%)–LLC (PMAA-co-EA, 12%) blends. Debonding rate is 0.1 mm/s. B: Effect of LLC (PMAA-co-EA) concentration on probe-tack stress–strain curves of PVP–PEG (50 wt%)–LLC ternary blends. The content of absorbed water is 7 wt%. Debonding rate is 0.1 mm/s.
[72], Copyright 2007. Reproduced with permission from Taylor & Francis.

strain hardening, while the blend with 60% PEG reveals a comparatively much more distinct liquid-like behavior. The PEG is a good plasticizer for the PVP blends with the PMAA-co-EA LLC [48]. As follows from the data in Fig. 50B, the increase in PEG content promotes ductility of PVP–PEG–LLC blends by increasing the free volume.

The data in Fig. 51 [72] indicates an essential difference in the effects of the LLC (PMAA-co-EA) and the telechelic oligomer (PEG-400) on tensile deformation of the ternary PVP–PEG–PMAA-co-EA blends. Recall that the values of ultimate tensile stress (σ_b) and maximum elongation-at-break (ε_b) of a stretched polymer film are, respectively, indirect measures of cohesive strength and free volume of the strained polymer [38,84], whereas the work of viscoelastic deformation up to the break of the polymer film W_b characterizes the amount of energy required to stretch and break the polymer film. For binary PVP–PEG blends a fairly reasonable correlation has been established between the W_b, the adhesion characteristics such as peel strength [41] and the practical work of adhesion measured with probe tack test [42,61].

As is evident from the data in Fig. 51 [72], the LLC (PMAA-co-EA) appreciably increases the cohesive strength (σ_b) and decreases the free volume (ε_b), acting like an interpolymer noncovalent cross-linker. While the maximum elongation as a function the LLC content monotonically decreases, the tensile strength σ_b goes through a maximum at 8% LLC concentration and then decreases slightly. At the same time, the PEG-400, serving as a typical plasticizer in PVP–PEG–PMAA-co-EA system, causes a smooth decrease of cohesive strength (σ_b) and an appreciable increase in free volume (ε_b). The role of PEG as crosslinker is, thus, diminished in the ternary blends, in contrast to the binary PVP–PEG blends [72].

7.3. Effects of the ladder-like and telechelic oligomer crosslinkers on adhesion of ternary PVP–PEG–Polyacid complexes

Because the ratio between the cohesive strength and the free volume is a factor that accounts for adhesive capability of a material, and taking into consideration that the binary PVP–PEG complex is tacky, it is logical to expect that adding the LLC (PMAA-co-EA) to the PVP–PEG complex would destabilize the specific balance between the cohesion and free volume and as a result of this the adhesion would deteriorate. In fact, as is seen from the probe tack curves presented in Fig. 52 [72], incorporation of the LLC (PMAA-co-EA) into the binary PVP–PEG adhesive blend has only a negligible effect on the value of maximum stress,

but decreases considerably the work of debonding (the area under the stress–strain curve).

The probe-tack profiles in Fig. 52A and B tell us about the mechanism of the debonding process. As follows from the curves in Fig. 52A, the ladder-like noncovalent cross-linking of FFP (PVP) results in a dramatic change of the debonding mechanism from twofold, typical of PSAs (binary PVP–PEG blend), to the solid-like, found for ternary PVP–PEG–PMAA-co-EA blends. The transition from a liquid-like mechanism of deformation to solid-like with an increase of LLC concentration is shown in Fig. 52B. The blend containing 2 wt.% PMAA-co-EA deforms as a typical PSA. A twofold increase in the LLC content rapidly reduces the free volume and, as a consequence, decreases the maximum elongation. Further increase in the LLC concentration increases both cohesive strength and cavitation stress, which reach maximum values at 8 wt.% of the PMAA-co-EA in the blends. If the LLC concentration increases further the maximum stress begins to decrease since the material under such a debonding rate becomes brittle. The practical work of adhesion W_a is a decreasing function of PMAA-co-EA concentration and achieves its limiting value ($W_a = 37\ J/m^2$) at 4 wt.% LLC. The W_a value (J/m^2) should not be confused with the W_b (MJ/m^3), the latter refers to the total work of viscoelastic deformation up to break of the adhesive film in the course of uniaxial drawing [72].

The PMAA-co-EA is not a unique carboxyl-containing polymer that can be employed as an LLC for a film-forming polymer (PVP). Similar effects are exhibited by another polyacid, namely hydroxypropylmethylcellulose phthalate (HPMCP). The transition to a solid-like behavior with the increase of LLC concentration is typical for HPMCP, which is a much more rigid-chain polymer than the PMAA-co-EA. This is likely the reason why the peak stress of the PVP–PEG–HPMCP blend is higher than that of the PVP–PEG–PMAA-co-EA system. In the PVP–PEG–HPMCP complex both the maximum stress and the work of debonding go through the maximum at 15 wt.% LLC concentration [72].

Due to the presence of carboxyl groups, an LLC is a pH-sensitive polymer. With the increase of pH value, neutralization occurs that renders the carboxyl groups partially ionized. The effect of LLC ionization by treatment of polyacid with NaOH solution impacts adhesion due to the following reasons:

(1) Only nonionized carboxyl groups are capable of forming H-bonds with complementary groups in PVP and PEG [49]. This factor affects the network density of H-bonds and, consequently, the cohesive strength and adhesion;
(2) Due to the electrostatic repulsion between carboxylate anions, the LLC chains become extended and increase the free volume.

As is obvious from the probe tack data shown in Fig. 53, partial ionization of ionogenic groups in PMAA-co-EA results in tack improvement, but does not change the mechanism of debonding that remains solid-like and is not accompanied by fibrillation for PVP–PEG–LLC blends [72].

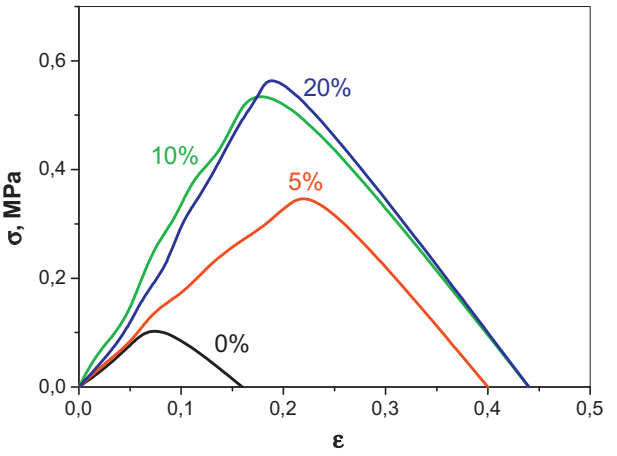

Fig. 53. Impact of ionization of carboxyl groups of LLC (PMAA-co-EA) on the probe tack curves of the PVP–PEG–LLC ternary blend containing 12 wt% absorbed water. The degree of ionization (%) is shown in the Figure. [72], Copyright 2007. Reproduced with permission from Taylor & Francis.

Fig. 54 demonstrates the effect of PEG-400 on probe tack in PVP–PEG–PMAA-co-EA blends. The PEG-400 acts as a plasticizer in PVP–PEG–LLC blends by promoting the fibrillation process and increasing the value of maximum elongation. In this respect, the effect of PEG concentration increase is similar to the decrease of LLC content (Fig. 52A and B).

As is obvious from a comparison of the curves in Fig. 54, the practical work of adhesion increases with the increase of PEG-400 concentration up to 60 wt.%. It follows that PEG is an enhancer of adhesion for PVP–PEG–PMAA-co-EA blends, while the peak stress goes through a maximum at 40 wt.% PEG-400 in the blend. The value of the maximum of debonding force is traditionally considered as the tack [351]. The observed disagreement between the amplitudes of the peak stress and the work of debonding indicates that the former value cannot always be accepted as an unequivocal characteristic of adhesion. This conclusion is

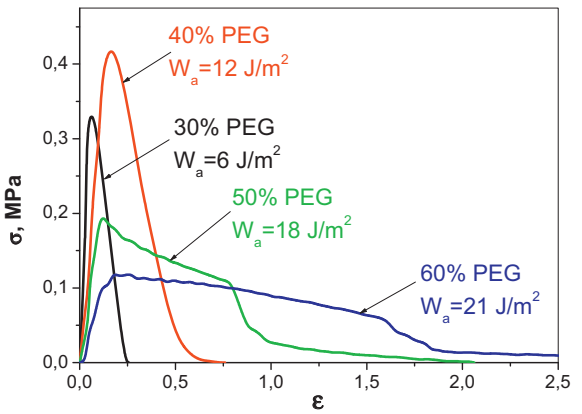

Fig. 54. Effect of PEG-400 wt % on probe tack stress–strain curves of PVP–PEG–LLC system. The PEG content in the blends is indicated in the Figure, the contents of LLC (PMAA-co-EA) and water are 8.3 and 12 wt %, respectively. Debonding rate is 0.1 mm/s.
[72], Copyright 2007. Reproduced with permission from Taylor & Francis.

confirmed by the data for other PSA systems reported in the literature [346].

The appropriate value of the glass-transition temperature T_g is a necessary but insufficient condition for pressure-sensitive adhesion [38]. PSAs possess generally the T_g values below −50 °C. Being a good plasticizer of the PVP–LLC interpolymer complex, the PEG decreases the T_g of ternary PVP–PEG–PMAA-co-EA blends from −14 to −59 °C as the PEG concentration increases from 15 to 60 wt.% [49]. PSAs based on PVP–PEG binary blends display T_g values below −55 °C [44,80]. In this connection we can expect that the ternary blends containing 50 wt.% PEG or higher and featuring a T_g below −55 °C may serve as PSAs. The glass transition temperatures of PVP–PEG blends with relatively low values of the PVP:LLC ratio have been found to be too high for good adhesion [49]. However, the T_g can be decreased to meet the value desired for PSAs by incorporating an additional plasticizer. One such auxiliary plasticizer, compatible with the PVP–PEG–LLC system, is water.

7.4. Mechanisms of swelling and dissolution of ternary PVP–PEG–Polyacid complex in water

Wedge micro-interferometry (WMI) [352] was used to study swelling and dissolution of films in phosphate buffers at different pH. The principles underlying the wedge micro interferometry (WMI) technique have been described in detail elsewhere [45,352]. Briefly, this technique utilizes information provided by evolving interference fringe patterns of light transmitted through a sample which thickness varies gently along one axis, and its composition varies in the perpendicular direction. Uniform samples exhibit equally spaced interference fringes perpendicular to the axis of increasing sample thickness, while the composition gradients in the perpendicular direction cause sharp bending and crowding of the fringes. When all components of the polymer blend are soluble in the solvent, the composition gradient and fringe density are large at early times following initial contact at the interface, but later relax to uniform composition, with an associated parallel fringe pattern. When some of the components are immiscible, however, a sharp phase boundary between the polymer and the solvent and dissolved components will appear. This phase boundary may block light transmission, and will show up as a dark band in the interferogram. At equilibrium parallel fringes are expected on both sides of the interface, but fringe spacing on the two sides will not be the same due to differences in refractive index.

Typical WMI interferograms of the contact interface between PVP–PEG–PMAA-*co*-EA films and phosphate buffers at two pH values, 5.6 and 7.4, are shown in Fig. 55 [352]. These pH values represent the nonionized and ionized states of the PMAA-*co*-EAA component. At pH = 7.4 (Fig. 55A), the micrographs reveal interference patterns that are typical of systems with unlimited solubility. No phase discontinuity is observed, but a steep compositional gradient is inferred in the region where the fringes are bent and crowded. This region, which corresponds to the dissolution zone, separates the region of nearly pure buffer (right) from the yet undissolved hydrogel (left). Curvature in the fringes in the undissolved region is probably due

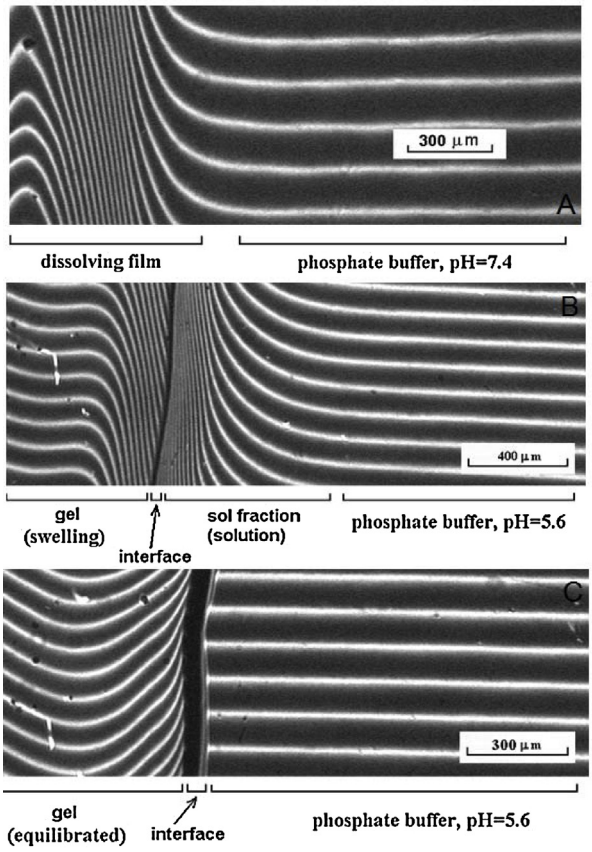

Fig. 55. Effects of pH and contact time on micro-interferograms of the contact interface between PVP(59%)–PEG(29%)–PMAA-co-EA (12%) film (left) and phosphate buffer (right). A: pH = 7.4 (50 mM). Contact time is 2 min, T = 36 °C. B: pH = 5.6 (50 mM), at 36 °C. Contact time = 3 min. C: Contact time = 20 h for the same system as in B.
[352], Copyright 2008. Reproduced with permission from Society of Chemical Industry.

to variations in composition resulting from selection of components that dissolve at different rates. With time, the dissolution zone broadens as interdiffusion proceeds. At very long times, the sample composition becomes uniform and displays parallel fringes [352].

At pH 5.6 (Fig. 55B,C) the interference patterns display a sharp persistent phase boundary, which indicates immiscibility. At the early stages (Fig. 55B), there is a rapid leaching of certain blend components, as the fringe bending/crowding near the phase boundary indicates. At later stages (Fig. 55C), buffer appears to be of uniform composition, while the composition gradient remains in the hydrogel. In the latter case, slow leaching of soluble blend components from the gel occurs, but these components equilibrate rapidly in the buffer. The nonmonotonic behavior of fringes on the hydrogel side is probably due to the multiplicity of interdiffusing components.

Fig. 56 shows the relationship between the fraction of PEG initially incorporated in the hydrogel and the fraction of polymer that is leached out as sol after 2 days. This sol fraction increases linearly with PEG content. From these graphs it can be concluded that PEG is the primary com-

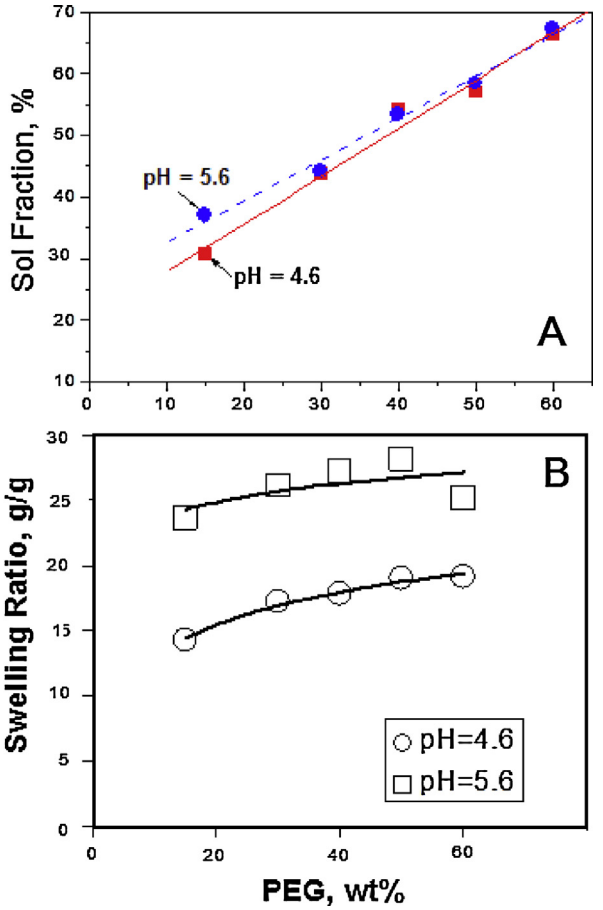

Fig. 56. Sol–Gel behavior of PVP–PEG–PMAA-*co*-EA hydrogels. A: Impact of PEG loading on sol fraction. B: Effect of pH and PEG loading on PVP–PEG–PMAA-co-EA hydrogel swelling.
[352], Copyright 2008. Reproduced with permission from Society of Chemical Industry.

ponent of the sol fraction. However, sol fraction is always greater than PEG fraction, indicating that other components such as low molecular weight PVP fractions are also leached, but to a lesser extent. Except for the lowest PEG fraction, the sol fraction is the same at pH 4.6 and 5.6. It is evident that the most stable three-dimensional hydrogen bonded network in the swollen state is formed predominantly between PVP and the PMAA-co-EA copolymer.

As illustrated in Fig. 56A [352], swelling of PVP–PEG–PMAA-co-EA hydrogel after 2 days is pH dependent. The hydrogels swell 15–30 fold, with the PEG concentration only weakly affecting the swelling ratio. The swelling ratio increases appreciably at higher pH due to partial neutralization and ionization of PMAA-co-EA carboxylic groups present in the hydrogen bonded hydrogel. Ionization provokes swelling in part due to the electrostatic osmotic repulsion of polyelectrolyte chains and in part due to loss of carboxylic acid H-bond donors sites. It is obvious that the same mechanism of PMAA-co-EA ionization governs eventual dissolution of the hydrogels at higher pHs, as seen in Fig. 56B [352].

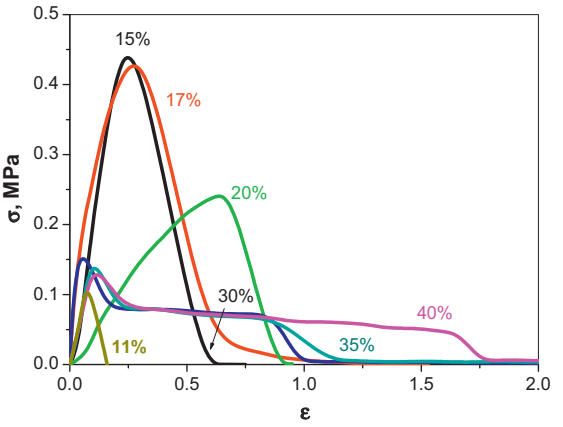

Fig. 57. Effect of absorbed water (wt %) on probe tack stress-strain curves of PVP–PEG –PMAA-*co*-EA blends. The PVP/PMAA-co-EA ratio is 5:1, and PEG content is 29 wt%. Debonding rate is 0.1 mm/s.
[351], Copyright 2008. Reproduced with permission from Society of Chemical Industry.

7.5. Effect of absorbed water on adhesion of PVP–PEG–Polyacid hydrogels

The capacity of PVP–PEG–PMAA-*co*-EA hydrogels to adhere to a variety of substrates is a significant feature. The blends are nontacky or have low tack in the dry state. However, as shown in Figs. 57 and 58B, they develop appreciable tack upon hydration [71]. As the hydration increases, the tack passes through a maximum and stabilizes at a moderate level as the swollen hydrogel becomes softer and more compliant. Such an adhesive profile is characteristic of bioadhesives that are designed to adhere to highly moistened biological tissues.

Fig. 58 compares the effects of absorbed water on the probe tack adhesion of a traditional synthetic bioadhesive Carbopol® 974P (a slightly covalently crosslinked poly(acrylic acid), PAA), binary PVP–PEG and ternary PVP–PEG–PMAA-co-EA hydrogels. Note that in Fig. 58B the values of practical work of adhesion for binary and ternary blends are plotted against different scales. Qualitatively, the behaviors of traditional and novel bioadhesive hydrogels are very similar. Carbopol bioadhesive exhibits no tack in dry state, but becomes tacky upon absorption of moisture and demonstrates no signs of probe tack adhesion reduction until absorption of 100% of water by weight. In a similar manner, for PVP–PEG binary blends and for ternary PVP–PEG–Polyacid blends containing 17 wt.% of PMAA-co-EA, the adhesion increases with blend hydration going through a maximum at 9 wt.% water (PVP–PEG) and 17% for the ternary blend. However, taking into account the scales of debonding work in Fig. 58A and B, we see that both the PVP–PEG and PVP–PEG–Polyacid hydrogels display unprecedently high adhesion as compared with the Carbopol bioadhesive. In this way, noncovalently crosslinked ternary PVP–PEG–Polyacid complexes combine high tack (an intrinsic feature of hydrophobic PSAs) with the capability of forming adhesive joints with wet substrates, featured for bioadhesives.

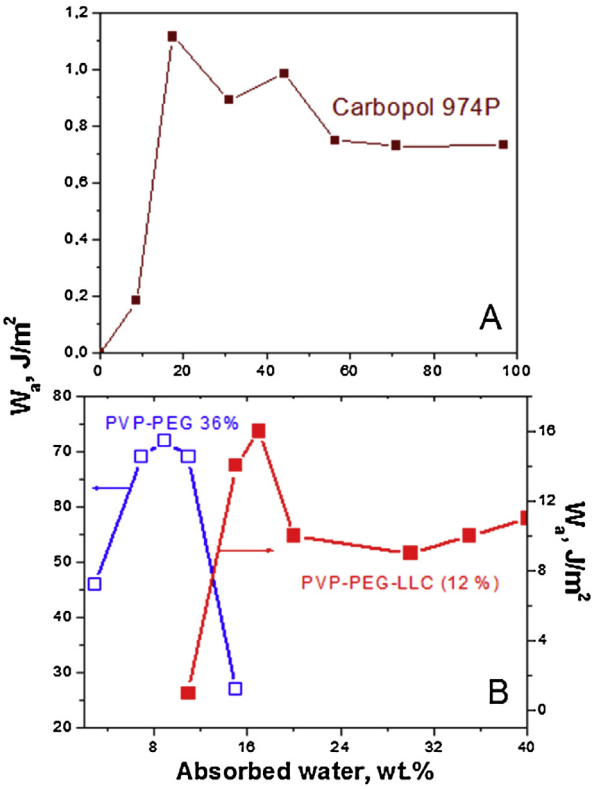

Fig. 58. Comparative effects of hydration on the practical work of adhesion (W_a) of Carbopol® 974P bioadhesive (A), PVP–PEG and PVP–PEG–LLC (PMAA-co-EA) hydrogels (B). Debonding rate is 0.1 mm/s.
[72], Copyright 2007. Reproduced with permission from Taylor & Francis.

This behavior enables the hydrophilic adhesives to perform as typical bioadhesives [26] and, thus, they are useful for medical applications as they adhere to highly hydrated biological substrates such as teeth and mucosal membranes [31]. It is noteworthy that the PVP blend containing 36 wt.% PEG-400 demonstrates the best adhesion at ambient conditions (room temperature and a typical relative humidity), because being exposed to the relative humidity of the surrounding atmosphere of 50% at 20 °C, it contains 9–11 wt.% of absorbed water (see Fig. 8, Section 3.4). In contrast to the behavior of binary PVP–PEG blends, the ternary PVP–PEG–LLC blends demonstrate much lower values of practical work of adhesion (Fig. 58) [72]. Since addition of LLC leads to a reduction in free volume and an increase in intermolecular cohesion energy, it is not surprising that the binary PVP–PEG complexes dissipate more detaching energy and thus demonstrate higher adhesion than the ternary PVP–PEG–PMAA-co-EA blends that combine polymer–oligomer and ladder-like types of noncovalent cross-linking (Fig. 57).

By comparing the probe tack data in Figs. 54 and 57, it is apparent that the effect of absorbed water on tack is similar to the effect of the other plasticizer, PEG. While relatively dry PVP–PEG–PMAA-co-EA compositions (containing up to 11 wt.% of water) are initially nontacky and reveal solid-like mechanism of debonding without fibrillation, the adhesion increases with an increase of the content of absorbed water up to 17 wt.% (Figs. 57 and 58B) [72]. A sharp transition in the deformation type showing a pronounced plateau in the stress–strain curves and, thereby, a well-expressed mechanism of fibrillation, occurs between 7 and 11 wt.% of absorbed water for the binary PVP–PEG blends [72] and between 20% and 30% degrees of hydration for the ternary PVP–PEG–PMAA-co-EA blends (Fig. 57). Thus, in strong contrast to the behavior of conventional hydrophobic PSAs, water acts as an enhancer of adhesion in ternary PVP–PEG–LLC blends.

PVP–PEG–PMAA-co-EA hydrogel films retain their integrity upon hydration – a feature characteristic of covalently crosslinked hydrogels. Since the PVP–PEG–PMAA-co-EA hydrogels do not develop weak spots, they do not leave residue after removal from a substrate. The observed adhesive profile of the blends is also consonant with improved ease of handling during manufacturing, since in dry state the low tack prevents the blends from sticking to machinery tools or packaging materials.

The PVP–PEG–PMAA-co-EA hydrogen bonded networks, described in this review, behave like covalently crosslinked hydrogels over reasonably long timescales. The components are all of pharmaceutical grade, and the blends can be formed without introduction or formation of toxic by-products. Moreover, since the hydrogen bonding interactions that form the network are reversible, the blends are much more readily processed by controlling temperature, solvent choice, etc. The materials are malleable under various processing conditions such as drawing, molding, and extrusion. Therefore, the blends appear to present several advantages from the manufacturing and regulatory points of view. These favorable properties such as the ability to swell but yet retain both cohesive strength and tack, combined with processability, suggest a wide range of applications of these materials in the biomedical, cosmetic, industrial, and household fields.

8. Hydrophilic adhesives based on interpolymer and polymer–oligomer complexes compared with conventional PSAs and bioadhesives

As has been mentioned above (see Table 1), the vast majority of commercial PSAs are made of hydrophobic polymers and their common disadvantage is a lack of tack toward wet substrates. Traditional synthetic bioadhesives, based on covalently crosslinked hydrogels, adhere to moistened substrates but demonstrate much lower adhesion (compare Fig. 58 A and B).

Covalently cross-linked hydrogels have received much attention due to their permanence of shape, their elastic behavior under stress, and their ability to house, release, and serve as a medium for controlled permeation of active substances. Unfortunately, covalently cross-linked hydrogels have not been applied as broadly as was hoped particularly in the biomedical arena. One limiting factor has been the difficulty in guaranteeing removal of impurities such as unreacted monomers, sol fractions, nonaqueous solvents, and initiators. A second limitation is that once the three-dimensional covalent network is formed, it cannot be readily processed.

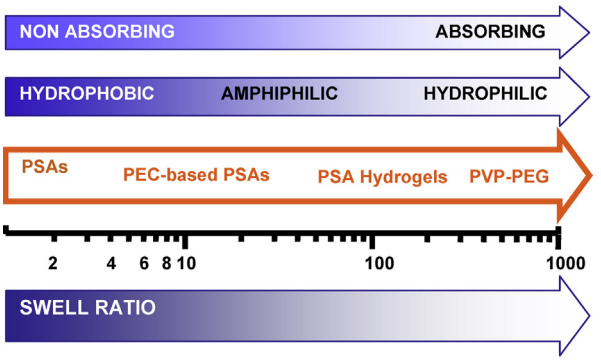

Fig. 59. Classification guide of pressure sensitive adhesives of controlled hydrophilicity and water-absorbing capability based on polymer–oligomer and interpolymer complexes.
[31], Copyright 2009. Adapted with permission from Taylor & Francis.

Innovative technology of PSA formulation is based on the molecular design of PSA materials and coupling high molecular mobility with strong intermolecular cohesion offers products with varying adhesion, mechanical, and water-absorbing capabilities. This technology provides a convenient tool for obtaining the desired material performance by simply varying the composition of polymer blends. The values of swell ratio and sol fraction can be used as a basis for the classification of novel adhesives in terms of their hydrophilicity. The higher the swell ratio and sol fraction values, the higher the hydrophilicity of the adhesive and the lower the density of noncovalent cross-linking. The binary blends of PVP–PEG demonstrate SF = 100% and the value of swell ratio tends to be exceptionally high. Conventional hydrophobic PSAs such as acrylic Duro-Tak 87-900A and SIS-based Duro-Tak 387 2287 adhesives fall on the other side of the scale of hydrophilicity (SF ≈ 0% and swell ratio $\alpha \approx 0.1$). This means that their percentage water absorbency (based on the grams of water absorbed per 1 g of dry material at 25 °C and 100% relative humidity) does not exceed 10%.

Hydrophilic adhesives fill the range between these two extremes on the scale of hydrophilicity (Fig. 59). The swell ratio scale is used in Fig. 59 to classify the adhesive absorbents of moisture in three broad categories [31]: amphiphilic PSAs based on polyelectrolyte complexes, water swellable but mainly insoluble PSA hydrogels based on ternary polybase–polyacid–telechelic oligomer complexes (PVP–PEG–Polyacid), and water-soluble PSAs (PVP–PEG).

Comparison of the adhesive, viscoelastic and relaxation properties of traditional PSAs and the PSAs based on interpolymer complexes is described in a range of publications [17,31,38,51,61,100,101,103]. In spite of the fact that chemical compositions of traditional, hydrophobic and innovative hydrophilic PSAs have little in common, the same general factors govern their adhesive and viscoelastic behaviors. For instance, the Dahlquist criterion of tack holds for all PSA classes [51], longer relaxation times govern the elasticity and adhesion of different PSAs [99–102] and similar glass transition temperatures and coefficients of self-diffusion are inherent in a variety of PSAs [38]. The adhesive joint strengths of hydrophilic PSAs fall generally in the range usually found for covalently uncrosslinked hydrophobic PSAs, though they can be somewhat exceeded by covalently crosslinked PSAs and adhesives based on triblock copolymers [31]. While molecular theory of pressure sensitive adhesion [38] predicts correctly the position of the adhesion maximum along the scale of the ratio of molecular mobility to intermolecular cohesive interaction energy, the absolute magnitude of adhesion strength depends also on supramolecular architecture of adhesive material.

9. Conclusions

Earlier the phenomenon of pressure sensitive adhesion was considered not only in its traditional aspect, as a specific property of viscoelastic materials under applied compressive and tensile forces, but as a permanent three-stage process that includes three indivisible consecutive stages: adhesive bond formation, adhesive material relaxation and debonding [353]. This implies that the second (relaxation) and the third (debonding) stages cannot be studied separately if the adhesive joint in the course of the first stage is never formed. The PSA behavior at each subsequent stage is affected by the earlier stages, providing a “memory effect”. In other words, at each stage of the process the PSA “remembers” what happened at earlier stages [100]. The relaxation represents continuous rearrangements of PSA supramolecular structure that includes diffusion and translational movement of polymer segments as a constituent mechanism induced and driven by macromolecular interaction. In addition, the pressure sensitive adhesion should also be treated as an interfacial phenomenon, wherein the strength of an adhesion joint depends on the properties of the adhesive material and a substrate. In the present review we consider only those aspects of pressure sensitive adhesion which are indispensable for molecular design of innovative PSAs: their molecular and supramolecular structures.

At the most fundamental molecular level, a high strength of PSA joints requires a compromise between two mutually conflicting factors, namely high energy of intermolecular cohesion and large free volume. The former factor governs the amount of mechanical energy dissipated in the course of debonding process, whereas the latter contributes both to adhesive bond formation (tack) and the ability of a PSA material to develop large deformations under a detaching force, when the PSA polymer demonstrates large tensile strain and fibrillation. Insights gained into the molecular structures responsible for the pressure sensitive adhesion have opened the doors to molecular design of new PSAs with optimized performance properties. The production of innovative PSAs has been made possible by blending nonadhesive polymers and oligomers bearing complementary functional groups capable of forming intermolecular hydrogen or electrostatic bonds.

Considering that the functions of adhesive blend components in PSA performance are clearly characterized, as described in this review, the molecular design method

Table 11
Functional groups of complementary polymers and oligomers capable of serving as parent components of PSA composites based on polymer–oligomer and interpolymer complexes.

Component 1	Component 2	Bonding Type
—COOH	$-NH_2$, —NHR, $-NR_2$	Electrostatic
$-SO_3H$	—OH, —C—O—C—, $-CONH_2$, —CONHR, $-CONR_2$	Hydrogen
$-COO^-$ $-SO_3^-$	$-NH_3^+$, $-NH_2R^+$, $-NHR_2^+$, $-NR_3^+$	Ionic
—PhOH —OH	$-CONH_2$,—CONHR,$-CONR_2$—PhOH—OH—COOH	Hydrogen

suggests in a very illustrative manner how the adhesive and mechanical properties of the hydrophilic PSA materials may be improved by a change of PSA composition. Additive tools to optimize adhesion include conventional practice employed in adhesive technology: incorporation of plasticizers, fillers and tackifiers, variation of absorbed water content and debonding rate. Also it must be remembered that the PSA of each type exhibit best adhesion in its own specific temperature interval. For instance, the adhesion strength of PVP–PEG blend increases from 114 to 152 J/m^2 as the temperature rises from 20 to 30–40 °C. Adhesion of the polyelectrolyte complex reaches its maximum at 60 °C, etc. [51].

The time has passed when the efforts of adhesive material designers were solely directed to the achievement of strongest adhesion. The time is ripe for the adhesion scientists to develop innovative materials with a wide and well-balanced spectrum of various and often unprecedented performance properties. Adhesive superabsorbents of moisture, "smart" thermoswitchable and electroconductive PSAs are the typical examples of such innovative materials. Currently they are in well-advanced stage of the development in our laboratory.

Table 11 summarizes the types of major complementary functional groups in numerous polymers and oligomers that are feasible for use as parent components in novel PSA composites. The number of functional polymers suitable as parent components for novel PSAs with tailored performance properties is very large, suggesting that the blending approach, based on molecular design considerations, will lead to significant innovations by the adhesives industry in the coming decades.

The PSAs of controlled hydrophilicity and water-absorbing capacity, as described in the present review, find use in health and personal care as skin contact adhesives (see Section 3.11), adhesive platforms for tooth whitening strips [354,355], and "smart", thermoswitchable, painlessly removable from skin surface superabsorbents of moisture in wound and ulcer dressings [356]. They are also miscible and compatible with numerous low and high molecular weight compounds, leading to a broad spectrum of future commercial products with presently unachieved or unexplored performance properties. Such adhesive innovations include hybrid PSAs based on biomacromolecules. The hybrid PSAs combine the conventional rheological principles of pressure sensitive adhesion with biospecific mechanisms of cell adhesion, as well as bioinspired PSAs for various medical, household, and industrial applications. The age of rationally designed adhesives is just around the corner.

Acknowledgements

Part of the work described in this review was supported by the Ministry of Education and Science of Russian Federation, State Contract No. 14.574.21.0073. The authors thank their former and present associates, Dr. D. Bayramov, Dr. M. Novikov, Dr. T. Levada, Dr. E. Bermesheva, Dr. A. Moscalets, Dr. A. Eliseev, Dr. Georgy A. Shandryuk, Mr. B. Gdalin, Mr. I. Rodionov, Mrs. P. Kireeva, Mrs. G. Perepelitsa, Mrs. N. Sherstneva, Mrs. K. Bovaldinova and Mrs. K. Shchepetova for their appreciable contribution to the development of novel pressure sensitive adhesives and a number of products on their basis. Within the period from 1999 to 2008 the research described in this review was supported by the Corium International, Inc., and the US Civilian Research & Development Foundation (CRDF). The authors appreciate stimulating advise, fruitful research collaborations and significant contributions to this work by Prof. Alexaner Yu. Grosberg, Prof. Costantino Creton, Prof. Ronald A. Siegel, Prof. Anatoly E. Chalykh, Prof. Ivan M. Papisov, Prof. Alexander B. Zezin, Prof. Elena Y. Kramarenko, Prof. Igor Ya. Erukhimovich, and Prof. Jasper van der Gucht. Valuable discussions and the support of Acad. Nikolai A. Platé are gratefully acknowledged. The text contains segments reproduced with permission from the following sources: [38], Copyright 2012, Wiley; [80], Copyright 2000, Elsevier; [186], Copyright 2012, Wiley; [223], Copyright 2006, ACS; [272], Copyright 2005, Taylor & Francis; and [303], Copyright 2003, ACS.

References

[1] Michaels AS. Polyelectrolyte complexes. Ind Eng Chem 1965;57:32–40.
[2] Ikkala O, ten Brinke G. Functional materials based on self-assembly of polymeric supramolecules. Science 2002;295:2407–9.
[3] Kabanov VA. Polyelectrolyte complexes in solution and in condensed phase. Russ Rev Chem 2005;74:3–20.
[4] Khutoryanskiy VV, Staikos G, editors. Hydrogen-bonded interpolymer complexes: formation, structure and applications. World Scientific Publishing Co.; 2009. p. 366pp.
[5] Tünemann AF, Müller M, Dautzenberg H, Joanny JF, Löwen H. Polyelectrolyte complexes. Adv Polym Sci 2004;166:113–71.
[6] Anonymous. Glossary of terms. Test methods for pressure sensitive adhesive tapes. Pressure Sensitive Adhesive Tape Council; 1996 http://www.pstc.org/i4a/pages/index.cfm?pageID=3336(1 pp) [accessed October 2014].
[7] Everaerts AI, Clemens LM. Pressure sensitive adhesives. In: Chaudhury M, Pocius AV, editors. Adhesion science and engineering – 2. Surfaces, chemistry and applications. Amsterdam: Elsevier Ltd.; 2002. p. 465–534.
[8] Kinloch AJ. Adhesion and adhesives: science and technology. London, New York: Chapman and Hall; 1987. p. 441pp.
[9] Dahlquist CA. Pressure-sensitive adhesives. In: Patrick R, editor. Treatise on adhesion and adhesives, vol. 2. New York: M Dekker; 1969. p. 219–60.

[10] Dahlquist CA. Tack. In: Ministry of technology, editor. Adhesion: fundamentals and practice. London: McLaren and Sons Ltd.; 1996. p. 143–51.
[11] Dahlquist CA. Creep. In: Satas D, editor. Handbook of pressure sensitive adhesive technology. New York: Van Nostrand Reinhold; 1989. p. 97–114.
[12] Kraus G, Jones FB, Mars OL, Rollman KW. Morphology and Viscoelastic behavior of styrene-diene block copolymers in pressure sensitive adhesives. J Adhes 1976;8:235–58.
[13] Tse MF. Studies of triblock copolymer – tackifying resin interactions and adhesive performance. J Adhes Sci Technol 1989;3:551–70.
[14] CretonC, Fabre P. Tack. In: Dillard DA, Pocius AV, editors. Adhesion science and engineering – 1. The mechanics of adhesion. Amsterdam: Elsevier Ltd.; 2002. p. 535–76.
[15] Heddleson SS, Hamann DD, Linebach DR. The Dahlquist criterion: applicability of a rheological criterion to the loss of pressure-sensitive tack in flour–water dough. Cereal Chem 1993;70:744–8.
[16] Bates R. Studies in the nature of adhesive tack. J Appl Polym Sci 1976;20:2941–54.
[17] Feldstein MM. Molecular nature of pressure-sensitive adhesion. In: Benedek I, Feldstein MM, editors. Fundamentals of pressure sensitivity (handbook of pressure-sensitive adhesives and products). Boca Rato, London, New York: CRC-Taylor & Francis; 2009. p. 10.1–43.
[18] Ferry JD. Viscoelastic properties of polymers. New York: John Wiley & Sons; 1980, 672pp.
[19] Chu SG. Viscoelastic properties of pressure sensitive adhesives. In: Satas D, editor. Handbook of pressure sensitive adhesive technology. New York: Van Nostrand Reinhold; 1989. p. 191–241.
[20] Chang EP. Viscoelastic properties and windows of pressure sensitive adhesives. In: Benedek I, Feldstein MM, editors. Fundamentals of pressure sensitivity (handbook of pressure-sensitive adhesives and products). Boca Rato, London, New York: CRC-Taylor & Francis; 2009. p. 5.1–22.
[21] Kinloch AJ. The durability of adhesive joints. In: Dillard DA, Pocius AV, editors. Adhesion science and engineering – 1. The mechanics of adhesion. Amsterdam: Elsevier Ltd.; 2002. p. 661–98.
[22] Lehman RL. Adhesives. In: Kreith F, Goswani Y, editors. The CRC handbook of mechanical engineering. Boca Raton, London, New York: CRC-Taylor & Francis; 2005. p. 12.31–40.
[23] Moon S, Foster M. Influence of humidity on surface behavior of pressure sensitive adhesives studied using scanning probe microscopy. Langmuir 2002;18:8108–15.
[24] Ghosh TK, Pfister WR, Yum SI. Transdermal and topical drug delivery systems. Buffalo Grove, IL: Interpharm Press Inc.; 1997. p. 736pp.
[25] Venkatraman S, Gale R. Skin adhesives and skin adhesion: 1. Transdermal drug delivery systems. Biomaterials 1998;19:1119–36.
[26] Peppas N, Sahlin JJ. Hydrogels as mucoadhesive and bioadhesive materials: a review. Biomaterials 1996;17:1553–61.
[27] Woodley J. Bioadhesion: new possibilities for drug administration. Clin Pharmacokinet 2001;40:77–84.
[28] Ovington L. Wound care products. Adv Skin Wound Care 2001;14:259–68.
[29] Knight J. Proper use of skin adhesives for wound repair. J Am Acad Nurse Pract 2001;13:13–4.
[30] Eliades T, Katsavrias E, Eliades G. Moisture-insensitive adhesives: reactivity with water and bond strength to wet and saliva-contaminated enamel. Eur J Orthod 2002;24:35–42.
[31] Feldstein MM, Cleary GW, Singh P. Hydrophilic adhesives. In: Benedek I, Feldstein MM, editors. Fundamentals of pressure sensitivity (handbook of pressure-sensitive adhesives and products). Boca Rato, London, New York: CRC-Taylor & Francis; 2009. p. 7.1–80.
[32] Hoffman HR, Roreger M. Hydrophilic pressure sensitive hot melt adhesives. US 6190689 LTS. Lohman Therapie Systems Gmbh; 1995.
[33] Yamaguchi Y, Sugibayashi K, Tekeda T, Seki T, Morimoto Y. Release of clonidine hydrochloride from pressure sensitive adhesive matrices prepared by emulsion type acrylate polymers. Chem Pharm Bull 1995;43:1807–9.
[34] Bonfanti L, Lunetto P, Corzani I, Marchezini M. Improved thermoplastic hydrophilic adhesive composition for attachment in dry and wet surfaces and with increased water adhesion stability. PCT Application WO/2004/016704. The Procter and Gamble Company; 2005.
[35] Sulc J, Krkova Z. Composite pressure sensitive hydrophilic adhesive and method of preparing the same. US 6005039, 1999.
[36] Yang YK, Li H, Wang F. Studies of water resistance of acrylic emulsion pressure sensitive adhesives. J Adhes Sci Technol 2003;17:1741–50.
[37] Kubo T. Adhesive medical composition with sustained medicament release. US 6146654. Alcare Co Ltd.; 2000.
[38] Feldstein MM, Siegel RA. Molecular and nanoscale factors governing pressure-sensitive adhesion strength of viscoelastic polymers. J Polym Sci Part B Polym Phys 2012;50:739–72.
[39] Chalykh AA, Chalykh AE, Novikov MB, Feldstein MM. Pressure-sensitive adhesion in the blends of poly(N-vinylpyrrolidone) and poly(ethyleneglycol) of disparate chain lengths. J Adhes 2002;78:667–94.
[40] Fujita H. Diffusion in polymer–diluent systems. Adv Polym Sci 1961;3:1–47.
[41] Feldstein MM. Molecular fundamentals of pressure-sensitive adhesion. In: Benedek I, editor. Developments in pressure-sensitive products. 2nd ed. Boca Raton, New York, London: CRC-Taylor & Francis; 2006. p. 119–43.
[42] RoosA, CretonC, NovikovMB FeldsteinMM. Viscoelasticity and tack of poly(N-vinylpyrrolidone) – poly(ethyleneglycol) blends. J Polym Sci Part B Polym Phys 2002;40:2395–409.
[43] Feldstein MM, Bovaldinova KA, Bermesheva EV, Moscalets AP, Dormidintova EE, Grinberg VY, Khokhlov AR. Thermo-switchable pressure-sensitive adhesives based on poly(N-vinyl caprolactam) non-covalently crosslinked by poly(ethylene glycol). Macromolecules 2014;47:5759–67.
[44] Feldstein MM. Adhesive hydrogels: structure, properties and application. Polym Sci Ser A 2004;46:1265–91.
[45] Bairamov DF, Chalykh AE, Feldstein MM, Siegel RA, Platé NA. Dissolution and mutual diffusion of poly(N-vinylpyrrolidone) in short chain poly(ethyleneglycol) as observed by optical wedge microinterferometry. J Appl Polym Sci 2002;85:1128–36.
[46] Bairamov DF, Chalykh AE, Feldstein MM, Siegel RA. Impact of molecular weight on miscibility and interdiffusion between poly(N-vinylpyrrolidone) and poly(ethylene glycol). Macromol Chem Phys 2002;203:2674–85.
[47] Painter PC, Coleman MM. Hydrogen bonding systems. In: Paul DR, Bucknall CB, editors. Polymer blends, vol. 1. New York, Chichester, Toronto: John Wiley & Sons; 2000. p. 93–140.
[48] Feldstein MM, Lebedeva TL, Shandryuk GA, Kotomin SV, Kuptsov SA, Igonin VE, Grokhovskaya TE, Kulichikhin VG. Complex formation in poly(N-vinylpyrrolidone–poly(ethylene glycol) blends. Polym Sci Ser A 1999;41:854–66.
[49] Kireeva PE, Shandryuk GA, Kostina JV, Bondarenko GN, Singh P, Cleary GW, Feldstein MM. Competitive hydrogen bonding mechanisms underlying phase behavior of triple poly(N-vinylpyrrolidone)–poly(ethyleneglycol)–poly(methacrylicacid-co-ethylacrylate) blends. J Appl Polym Sci 2007;105:3017–36.
[50] Coleman MM, Painter PC, Graf JF. Specific interactions and the miscibility of polymer blends. Boca Raton: CRC Press; 1995. p. 516pp.
[51] Gdalin BE, Bermesheva EV, Shandryuk GA, Feldstein MM. Effect of temperature on probe tack adhesion: extension of the Dahlquist criterion of tack. J Adhes 2011;87:111–38.
[52] Deplace F, Carelli C, Mariot S, Retsos H, Chateauminois A, Ouzineb K, Creton C. Optimizing the microstructure of a soft material made from latex particles for adhesive properties. J Adhes 2009;85:18–54.
[53] Derail C, Marin G. Rheology of hot-melt PSAs: influence of polymer structure. In: Possart W, editor. Adhesion – current research and applications. Weinheim: Wiley-VCH; 2005. p. 229–48.
[54] Lakrout H, Sergot P, Creton C. Direct observation of cavitation and fibrillation in AP robe-tack experiment on model acrylic pressure-sensitive adhesives. J Adhes 1999;69:307–59.
[55] Creton C, Shull KR. Probe tack. In: Benedek I, Feldstein MM, editors. Fundamentals of pressure sensitivity (handbook of pressure-sensitive adhesives and products). Boca Rato, London, New York: CRC-Taylor & Francis; 2009. p. 6.1–26.
[56] Lindner A, Maevis T, Brummer R, Lůhmann B, Creton C. Sub-critical failure of soft acrylic adhesives under tensile stress. Langmuir 2004;20:9156–69.
[57] Kaelble DH. Theory and analysis of peel adhesion. In: Satas D, editor. Handbook of pressure sensitive adhesive technology. Warwick, Rhode Island: Satas & Associates; 1999. p. 145–61.
[58] Hui CY, Lin YY, Baney JM. The mechanics of tack: viscoelastic contact on rough surface. J Polym Sci Part B Polym Phys 2000;38:1485–95.
[59] Yamaguchi T, Koike K, Doi M. In situ observation of stereoscopic shapes of cavities in soft adhesives. Europhys Lett 2007;77:64002.
[60] Yamaguchi T, Morita H, Doi M. Modeling on debonding dynamics of pressure-sensitive adhesives. Eur Phys J E 2006;20:7–17.
[61] Novikov MB, Roos A, Creton C, Feldstein MM. Dynamic mechanical and tensile properties of poly(N-vinyl pyrrolidone)–poly(ethylene glycol) blends. Polymer 2003;44:3559–76.

[62] Ward IM. The mechanical properties of solid polymers. 2nd ed. West Sussex: John Wiley and Sons Ltd.; 1985. p. 475pp.
[63] Feldstein MM, Kuptsov SA, Shandryuk GA, Platé NA, Chalykh AE. Coherence of thermal transitions in poly(N-vinyl pyrrolidone)–poly(ethylene glycol) compatible blends. 3. Impact of sorbed water upon phase behavior. Polymer 2000;41:5349–59.
[64] Kirsh YE. Water soluble poly (N-vinyl amides). New York: John Wiley and Sons Ltd.; 1998. p. 233pp.
[65] Kirsh YE. Water-soluble poly(N-vinylamides) – microstructure, solvation, conformational state and complex formation in aqueous solutions. Prog Polym Sci 1993;18:519–42.
[66] Buehler V. Kollidon: polyvinylpyrrolidone for the pharmaceutical industry. 9th ed. Ludwigshafen: BASF; 2008. p. 330pp.
[67] Lebedeva TL, Kuptsov SA, Feldstein MM, Platé NA. Molecular arrangement of water associated with poly (N-vinylpyrrolidone) in the first hydrate shell. In: Iordanskii AL, Starzev OV, Zaikov GE, editors. Water transport in synthetic polymers. New York: Nova Science Publishers Inc.; 2003. p. 69–94.
[68] Chalykh AE, Bairamov DF, Gerasimov VK, Chalykh AA, Fel'dshtein MM. Diffusion and thermodynamics of mixing in poly(vinyl pyrrolidone)–water system. Polym Sci Ser A 2003;45:1115–9.
[69] Zhang J, Zografi G. The relationship between "BET" and "free volume"-derived parameters for water vapor absorption into amorphous solids. J Pharm Sci 2000;89:1063–72.
[70] Hancock BC, Zograf iG. The use of solution theories for predicting water vapor absorption by amorphous pharmaceutical solids: a test of the Flory–Huggins and Vrentas models. Pharm Res 1993;10:1262–7.
[71] Ramesh N, Davis PK, Zielinski JM, Danner RP, Duda JL. Application of free-volume theory to self-diffusion of solvents in polymers below the glass transition temperature: a review. J Polym Sci Part B Polym Phys 2011;49:1629–44.
[72] Kireeva PE, Novikov MB, Singh P, Cleary GW, Feldstein MM. Tensile properties and adhesion of water absorbing hydrogels based on triple poly(N-vinylpyrrolidone)/poly(ethyleneglycol)/poly(methacrylicacid-co-ethylacrylate) blends. J Adhes Sci Technol 2007;21:531–57.
[73] Harris JM, Zalipsky S, editors. Poly(ethyleneglycol): chemistry and biological applications. ACS Symp Series, vol. 680. 1997, 489 pp.
[74] Newman S, Paul DR. Polymer blends. New York: Academic Press; 1978. p. 435pp.
[75] Fox TG. Influence of diluents and copolymer composition on the glass transition temperature of a polymer system. Bull Am Phys Soc 1956;1:123.
[76] Feldstein MM, Shandryuk GA, Kuptsov SA, Platé NA. Coherence of thermal transitions in poly(N-vinyl pyrrolidone)–poly(ethylene glycol) compatible blends. 1. Interrelations among the temperatures of melting, maximum cold crystallization rate and glass transition. Polymer 2000;41:5327–38.
[77] Feldstein MM, Kuptsov SA, Shandryu GA. Coherence of thermal transitions in poly(N-vinyl pyrrolidone)–poly(ethylene glycol) compatible blends. 2. The temperature of maximum cold crystallization rate versus glass transition. Polymer 2000;41:5339–48.
[78] Feldstein MM, Shandryuk GA, Platé NA. Relation of glass transition temperature to the hydrogen-bonding degree and energy in poly(N-vinylpyrrolidone)blends with hydroxyl-containing plasticizers. Part1. Effects of hydroxyl group number in plasticizer molecule. Polymer 2001;42:971–9.
[79] Feldstein MM, Kuptsov SA, Shandryuk GA, Platé NA. Relation of glass transition temperature to the hydrogen-bonding degree and energy in poly(N-vinyl pyrrolidone) blends with hydroxyl-containing plasticizers. Part 2. Effects of poly(ethylene glycol) chain length. Polymer 2001;42:981–90.
[80] Feldstein MM, Roos A, Chevallier C, Creton C, Dormidontova EE. Relation of glass transition temperature to the hydrogen bonding degree and energy in poly(N-vinyl pyrrolidone) blends with hydroxyl-containing plasticizers: 3. Analysis of two glass transition temperatures featured for PVP solutions in liquid poly(ethylene glycol). Polymer 2003;44:1819–34.
[81] Feldstein MM. Peculiarities of glass transition temperature relation to the composition of poly(N-vinyl pyrrolidone) blends with short chain poly(ethylene glycol). Polymer 2001;42:7719–26.
[82] Askadskii AA. Computational materials science of polymers. Cambridge UK: Cambridge International Science Publishing; 2001. p. 650pp.
[83] Askadskii AA. Physical properties of polymers. prediction and control. Amsterdam, New York: Gordon and Breach Publishers; 1996. p. 333pp.
[84] Feldstein MM, Bermesheva EV, Jean YC, Misra GP, Siegel RA. Free volume, adhesion and viscoelastic properties of model nanostructured pressure-sensitive adhesive based on stoichiometric complex of poly(N-vinylpyrrolidone) and poly(ethylene glycol)of disparate chain lengths. J Appl Polym Sci 2011;119:2408–21.
[85] Bershtein VA, Egorov VM. Differential scanning calorimetry of polymers. New York: Horwood; 1994. p. 253pp.
[86] Maes C, Devaux J, Legras R, McGrail PT. Glass transition temperature of crosslinked poly(ether sulfone)s. Polymer 1995;36:3159–64.
[87] Feldstein MM, Lebedeva TL, Shandryuk GA, Igonin VE, Avdeev NN, Kulichikhin VG. Stoichiometry of poly(N-vinyl pyrrolidone)–poly(ethylene glycol) complex. Polym Sci Ser A 1999;41:867–75.
[88] Vartapetian RS, Khozina EV, Karger J, Geschke D, Rittig F, Feldstein MM, Chalykh AE. Self-diffusioninpoly(N-vinylpyrrolidone)-poly(ethyleneglycol)system. Colloid Polym Sci 2001;279:532–8.
[89] Vartapetian RSh, Khozina EV, Karger J, Geschke D, Rittig F, Feldstein MM, Chalykh AE. Molecular dynamics in poly(N-vinylpyrrolidone)–poly(ethylene glycol) blends by pulsed field gradient NMR method: effects of aging, hydration and PEG chain length. Macromol Chem Phys 2001;202:2648–52.
[90] Feldstein MM, Kulichikhin VG, Kotomin SV, Borodulina TA, Novikov MB, Roos A, Creton C. Rheology of poly(N-vinylpyrrolidone)–poly(ethyleneglycol) adhesive blends under shear flow. J Appl Polym Sci 2006;100:522–37.
[91] Bessmertnaya LYa, Goncharova AI, Rumsh LD, Grokhovskaya TE, Feldstein MM. Thermostability and phase behavior of enzymes in solid state and within polymer matrices. Proc Intern Symp Control Release Bioactive Mater 1999;26:383–4.
[92] Privalov PI, Khechiashvili NN, Atanasov BP. Thermodynamic analysis of thermal transitions in globular proteins. Calorimetric study of trypsinogen, ribonuclease and myoglobin. J Biopolym 1971;10:1865–90.
[93] Lyubarev AE, Kurganov BI. Analysis of DSC data relating to proteins undergoing irreversible thermal denaturation. J Therm Anal Cal 2000;62:49–60.
[94] Sochava IV, Belopolskaya TV, Smirnova OI. DSC study of reversible and irreversible thermal denaturation of globular proteins. Biophys Chem 1985;22:323–36.
[95] Leon A, Rosell CM, deBarber CB. A differential scanning calorymetry of wheat proteins. Eur Food Res Technol 2003;217:13–6.
[96] Bruylants G, Wouters J, Michaux C. Differential scanning calorymetry in life science: thermodynamics, stability, molecular recognition and application in drug design. Current Med Chem 2005;12:2011–20.
[97] Sauer BB, Kampert WG, Blanchard EN, Threefour SA, Hsiao BS. Temperature modulated DSC studies of melting and recrystallization in polymers exhibiting multiple endotherms. Polymer 2000;41:1099–108.
[98] Novikov MB, Borodulina TA, Kotomin SV, Kulichikhin VG, Feldstein MM. Relaxation properties of pressure-sensitive adhesives upon withdrawal of bonding pressure. J Adhes 2005;81:77–107.
[99] Novikov MB, Gdalin BE, Anosova JV, Feldstein MM. Stress relaxation during bond formation and adhesion of pressure-sensitive adhesives. J Adhes 2008;84:164–90.
[100] Feldstein MM, Novikov MB, Creton C. Significance of relaxation for adhesion of pressure-sensitive adhesives. In: Benedek I, Feldstein MM, editors. Fundamentals of pressure sensitivity (handbook of pressure-sensitive adhesives and products). Boca Rato, London, New York: CRC-Taylor & Francis; 2009. p. 11.1–62.
[101] Feldstein MM. Contribution of relaxation processes to adhesive-joint strength of viscoelastic polymers. Polym Sci Ser A 2009;51:1341–54.
[102] Chuvaev VF, Vartapetian RSh, Feldstein MM. Influence of physical aging on the state of water strongly bound by the poly(vinyl pyrrolidone)–poly(ethylene glycol) complex by Broad-Line 1H NMR data (in Russia). Colloid J 2004;66:95–9.
[103] Feldstein MM, Cleary GW, Platé NA. Molecular design of hydrophilic pressure-sensitive adhesives for medical applications. In: Benedek I, editor. Developments in pressure-sensitive products. 2nd ed. Boca Raton, New York, London: CRC-Taylor & Francis; 2006. p. 473–503.
[104] Feldstein MM, Kireeva PE, Kiseleva TI, Gdalin BE, Novikov MB, AnosovaY uV, Shandryuk GA, Singh P, Cleary GW. A new class of pressure-sensitive adhesives based on interpolymer and polymer–oligomer complexes. Polym Sci Ser A 2009;51:799–814.
[105] Kamperman M, Synytska A. Switchable adhesion by chemical functionality and topography. J Mater Chem 2012;22:19390–401.
[106] de las Heras Alarcón C, Pennadam S, Alexander C. Stimuli responsive polymers for biomedical applications. Chem Soc Rev 2005;34:276–85.

[107] O'Mahony J, McCarthy KE, Monaghan E, Sullivan A. A novel way to reversibly detackify PSA compositions using thermoresponsive polymers. PSTC (Pressure-Sensitive Tape Council), Advanced polymer design for adhesives; 2007 http://www.pstc.org/files/public/OMahony.pdf, 10 pp. [accessed October 2014].
[108] Kirsh YE. Water-soluble poly-N-vinylamides: synthesis and physico-chemical properties. Chichester: John Wiley & Sons Inc.; 1998. p. 232pp.
[109] Agular MR, Roman JS, editors. Smart polymers and their applications. Oxford: Elsevier Ltd.; 2014. p. 552pp.
[110] Meeussen F, Nies E, Berghams H, Verbrugghe S, Goethals E, Prez FD. Phase behaviour of poly(N-vinyl caprolactam) in water. Polymer 2000;41:8597–602.
[111] Maeda Y, Nakamura T, Ikeda I. Hydration and phase behavior of poly(N-vinylcaprolactam) and poly(N-vinylpyrrolidone) in water. Macromolecules 2002;35:217–22.
[112] Makhaeva EE, Thanh LTM, Starodubtsev SG, Khokhlov AR. Thermoshrinking behavior of poly(vinylcaprolactam) gels in aqueous solution. Macromol Chem Phys 1996;197:1973–82.
[113] Dubovik AS, Makhaeva EE, Grinberg VY, Khokhlov AR. Energetics of cooperative transitions of *N*-vinylcaprolactam polymers in aqueous solutions. Macromol Chem Phys 2005;206:915–28.
[114] Mikheeva EE, Grinberg NV, Mashkevich AY, Grinberg VY, Makhaeva EE, Khokhlov AR. Microcalorimetric study of thermal cooperative transitions in poly(N-vinylcaprolactam) hydrogels. Macromolecules 1997;30:2693–9.
[115] Laukkanen A, Valtola L, Winnik FM, Tenhu H. Formation of colloidally stable phase separated poly(N-vinylcaprolactam) in water: a study by dynamic light scattering, microcalorimetry, and pressure perturbation calorimetry. Macromolecules 2004;37:2268–74.
[116] Spěváček J, Dybal J, Starovoytova L, Zhigunov A, Sedláková Z. Temperature-induced phase separation and hydration in poly(*N*-vinylcaprolactam) aqueous solutions: a study by NMR and IR spectroscopy, SAXS, and quantum-chemical calculations. Soft Matter 2012;8:6110–9.
[117] Anufrieva EV, Gromova RA, Kirsh YE, Yanul NA, Krakovyak MG, Lushchik VB, Pautov VD, Sheveleva TV. Complexing properties and structural characteristics of thermally sensitive copolymers of N-vinylpyrrolidone and N-vinylcaprolactam. Eur Polym J 2001;37:323–8.
[118] Feldstein MM, Dlickman IF, Pavperova SV, Pariy IV, Pudel ME, Vasiliev AE, Platé NA. Effect of hydrophilic matrix hydration on transdermal drug delivery kinetics: I. Matrix hydration in vivo and in vitro. In: Brain KR, James VJ, Walters KA, editors. Prediction of percutaneous penetration. Cardiff: 4 b STS Publishing; 1996. p. 61–4.
[119] Feldstein MM, Pariy IV, Dlickman IF, Malkhazov LB, Tohmakhchi VN, Petukhova NM, Vasiliev AE, Platé NA. Effect of hydrophilic matrix hydration on transdermal drug delivery kinetics: II. In vitro cytisine delivery from Cypercuten TTS. In: Brain KR, James VJ, Walters KA, editors. Prediction of percutaneous penetration. Cardiff: 4 b STS Publishing; 1996. p. 65–7.
[120] Feldstein MM, Petukhova NM, Dlickman IF, Malkhazov LB, Kadenatsi IB, Vasiliev AE, Platé NA. Effect of hydrophilic matrix hydration on transdermal drug delivery kinetics: III. In vitro clonidine delivery from Clopercuten TTS. In: Brain KR, James VJ, Walters KA, editors. Prediction of percutaneous penetration. Cardiff: 4 b STS Publishing; 1996. p. 68–70.
[121] Feldstein MM, Vasiliev AE, Platé NA. Effect of hydrophilic matrix hydration on transdermal drug delivery kinetics: IV. In vitro–in vivo correlation. In: Brain KR, James VJ, Walters KA, editors. Prediction of percutaneous penetration. Cardiff: 4 b STS Publishing; 1996. p. 71–3.
[122] Feldstein MM, Tohmakhchi VN, Malkhazov LB, Vasiliev AE, Platé NA. Hydrophilic polymeric matrices for enhanced transdermal drug delivery. Int J Pharm 1996;131:229–42.
[123] Iordanskii AL, Feldstein MM, Markin VS, Hadgraft J, Platé NA. Modeling of the drug delivery from a hydrophilic transdermal therapeutic system across polymer membrane. Eur J Pharm Biopharm 2000;49:287–93.
[124] Feldstein MM, Raigorodskii IM, Iordanskii AL, Hadgraft J. Modeling of percutaneous drug transport in vitro using skin-imitating Carbosil membrane. J Control Release 1998;52:25–40.
[125] Starodubtsev AK, Rumyantsev AS, Pavlova LI, Vasiliev AE, Feldstein MM. Pharmacodynamics of nitroglycerin following continuous controlled transdermal delivery from Nitropercuten TDS in patients with ischaemic heart disease (in Russian). In: Kukes VG, editor. Actual problems of traditional medicine and pharmacotherapy. Moscow: I.M. Sechenov First Moscow State Medical University; 1995. p. 205–15.
[126] Pavlova LI, Rumyantsev AS, Starodubtsev AK. Pharmacodynamics of isosorbide dinitrate following continuous controlled transdermal delivery from Sorbopercuten TDS in patients with ischaemic heart disease. In: Kukes VG, editor. Actual problems of traditional medicine and pharmacotherapy. Moscow: I.M. Sechenov First Moscow State Medical University; 1995. p. 195–205 [in Russian].
[127] Menke G, Schellhammer R, Rietbrock N. Konzentrations – Zeitprofil von Isosorbiddinitrat und seinen Metaboliten im Plasma nach perkutaner Resorption aus einen transdermalen therapeutischen System (in German). Arzneim-Forsch 1987;37:1301–3.
[128] Takemoto Y, Ajiro H, Akashi M. Amphiphilic poly(N-vinyl acetamide) gels strengthened with swelling solvent. Macromol Chem Phys 2014;215:384–90.
[129] Feldstein MM, Platé NA, Chalykh AE, Cleary GW. Preparation of hydrophilic pressure sensitive adhesives having optimized adhesive properties. US 6576712. Corium International Inc.; 2003.
[130] Silva CL, Pereira JC, Ramalho A, Pais AACC, Sousa JJS. Films based on chitosan polyelectrolyte complexes for skin drug delivery: development and characterization. J Membr Sci 2008;320:268–79.
[131] Feldstein MM, Platé NA. A structure–property relationship and quantitative approach to the development of universal transdermal drug delivery system. In: Sohn T, Voicu VA, editors. Nuclear, biological and chemical risks – current capabilities and future perspectives for protection. Dordrecht, Boston, London: Kluwer Academic Publishers; 1999. p. 441–58.
[132] Tsuchida E, Abe K. Interactions between macromolecules in solution and intermacromolecular complexes. Adv Polym Sci 1982;45:1–119.
[133] Antipina AD, Papisov IM, Kabanov VA. Critical chain dimension for cooperative interaction of poly(ethylene glycol) with polymethacrylic acid (in Russian). Vysokomol Soyed B 1970;12:329–31.
[134] Kabanov VA, Papisov IM. Formation of complexes between complementary synthetic polymers and oligomers in dilute solution. Review. Polym Sci USSR 1979;21:261–307. Soyed A 1979;21:243–81.
[135] Papisov IM, Litmanovich AA. Intermolecular reactions. In: Platé NA, Litmanovich AD, Noah OV, editors. Macromolecular reactions. Chichester: John Wiley & Sons; 1995. p. 283–344.
[136] Baranovsky VYu, Litmanovich AA, Papisov IM, Kabanov VA. Quantitative studies of interaction between complementary polymers and oligomers in solution. Eur Polym J 1981;17:669–79.
[137] Zezin AB, Lutsenko VV, Rogacheva VB, Aleksina OA, Kalyuzhnaya RI, Kabanov VA, Kargin VA. Cooperative interactions between synthetic polyelectrolytes in aqueous solutions. Polym Sci USSR 1972;14:857–65. Vysokomol Soyed A 1972;14:772–9.
[138] Papisov IM, Litmanovich AA. Molecular récognition in interpolymer interactions and matrix polyreactions. Adv Polym Sci 1989;90:139–79.
[139] Litmanovich AA, Papisov IM, Kabanov VA. Selectivity of complex formation between macromolecules and its usage for the composition fractionation. Polym Sci USSR 1980;22:1297–302. Vysokomol Soyed A 1980;22:1180–4.
[140] Rogacheva VB, Zezin AB, Kargin VA. Interaction of polymeric acids with polybase salts (in Russian). Vysokomol Soyed B 1970;12:826–30.
[141] Lutsenko VV, Zezin AB, Lopatkin AA. Statistical model of cooperative reaction between weak polyelectrolytes. Polym Sci USSR 1974;16:2819–26. Vysokomol Soyed A 1974;16:2429–34.
[142] Lutsenko VV, Zezin AB, Kalyuzhnaya RI. Thermodynamics of polyelectrolyte cooperative interaction in aqueous solutions. Polym Sci USSR 1974;16:2797–805. Vysokomol Soyed A 1974;16:2411–17.
[143] Zezin AB, Lutsenko VV, Izumrudov VA, Kabanov VA. The cooperation characteristics between polyelectrolytes during their reactions. Polym Sci USSR 1974;16:694–8. Vysokomol Soyed A 1974;600–4.
[144] Aleksina OA, Papisov IM, Zezin AB. Separation of polymer–polymer complexes. J Membr Sci 1971;13:1199–205.
[145] Tsuchida E, Osada Y. The role of the chain length in the stability of polyion complexes. Makromol Chem 1974;175:593–601.
[146] Tsuchida E, Osada Y, Ohno H. Formation of interpolymer complexes. J Macromol Sci Phys B 1980;17:683–714.
[147] Osada Y, Antipina AD, Papisov IM, Kabanov VA, Kargin VA. Role of cooperative interaction of growing chains and macromolecular matrices under polymerization. Dokl Akad Nauk SSSR 1970;191:339–402.

[148] Litmanovich AA, Papisov IM, Kabanov VA. "Recognition" of copolymers and stereoisomers in macromolecule complexation reactions in dilute solutions. Eur Polym J 1981;17:981–8.
[149] Finkelstein AV, Ptitsyn OB. Protein physics. A course of lectures. San Diego, Hong Kong: Academic Press; 2002. p. 354pp.
[150] Lumry R, Rajender S. Enthalpy–entropy compensation phenomena in water solutions of proteins and small molecules: a ubiquitous properly of water. Biopolymers 1970;9:1125–227.
[151] Bekturov EA, Bimendina LA. Interpolymer complexes. Adv Polym Sci 1981;41:99–147.
[152] Dumitriu S, Chornet E. Inclusion and release of proteins from polysaccharide-based polyion complexes. Adv Drug Deliv Rev 1998;3:223–46.
[153] Burkart P, Datzenberg H, Linow KJ, Kötz J, Dawydoff W. Polyelectrolyte complexes – recent development and open problems. Prog Polym Sci 1989;14:91–172.
[154] Dubin P, Bock J, Davis R, Schulz D, Thies C. Macromolecular complexes in chemistry and biology. Berlin, Heidelberg, New York: Springer; 1994. p. 359pp.
[155] Jiang M, Li M, Xiang M, Zhou H. Interpolymer complexation and miscibility enhancement by hydrogen bonding. Adv Polym Sci 1999;146:121–96.
[156] Zhang G, Jiang M, Zhu L, Wu C. Intermacromolecular complexation because of specific interactions: 11. Ionic interaction complexation and its comparison with hydrogen-bonding complexation. Polymer 2001;42:151–9.
[157] Philippova OE, Khokhlov AR. Polyelectrolyte/ionomer behavior of polymer gels. In: Osada Y, Kokhlov AR, editors. Polymer gels and networks. New York: Marcel Dekker Inc.; 2001. p. 163–75.
[158] Kabanov VA, Zezin AB. Soluble interpolymeric complexes as a new class of synthetic polyelectrolytes. Pure Appl Chem 1984;65:343–54.
[159] Jaber JA, Schlenoff JB. Mechanical properties of reversibly crosslinked ultrathin polyelectrolyte complexes. J Am Chem Soc 2006;126:2940–7.
[160] Kiseleva TI, Shandryuk GA, Khasbiullin RR, Shcherbina AA, Chalykh AE, Feldstein MM. Phase state of polyelectrolyte complexes based on blends of acrylic copolymers. J Appl Polym Sci 2011;122:2926–43.
[161] Iliopoulos I, Audebert R. Polymer complexes stabilized through hydrogen bonds: a semiquantitative theoretical model. J Polym Sci Part B Polym Phys 1988;26:2093–112.
[162] Iliopoulos I, Audebert R. Complexation of acrylic acid copolymers with polybases: importance of cooperative effects. Macromolecules 1991;24:2566–75.
[163] Borue VYu, Erukhimovich IYa. A statistical theory of globular polyelectrolyte complexes. Macromolecules 1990;23:3625–32.
[164] Lifshitz IM, Grosberg AYu, Khokhlov AR. Some problems of the statistical physics of polymer chains with volume interactions. Rev Mod Phys 1978;50:683–713.
[165] Grosberg AYu, Khokhlov AR. Statistical physics of macromolecules. New York: American Institute of Physics; 1994. p. 350pp.
[166] Veis A. Biological polyelectrolytes. New York: Dekker; 1970. p. 291pp.
[167] Dautzenberg H. Polyelectrolyte complex formation in highly aggregating systems. 1. Effect of salt. Polyelecrolyte complex formation in the presence of NaCl. Macromolecules 1997;30:7810–5.
[168] Hayashi Y, Ullner M, Linse P. Complex formation in solutions of oppositely charged polyelectrolytes at different polyion compositions and salt content. J Phys Chem B 2003;107:8198–207.
[169] de Vasconcelos CL, Bezerril PM, dos Santos DES, Dantas TNC, Pereira MR, Fonseca JLC. Effect of molecular weight and ionic strength on the formation of polyelectrolyte complexes based on poly(methacrylic acid) and chitosan. Biomacromolecules 2006;7:1245–52.
[170] Sedlak M, Amis EJ. Concentration and molecular weight regime diagram of salt-free polyelectrolyte solutions as studied by light scattering. J Chem Phys 1992;96:826–34.
[171] Sedlak M, Amis EJ. Dynamics of moderately concentrated salt-free polyelectrolyte solutions: molecular weight dependence. J Chem Phys 1992;96:817–25.
[172] Förster S, Schmidt M. Polyelectrolytes in solution. Adv Polym Sci 1995;120:51–133.
[173] Yethiraj A. Liquid state theory of polyelectrolyte solutions. J Phys Chem B 2009;113:1539–51.
[174] Zhou KJ, Li JF, Lu YJ, Zhang GZ, Xie ZW, Wu C. Re-examination of dynamics of polyeletrolytes in salt-free dilute solutions by designing and using a novel neutral-charged-neutral reversible polymer. Macromolecules 2009;42:7146–54.
[175] Lin SC, Lee WI, Schurr JM. Brownian-motion of highly charged poly(l-lysine)—effects of salt and polyion concentration. Biopolymers 1978;17:1041–64.
[176] Li J, Ngai T, Wu C. The slow relaxation mode: from solutions to gel networks. Polymer J 2010;42:609–25.
[177] Muthukumar M. Double screening in polyelectrolyte solutions: limiting laws and crossover formulas. J Chem Phys 1996;105:5183–99.
[178] Sedlak M, Konak C, Stepanek P, Jakes J. Semidilute solutions of poly(methacrylic acid) in the absence of salt—dynamic light-scattering study. Polymer 1987;28:873–80.
[179] Schmitz KS, Yu JW. On the electrostatic contribution to the persistence length of flexible polyelectrolytes. Macromolecules 1988;21:484–93.
[180] Forster S, Schmidt M, Antonietti M. Static and dynamic light-scattering by aqueous polyelectrolyte solution: effect of molecular weight, charged density and added salt. Polymer 1990;31:781–92.
[181] Mattoussi H, Karasz FE, Langley KH. Electrostatic and screening effects on the dynamic aspects of polyelectrolyte solutions. J Chem Phys 1990;93:3593–603.
[182] Son JM, Pak H. Topological analysis on the degree of complexation and viscosity of polymer complexes. Bull Kor Chem Soc 1995;16:1046–56.
[183] Iwata K, Kurata M. Brownian motion of lattice-model polymer chains. J Chem Phys 1969;50:4008–13.
[184] Iwata K. Topological rubber-elasticity theory. III. Comparison of rigidities computed for model tetra-functional networks with experiments. J Chem Phys 1985;83:1969–79.
[185] Deng L, Wang C, Li ZC, Liang D. Re-examination of the "zipper effect" in hydrogen-bonding complexes. Macromolecules 2010;43:3004–10.
[186] Lazutin A, Semenov AN, Vasilevskaya VV. Polyelectrolyte complexes consisting of macromolecules with varied stiffness: computer simulation. Macromol Theory Simul 2012;21:328–39.
[187] Srivastava D, Muthukumar M. Interpenetration of interacting polyelectrolytes. Macromolecules 1994;27:1461–5.
[188] Winkler RG. Complex formation in systems of oppositely charged polyelectrolytes: a molecular dynamics simulation study. Phys Rev E 2002;66, 021802/1-7.
[189] Winkler RG. Universal properties of complexes formed by two oppositely charged flexible polyelectrolytes. New J Phys 2004;6:11.1–10.
[190] Ou Z, Muthukumar M. Entropy and enthalpy of polyelectrolyte complexation: Langevin dynamics simulations. J Chem Phys 2006;124, 154902/1-11.
[191] Trejo-Ramos MA, Tristan F, Menchaca JL, Perez E, Chavez-Paez M. Structure of polyelectrolyte complexes by Brownian dynamics simulation: effects of the bond length asymmetry of the polyelectrolytes. J Chem Phys 2007;126, 014901/1-8.
[192] Hayashi Y, Ullner M, Linse P. Oppositely charged polyelectrolytes. Complex formation and effects of chain asymmetry. J Phys Chem B 2004;108:15266–77.
[193] Jorge AF, Sarraguça JF, Dias JMG, Paes AACC. Polyelectrolyte compaction by pH-responsive agents. Phys Chem Chem Phys 2009;11:10890–8.
[194] Narambuena CF, Leiva EPM, Chávez-Páez M, Pérez E. Effect of chain stiffness on the morphology of polyelectrolyte complexes. A Monte Carlo simulation study. Polymer 2010;51:3293–302.
[195] Gus'kova O.A., Pavlov AS, Khalatur PG. Complexes based on rigid-chain polyelectrolytes: computer simulation. Polym Sci Ser A 2006;48:763–70.
[196] Kriz J, Dybal J, Dautzenberg H. Cooperative interactions of unlike macromolecules: 3. NMR and theoretical study of the electrostatic coupling of sodium polyphosphates with diallyl(dimethyl)ammonium chloride-acrylamide copolymers. J Phys Chem A 2001;105:7486–93.
[197] Komarov PV, Zherenkova LV, Khalatur PG. Ribbonlike nanostructures from stiff polyanions and short cationic chains. Chem Phys Lett 2006;420:29–34.
[198] Izumrudov VA, Zezin AB, Kabanov VA. Equilibria in interpolyelectrolyte reactions and the phenomenon of molecular "recognition" in solutions of interpolyelectrolyte complexes. Russ Chem Rev 1991;60:792–806.
[199] Tanaka T. Collapse of gels and the critical end point. Phys Rev Lett 1978;40:820–3.
[200] Osada Y. Effects of polymers and their chain lengths on the contraction of poly(methacrylic acid) network. J Polym Sci Polym Lett Ed 1980;18:281–6.

[201] Khokhlov AR, Kramarenko EYu, Makhaeva EE, Starodubtzev SG. Collapse of polyelectrolyte networks induced by their interaction with an oppositely charged surfactant. Theory Macromol Chem Theory Simul 1992;1:105–18.
[202] Kramarenko EYu, Khokhlov AR. Collapse of a polymer gel induced by complex formation with linear polymers. Macromol Chem Theory Simul 1993;2:169–76.
[203] Khokhlov AR. On the collapse of weakly charged polyelectrolytes. J Phys A 1980;13:979–87.
[204] Khokhlov AR, Makhaeva EE, Philippova OE, Starodubtsev SG. Supramolecular structures and conformational transitions in polyelectrolyte gels. Macromol Symp 1994;87:69–91.
[205] Mann BAF, Kremer K, Lenz O, Holm C. Hydrogels in poor solvents: a molecular dynamics study. Macromol Theory Simul 2011;20:721–34.
[206] Grinberg VYa, Grinberg NV, Mikheeva LM, Dembo AT, Makhaeva EE, Khokhlov AR, Grosberg AYu, Tanaka T. A new hydrogel system undergoing a volume phase transition upon heating. Macromol Chem Phys 1999;200:1603–7.
[207] Makhaeva EE, Tenhu H, Khokhlov AR. Behavior of Poly(N-vinylcaprolactam-co-methacrylic acid) macromolecules in aqueous solution: interplay between coulombic and hydrophobic interaction. Macromolecules 2002;35:1870–6.
[208] Kozhunova EYu, Makhaeva EE, Khokhlov AR. Collapse of thermosensitive polyelectrolyte semi-interpenetrating networks. Polymer 2012;53:2379–84.
[209] Dautzenberg H, Gao Y, Hahn M. Formation, structure, and temperature behavior of polyelectrolyte complexes between ionically modified thermosensitive polymers. Langmuir 2000;16:9070–81.
[210] Cherstvy AG. Collapse of highly charged polyelectrolytes triggered by attractive dipole–dipole and correlation-induced electrostatic interactions. J Phys Chem B 2010;114:5241–9.
[211] Loh P, Deen GR, Vollmer D, Fischer K, Schmidt M, Kundagrami A, Muthukumar M. Collapse of linear polyelectrolyte chains in a poor solvent: when does a collapsing polyelectrolyte collect its counterions? Macromolecules 2008;41:9352–8.
[212] Potemkin II, Palyulin VV. Complexation of oppositely charged polyelectrolytes: effect of discrete charge distribution along the chain. Phys Rev E 2010;81, 041802 6 pp.
[213] van der Gucht J, Spruijt E, Lemmers M, Cohen Stuart MA. Polyelectrolyte complexes: bulk phases and colloidal systems. J Colloid Interface Sci 2011;361:407–22.
[214] Kabanov VA. Basic properties of soluble complexes applied to bioengineering and cell transformations. In: Dubin P, Bock J, Davies RM, Schulz DN, Thies C, editors. Macromolecular complexes in chemistry and biology. Berlin: Springler-Verlag; 1994. p. 151–74.
[215] Krotova MK, Vasilevskaya VV, Leclercq L, Boustta M, Vert M, Khokhlov AR. Salt effects on complexes of oppositely charged macromolecules having different affinity to water. Macromolecules 2009;42:7495–503.
[216] Harada A, Kataoka K. Chain length recognition: core–shell supramolecular assembly from oppositely charged block copolymers. Science 1999;238:65–7.
[217] Kabanov AV, Vinogradov SV, Suzdaltseva YuG, Alakhov VYu. Water-soluble block polycations as carriers for oligonucleotide delivery. Bioconjugate Chem 1995;6:639–43.
[218] Kabanov AV, Bronich TK, Kabanov VA, Yu K, Eisenberg A. Soluble stoichiometric complexes from poly(N-ethyl-4-vinylpyridinium) cations and poly(ethylene oxide)-block-polymethacrylate anions. Macromolecules 1996;29:6797–802.
[219] Kramarenko EYu, Khokhlov AR, Reineker P. Micelle formation in a dilute solution of block copolymers with a polyelectrolyte block complexed with oppositely charged linear chains. J Chem Phys 2003;l19:4945–52.
[220] Kramarenko EYu, Khokhlov AR, Reineker P. Stoichiometric polyelectrolyte complexes of ionic block copolymers and oppositely charged polyions. J Chem Phys 2006;125, 194902/1-8.
[221] Castelnovo M. Thermodynamics of micellization of oppositely charged polymers. Europhys Lett 2003;62:841–7.
[222] Vasilevskaya VV, Leclercq L, Boustta M, Vert M, Khokhlov AR. Study of interpolymer complexes of oppositely charged macromolecules with different affinity to solvent. Macromolecules 2007;40:5934–40.
[223] Jeon J, Dobrynin AV. Molecular dynamics simulations of polyelectrolyte–polyampholyte complexes. effect of solvent quality and salt concentration. J Phys Chem B 2006;110:24652–65.
[224] Dobrynin AV, Rubinstein M. Theory of polyelectrolytes in solutions and at interfaces. Prog Polym Sci 2005;30:1049–118.
[225] Dobrynin AV, Rubinstein M, Obukhov SP. Cascade of transitions of polyelectrolytes in poor solvent. Macromolecules 1996;29:2974–9.
[226] Dobrynin AV, Rubinstein M. Hydrophobic polyelectrolytes. Macromolecules 1999;32:915–22.
[227] Solis FJ, de la Cruz MO. Variational approach to necklace formation in polyelectrolytes. Macromolecules 1998;31:5502–6.
[228] Micka U, Kremer K. Strongly charged flexible polyelectrolytes in poor solvents—from stable spheres to necklace chains. Europhys Lett 2000;49:189–95.
[229] Micka U, Holm C, Kremer K. Strongly charged, flexible polyelectrolytes in poor solvents: molecular dynamics simulations. Langmuir 1999;15:4033–44.
[230] Lyulin AV, Dunweg B, Borisov OV, Darinskii AA. Computer simulation studies of a single polyelectrolyte chain in poor solvent. Macromolecules 1999;32:3264–78.
[231] Limbach HJ, Holm C. Conformational properties of poor solvent polyelectrolytes. Comput Phys Commun 2002;147:321–4.
[232] Limbach HJ, Holm C. Single-chain properties of polyelectrolytes in poor solvent. J Phys Chem B 2003;107:8041–55.
[233] Limbach HJ, Holm C, Kremer K. Conformations and solution structure of polyelectrolytes in poor solvent. Macromol Symp 2004;211:43–53.
[234] Liao Q, Dobrynin AV, Rubinstein M. Molecular dynamics simulations of polyelectrolyte solutions: nonuniform stretching of chains and scaling behavior. Macromolecules 2003;36:3386–98.
[235] Liao Q, Dobrynin AV, Rubinstein M. Counterion-correlation-induced attraction and necklace formation in polyelectrolyte solutions: theory and simulations. Macromolecules 2006;39:1920–38.
[236] Dormidontova EE, Erukhimovich IY, Khokhlov AR. Microphase separation in poor-solvent polyelectrolyte solutions—phase-diagram. Macromol Theory Simul 1994;3:661–75.
[237] Prevysh VA, Wang BC, Spontak RJ. Effect of added salt on the stability of hydrogen-bonded interpolymer complexes. Colloid Polym Sci 1996;274:532–9.
[238] Spruijt E, Sprakel J, Lemmers M, Cohen Stuart MA, van der Guht J. Relaxation dynamics at different time scales in electrostatic complexes: time-salt superposition. Phys Rev Lett 2010;105, 208301/1-4.
[239] Hariri HH, Lehaf AM, Schlenoff JB. Mechanical properties of osmotically stressed polyelectrolyte complexes and multilayers: water as a plasticizer. Macromolecules 2012;45:9364–72.
[240] Liu T, An QF, Zhao Q, Lee KR, Zhu BK, Qian JW, Gao CJ. Preparation and characterization of polyelectrolyte complex membranes bearing alkyl side chains for the pervaporation dehydration of alcohols. J Membr Sci 2013;429:181–9.
[241] Wang XS, An QF, Zhao Q, Lee KR, Qian JW, Gao CJ. Homogenous polyelectrolyte complex membranes incorporated with strong ion-pairs with high pervaporation performance for dehydration of ethanol. J Membr Sci 2013;435:71–9.
[242] Thuresson K, Nilsson S, Lindman B. Effect of hydrophobic modification on phase behavior and rheology in mixtures of oppositely charged polyelectrolytes. Langmuir 1996;12:530–7.
[243] dos Santos S, Piculell L, Medronho B, Miguel MG, Lindman B. Phase behavior and rheological properties of DNA–cationic polysaccharide mixtures. J Colloid Interface Sci 2012;383:63–74.
[244] Gratson GM, Lewis JA. Phase behavior and rheological properties of polyelectrolyte inks for direct-write assembly. Langmuir 2005;21:457–64.
[245] Liu T, Burger C, Chu B. Nanofabrication in polymer matrices. Prog Polym Sci 2003;28:5–26.
[246] Parthasarathy M, Kakade BA, Pillai VK. Tuning the transport properties of poly(oxyethylene)bisamine-nafion polyelectrolyte complexes by dielectric manipulation. Macromolecules 2008;41:3653–8.
[247] Shchipunov YA, Postnova IV. Water-soluble polyelectrolyte complexes of oppositely charged polysaccharides. Compos Interfaces 2009;16:251–79.
[248] ten Brinke G, Ruokolainen J, Ikkala O. Supramolecular materials based on hydrogen-bonded polymers. Adv Polym Sci 2007;207:113–77.
[249] Wyss HM, Miyazaki K, Mattsson J, Hu Z, Reichman DR, Weitz DA. Strain-rate frequency superposition: a rheological probe of structural relaxation in soft materials. Phys Rev Lett 2007;98, 238303/1-4.
[250] Liu RCW, Morishima Y, Winnik FM. Rheological properties of mixtures of oppositely charged polyelectrolytes. Polym J 2002;34:340–6.
[251] Spruijt E, Cohen Stuart MA, van der Gucht J. Linear viscoelasticity of polyelectrolyte complex coacervates. Macromolecules 2013;46:1633–41.

[252] Wang Y, Kimura K, Huang Q, Dubin PL, Jaeger W. Effects of salt on polyelectrolyte-micelle coacervation. Macromolecules 1999;32:7128–34.
[253] Piculell L, Lindman B. Association and segregation in aqueous polymer/polymer, polymer/surfactant, and surfactant/surfactant mixtures: similarities and differences. Adv Colloid Interface Sci 1992;41:149–78.
[254] Chollakup R, Beck JB, Dirnberger K, Tirrel M, Eisenbach CD. Polyelectrolyte molecular weight and salt effects on the phase behavior and coacervation of aqueous solutions of poly(acrylic acid) sodium salt and poly(allylamine) hydrochloride. Macromolecules 2013;46:2376–90.
[255] Chollakup R, Smitthipong W, Eisenbach CD, Tirrell M. Phase behavior and coacervation of aqueous poly(acrylic acid)-poly(allylamine) solutions. Macromolecules 2010;43:2518–28.
[256] Spruijt E, Westphal AE, Borst JW, Cohen Stuart MA, van der Gucht J. Binodal compositions of polyelectrolyte complexes. Macromolecules 2010;43:6476–84.
[257] Dautzenberg H, Karibyants N. Polyelectrolyte complex formation in highly aggregating systems. Effect of salt: response to subsequent addition of NaCl. Macromol Chem Phys 1999;200:118–25.
[258] Dautzenberg H, Kriz J. Response of poly electrolyte complexes to subsequent addition of salts with different cations. Langmuir 2003;19:5204–11.
[259] Solis FJ, de la Cruz MO. Flexible linear polyelectrolytes in multivalent salt solutions: solubility conditions. Eur Phys J E 2001;4:143–52.
[260] Solis FJ. Phase diagram of dilute polyelectrolytes: collapse and redissolution by association of counterions and co-ions. J Chem Phys 2002;117:9009–15.
[261] Litmanovich EA, Chernikova EV, Stoychev GV, Zakharchenko SO. Unusual phase behavior of the mixture of poly(acrylic acid) and poly(diallyldimethylammonium chloride) in acidic media. Macromolecules 2010;43:6871–6.
[262] Overbeek J, Voorn M. Phase separation in polyelectrolyte solutions. Theory of complex coacervation. J Cell Comp Phys 1957;49:7–26.
[263] Chodanowski P, Stoll S. Polyelectrolyte adsorption on charged particles: a Monte Carlo approach. Macromolecules 2001;34:2320–8.
[264] Song B, Schönherr H. Atomic force microscopy measurements of supramolecular interactions. In: Steed JW, Gale PA, editors. Supramolecular Chemistry: from molecules to nanomaterials. Nanotechnology, vol. 8. New York: John Wiley & Sons Inc.; 2012. p. 3825–40.
[265] Zhang WK, Zhang X. Single molecule mechanochemistry of macromolecules. Prog Polym Sci 2003;28:1271–95.
[266] Cappella B, Dietler G. Force-distance curves by atomic force microscopy. Surf Sci Rep 1999;34:1–104.
[267] Noy A. Handbook of molecular force spectroscopy. New York: Springer; 2008. p. 291pp.
[268] Duwez N, Willet AS, editors. Molecular manipulation with atomic force microscopy. Boca Raton: CRS Press; 2011. p. 287pp.
[269] Butt HJ, Cappella B, Kappl M. Force measurements with the atomic force microscope: technique, interpretation and applications. Surf Sci Rep 2005;59:1–152.
[270] Hugel T, Seitz M. The study of molecular interactions by AFM force spectroscopy. Macromol Rapid Commun 2001;22:989–1016.
[271] Noy A, Vezenov DV, Lieber CM. Chemical force microscopy: nanoscale probing of fundamental chemical interactions. In: Noy A, editor. Handbook of molecular force spectroscopy. New York: Springer; 2000. p. 97–122.
[272] Vezenov DV, Noy A, Ashby P. Chemical force microscopy: probing chemical origin of interfacial forces and adhesion. J Adhes Sci Technol 2005;19:313–64.
[273] Schönherr H. Scanning force microscopy. In: Mark H, editor. Encyclopedia of polymer science and technology, vol. 11, 3rd ed. New York: John Wiley & Sons; 2004. p. 699–745.
[274] Evans E. Probing the relation between force – lifetime – and chemistry in single molecular bonds. Annu Rev Biophys Biomol Struct 2001;30:105–28.
[275] Strunz T, Oroszlan K, Shafer R, Guntherodt HJ. Dynamic force spectroscopy of single DNA molecules. Proc Natl Acad Sci USA 1999;96:11277–82.
[276] Rief M, Gautel M, Osterhelt F, Fernandez JM, Gaub HE. Reversible unfolding of individual titin immunoglobulin domains by AFM. Science 1997;276:1109–12.
[277] van der Vegte EW, Hadziioannou G. Scanning force microscopy with chemical specificity: an extensive study of chemically specific tip-surface interactions and the chemical imaging of surface functional groups. Langmuir 1997;13:4357–68.
[278] Israelachvili JN. Intermolecular and surface forces. 3rd ed. Amsterdam: Elsevier Ltd.; 2011. p. 704pp.
[279] Johnson KL, Kendall K, Roberts AD. Surface energy and the contact of elastic solids. Proc R Soc London A 1971;324:301–13.
[280] van der Vegte EW, Hadziioannou G. Acid-base properties and the chemical imaging of surface-bound functional groups studied with scanning force microscope. J Phys Chem 1997;101:9563–9.
[281] Cranford SW, Ortiz C, Buehler M. Mechanomutable properties of a PAA/PAH polyelectrolyte complex: rate dependence and ionization effects on tunable adhesion strength. Soft Matter 2010;6:4175–88.
[282] Granbois M, Beyer M, Rief M, Clausen-Schaumann H, Gaub HE. How strong is a covalent bond? Science 1999;283:1727–30.
[283] Garnier L, Gauthier-Manuel B, van der Vegte EW, Snijders J, Hadzioannou G. Covalent bond force profile and cleavage in a single polymer chain. J Chem Phys 2000;113:2497–503.
[284] Beyer MK. The mechanical strength of a covalent bond calculated by density functional theory. J Chem Phys 2000;112:7307–12.
[285] Beyer MK, Clausen-Schaumann H. Mechanochemistry: the mechanical activation of covalent bonds. Chem Rev 2005;105:2821–948.
[286] Ray C, Brown JR, Akhremitchev BB. Single-molecule force spectroscopy measurements of "hydrophobic bond" between tethered hexadecane molecules. J Phys Chem B 2006;110:17578–83.
[287] Cui SX, Liu CJ, Zhang W, Zhang X, Wu C. Desorption force per polystyrene segment in water. Macromolecules 2003;36:3779–82.
[288] Li ITS, Walker GC. Single polymer studies of hydrophobic hydration. Acc Chem Res 2012;45:2011–21.
[289] Bai C, Wang C. Single molecule chemistry and physics. An introduction. New York: Springer; 2006. p. 131–58.
[290] Grzybowski BA, Wilmer CE, Kim J, Browne KP, Bishop KJ. Self-assembly: from crystals to cells. Soft Matter 2009;5:1110–28.
[291] Spruijt E, van den Berg SA, Cohen Stuart MA, van der Gucht J. Direct measurement of the strength of single ionic bonds between hydrated charges. ACS Nano 2012;6:5297–303.
[292] Kufer SK, Puchner EM, Gumpp H, Liedl T, Gaub HE. Single molecule cut-and-paste surface assembly. Science 2008;319:594–6.
[293] Oesterhelt F, Rief M, Gaub HE. Single molecule force spectroscopy by afm indicates helical structure of poly-(ethylene-glycol) in water. New J Phys 1999;1:6.1–11.
[294] Spruijt E, Bakker HE, Kodger TE, Sprakel J, Cohen Stuart MA, van der Gucht J. Reversible assembly of oppositely charged hairy colloids in water. Soft Matter 2011;7:8281–90.
[295] Spruijt E, Cohen Stuart MA, van der Guht J. Dynamic force spectroscopy of oppositely charged polyelectrolyte brushes. Macromolecules 2010;43:1543–50.
[296] Sanz E, Leunissen ME, Fortini A, van Blaaderen A, Dijkstra M. Gel formation in suspensions of oppositely charged colloids: mechanism and relation to the equilibrium phase diagram. J Phys Chem B 2008;112:10861–72.
[297] Rief M, Oesterhelt F, Heymann B, Gaub HE. Single molecule force spectroscopy on polysaccharides by AFM. Science 1997;275:1295–7.
[298] Li HB, Rief M, Oesterhelt F, Gaub HE. Single molecule force spectroscopy of xanthan by AFM. Adv Mater 1998;10:316–9.
[299] Li H, Zhang W, Zhang X, Shen J, Liu B, Gao C, Zou G. Single molecule force spectroscopy on poly(vinyl alcohol) by atomic force microscopy. Macromol Rapid Commun 1998;19:609–11.
[300] Li H, Liu B, Zhang H, Gao C, Shen J, Zou G. Single – molecule force spectroscopy on poly(acrylic acid) by AFM. Langmuir 1999;15:2120–4.
[301] Cui S, Pang X, Zhang S, Yu Y, Ma H, Zhang X. Unexpected temperature-dependent single chain mechanics of poly(N-isopropyl-acrylamide) in water. Langmuir 2012;28:5151–7.
[302] Liu K, Song Y, Feng W, Liu N, Zhang W, Zhang X. Extracting a polyetylene oxide chain from a single crystal by a combination of atomic force microscopy imaging and single-molecule force spectroscopy: toward the investigation of molecular interactions in their condensed states. J Am Chem Soc 2011;133:3226–9.
[303] Li H, Zhang W, Xu W, Zhang X. Hydrogen bonding governs the elastic properties of poly(vinyl alcohol) in water: single-molecule force spectroscopy studies of PVA by AFM. Macromolecules 2000;33:465–9.
[304] Wang K, Pang X, Cui S. Inherent stretching elasticity of a single polymer chain with carbone-carbone backbone. Langmuir 2013;29:4315–9.
[305] Flory PJ. Statistical mechanics of chain molecules. Munchen: Hanser; 1988. p. 432pp.
[306] Doi M, Edwards SF. The theory of polymer dynamics. Oxford: Oxford University Press; 1998. p. 391 pp.

[307] Kratky O, Porod G. Röntgenuntersuchung gelöster Fadenmoleküle. Rec Trav Chim 1949;68:1106–23.
[308] Rubinstein M, Colby RH. Polymer Physics. Oxford: Oxford University Press; 2003. p. 456pp.
[309] Janshoff A, Neitzert M, Oberdörfer Y, Fuchs H. Force spectroscopy of molecular systems – single molecule spectroscopy of polymers and biomolecules. Angew Chem Int Ed 2000;39:3212–37.
[310] Liu N, Zhang W. Feeling inter- or intramolecular interactions with the polymer chain as probe: recent progress in SMFS studies on macromolecular interactions. ChemPhysChem 2012;13:2238–56.
[311] Bustamante C, Marko JF, Siggia ED, Smith S. Entropic elasticity of lambda-phage DNA. Science 1994;265:1599–600.
[312] Murnen HK, Rosales AM, Dobrynin AV, Zuckermann RN, Segalman RA. Persistence length of polyelectrolytes with precisely located charges. Soft Matter 2013;9:90–8.
[313] Bouchiat C, Wang MD, Allemand JF, Strick T, Block SM, Croquette V. Estimating the persistence length of a worm-like chain molecule from force-extension measurements. Biophys J 1999;76:409–13.
[314] Hugel T, Grosholz M, Clausen-Schaumann H, Pfau A, Gaub H, Seitz M. Elasticity of single polyelectrolyte chains and their desorption from solid supports studied by AFM based single molecule force spectroscopy. Macromolecules 2001;34:1039–47.
[315] Odijk T. Stiff chains and filaments under tension. Macromolecules 1995;28:7016–8.
[316] Bustamante C, Smith SB, Liphardt J, Smith D. Single-molecule studies of DNA mechanics. Curr Opin Struct Biol 2000;10:279–85.
[317] Odijk T. Polyelectrolytes near the rod limit. J Polym Sci Part B Polym Phys 1977;15:477–83.
[318] Skolnick J, Fixman M. Electrostatic persistence length of a wormlike polyelectrolyte. Macromolecules 1977;10:944–8.
[319] Zhang D, Ortiz C. Synthesis and single molecule force spectroscopy of graft copolymers of poly(2-hydroxyethyl methacrylate-g-ethylene glycol). Macromolecules 2004;37:4271–82.
[320] Zhang D, Ortiz C. Single macromolecule nanomechanical design: poly(2-hydroxyethyl methacrylate-g-ethylene glycol) graft copolymers of varying architecture. Macromolecules 2005;38:2535–9.
[321] Liu C, Cui S, Wang Z, Zhang X. Single-chain mechanical property of poly(N-vinyl-2-pyrrolidone) and interaction with small molecules. J Phys Chem B 2005;109:14807–12.
[322] Livadaru L, Netz RR, Kreuzer HJ. Stretching response of discrete semiflexible polymers. Macromolecules 2003;36:3732–44.
[323] Hugel T, Rief M, Seitz M, Gaub HE, Netz RR. Highly stretched single polymers: atomic-force-microscope experiments versus ab-initio theory. Phys Rev Lett 2005;94, 048301/1-4.
[324] Zhang W, Yu Y, Zhang X. Mechanics of synthetic polymers. In: Duwez N, Willet AS, editors. Molecular manipulation with atomic force microscopy. Boca Raton: CRC Press; 2011. p. 149–63.
[325] Zhang WK, Zou S, Wang C, Zhang X. Single polymer chain elongation of poly(N-isopropylacrylamide) and poly(acrylamide) by atomic force microscopy. J Phys Chem B 2000;104:10258–64.
[326] Wang C, Shi WQ, Zhang WK, Zhang X, Katsumoto Y, Ozaki Y. Force spectroscopy study on poly(acrylamide) derivatives: effects of substitutes and buffers on single-chain elasticity. Nano Lett 2002;2:1169–72.
[327] Borchard W. Thermoreversible gelation. In: Finch AA, editor. Chemistry and technology of water-soluble polymers. New York: Plenum Press; 1983. p. 113–24.
[328] Derjaguin BV, Muller VM, Toporov YP. Effect of contact deformations on the adhesion of particles. J Colloid Interface Sci 1975;53:314–26.
[329] Maugis D. Extension of the Johnson–Kendall–Roberts theory of the elastic contact of spheres to large contact radii. Langmuir 1995;11:679–82.
[330] Carpick RW, Sasaki DY, Burns AR. Large friction anisotropy of a polydiacetylene monolayer. Tribol Lett 1999;7:79–85.
[331] Dzyaloshinskii IE, Lifshitz EM, Pitaevskii LP. General theory of van der Waals' forces. Sov Phys Usp 1961;4:153–76.
[332] van Oss CJ, Chaudhury MK, Good RJ. Interfacial Lifshitz-van der Waals and polar interactions in macroscopic systems. Chem Rev 1988;88:927–41.
[333] Christendat D, Abraham T, Xu Z, Masliyah J. Adhesion forces between functionalized probes and hydrophilic silica surfaces. J Adhes Sci Technol 2005;19:149–63.
[334] Vezenov DV, Noy A, Lieber CM. Chemical force microscopy: force spectroscopy and imaging of complex interactions in molecular assemblies. In: Noy A, editor. Handbook of molecular force spectroscopy. New York: Springer; 2008. p. 123–41.
[335] Brown MA, Huthwelker T, Beloqui Redondo A, Janousch M, Faubel M, Arrell CA, Scarongella M, Chergui M, van Bokhoven JA. Changes in the silanol protonation state measured in situ at the silica–aqueous interface. J Phys Chem Lett 2012;3:231–5.
[336] Feldstein MM, Kiseleva TI, Bondarenko GN, Kostina JV, Singh P, Cleary GW. Mechanisms of molecular interactions in polybase – polyacid complex formed by copolymers of N,N-dimethylaminoethyl methacrylate with alkylmethacrylates and methacrylic acid with ethylacrylate. J Appl Polym Sci 2009;112:1142–65.
[337] Vezenov DV, Noy A, Rozsnyai LF, Lieber CM. Force titration and ionization state sensitive imaging of functional groups in aqueous solutions by chemical force microscopy. J Am Chem Soc 2007;119:2006–15.
[338] Vezenov DV, Zhuk AV, Whitesides GM, Lieber CM. Chemical force spectroscopy in heterogeneous systems: intermolecular interactions involving epoxy polymer, mixed monolayers, and polar solvents. J Am Chem Soc 2002;124:10578–88.
[339] Borkovec M, Papastavrou G. Interactions between solid surfaces with adsorbed polyelectrolytes of opposite charge. Curr Opin Colloid Interface Sci 2008;13:429–37.
[340] Geisler M, Horinek D, Hugel T. Single molecule adhesion mechanics on rough surfaces. Macromolecules 2009;42:9338–43.
[341] Balzer BN, Micciulla S, Dodoo S, Zerball M, Gallei M, Rehahn M, von Klitzing R, Hugel T. Adhesion property profiles of supported thin polymer films. ACS Appl Mater Interfaces 2013;5:6300–6.
[342] Sheiko SS, Magonov SN. Scanning probe microscopy of polymers. In: Matyjaszewski K, Möller M, editors. Polymer science: a comprehensive reference. Vol. 2: polymer characterization. Amsetdam: Elsevier Ltd; 2012. p. 559–605.
[343] Levada (Kiseleva) TI, Feldstein MM. Relationship between intermolecular bonding, nanostructure, phase behavior and macroscopic physical properties of pressure-sensitive adhesives based on polyelectrolyte complexes. J Appl Polym Sci 2012;125:448–70.
[344] Yamaguchi T, Doi M. Debonding dynamics of pressure-sensitive adhesives: 3D block model. Eur Phys J E 2006;21:331–9.
[345] Omidian H, Park K. Introduction to Hydrogels. In: Otternbrite RM, Park K, Okano T, editors. Biomedical applications of hydrogels handbook. New York, Heidelberg, London: Springer; 2010. p. 1–16.
[346] Shull KR, Creton C. Deformation behavior of thin, compliant layers under tensile loading conditions. J Polym Sci Part B Polym Phys 2004;42:4023–43.
[347] Miquelard-Garnier G, Hourdet D, Creton C. Large strain behaviour of nanostructured polyelectrolyte hydrogels. Polymer 2009;50:481–90.
[348] Webber RE, Shull KR. Strain dependence of the viscoelastic properties of alginate hydrogels. Macromolecules 2004;37:6153–60.
[349] Shull KR. Fracture and adhesion of elastomers and gels: large strains at small length scales. J Polym Sci Part B Polym Phys 2006;44:3436–9.
[350] Courtois J, Baroudi I, Nouvel N, Degrandi E, Pensec S, Ducouret G, Chanéac C, Bouteiller L, Creton C. Supramolecular soft adhesive materials. Adv Funct Mater 2010;20:1803–11.
[351] Satas D, editor. Handbook of pressure sensitive adhesive technology. 3rd ed. Warwick, Rhode Island: Satas & Associates; 1999, 1017 pp.
[352] Bayramov DF, Singh P, Cleary GW, Siegel RA, Chalykh AE, Feldstein MM. Non-covalently crosslinked hydrogels displaying a unique combination of water-absorbing, elastic and adhesive properties. Polym Int 2008;57:785–90.
[353] Feldstein MM, Creton C. Pressure-sensitive adhesion as a material property and as a process. In: Benedek I, editor. Pressure-sensitive design, theoretical aspects. Leiden, Boston: VSP-Brill; 2006. p. 27–62.
[354] Feldstein MM, Perepelitsa GG, Khokhlov AR. Hydrophilic pressure-sensitive bioadhesives with targeted adhesion towards teeth and tooth-care compositions based thereon. PCT Application PCT/RU2012/000377WO2013/162404 A1. INPOLYA Ltd.; 2013.
[355] Singh P, Cleary GW, Mudumba S, Feldstein MM, Bairamov DF. Hydrogel composition for tooth whitening. US Patent Application US2003/0152528; Corium International Inc; PCT Application WO2004/071323; Corium International Inc., 2004.
[356] Feldstein MM. Hydrophilic thermo-switchable pressure-sensitive adhesive composition, reversibly detaching in aqueous media under temperature elevation. PCT Application RU2013/001107; INPOLYA Int., 2013.